Definition and implementation of a new service for precise GNSS positioning

Paulo Sérgio De Oliveira Junior

unesp le cnam

ECOLE DOCTORALE Sciences pour L'Ingénieur, Géosciences et Architecture

Laboratoire Géomatique et Foncier

Faculdade de Ciências e Tecnologia

Programa de Pós-graduação em Ciências Cartográficas

Laboratório de Geodésia Espacial

THÈSE présentée par :

Paulo Sérgio de Oliveira Jr.

soutenue le : **05 Septembre 2017**

pour obtenir le grade de : **Docteur du Conservatoire National des Arts et Métiers**

Discipline: Astronomie, astrophysique / Spécialité : Géomatique

Definition and implementation of a new service for precise GNSS positioning

THÈSE dirigée par :

M. MOREL Laurent	Professeur des Universités, CNAM
M. MONICO João F. G.	Professeur des Universités, Unesp

RAPPORTEURS :

M. PEROSANZ Félix	Ingénieur de Recherche, HDR, CNES
M. SANTOS Marcelo	Professeur des Universités, University of New Brunswick

---

EXAMINATEURS :

M. MOURGUES Régis	« Président du jury »	Professeur des Universités, Université du Maine
Me. ALVES Daniele B. M.		Professeure Assistante, Dre., Unesp
M. REBISCHUNG Paul		Chercheur, Dr., IGN
M. FUND François	« Membre absent »	Dr., Geodata-Diffusion/Hexagon Geosystems
M. DURAND Stéphane	« Membre absent »	Professeur Assistant, Dr, CNAM
M. DURAND Frédéric	« Membre absent »	Ingénieur de Recherche, CNAM

"*Whether you think you can, or you think you can't – you're right.*"

Henry Ford

Acknowledgements

I believe that God is the name we found for the positive feelings, energy and all good. So yes, I thank God for his constant presence in my life.

I would like to express my sincere gratitude to my supervisor at ESGT, Laurent Morel, who has encouraged me during this work and provided the opportunity to realize such project. Merci beaucoup!

I also thank François Fund, my supervisor at Geodata Diffusion, who has been a friend, provided interesting discussions and substantial contributions to 'aiguiser' this subject.

An 'obrigado' to my supervisor at Unesp, João F. Galera Monico for his motivation and guidance in GNSS related research.

Big thanks to Romain Legros for his initiative in this project and for following part of my work at Geodata Diffusion, providing me his advice, knowledge and friendship.

A 'merci' also goes to Frédéric Durand and Stéphane Durand, who have provided valuable supervision and technical support.

I acknowledge project funders, Geodata Diffusion Company (Hexagon Geosystems), CNPq (*Conselho Nacional de Desenvolvimento Científico e Tecnológico*) (process: 229828/2013-2). Thanks go also to ANRT (*Association Nationale de la Recherche et de la Technologie*) responsible for CIFRE conventions. Without their support this work would not be possible.

I am also very thankful to the data providers: IGS (International GNSS Service), CNES (*Centre National d'Études Spatiales*) and IGN (*Institut national de l'information géographique et forestière*).

I would like to thank Denis Laurichesse for his work developing PPP-Wizard 1.3 software package, used in part of this thesis, and also for his attention and contribution several times during our research. I also thank Tomoji Takasu for his efforts developing the program package RTKLib used in part of the studies realized in this work.

I will not forget the good moments shared with my friends from Geodata Diffusion: Audrey Gouzer, Sébastien Hutin, Maxime Guerin (& Angèle Caillé), Philippe Bouquerel, Catherine Foulatier, Marianne Vallée, Sandrine Bardotte, Patricia Beauverger, Didier Martinez and Jose-Maria Cabrera. The essential help provided by Corinne Domiter dealing with administrative aspects and the support of Jaime Hernandez. The motivation from friends of GeoAction group, in special Sonia Ikhlef, Mireille Blain, George Soares, Emilie Crasset, Marcel Tardivon, Renée Monot, Thierry Museux, Thomas Longchamp, Alice Simonin.

Friend and previous director of ESGT, Laurent Polidori, is acknowledged for his encouragement during this thesis and for his efforts in Brazil-France research cooperation.

Many thanks to my fellow PhD and post-doc mates, in France: Marcell Ferenc, Clément Roussel, Lina Jarboui, Adèle, André Leite, Mhamad El Hage, and Thomas Leroux; and in Brazil: Mariana Campos, Tayna Gouveia, Gabriel Jerez, Vinicius Stuani, Crislaine Menezes, Erico Martins, Fabricio Prol, Gabriela Takahashi, Marcos, Rodrigo.

Special thanks go to Monica David, for her friendship, motivation and help, as well as her family, for being my family in France, in several moments.

I thank all professors, technical engineers and staff from ESGT/Cnam and FCT/Unesp. They keep these institutions alive and make possible the realization of researches like mine. Thank you! At ESGT, these thanks goes specially to Nelly Decosses, Marlène Cormier, Helène Massot, Jerôme Verdun, Patricia Busson, Sandra Linais, Sylvie Lebfèvre, Elisabeth Simonetto, Elisabeth Botrel, Christelle Mantegari, Christophe Proudhom, Christophe Charlet, Eric Labergerie, Jérémie, Gislain, Nathalie, Matthieu, Jean-Michel, Michel, Dani, Aisha, Thierry, Xavier, Arnaud, Charlet and at Unesp to Prof. Amilton Amorim, Profa. Daniele Barrocá, Italo, Prof. J. C. Chaves, Prof. M. Galo, Prof. Paulo Camargo, Prof. A. M. Tommaselli, Cinthia, Ivonette and André.

Last but not least, I would like to thank my parents, my sister and all my family for being close to me even when I am far, with their love and support. I also thank all my friends from Brazil and France, for being my chosen family.

Abstract

PPP (Precise Point Positioning) is a positioning method by GNSS (Global Navigation Satellite Systems), based on SSR (State Space Representation) concept that can provide centimeter accuracy solutions. Real-time PPP (RT-PPP) is possible thanks to the availability of precise products, for orbits and clocks, provided by the International GNSS Service (IGS), as well as by its analysis centers such as CNES (*Center National d'Etudes Spatiales*). One of the remaining challenges on RT-PPP is the mitigation of atmospheric effects (troposphere and ionosphere) on GNSS signals. Thanks to recent improvements in atmospheric models, RT-PPP can be enhanced, allowing accuracy and centimeter initialization time, comparable to the current NRTK (Network Real-Time Kinematic) method. Such performance depends on topology of permanent stations networks and atmospheric conditions. The main objective of this project is to study the RT-PPP and the optimized infrastructure in terms of costs and benefits to realize the method using atmospheric corrections. Therefore, different configurations of a dense and regular GNSS network existing in France, the Orpheon network, are used. This network has about 160 sites and is owned by Geodata-Diffusion (Hexagon Geosystems). The work was divided into two main stages. Initially, 'float PPP-RTK' was evaluated, it corresponds to RT-PPP with improvements resulting from network corrections, although with ambiguities kept float. Further on, network corrections are applied to improve "PPP-RTK" where ambiguities are fixed to their integer values. For the float PPP-RTK, a modified version of the RTKLib 2.4.3 (beta) package is used to take into account for the network corrections. First-order ionospheric effects were eliminated by the iono-free combination and zenith tropospheric delay estimated. The corrections were applied by introducing a priori constrained tropospheric parameters. Periods with different tropospheric conditions were chosen to carry out the study. Adaptive modeling based on OFCs (Optimal Fitting Coefficients) has been developed to describe the behavior of the troposphere, using estimates of tropospheric delays for Orpheon stations. This solution allows one-way communication between the server and the user. The quality of tropospheric corrections is evaluated by comparison to external tropospheric products. The gains achieved in convergence time to 10 centimeters accuracy were statistically quantified. Network topology was assessed by reducing the number of reference stations (up to 75%) using a sparse Orpheon network configuration to perform tropospheric modeling. This did not degrade the tropospheric corrections and similar performances were obtained on the user side. In the second step, PPP-RTK is realized using the PPP-Wizard 1.3 software and CNES real-time products for orbits, clocks and phase biases of satellites. RT-IPPP (Real-Time Integer PPP) is performed with estimation of tropospheric and ionospheric delays. Ionospheric and tropospheric corrections are introduced as a priori parameters constrained to the PPP-RTK of the user. To generate ionospheric corrections, it was implemented a solution aligned with RTCM (Real-Time Maritime Services) conventions, regarding the transmission of ionospheric parameters SSR, which is a standard Inverse Distance Weighting (IDW) algorithm. The choice of the periods for this experiment was made mainly with respect to the ionospheric activity. The comparison of the atmospheric corrections with the external products and the evaluation of different network topologies (dense and sparse) were also carried out in this stage. Statistically, the standard RT-IPPP takes ~ 25 min to achieve a 10 cm horizontal accuracy, which is significantly improved by our method: 46% (convergence in 14 min) with dense network corrections and 24% (convergence in 19 min) with the sparse network. Nevertheless, vertical positioning sees its convergence time slightly increased, especially when corrections are used from a sparse network solution. However, improvements in horizontal positioning due to external SSR corrections from a (dense or sparse) network are promising and may be useful for applications that depend primarily on horizontal positioning.

Keywords: GNSS; PPP-RTK; ZWD; Troposphere; Ionosphere; Modeling; Reference network; Ambiguity resolution.

Résumé

Le PPP (*Precise Point Positioning*) est une méthode de positionnement par GNSS (*Global Navigation Satellite Systems*), basée sur le concept SSR (*State Space Representation*), qui peut générer solutions de précision centimétrique. Le PPP en temps réel (RT-PPP) est possible grâce à la disponibilité des produits précis, pour les orbites et horloges, fournis par l'IGS (*International GNSS Service*), ainsi que par ses centres d'analyse, tels que le CNES (Centre National d'Etudes Spatiales). Un des défis restants sur le RT-PPP est la mitigation des effets atmosphériques (troposphère et ionosphère) sur les signaux GNSS. Grâce aux améliorations récentes des modèles atmosphériques, le RT-PPP peut être amélioré, ce qui permet une précision et un temps d'initialisation au niveau du centimètre, comparables à la méthode NRTK (*Network Real-Time Kinematic*) actuelle. De telles performances dépendent de la topologie du réseau de stations GNSS permanentes et des conditions atmosphériques. L'objectif principal de ce projet est d'étudier le RT-PPP et l'infrastructure optimisée en termes de coûts et d'avantages pour réaliser la méthode en utilisant des corrections atmosphériques. Pour cela, différentes configurations d'un réseau GNSS dense et régulier existant en France, le réseau Orphéon, sont utilisées. Ce réseau compte environ 160 sites, propriété de Geodata-Diffusion (Hexagon Geosystems). Le travail est divisé en deux étapes principales. Dans un premier temps, le mode «PPP-RTK flottant» a été évalué, il correspond au RT-PPP avec des améliorations issues des corrections de réseau, mais avec les ambiguïtés flottantes. Ensuite, des corrections de réseau sont appliquées pour améliorer le mode « PPP-RTK » où les ambiguïtés sont fixées à leurs valeurs entières. Pour le PPP-RTK flottant, une version modifiée du package RTKLib 2.4.3 (beta) est utilisée pour prendre en compte les corrections réseau. Les effets ionosphériques de premier ordre ont été éliminés par la combinaison *iono-free* et le retard troposphérique zénithal est estimé. Les corrections ont été appliquées en introduisant des paramètres troposphériques a priori contraints. Des périodes avec différentes conditions troposphériques ont été choisies pour réaliser l'étude. Une modélisation adaptative basée sur les OFCs (*Optimal Fitting Coefficients*) a été mise en place pour décrire le comportement de la troposphère, en utilisant des estimations des retards troposphériques pour les stations Orphéon. Cette solution permet une communication mono-directionnelle entre le serveur et l'utilisateur. La qualité des corrections troposphériques est évaluée par comparaison avec des produits troposphériques externes. Les gains réalisés sur le temps de convergence pour obtenir un positionnement de 10 centimètres de précision ont été quantifiés statistiquement. La topologie du réseau a été évaluée, en réduisant le nombre de stations de référence (jusqu'à 75%), via une configuration de réseau Orphéon lâche pour effectuer la modélisation troposphérique. Cela n'a pas dégradé les corrections troposphériques et des performances similaires ont été obtenues du côté de l'utilisateur. Dans la deuxième étape, le PPP-RTK est réalisé grâce au logiciel PPP-Wizard 1.3 et avec les produits temps réel CNES pour les orbites, les horloges et les biais de phase des satellites. Le RT-IPPP (*Real-Time Integer* PPP) est réalisé avec estimation des délais troposphériques et ionosphériques. Les corrections ionosphériques et troposphériques sont introduites en tant que paramètres a priori contraints au PPP-RTK de l'utilisateur. Pour générer des corrections ionosphériques, il a été mis en place une solution alignée avec les conventions RTCM (Real-Time Maritime Services) pour la transmission des paramètres ionosphériques SSR, un algorithme standard d'interpolation à distance inversée (IDW – *Inverse Distance Weighting*). Le choix des périodes pour cette expérience a été fait principalement en regard de l'activité ionosphérique. La comparaison des corrections atmosphériques avec les produits externes et l'évaluation de différentes topologies de réseau (dense et lâche) ont également été effectuées dans cette étape. Statistiquement le RT-IPPP standard prend ~25 min pour atteindre une précision horizontale de 10 cm, ce que nous améliorons significativement par notre méthode : 46% (convergence en 14 min) avec le réseau dense et 24% (convergence en 19 min) avec le réseau restreint. Néanmoins le positionnement vertical voit son temps de convergence légèrement augmenté, en particulier lorsque l'on utilise des corrections à partir d'une solution de réseau lâche. Cependant, les améliorations apportées au positionnement horizontal dues aux corrections atmosphériques SSR externes provenant d'un réseau (dense ou lâche) sont prometteuses et peuvent être utiles pour les applications qui dépendent principalement du positionnement horizontal.

Mots-clés: GNSS; PPP-RTK; ZWD; Troposphère; Ionosphère; Modèles; Réseau de référence; Résolution des ambiguïtés.

Resumo

O PPP (*Precise Point Positioning*) é um método de posicionamento pelo GNSS (*Global Navigation Satellite Systems*), baseado no conceito SSR (*State Space Representation*) o qual pode fornecer soluções de acurácia centimétrica. O PPP em tempo real (RT-PPP) é possível graças à disponibilidade de produtos precisos, para órbitas e relógios, fornecidos pelo IGS (*International GNSS Service*), bem como por seus centros de análise, como o CNES (*Centre National d'Etudes Spatiales*). Um dos desafios restantes no RT-PPP é a mitigação dos efeitos atmosféricos (troposfera e ionosfera) nos sinais GNSS. Graças às melhorias recentes nos modelos atmosféricos, o RT-PPP pode ser aprimorado, permitindo tempo de inicialização com acurácia centimétrica, comparável ao atual método NRTK (Network Real-Time Kinematic). Esse desempenho depende da topologia das redes de estações permanentes e das condições atmosféricas. O objetivo principal deste projeto é estudar o RT-PPP e a infraestrutura optimizada em termos de custos e benefícios para realizar o método usando correções atmosféricas. Portanto, são utilizadas diferentes configurações de uma rede GNSS densa e regular existente na França, a rede Orphéon. Esta rede tem cerca de 160 estações, sendo propriedade da Geodata-Diffusion (Hexagon Geosystems). O trabalho foi dividido em duas etapas principais. Inicialmente, foi avaliado o "*float* PPP-RTK", que corresponde ao RT-PPP com melhorias resultantes de correções de rede, embora mantendo as ambiguidades como *float*. Em um segundo momento, as correções de rede são aplicadas para aprimorar o "PPP-RTK", onde ambiguidades são fixadas para seus valores inteiros. Para o *float* PPP-RTK, uma versão modificada do software RTKLib 2.4.3 (beta) é empregada de modo a levar em consideração as correções de rede. Os efeitos ionosféricos de primeira ordem são eliminados pela combinação iono-free e atraso zenital troposférico é estimado. As correções são aplicadas introduzindo parâmetros troposféricos a priori injuncionados. Períodos com diferentes condições troposféricas foram escolhidos para realizar o estudo. Uma modelagem adaptativa baseada em OFCs (*Optimal Fitting Coefficients*) foi implementada para descrever o comportamento da troposfera, utilizando estimativas de atraso troposférico para estações da rede Orphéon. Tal solução permite a comunicação unidirecional entre o servidor e o usuário. A qualidade das correções troposféricas foi avaliada através de comparação com produtos externos troposféricos. Os ganhos alcançados no tempo de convergência para acurácia de 10 centímetros foram quantificados estatisticamente. A topologia de rede foi avaliada reduzindo o número de estações de referência (em até 75%) usando uma configuração da rede Orphéon esparsa para realizar a modelagem troposférica. Isso não degradou as correções troposféricas e foram obtidas performances similares para os usuários simulados. Na segunda etapa, o PPP-RTK é realizado usando o software PPP-Wizard 1.3, bem como os produtos para tempo real do CNES de órbitas, relógios e *biases* de fase dos satélites. O RT-IPPP (*Real-Time Integer* PPP) é realizado com estimativa de atrasos troposféricos e ionosféricos. As correções ionosféricas e troposféricas são introduzidas como parâmetros a priori injuncionados no PPP-RTK do usuário. Para gerar correções ionosféricas, foi implementada uma solução alinhada com as convenções RTCM (*Real-Time Maritime Services*), em relação à transmissão de correções ionosféricas SSR, o qual é um algoritmo baseado na ponderação pelo inverso da distância (IDW – *Inverse Distance Weighting*). A escolha dos períodos para este experimento foi realizada principalmente em relação à atividade ionosférica. A comparação das correções atmosféricas com produtos externos, assim como a avaliação de diferentes topologias de rede (densa e esparsa) também foram realizadas nesta etapa. Estatisticamente, o RT-IPPP padrão leva ~ 25 min para alcançar uma acurácia horizontal de 10 cm, a qual é significativamente melhorada pelo método implementado: 46% (convergência em 14 min) com correções de rede densa e 24% (convergência em 19 min) com a rede esparsa. No entanto, o posicionamento vertical vê o seu tempo de convergência ligeiramente aumentado, especialmente quando as correções são usadas a partir de uma solução de rede esparsa. No entanto, as melhorias no posicionamento horizontal com o uso das correções de SSR externas de uma rede (densa ou esparsa) são promissoras e podem ser úteis para aplicações que dependem principalmente do posicionamento horizontal.

Palavras chave: GNSS; PPP-RTK; ZWD; Troposfera; Ionosfera; Modelos; Rede de Referência; Resolução das ambiguidades.

Résumé long

Introduction

L'information sur la position est essentielle au développement scientifique de notre société. Lorsque la position est fournie avec une précision élevée (cm) et en temps réel, la valeur de cette information augmente considérablement, ainsi que le nombre d'applications pour le positionnement. Le GNSS (*Global Navigation Satellite Systems*) s'est affirmé comme une technologie puissante pour une telle tâche. Le PPP (*Precise Point Positioning*) est l'une des méthodes les plus remarquables pour obtenir la position d'un utilisateur par GNSS.

Le concept de PPP commence son développement par la communauté scientifique à la fin des années 1990, dans le contexte du traitement de données GPS de manière efficace de pour grandes quantités données (*Global Positioning System*) (Zumberge et al., 1997). Par la suite, le PPP a été développé et amélioré grâce à la disponibilité de produits d'orbites et d'horloges des satellites destinés aux applications de post-traitement. Depuis plusieurs années, ces produits sont générés et diffusés par des organisations telles que la NASA (*National Aeronautics and Space Administration*), JPL (*Jet Propulsion Laboratory*), IGS (*International* GNSS *Service*), RNCan (*Natural Resources Canada*), entre autres (Morel et al., 2014). Des études précédentes ont montré que la méthode PPP peut fournir des solutions avec une précision centimétrique (Kouba et Hero, 2001) lors de l'utilisation de produits finaux générés par l'IGS pour les orbites et les horloges des satellites. Après cela, le nombre d'applications employant le PPP a augmenté rapidement. La méthode est devenue essentielle, par exemple, dans la surveillance glaciaire, la volcanologie, ainsi que dans tout endroit où les lignes de base avec des stations de référence sont trop longues pour un positionnement relatif (Morel, 2015).

Les efforts de la communauté géodésique dans le PPP ont été conduits vers des solutions réelles ou quasi réelles. L'IGS RTWG (*Real-Time Working Group*) a été créé en 2001 pour étudier les produits de précision destinés aux utilisateurs de solutions en temps réel (Caissy et Agrotis, 2011). Par la suite, Gao et Chen (2004) ont effectué des analyses PPP en utilisant des produits précis en temps réel pour les orbites et horloges des satellites, et ils ont obtenu des résultats prometteurs pour le positionnement avec une précision centimétrique.

Plusieurs sessions à l'ION (*Institute of Navigation*), un événement annuel sur le

GNSS, sont dédiées au PPP et la plupart des travaux montrent son potentiel pour les applications en temps réel (Laurichesse et al, 2009 ; Laurichesse et Mercier, 2007; Monico , 2008 ; Wübbena et al., 2005).

L'IGS a lancé le RTPP (*Real-Time Pilot Project*) en 2007, en utilisant des observations GNSS en temps réel obtenues à partir d'un réseau mondial. En avril 2013, le RTS (*Real Time Service*) a été officiellement lancé. Ses produits officiels comprenaient des corrections pour les orbites et les horloges transmises par les satellites GPS (http://www.rtigs.net). Le centimètre de précision est devenu possible avec le RT-PPP en fonction des produits obtenus avec les réseaux GNSS mondiaux (Grinter et Roberts, 2013; Morel, 2015, Rizos et al, 2012.).

L'inconvénient de la méthodologie PPP temps réel, la plus utilisée, c'est le temps nécessaire pour que la solution atteigne la convergence. À l'heure actuelle, la stratégie standard PPP nécessite l'estimation des paramètres d'état (par exemple : les retards troposphériques) ainsi que les ambiguïtés « *float* », ce qui nécessite un temps d'initialisation considérable (au moins 30 min) pour obtenir une bonne convergence des valeurs réelles des ambiguïtés, même dans de bonnes conditions de géométrie des satellites et sans la présence d'effets de multitrajet significatifs (Ge et al., 2012, Rovira-Garcia et al., 2015). Par conséquent, pour les utilisateurs GNSS temps réel qu'ont le besoin d'une précision centimétrique, les méthodes RTK (*Real Time Kinematic*) ou NRTK (*Network* RTK) sont généralement utilisées. La méthode RTK nécessite l'utilisation d'au moins deux récepteurs GNSS connectés via une liaison de communication. Dans le cas du NRTK, l'utilisateur n'a besoin que d'un récepteur, mais il faut l'accès aux corrections OSR (*Observation Space Representation*) obtenues à partir d'un réseau local dense de CORS (*Continuously Operating Reference Station*). Ainsi, le positionnement NRTK a favorisé une augmentation du nombre de réseaux CORS dans le monde (Grinter et Roberts, 2013).

L'efficacité en termes de coût du PPP et la disponibilité des produits précis en temps réel ont motivé beaucoup de recherches pour améliorer la méthode et définir à valeurs entières les paramètres des ambiguïtés de phase (Collins et al, 2010; Ge et al, 2012; Laurichesse et al., 2010, Laurichesse et Mercier, 2007, Mervart et al., 2008). Des améliorations significatives ont été obtenues lorsque, en plus des orbites et horloges, des informations précises des biais de phase sont disponibles, ce qui permet de fixer les ambiguïtés de phase à des valeurs entières (Shi et Gao, 2014, Teunissen et Khodabandeh,

2015). Ces avancées ont conduit au concept connu comme SSR (*State Space Representation*), qui consiste à isoler et corriger toutes les erreurs physiques affectant les mesures GNSS (Mervart et al, 2013; Wübbena et al, 2005). Des études ont montré que les corrections SSR pour les paramètres atmosphériques, tels que les retards ionosphériques et troposphériques, peuvent réduire le temps de convergence du PPP pour une solution de qualité centimétrique à quelques minutes ou même les secondes (Leandro et al., 2011, Li et al., 2014b, Rovira-Garcia et al., 2015). Dans ce cas, l'amélioration du temps de convergence de la solution est favorisée non seulement au profit de la corrections des biais de phase, mais aussi grâce à des corrections atmosphériques fournies par l'augmentation des réseaux, menant à ce que l'on appelle PPP-RTK (Stürze et al., 2012 Wübbena et al., 2014, 2005). Ces études montrent le positionnement basé sur les corrections SSR comme une solution potentielle rivale ou complémentaire aux méthodes RTK ou NRTK. Dans ce cas, en particulier si la correction atmosphérique SSR peut être généré à partir des réseaux GNSS plus lâches que ceux requis pour générer des corrections OSR, la solution PPP-RTK devient moins coûteuse que le NRTK. Cependant, les performances de la modélisation atmosphérique pour générer les corrections SSR dépendent de la topologie du réseau et des conditions atmosphériques.

En France, l'entreprise Geodata-Diffusion, filiale du groupe Hexagon Geosystems, fournit des services industriels pour le positionnement basé sur les réseaux GNSS. Ces services sont disponibles depuis 2004 en utilisant les données GNSS du réseau Orphéon. Afin de continuer à fonctionner de manière efficace et maintenir son leadership dans leur domaine, la société Geodata-Diffusion a besoin d'approfondir la compréhension et les détails techniques des performances du PPP, ainsi que l'impact potentiel d'une telle méthode dans l'industrie du GNSS. Dans ce contexte, il a été proposé le développement de cette thèse CIFRE-Brésil (Convention Industrielle de Formation par la Recherche - Brésil) sous cotutelle internationale entre deux laboratoires de recherche : le GeF (Géomatique et Foncier) en France et le LGE (Laboratoire de géodésie spatiale) au Brésil.

Objectif

L'objectif principal de cette thèse est d'évaluer les solutions PPP en temps réel existantes augmentées par l'apport de corrections SSR atmosphériques, ainsi que d'améliorer les solutions ou modèles employés, tout en s'adaptant au contexte industriel du projet. Ainsi, la faisabilité et la démonstration d'un nouveau service de positionnement GNSS précis en

temps réel basé sur la méthode PPP sont étudiées.

Afin d'atteindre les objectifs mentionnés ci-dessus, les objectifs spécifiques suivants doivent être atteints :

- Effectuer une révision bibliographique pour comprendre les avancées et les aspects de base impliqués dans le sujet de cette thèse,
- Assurer l'efficacité économique par rapport à la communication entre le serveur et les utilisateurs, ainsi que l'alignement des solutions adoptées avec les normes définies pour les correctifs SSR.
- Contribuer à la modélisation de la variabilité atmosphérique ainsi qu'à la compréhension de l'impact des corrections atmosphériques sur les paramètres du traitement GNSS.
- Étudier la qualité et la fiabilité du positionnement de l'utilisateur avec des corrections atmosphériques.
- Évaluer la corrélation entre qualité du positionnement GNSS basée sur les corrections SSR et la topologie du réseau de référence utilisé pour la génération de ces corrections.

Contributions de ce travail

Ce travail est divisé en deux étapes principales : 1) l'utilisation des corrections troposphériques et 2) l'utilisation de corrections troposphériques et ionosphériques. L'impact de la topologie du réseau utilisée pour générer les corrections est étudié dans les deux cas, en réduisant le nombre de stations de référence jusqu'à 75%, ce qui correspond à une configuration de réseau lâche. Pour cela, on s'appuiera sur un réseau GNSS permanent, dense et régulier, le réseau Orphéon. Ce réseau compte environ 160 sites en France et appartient à la société Geodata-Diffusion, filiale du groupe Hexagon Geosystems directement impliquée dans ce projet.

Concernant la première étape, le logiciel RTKLib 2.4.3-beta (Takasu, 2013) est utilisé avec des modifications mises en œuvre pour prendre en compte les corrections troposphériques SSR issues du réseau Orphéon. Les observables iono-free sont utilisées pour réduire les effets ionosphériques, et le PPP en temps réel est réalisé avec l'utilisation de

corrections troposphériques. Cette solution de positionnement avec ambiguïtés flottantes est appelée ici "*float* PPP-RTK". La génération de corrections troposphériques est basée sur une modélisation polynomiale adaptative, l'OFC (*Optimal Fitting Coefficients*), qui convient à une communication monodirectionnelle entre le serveur et les utilisateurs, et permet ainsi une communication plus légère (Shi et al., 2014). Dans cette recherche, la méthode OFC au deuxième ordre a été mise en œuvre et évaluée, ce qui n'a pas été réalisé dans des travaux antérieurs, permettant la génération de corrections troposphériques pour de plus grandes zones.

Dans un deuxième temps, le logiciel CNES PPP-Wizard 1.3 est utilisé pour introduire des corrections ionosphériques et troposphériques en tant que paramètres a priori. Dans cette solution PPP-RTK, des observations non combinées sont utilisées et la fixation des ambiguïtés est effectuée, en utilisant des produits CNES orbitaux, d'horloge et de biais de phase. L'interface existante pour appliquer les contraintes atmosphériques dans ce logiciel est améliorée pour prendre en compte la variation de la précision des corrections atmosphériques SSR (utilisée comme contrainte) au cours du temps. La génération de corrections troposphériques et ionosphériques SSR est alignée sur les conventions RTCM (*Radio Technical Commission for Maritime Services*) grâce à un algorithme d'interpolation classique supposant que les utilisateurs auraient accès directement aux informations des retards ionosphériques et troposphériques estimées aux stations de référence.

Premier stage : *float* PPP-RTK avec modélisation troposphérique

Méthodologie

Le ZTD (*Zenith Total Delay*) troposphérique a une composante résiduelle, le ZWD (*Zenith Wet Delay*), qui doit être estimée comme un paramètre supplémentaire dans le traitement GNSS. Par conséquent, l'utilisation des valeurs de ZWD a priori précis peut aider à réduire le temps de convergence de la position.

Afin de réduire le temps nécessaire pour que le PPP-RTK atteigne une précision de 10 cm, la stratégie de ce premier stage de la recherche s'est concentrée sur deux points : 1) réaliser la modélisation troposphérique pour fournir des corrections de ZWD et 2) vérifier les

impacts de ces corrections du côté utilisateur sur le traitement *float* PPP-RTK. La technique de modélisation OFC (Shi et al., 2014) est utilisée car elle ne nécessite qu'une liaison de communication monodirectionnelle.

Les principales données d'entrée, ainsi que la stratégie utilisée pour effectuer la modélisation troposphérique, sont présentées sur la Figure 1. Dans la première étape, les valeurs de ZWD sont estimées en temps réel pour un réseau GNSS de référence, où les positions de la station sont fortement contraintes (1 cm). Dans la deuxième étape, les estimatives de ZWD sont utilisées pour générer un modèle ZWD utilisable à n'importe quel endroit dans la zone de couverture du réseau. Au cours de ce processus, des paramètres de contrôle qualité sont vérifiés pour éliminer les éventuels *outliers*. Dans cette étape, la modélisation doit permettre à une liaison de communication monodirectionnelle entre le serveur et les utilisateurs. Enfin, ce modèle ZWD peut être transmis aux mobiles afin de dériver des valeurs ZWD a priori utilisées dans l'algorithme de *float* PPP-RTK.

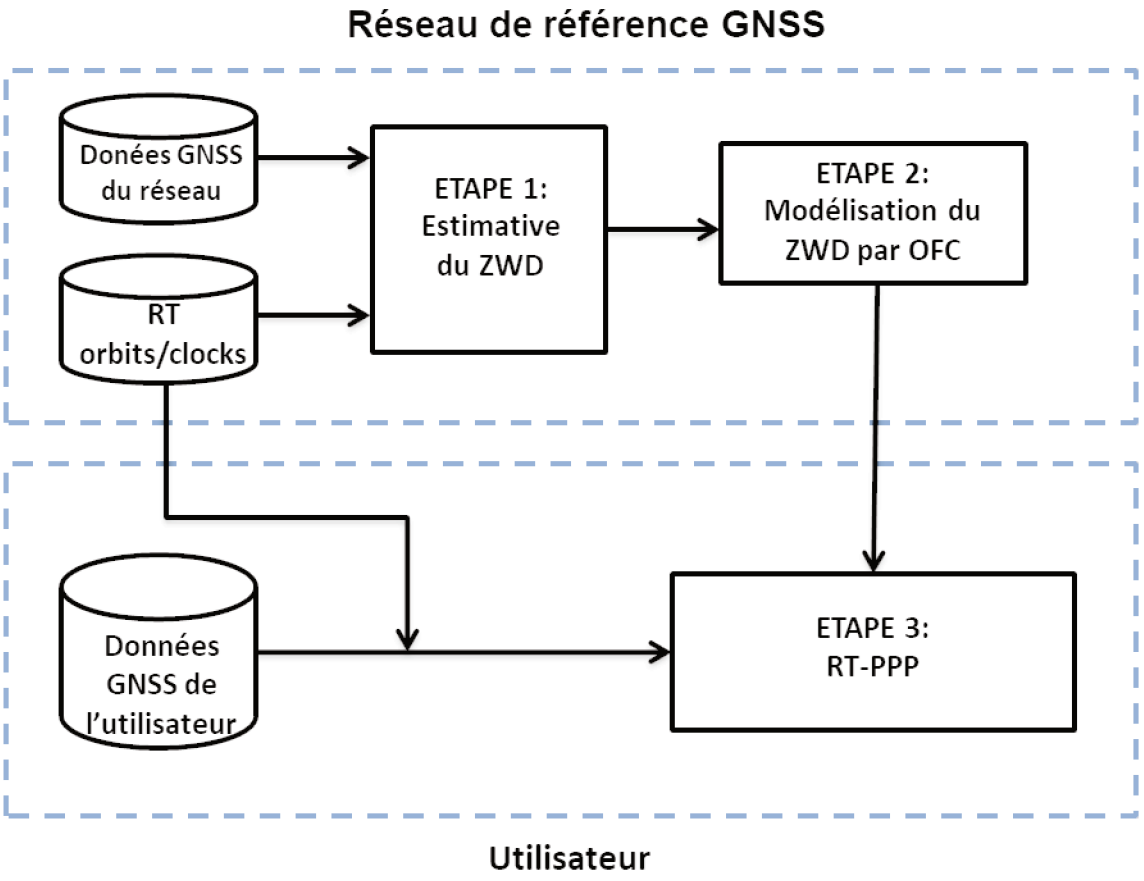

Figure 1 – Stratégie adoptée pour générer le modèle ZWD pour le *float* PPP-RTK.

Pour exécuter le *float* PPP-RTK, on utilise le logiciel RTKLib 2.4.2 (Takasu, 2013) modifié dans cette recherche pour ajouter une option qui permet d'introduire des valeurs de ZWD a priori contraintes pour ce paramètre. Les stratégies de traitement GNSS utilisées pour estimer les valeurs de ZWD du côté réseau GNSS de référence (étape 1) et pour exécuter le *float* PPP-RTK au niveau de l'utilisateur (étape 3) sont présentées par le Tableau 1. Les principales différences entre eux sont le mode de positionnement, statique ou cinématique. Au cours de l'étape 1, les coordonnées des stations de référence sont bien connues, de sorte qu'elles sont fortement contraintes tandis que les valeurs ZWD sont estimées. Du côté de l'utilisateur, on estime les coordonnées du récepteur lors de l'étape 3, et les valeurs de ZWD sont contraintes en utilisant des valeurs a priori provenant des corrections à chaque *cold-start*. La qualité de la correction (sa précision) est utilisée comme contrainte pour les retards troposphériques dans l'algorithme PPP-RTK.

Tableau 1 – Configurations du traitement GNSS pour le serveur et pour l'utilisateur.

	Traitement GNSS du côté réseau	**Traitement GNSS du côté utilisateur**
Mode	PPP statique (solution *float*)	PPP cinématique (solution *float*)
Orbites et horloges	Produits d'horloge et orbites du CNES RT	Produitsd'horloge et orbites du CNES RT
Ionosphère	*Ionospheric-free*	*Ionospheric-free*
Zenith Tropospheric Delay	ZHD: (Saastamoinen, 1972) + atmosphère standard ZWD: estimé Mapping functions: (Niell, 1996)	ZHD: (Saastamoinen, 1972) + atmosphère standard ZWD: Contraintes (correction introduite à chaque *cold-start*) Mapping functions: (Niell, 1996)
Coordonnées	Contraintes (1 cm)	Estimées
Cut-off	10 degrés	10 degrés
Intervalle des observations	30 s	30 s
Process Kalman	*Forward*	*Forward*
Autres paramètres	*IERS Conventions 2010* (Petit and Luzum, 2010)	*IERS Conventions 2010* (Petit and Luzum, 2010)
Logiciel	RTKLib 2.4.2 (Takasu, 2013)	RTKLib 2.4.2 (Takasu, 2013)

Pour simuler les conditions de positionnement en temps réel, les produits du CNES sont utilisés pour l'orbite et l'horloge en temps réel (Laurichesse et al., 2009). Les observables GPS et GLONASS sont utilisées à intervalle de 30 secondes et traitées en considérant l'angle d'élévation supérieur à 10 degrés. Dans ces conditions, l'adoption d'un modèle troposphérique standard pour le ZHD (Saastamoinen, 1972) et de la NMF (Niell, 1996) ne présentent pas de biais significatifs par rapport à l'usage de modèles plus sophistiqués tels que GPT2w (Böhm et al., 2015) et de la GMF (Boehm et al., 2006) dans le positionnement tel que vérifié par Fund et al. (2011).

Modélisation troposphérique

Une fois que les valeurs de ZWD temps réel sont estimées avec le logiciel RTKLib pour toutes les stations de référence, le modèle troposphérique OFC peut être généré. Le modèle est appliqué au second ordre, adapté de Shi et al. (2014), équation (1).

$$ZWD_i = a_0 + a_1 x_i + a_2 y_i + a_3 z_i + a_4 x_i y_i + a_5 x_i z_i + a_6 y_i z_i + a_7 x_i^2 + a_8 y_i^2 + a_9 z_i^2 (i = 1, \dots n) \quad (1)$$

L'équation (1) est utilisée avec les contraintes suivantes (2) :

$$0 = \varphi_j a_j \quad (2)$$

com $\varphi_j = \{0,1\}$, $j = \{0, \dots, 9\}$

Dans l'équation (1), le paramètre ZWD_i représente la valeur de ZWD de la station de référence i, les termes (a_0, a_1, ..., a_9) représentent les coefficients du modèle, qui sont les paramètres à estimer. x_i, y_i et z_i sont les coordonnées géodésiques, j est le nombre de coefficients. Différents ensembles de coefficients sont estimés, en fonction de l'application des contraintes de mode décroissant aux coefficients lors de l'ajustement par moindres carrés. Le nombre d'ensembles de coefficients à tester (c) est donné par (3) :

$$c = \sum_{k=0}^{m} \frac{m!}{k!\,(m-k)!} \quad (3)$$

où m est le nombre de coefficients du modèle et k est le numéro du coefficient (a_j). Par exemple, si le nombre de coefficients est 4 (cas du premier ordre), c est égal à 16. Mais lorsque le nombre de coefficients utilisé est 10 (cas du second ordre), le nombre d'ensembles

de coefficients testés augmente à 1024. Dans notre étude, la modélisation de second ordre a été implémentée, avec quelques modifications mineures pour couvrir une grande surface.

Le paramètre de qualité interne pour le modèle OFC est le RMS des résidus (4) dérivés de l'estimation des coefficients.

$$RMS_{Trop} = \sqrt{\frac{v_1^2 + v_2^2 + v_3^2 + \cdots + v_n^2}{n}} \tag{4}$$

Dans l'équation (4), RMS_{Trop} est la valeur utilisée comme information de contrôle qualité pour l'application de la correction troposphérique, *v* est la différence entre le ZWD estimée dans le traitement RT-PPP avec les observations du réseau de CORS et la valeur ajusté sur la surface troposphérique.

Afin de détecter les erreurs aberrantes entre les ZWD utilisées pour estimer les coefficients, une méthode classique d'identification des *outliers* (Leick, 2004) est appliquée, en comparant les valeurs absolues de chaque résidu ZWD avec le RMS résiduel global si le résidu individuel dépasse 4 fois la valeur du résidu RMS, les coefficients sont à nouveau estimés avec une réduction du poids de l'observation en question.

Données GNSS

Les améliorations sur le positionnement ont été évaluées pour des corrections troposphériques obtenues avec une configuration de réseau dense et une configuration plus lâche (Figure 2) ainsi qu'avec des observations GPS uniquement et avec des observations GPS+GLONASS.

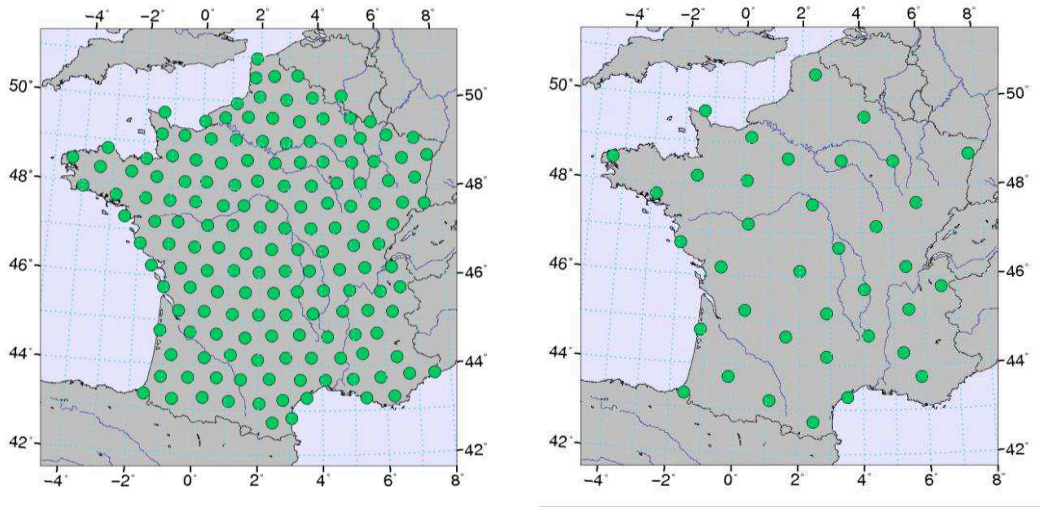

Figure 2 - Les configurations du réseau GNSS Orphéon utilisées pour générer les corrections troposphériques : dense (gauche) et lâche (droite).

Pour la réalisation de cette étude, 20 jours répartis en quatre périodes principales au cours de l'année 2014 sont sélectionnés (Tableau 2). Ces périodes sont choisies en fonction des saisons de l'année et des variations annuelles de température en France publiées par Météo-France.

Tableau 2 – Périodes de l'étude

	Printemps	**Eté**	**Automne**	**Hiver**
Jours sélectionnés dans 2014	121-126	205-210	289-294	357-362

En tant que référence externe indépendante pour les corrections troposphériques, les produits de ZTD disponibles par l'IGN (*Institut National de l'Information Géographique et Forestière*) sont utilisés pour évaluer les corrections troposphériques de ZWD modélisées par OFC. Cette comparaison montre que les ZWDs modélisés présentent une précision d'environ 1,3 cm par rapport aux produits IGN ZTD. En outre, une bonne cohérence entre le RMS des résidus de la modélisation OFC et les différences par rapport aux produits IGN est observée. Un tel résultat est important, puisque le RMS des résidus OFC est la quantité utilisée comme contrainte pour les corrections troposphériques, variant la plupart du temps entre 1 et 2 cm.

Les améliorations du temps de convergence lors de l'utilisation des corrections troposphériques pour le PPP-RTK sont quantifiées. Pour cela, 22 stations du RGP (Réseau GNSS Permanent) géré par l'IGN sont sélectionnées pour simuler des utilisateurs répartis

dans la zone de couverture du réseau Orphéon en France (Figure 3).

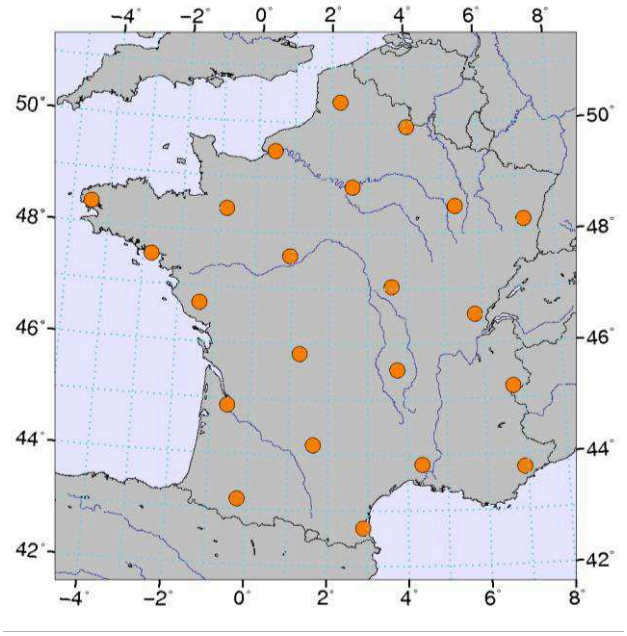

Figure 3 - Stations RGP sélectionnées pour simuler le positionnement du côté utilisateur et évaluer la qualité des corrections troposphériques.

Résultats et analyses

La Figure 4 montre les résultats du traitement GPS+GLONASS, en considérant les médianes et les quantiles à 68% de toutes les réinitialisations (10 réinitialisations par jour sur 20 jours) pour les 22 utilisateurs simulés. Quatre méthodes sont évaluées : 1) une solution standard sans corrections troposphériques (PPP standard en temps réel), 2) l'utilisation de produits IGN (solution post-traitée de haute précision utilisée comme référence) et l'utilisation de corrections externes générées à partir d'un réseau 3) dense et 4) lâche. Les barres verticales sur ces figures indiquent quand la méthode atteint une précision de 10 cm.

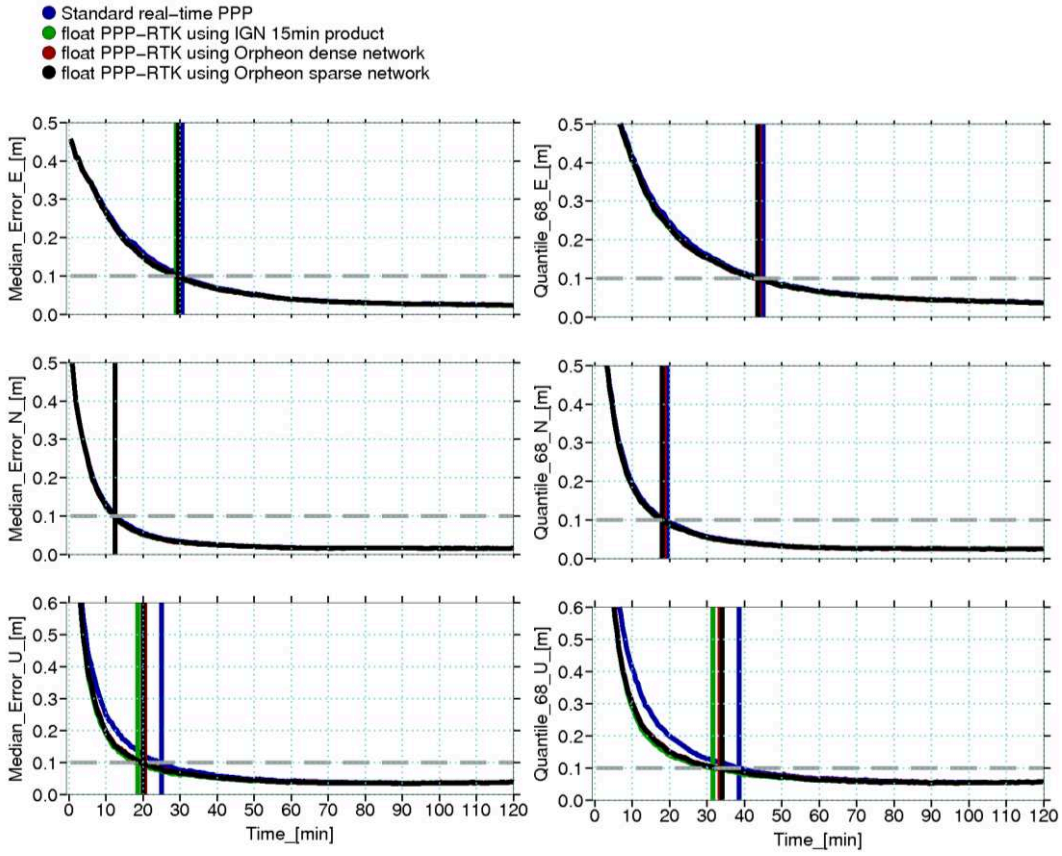

Figure 4 - Médianes (gauche) et quantiles à 68% (droite) des erreurs de positionnement cinématique RT-PPP (GPS + GLONASS) par époque aux stations IGN représentées sur la Figure 3.

Tableau 3 – Temps de convergence (min) de la solution de positionnement avec *float* PPP-RTK (GPS+GLONASS).

Correction troposphérique	Médianes Temps de convergence			Quantiles à 68% Temps de convergence		
	E	N	U	E	N	U
Standard (sans correction)	30,5	12,5	25,0	45,0	19,5	38,5
IGN ZWD produits	29,0	12,5	18,5	44,0	18,0	31,5
OFCs obtenus avec le réseau dense	29,5	12,5	20,5	44,0	18,5	33,5
OFCs obtenus avec le réseau lâche	29,5	12,5	20,0	43,5	18,0	34,0

Les gains en médianes observés sur le temps de convergence en utilisant les produits troposphériques de l'IGN (solution de référence) sont d'environ 1,5 min (4,9%) et 6,5 min (26,0%) sur les composants Est et Up, respectivement. Lors de l'application des ZWDs a

priori obtenus à partir de la modélisation OFC et en utilisant des configurations de réseau dense ou lâche, des améliorations semblables sont observées sur la composante Est : 1 min (3,3%). Sur la hauteur, l'utilisation des OFCs dérivés d'un réseau lâche a fournit des résultats légèrement meilleurs, avec un gain de 5,0 min (20,0%) contre 4,5 min (18,0%) avec le réseau dense. Aucun gain sur la composante Nord n'est observé. Une fois les impacts des corrections troposphériques quantifiés, l'ajout de corrections ionosphériques a été quantifié dans le deuxième stage de cette étude.

Deuxième stage : PPP-RTK avec corrections troposphériques et ionosphériques

Méthodologie

Dans le deuxième stage, le logiciel CNES PPP-Wizard 1.3 est utilisé pour faire du RT-IPPP (RT *Integer* PPP), ce qui correspond au PPP temps réel avec l'estimation des ambiguïtés entières. Cette méthode est utilisée pour estimer les retards ionosphériques et troposphériques en utilisant les données GNSS des stations Orphéon. Les retards atmosphériques estimés sont utilisés comme entrée dans un algorithme d'interpolation IDW (*Inverse Distance Weighting*) afin de générer les corrections. Les retards ionosphériques sont particulièrement compliqués à traiter étant donné qu'ils sont affectés par les biais de *hardware* du récepteur et du satellite.

La Figure 5 montre le schéma de la stratégie appliquée pour générer et appliquer les corrections atmosphériques SSR, respectivement, au serveur du réseau de référence et au positionnement de l'utilisateur. Par rapport à la stratégie précédemment utilisée dans le premier stage, les principales différences sont l'addition de l'estimation des retards ionosphériques inclinés au réseau de référence et l'utilisation de l'algorithme d'interpolation, aligné avec les normes RTCM pour les corrections atmosphériques SSR.

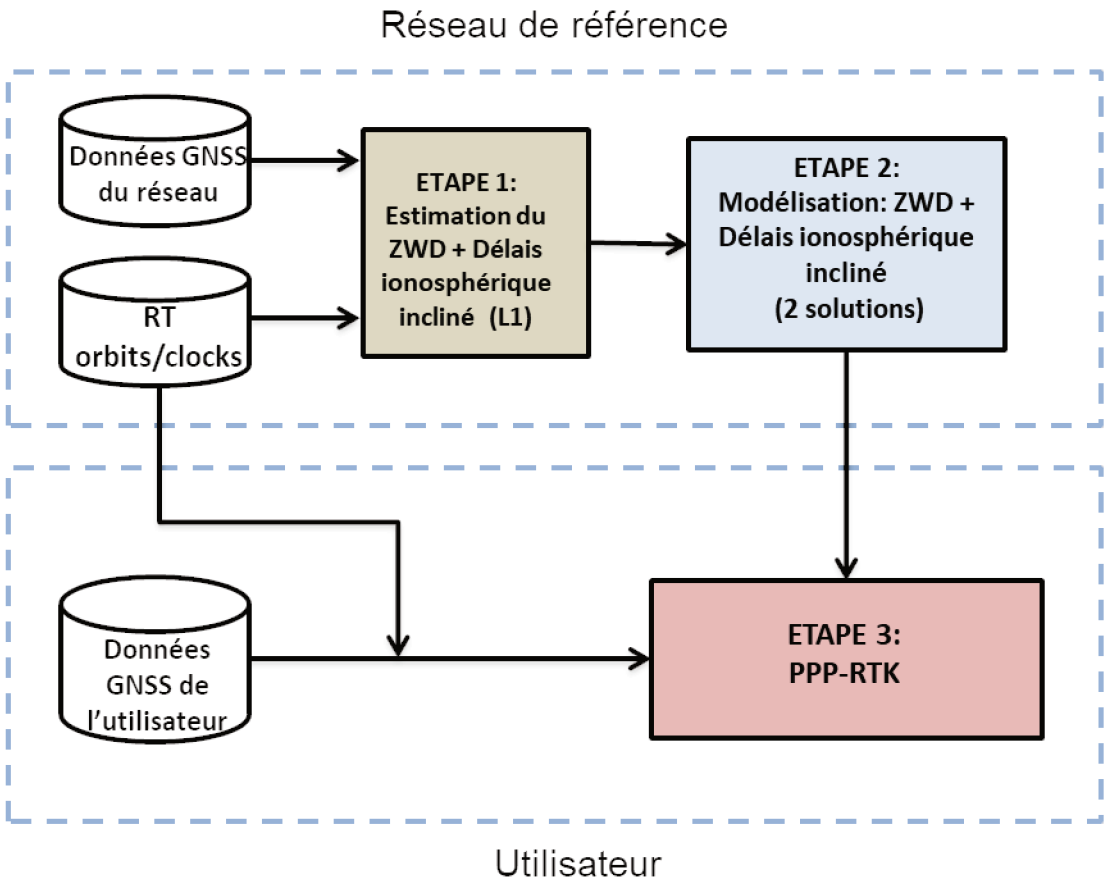

Figure 5 – Stratégie de réalisation du PPP-RTK, avec génération de corrections atmosphériques SSR et leur application au positionnement de l'utilisateur.

En estimant les retards atmosphériques du réseau sur le serveur, les coordonnées de la station sont connues et peuvent être fortement contraintes ou même fixes (c'est-à-dire, le sigma initial des positions mises à zéro). Cependant, dans cette étape, les coordonnées des stations sont considérées comme des paramètres inconnus, de sorte que les erreurs de positionnement puissent être utilisées comme indicateur de la qualité des paramètres atmosphériques estimés. Les paramètres de configuration du PPP-Wizard 1.3 définis du côté serveur (réseau Orphéon) sont présentés par le tableau 4. Les paramètres proposés par la documentation du PPP-Wizard 1.3 (Laurichesse, 2016) sont utilisés, à l'exception de deux changements : 1) limite appliquée à l'écart-type des ambiguïtés, requis pour la fonction de décision des ambiguïtés (*thrAmb*) et 2) le rejet maximum de RAIM (*maxReject*).

Tableau 4 – Paramètres du traitement GNSS avec le PPP-Wizard 1.3 pour estimer les retards atmosphériques

Numéro	Paramètre	Type/Unité	Description	Traitement GNSS au serveur
1	Mode	Enum	Mode de traitement: Mode_PPP_AR	Mode_PPP_AR
2	AntexFileName	String	Antex IGS file	igs08.atx
3	AR/JumpsIndicators	Boolean	Indicates ambiguities to be estimated. NL, WL and Extra WL. If 1: yes, 0: no.	1 1 0
4	useGPS	Boolean	Use GPS constellation. If 1: yes, 0: no.	1
5	useGLONASS	Boolean	Use GLONASS constellation. If 1: yes, 0: no.	1
6	sbasCorrection	Boolean	If 1: SBAS clock correction, otherwise 0: e.g. RTIGS or CNES clock correction	0
7	Reset	Int/sec	Time between consecutive reset (for convergence tests) 0 if no reset	0
8	OutputVerbose	Boolean	Verbose output	0
9	Step	Real/second	Measurement interval, i.e. the sampling interval of observations.	1
10	maxAge	Real/second	Maximum RTCM correction age	10
11	stepMin	Integer/S.U.	Minimum step before AR. Minimum number of epochs to start ambiguity fixing. If interval is 1 second, 3600 represents 1 hour.	3600
12	maxReject	Integer/S.U.	Maximum rejection RAIM (Receiver Autonomous Integrity Monitoring)	3
13	raim	Boolean	Advanced RAIM. Outlier detercion.	1
14	mapThr	Real/S.U.	Tropospheric mapping function threshold (1/sin(ele)). In this function (CNES mapping, 6 is equivalent to 10 degrees cutoff)	6
15	sigIniTro	Real/m	Tropo initial noise	0,5
16	sigModTro	Real/m	Tropo model noise	0,000005
17	nbSatFixAmb	Integer/S.U.	Minimum satellite for AR	0
18	thrAmb	Real/m	Ambiguity threshold for AR	0,25
19	sigIniBiasClk	Real/m	Initial clock bias noise	0
20	sigModBiasClk	Real/m	Model clock bias noise	0,001
21	sigIniIono	Real/m	Initial iono noise	10
22	sigModIono	Real/m	Model iono noise	0,002
23	sigMeasIono	Real/m	Iono measurement noise	1,0 1,0 1,0
24	IonoThr	Real/m	Iono measurement rejection threshold	5 0
25	sigMeasTropo	Real/m	Tropo measurement noise	0,1
26	tropoThr	Real/m	Tropo measurement rejection threshold	1
27	sigIniPos	Real/m	Initial position noise, 50 m position unknown or 0 (position fixed)	50
28	sigModPos	Real/m	Model position noise: 10 (mobile receiver), 0.02 (static receiver) or 0 (position fixed)	0,02
29	preDTMax	Real/sec	Maximum measurement gap	300
30	codeThr	Real/m	Code measurement rejection threshold	10
31	phaseThr	Real/m	Phase measurement rejection threshold	0,05
32	sigMeasCodeGps	Real/m	Code GPS measurement noise	1
33	sigMeasPhaseGps	Real/m	Phase GPS measurement noise	0,01
34	sigMeasCodeGlo	Real/m	Code GLONASS measurement noise	5
35	sigMeasPhaseGlo	Real/m	Phase GLONASS measurement noise	0,01

Pour le paramètre *thrAmb*, la valeur suggérée dans le fichier de configuration fourni avec le logiciel PPP-Wizard (cycle 0,25) est utilisée à la place de celle suggérée dans la documentation du logiciel (cycle 0,01). Ceci a été pris en compte puisque les tests initiaux ont montré que la précision du positionnement est réduite ainsi que le nombre d'ambiguïtés NL

fixes lors de l'utilisation de la valeur du cycle 0,01 pour *thrAmb*. Cependant, d'autres investigations pour définir un seuil optimal doivent être effectuées. Le paramètre *maxReject* pour le RAIM a été augmenté à 3 satellites, au lieu de 2. La configuration des satellites *maxReject* 3 a fourni des solutions légèrement meilleures lors des tests initiaux, mais des investigations supplémentaires doivent également être effectuées pour définir la meilleure configuration pour ce paramètre.

Aucune information externe pour les paramètres atmosphériques n'est utilisée du côté serveur. Ainsi, un modèle empirique (Saastamoinen, 1972) est utilisé pour obtenir le retard initial troposphérique a priori, qui est contraint à 10 cm (*sigMeasTropo*). Les retards ionosphériques sont initialisés à des valeurs nulles, avec précision de 1 m (*sigMeasIono*), comme suggéré dans la configuration du manuel du PPP-Wizard 1.3 (Laurichesse, 2016).

Les paramètres ionosphériques peuvent mettre un temps considérable pour converger correctement. Dans Rovira-Garcia (2015), par exemple, le traitement des stations du réseau de référence (côté serveur) est démarré un jour avant l'utilisation des paramètres liés à l'ionosphère pour assurer les limites de précision et de confiance de 1 TECU (~ 16cm). Dans ce travail, le traitement côté serveur commence à 0h00min UTC tous les jours et est continu tout au long de la journée. Avec le PPP-Wizard 1.3, la convergence peut mettre 1h, comme recommandé dans la documentation du PPP-Wizard 1.3 (Laurichesse, 2016) avant d'initier la fixation des ambiguïtés. Par conséquent, seules les premières heures de traitement sont impactées par la convergence de la solution. Donc, afin d'utiliser une solution atmosphérique appropriée, les 3 premières heures de traitement ne sont pas utilisées pour générer des corrections SSR. Cependant, une étude détaillée sur la convergence des paramètres atmosphériques avec le PPP-Wizard 1.3 est nécessaire.

Modélisation atmosphérique

Les retards ionosphériques et troposphériques estimés sont ensuite utilisés en tant qu'entrée dans l'algorithme d'interpolation IDW (*Inverse Distance Weighting*) pour générer les corrections du réseau. Au moins 3 stations de référence sont utilisées. Si l'utilisateur est à l'intérieur du réseau, les stations sélectionnées entourent son emplacement. Pour les utilisateurs situés aux bords du réseau, l'algorithme IDW fonctionne toujours, mais la qualité

des corrections peut être moins efficace en raison de la variabilité spatiale des retards atmosphériques.

Les corrections ionosphériques générées sont évaluées par rapport aux produits GIM (*Global Ionospheric Maps*) de l'IGS et aussi par rapport aux retards ionosphériques estimés au mobile dans le traitement du PPP-Wizard 1.3. Une précision de 20 ~ 40 cm a été trouvée en comparaison avec les produits iono de l'IGS. Ce résultat est cohérent avec la précision nominale de ce produit. D'un autre côté, comparées aux retards ionosphériques estimés sur le mobile lui-même, les corrections ionosphériques mises en œuvre présentent une précision de 10 ~ 20 cm. De tels résultats indiquent que même si les corrections ionosphériques peuvent être biaisées par les biais hardware du récepteur, elles restent précises et peuvent être utilisées comme corrections SSR. De plus, ces précisions sont cohérentes avec les valeurs des contraintes appliquées aux corrections ionosphériques.

Une fois les corrections ionosphériques et troposphériques générées, elles sont utilisées comme informations a priori et contraintes dans le traitement GNSS du PPP-Wizard 1.3 qui a été modifié pour permettre plus de flexibilité dans l'application des contraintes pour les corrections atmosphériques. Ces modifications permettent d'introduire des valeurs plus réalistes pour ces contraintes. La topologie du réseau avec une configuration dense et lâche pour générer des corrections atmosphériques a été évaluée (comme présenté sur la Figure 2).

Pour simuler les utilisateurs des corrections atmosphériques, 63 stations du RGP ont été sélectionnées en fonction de leur répartition géographique et de la disponibilité des données. Ces stations sont réparties de manière à couvrir pratiquement tout le périmètre du réseau Orphéon (Figure 6).

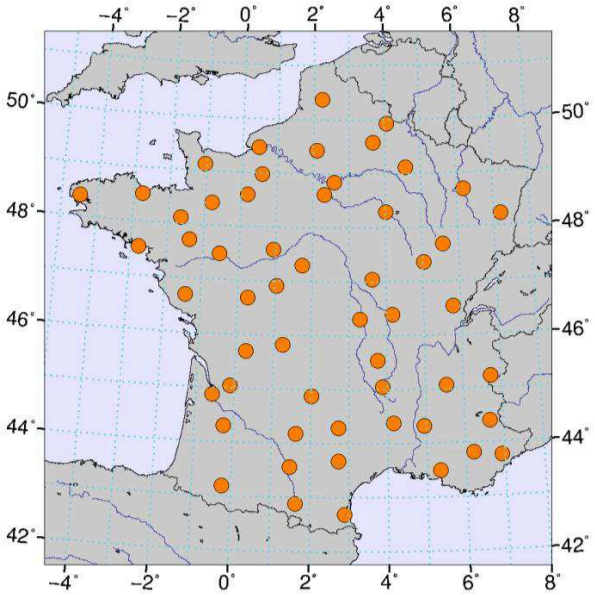

Figure 6 - Stations RGP sélectionnées pour simuler le positionnement du côté utilisateur et évaluer la qualité des corrections troposphériques et ionosphériques.

Les réinitialisations destinées à étudier la convergence de la solution de positionnement sur les stations sélectionnées sont effectuées toutes les 2 heures sur 10 jours sélectionnés. Ces jours sont sélectionnés pour assurer un échantillonnage représentatif des conditions ionosphériques, c'est-à-dire présentant des activités ionosphériques faibles, moyennes et élevées. Cette sélection est basée sur des informations du TEC (*Total Electron Contents*) et de l'indice F10.7 provenant de produits IRI (*International Ionospheric Reference*).

Résultats et analyses

La plupart du biais présent dans les corrections ionosphériques est absorbé par le paramètre correspondant à l'horloge du récepteur. Ce qu'on vérifie sur la Figure 7, par les statistiques des différences entre les horloges des récepteurs estimés sans et avec les corrections ionosphériques et le biais des corrections ionosphériques par rapport à l'ionosphère estimé sur le site. Sur cette figure, chaque point tracé correspond aux statistiques pour un site du réseau de mobiles simulés. Ces résultats montrent une anti-corrélation très forte (plus de 99%) des moyennes de ces différences. Cependant, il est important de souligner que comme les biais peuvent atteindre plusieurs mètres, l'impact de la partie non absorbée par l'horloge sur d'autres paramètres, comme par exemple les ambigüités, doit être mieux étudié.

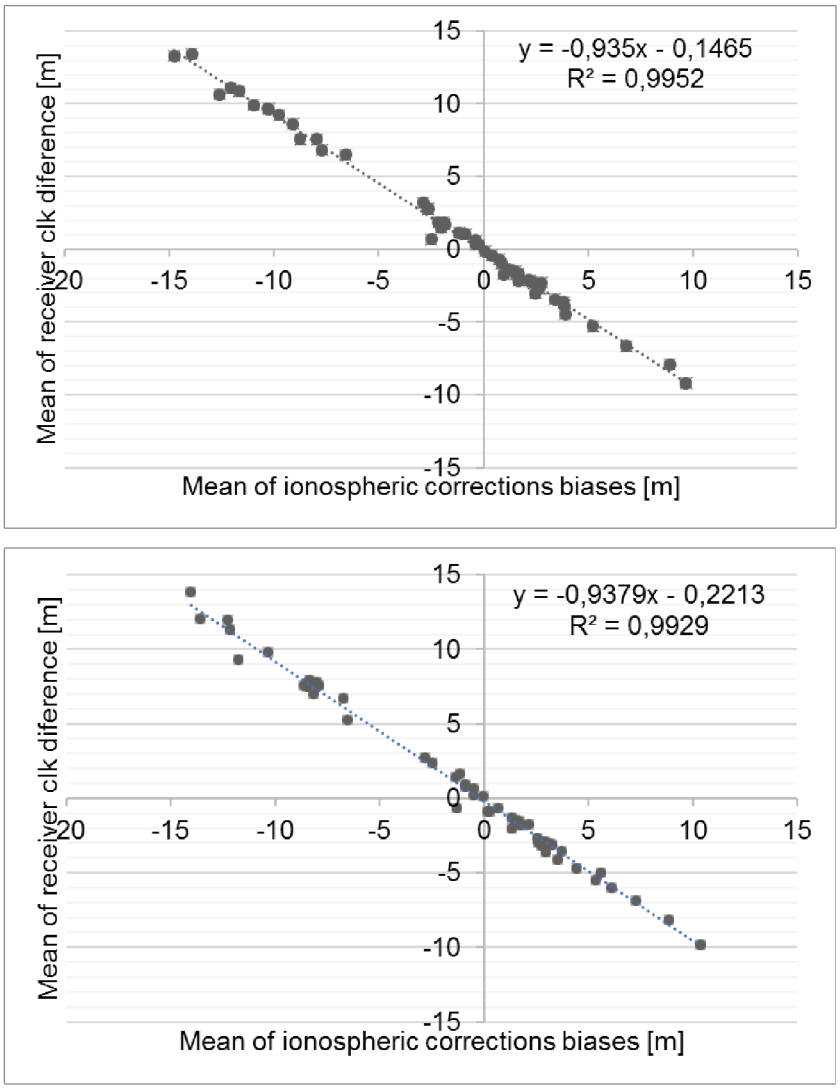

Figure 7 – Moyenne des différences entre les paramètres d'horloge du récepteur estimés sans et avec corrections ionosphériques par rapport aux moyennes des biais des corrections ionosphériques, générées avec le réseau dense (haut) et lâche (bas).

Le nombre d'ambiguïtés fixes avec chaque méthode évaluée est également analysé. La Figure 8 montre les statistiques par rapport à l'écart type et moyenne du nombre d'ambiguïtés WL et NL fixées sur les stations mobiles simulées.

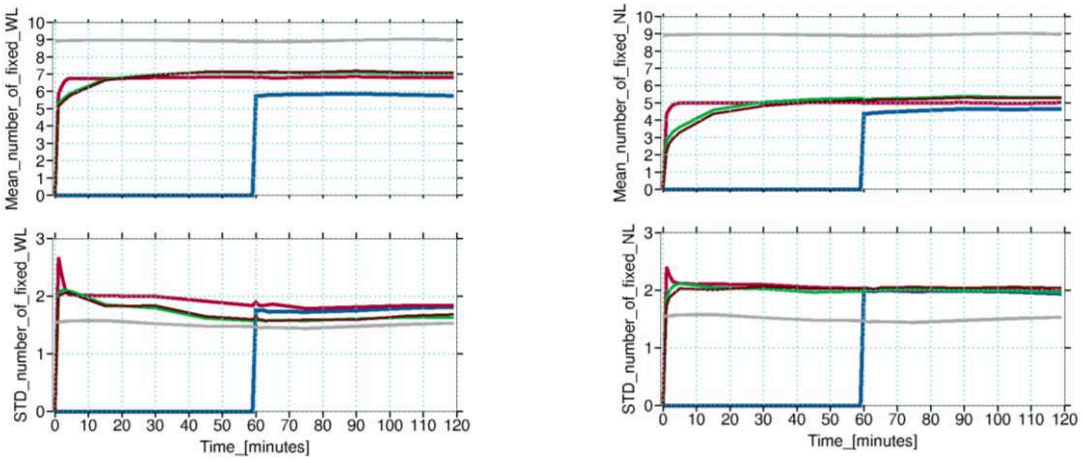

Figure 8 – Moyennes (haut) et écart-types (bas) du nombre d'ambiguïtés WL (gauche) et NL (droite) fixées à des valeurs entières ; la ligne grise correspond au nombre de satellites GPS disponibles.

Sur la Figure 8, les résultats montrent que la solution de ré-injection atteint une moyenne d'environ 7 WL (77%) et 5 NL (54%) fixée à 3 minutes. Les méthodes qui utilisent des corrections atmosphériques prennent 12 minutes pour atteindre les mêmes performances. Un aspect positif est que dans les solutions avec des corrections atmosphériques plus d'ambiguïtés sont résolues que dans la solution sans l'utilisation de corrections atmosphériques, et ce nombre est stable puisque toutes les méthodes présentent des écarts-types similaires sur le nombre d'ambiguïtés fixes.

La Figure 9 montre les médianes et quantiles à 68% de toutes les réinitialisations pour toutes les stations. Quatre solutions sont évaluées : 1) la solution standard sans corrections troposphériques (PPP standard en temps réel), 2) une solution de référence utilisant des estimations troposphériques et ionosphériques obtenues avec le traitement PPP-Wizard 1.3 au mobile lui-même, ce qu'on appelle « réinjection », et l'utilisation de corrections SSR externes générées à partir des configurations du réseau Orphéon 3) dense et 4) lâche. Ici encore, les barres verticales indiquent quand la méthode respective atteint une précision de 10 cm.

D'après la Figure 9 et le Tableau 5, on peut conclure que la médiane des erreurs de positionnement absolues à l'aide de corrections atmosphériques présente un temps de convergence à 10 cm sur la composante Est de 6 min et 4 min, pour les configurations de réseaux dense et lâche respectivement. Sur la composante Nord, ces valeurs sont de 4,5 min et

5 min. Ces chiffres représentent des gains en temps de convergence horizontale de 58% avec le réseau dense et de 43% avec la configuration de réseau lâche, par rapport à la solution RT-PPP standard. Pour la méthode de référence (réinjection), ce gain est d'environ 95%. Seule la méthode de réinjection présente un gain sur la composante Up (87%). D'après ces résultats le PPP-RTK utilisant des corrections atmosphériques externes présente une dégradation significative pour la composante altimétrique, principalement quand le réseau lâche est utilisé.

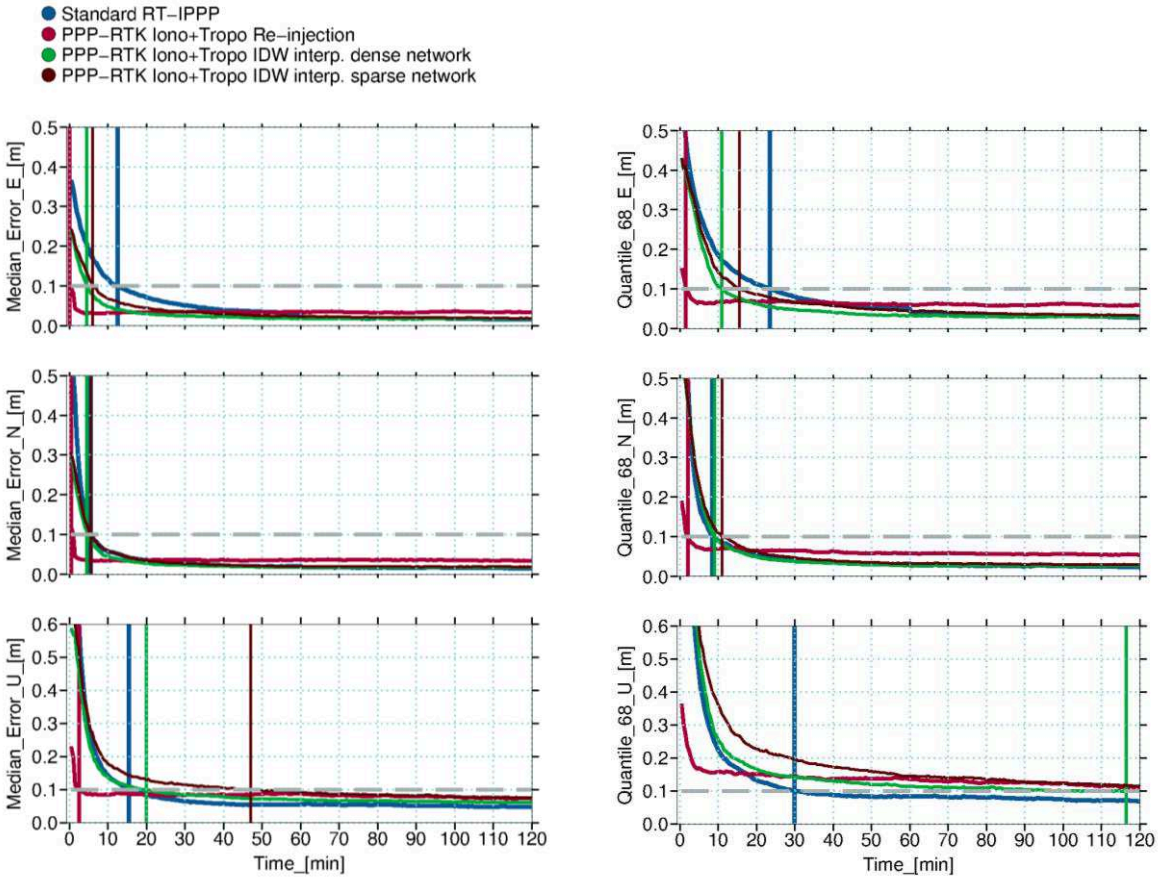

Figure 9 - Médianes (gauche) et quantiles à 68% (droite) des erreurs absolues de position en considérant le positionnement pour les « utilisateurs » simulés (sites RGP); les statistiques concernent les 63 stations, pendant les 10 jours d'expérimentation avec 10 réinitialisations par jour.

En ce qui concerne les quantiles-68% des composantes Est et Nord une durée de 24 min et 8,5 min, respectivement, permet d'atteindre une précision de 10 cm sans corrections atmosphériques (RT-IPPP standard). Lors de l'utilisation de corrections de réseau dense, les composantes Est et Nord convergent en 10,5 min et 9 min. Cela caractérise un positionnement horizontal meilleur de 47% par rapport au RT-IPPP standard. Avec le réseau lâche, ce gain sur le positionnement horizontal en termes de quantiles-68% vaut 24%, puisque les composantes Est et Nord mettent 16 min et 11 min à converger. La réinjection présente un gain de 85%,

montrant les performances qu'une modélisation parfaite peut atteindre. Une fois de plus une dégradation est observée sur la composante Up et même la solution de réinjection n'atteint pas vraiment la précision de 10 cm.

Tableau 5 – Statistiques du temps de convergence à 10 cm de précision pour chaque solution de positionnement (GPS + GLONASS).

Méthode	Médiane Temps de convergence [min]			Quantiles-68% Temps de convergence [min]		
	E	N	U	E	N	U
Standard RT-IPPP	13,5	5,0	16,5	24,0	8,5	30,0
PPP-RTK Réinjection	0,5	0,5	2,0	2,0	3,0	Non conv.
PPP-RTK – Réseau dense	4,0	4,5	19,5	10,5	9,0	117,0
PPP-RTK – Réseau lâche	6,0	5,5	47,0	16,0	11,0	Non conv.

Conclusions

La faisabilité d'un service de positionnement en temps réel basé sur la modélisation SSR pour le PPP a été étudiée. Les méthodes et les résultats ont été présentés en deux étapes et pour différentes solutions. La première étape s'est focalisée sur les corrections troposphériques et la deuxième sur les corrections troposphériques et ionosphériques.

Les améliorations du temps de convergence lors de l'utilisation de corrections troposphériques pour le *float* PPP-RTK (logiciel RTKLib modifié) ont été quantifiées. En considérant les quantiles-68% des erreurs de positionnement (GPS+GLONASS) pendant la convergence, on réduit le temps de convergence de la solution d'environ 2% sur la composante Est, 6% sur la composante Nord et 12% sur la composante Up. La réduction du nombre de stations de référence ne dégrade pas les corrections troposphériques générées par OFC, et des performances similaires sont obtenues entre les deux configurations.

Dans un second temps, le PPP-RTK a été réalisé grâce au logiciel CNES PPP-Wizard 1.3. Les corrections ionosphériques et troposphériques ont été introduites en tant que paramètres a priori contraints du côté utilisateur. Pour cela, le PPP-Wizard 1.3 a été modifié afin de permettre plus de flexibilité dans l'application de ces contraintes. De telles modifications ont permis d'introduire des valeurs plus réalistes pour contraindre les

corrections atmosphériques et de considérer la variation de leur qualité dans le temps.

Les retards ionosphériques ont été particulièrement compliqués à traiter étant donné qu'ils sont affectés par des biais hardware. Ce défi a été largement discuté dans la thèse, et plus particulièrement les résultats ont montré que les biais dans les corrections ionosphériques sont fortement anti-corrélés avec le paramètre d'horloge du récepteur.

La topologie des réseaux de configuration dense et lâche utilisée pour générer des corrections a été à nouveau étudiée. Le RT-PPP standard prend ~ 25 min pour atteindre 10 cm de précision horizontale, représentant un gain de 46% (~ 14 min) avec le réseau dense et 24% (~ 19 min) avec un réseau lâche. Par ailleurs le positionnement vertical présente un temps de convergence augmenté, en particulier lors de l'utilisation des corrections de la solution de réseau lâche. Cependant, les améliorations du positionnement horizontal avec des corrections atmosphériques SSR externes à partir d'un réseau dense ou lâche sont prometteuses et peuvent être utiles pour des applications qui dépendent principalement du positionnement horizontal.

Perspectives

Concernant la modélisation troposphérique, il faudra considérer des modèles empiriques plus récents, tels que GPT2w (Böhm et al., 2015; Kalita et Rzepecka, 2017) ainsi que des modèles de NWP (*Numerical Weather Prediction*) (Böhm et al., 2011; Urquhart et Santos, 2011). La combinaison de ces solutions avec les corrections troposphériques des réseaux GNSS, comme celles mises en œuvre dans cette thèse, permet d'améliorer sensiblement la qualité des corrections SSR.

En ce qui concerne les corrections ionosphériques, l'un des principaux défis reste la stratégie de gestion des biais hardware du récepteur pour modéliser les retards à l'échelle du réseau. Les dégradations observées sur la convergence de la composante Up doivent être étudiées, en tenant compte des corrections des biais hardware du récepteur et de l'évolution des algorithmes d'interpolation/modélisation mis en œuvre dans cette thèse. Par exemple, les limitations des fonctions de projection pour l'effet ionosphérique doivent être considérées, et l'utilisation de fonctions de projection ionosphérique basées sur le champ de densité électronique dérivé de l'IRI peut être une alternative intéressante (Zus et al., 2017).

Des améliorations de la stratégie de contrôle qualité pour sélectionner les retards

ionosphériques et troposphériques à utiliser dans l'algorithme d'interpolation IDW doivent être conduites. Cela permettrait de fixer ou contraindre fortement les coordonnées aux sites de référence. Cela pourrait aussi conduire à une convergence rapide de ces paramètres atmosphériques et augmenter leur qualité.

Les performances du PPP vont s'améliorer avec la disponibilité croissante de signaux GNSS, et des nouveaux GNSS en cours de déploiement. Ces aspects positifs doivent être fortement explorés pour optimiser la méthode. Ainsi, il est fortement recommandé d'étudier les avantages de l'utilisation de corrections atmosphériques avec l'ajout d'autres constellations GNSS, telles que Galileo et BDS (*BeiDou Navigation Satellite System*).

Resumo Longo

Introdução

A informação de posição possui valor chave para o desenvolvimento científico de nossa sociedade. Quando o seu conhecimento é proporcionado com alta acurácia (cm) e em tempo-real, seu valor agregado aumenta substancialmente, bem como o número de aplicações para o posicionamento. O GNSS (*Global Navigation Satellite Systems*) provou ser uma tecnologia poderosa para tal tarefa. Um dos métodos mais notáveis para se obter a posição de um usuário por GNSS é o PPP (*Precise Point Positioning*).

O conceito de PPP começou a ser de fato investigado pela comunidade científica no final dos anos 90, no contexto de processamento de grande quantidade de dados de redes GPS (*Global Positioning System*) globais de modo eficiente (Zumberge et al., 1997). Posteriormente, o PPP foi ainda mais desenvolvido e melhorado graças a disponibilidade de produtos de orbita e relógios dos satélites destinados para aplicações no modo pós-processado. Há vários anos, esses produtos são gerados e difundidos por organizações tais como a NASA (*National Aeronautics and Space Administration*), JPL (*Jet Propulsion Laboratory*), IGS (*International GNSS Service*), NRCan (*Natural Resources Canada*), dentre outros (Morel et al., 2014). Estudos posteriores mostraram que o método PPP pode fornecer soluções com acurácia centimétrica (Kouba and Héroux, 2001) quando usa-se produtos finais gerados pelo IGS para as órbitas e relógios dos satélites. Depois disso, o número de aplicações que empregam o PPP tem crescido rapidamente. O método se tornou essencial, por exemplo, em monitoramento glacial, vulcanologia, bem como em qualquer local onde as linhas de base com relação às estações de referência sejam demasiadamente longas para realização do posicionamento relativo (Morel, 2015).

Os esforços da comunidade geodésica no PPP têm sido direcionados para soluções em tempo real ou quase real. O IGS RTWG (*Real-Time Working Group*) foi estabelecido em 2001, para investigar produtos de precisão para os usuários de soluções em tempo real (Caissy and Agrotis, 2011). Posteriormente, Gao e Chen (2004) conduziram análises sobre PPP usando produtos precisos em tempo real para órbita e relógios dos satélites e obtiveram resultados promissores para o posicionamento com acurácia centimétrica.

Várias sessões no ION (*Institute of Navigation*), evento sobre GNSS realizado anualmente, tem sido dedicadas ao PPP e a maioria dos trabalhos tem evidenciado seu potencial para aplicações em tempo real (Laurichesse et al., 2009; Laurichesse and Mercier, 2007; Monico, 2008; Wübbena et al., 2005).

O IGS iniciou o RTPP (*Real-Time Pilot Project*) em 2007, através do emprego de observações GNSS em tempo-real obtidas de uma rede global. Em abril de 2013, o RTS (*Real Time Service*) foi lançado oficialmente. Seus produtos oficiais incluíram correções para as órbitas e relógios transmitidos dos satélites GPS (http://www.rtigs.net). A acurácia centimétrica tornou-se factível com PPP em tempo real baseado nos produtos obtidos com redes GNSS globais (Grinter and Roberts, 2013; Morel, 2015; Rizos et al., 2012).

O inconveniente da metodologia mais usual de PPP, em tempo real, é o tempo requerido para que a solução atinja convergência. Atualmente, a estratégia de PPP padrão requer a estimativa de parâmetros de estado (ex. atrasos troposféricos) conjuntamente com as ambiguidades "*float*", o que exige um tempo de inicialização considerável (no mínimo 30 min) para alcançar convergência apropriada dos valores reais das ambiguidades, mesmo sob boas condições de geometria dos satélites e sem significativos efeitos de multicaminho (Ge et al., 2012; Rovira-Garcia et al., 2015). Portanto, para os usuários GNSS de tempo real que requerem acurácia centimétrica, os métodos de RTK (*Real Time Kinematic*) ou NRTK (network RTK) são geralmente empregados. O método de RTK exige o uso de no mínimo dois receptores GNSS conectados através de um link de comunicação. No caso do NRTK, o usuário precisa somente de um receptor mas também é necessário o acesso a correções OSR (*Observation Space Representation*) de uma rede local densa de CORS (*Continuously Operating Reference Station*). Assim, o posicionamento NRTK promoveu um aumento no número de redes CORS no mundo todo (Grinter and Roberts, 2013).

A eficiência em termos de custo do PPP e a disponibilidade de produtos precisos em tempo real motivou muitas pesquisas para melhorar o método e fixar para valores inteiros os parâmetros das ambiguidades de fase (Collins et al., 2010; Ge et al., 2012; Laurichesse et al., 2010; Laurichesse and Mercier, 2007; Mervart et al., 2008). Melhorias significativas foram obtidas, quando em adição às informações precisas de orbita e relógios, produtos relacionados as tendências nas medidas de fase são fornecidos, permitindo fixar as ambiguidades de fase para valores inteiros (Shi and Gao, 2014; Teunissen and Khodabandeh, 2015). Tais avanços conduziram ao conceito conhecido como SSR (*State Space*

Representation) com o objetivo de isolar todos os erros físicos que afetam as observáveis GNSS (Mervart et al., 2013; Wübbena et al., 2005).

Resultados incluindo a aplicação de correções SSR para parâmetros atmosféricos, tais como os atrasos ionosférico e troposférico, tem demonstrado melhorias com convergência ao nível do centímetro nos primeiros minutos ou mesmo segundos (Leandro et al., 2011; Li et al., 2014b; Rovira-Garcia et al., 2015). Nesse caso, a melhoria no tempo de convergência da solução é promovida não somente pelo benefício das correções de tendências nas medidas de fase mas também graças às correções atmosféricas proporcionadas pelas redes de aumento, conduzindo ao chamado PPP-RTK (Stürze et al., 2012; Wübbena et al., 2014, 2005). Esses estudos mostram o posicionamento baseado em correções SSR como uma potencial solução rival ou complementar aos métodos de RTK ou NRTK. Nesse caso, especialmente se as correções atmosféricas SSR puderem ser geradas de redes GNSS mais esparsas do que aquelas requeridas para geração de correções OSR, tem-se uma infraestrutura menos onerosa que a necessária para o NRTK. No entanto, as performances da modelagem atmosférica para geração de correções SSR dependem da topologia da rede e das condições atmosféricas.

Na França, a companhia Geodata-Diffusion, subsidiária do grupo Hexagon Geosystems, oferece serviços industriais para posicionamento baseado em redes GNSS. Tais serviços estão disponíveis desde 2004, usando dados GNSS da rede Orphéon. No intuito de continuar operando efetivamente e manter a liderança em seu campo de atuação, a empresa Geodata-Diffusion necessita aprofundar o entendimento técnico e os detalhes das performances do PPP, bem como dos potenciais impactos de tal método na indústria GNSS. Nesse contexto, foi proposto o desenvolvimento desta tese CIFRE-Brasil (*Convention Industrielle de Formation par la Recherche - Brésil*), sob cotutela internacional entre dois laboratórios de pesquisa GeF (*Géomatique et Foncier*), e o LGE (Laboratório de Geodésia Espacial).

Objetivos

O objetivo principal desta tese é avaliar e aprimorar soluções de PPP em tempo real existentes, com o uso de correções atmosféricas SSR, levando-se em conta o contexto industrial envolvido no projeto, bem como a melhoria das soluções ou modelos empregados.

Desta forma, deverá buscar a demonstração da factibilidade e viabilidade de um novo serviço de posicionamento GNSS em tempo real com base no método PPP.

Para alcançar os objetivos mencionados acima, os seguintes objetivos específicos devem ser atingidos:

- Realizar revisão bibliográfica para compreender os avanços e os aspectos básicos envolvidos no assunto desse projeto,

- Assegurar a eficiência em termos de custo-benefício na comunicação entre o servidor e os usuários, bem como o alinhamento das soluções adotadas com os padrões definidos para correções SSR.

- Contribuir com a modelagem da variabilidade atmosférica, bem como com o entendimento dos impactos das correções atmosféricas nos parâmetros do processamento GNSS.

- Estudar a qualidade e a confiabilidade do posicionamento do usuário com as correções atmosféricas.

- Avaliar a correlação da qualidade do posicionamento GNSS baseado em correções SSR com relação a topologia da rede referência utilizada para a geração das correções atmosféricas SSR.

Contribuições

As contribuições deste trabalho estão divididas em duas etapas principais: 1) uso de correções de rede SSR, para o atraso troposférico e 2) correções para o atraso troposférico e ionosférico. A topologia da rede foi usada para gerar as correções, a qual foi avaliada em ambas as etapas, reduzindo-se o número de estações de referência em até 75%, testando assim uma configuração de rede mais esparsa para realizar a modelagem atmosférica. Em relação a este aspecto, foi avaliado o uso de diferentes configurações de uma rede GNSS densa e regular existente na França, a rede Orphéon. Esta rede tem cerca de 160 estações e é de propriedade da Geodata-Diffusion, subsidiária do grupo Hexagon Geosystems e diretamente envolvida neste projeto.

No que diz respeito ao primeiro estágio, o pacote RTKLib 2.4.3-beta (Takasu, 2013) é usado, mas é aprimorado com modificações introduzidas para levar em consideração as correções troposféricas de tipo SSR da rede. A combinação livre da ionosfera (*ionospheric-free*) é usada para mitigar a contribuição ionosférica, e o PPP em tempo real com o uso de correções para a troposfera é realizado. Essa solução de posicionamento com ambiguidades *float* é chamada neste trabalho como "*float* PPP-RTK". A geração de correções troposféricas baseia-se em uma modelagem polinomial adaptativa, o *Optimal Fitting Coefficients* (OFC), que permite comunicação mono-direcional entre servidor e usuários, reduzindo a largura de banda de comunicação necessária (Shi et al., 2014). Nesta pesquisa, o polinômio de segundo grau empregado pelo método OFC foi implementado e avaliado, algo não foi realizado em trabalhos anteriores, permitindo a geração de correções troposféricas para áreas maiores.

Na segunda fase, o software CNES PPP-Wizard 1.3 é utilizado e as correções ionosféricas e troposféricas são introduzidas como parâmetros a priori. Nesta solução PPP-RTK, são utilizadas observações não combinadas e a fixação de ambiguidades é realizada, utilizando os produtos CNES de órbita, relógio e tendências de fase dos satélites. A interface existente neste software, para aplicar injunções aos parâmetros atmosféricos, foi melhorada de modo a considerar a variação da precisão das correções atmosféricas de tipo SSR (valores usados para injunção) ao longo do tempo. Além disso, na segunda fase, a geração de correções SSR troposféricas e ionosféricas foi alinhada com as convenções RTCM (*Real-Time Maritime Services*), graças a um algoritmo de interpolação convencional (*Inverse Distance Interpolation*) assumindo que os usuários teriam acesso diretamente às informações de atrasos ionosféricos e troposféricos estimados em estações de referência, por exemplo, via conexão de internet.

Primeiro estágio: *Float* PPP-RTK com modelagem troposférica

Metodologia

O atraso total troposférico, também conhecido como ZTD (*Zenith Total Delay*) tem uma componente residual, o ZWD (*Zenith Wet Delay*) que deve ser estimado como um parâmetro adicional no processamento GNSS. Portanto, o uso do ZWD a priori pode contribuir com a redução do tempo de convergência da solução.

Para reduzir o tempo necessário para que o *float* PPP-RTK atinja convergência para uma precisão da ordem de 10 cm, a estratégia nesta etapa se concentrou em dois pontos: 1) modelagem troposférica para fornecer correções baseadas em rede de ZWD e 2) os impactos de usar esse modelo para injuncionar o ZWD a priori no processamento *float* PPP-RTK. A técnica de modelagem OFC (Shi et al., 2014) é utilizada pois requer apenas um link de comunicação (mono-direcional).

Os principais dados de entrada, bem como a estratégia utilizada para realizar a modelagem troposférica, são apresentados na Figura 1. No primeiro passo, os valores de ZWDs são estimados em tempo real para uma rede GNSS de referência, onde as posições das estações são fortemente injuncionadas (1 cm). Na segunda etapa, as estimativas de ZWD são usadas para gerar um modelo de ZWD utilizável em qualquer local na área de abrangência da rede. Durante este processo, os parâmetros de controle de qualidade são verificados para eliminar *outliers*. Nesta etapa, a modelagem deve ser de baixo consumo de largura de banda e permitir o *link* mono-direcional de comunicação com os usuários. Finalmente, este modelo de ZWD pode ser transmitido para *rovers* no intuito de derivar valores ZWDs a priori usados no algoritmo *float* PPP-RTK.

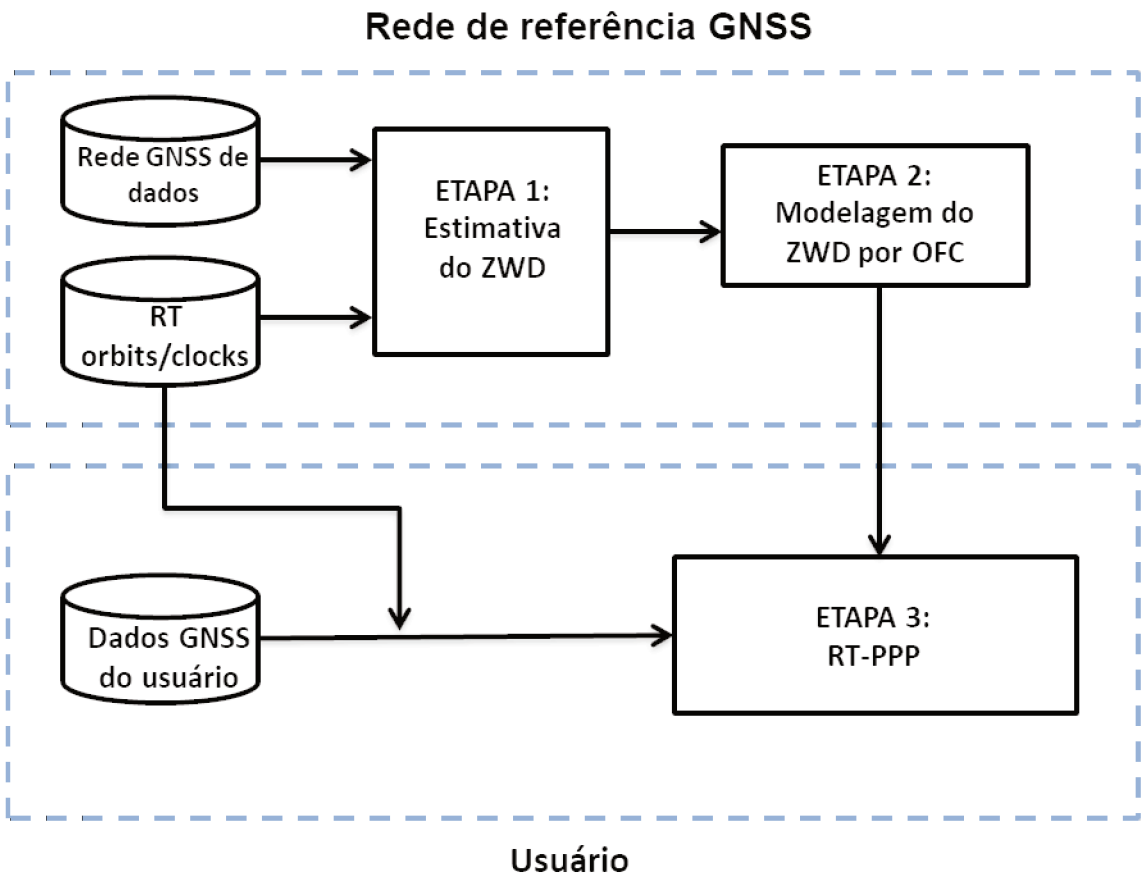

Figura 1 – Estratégia adotada para gerar o modelo de ZWD para o *float* PPP-RTK

Para executar o *float* PPP-RTK, utiliza-se o software RTKLib 2.4.2 (Takasu, 2013) modificado nesta pesquisa para adicionar uma opção para introduzir valores a priori injuncionados para o parâmetro de ZWD. As estratégias utilizadas para estimar os valores de ZWD na rede GNSS de referência (etapa 1) e para executar o *float* PPP-RTK a nível de usuário (etapa 3) estão resumidas na Tabela 1. As principais diferenças entre eles são o modo de posicionamento, estático ou cinemático e os parâmetros injuncionados. Durante a etapa 1, as coordenadas das estações de referência são bem conhecidas, logo as mesmas são fortemente injuncionados ao passo que os valores de ZWD são estimados. No usuário, as coordenadas do receptor são estimadas durante a etapa 3, enquanto os valores de ZWD são injuncionados usando valores a priori oriundos das correções, a cada *cold-start* (i.e. é fornecido o valor inicial na primeira época), proveniente da modelagem troposférica. A qualidade (precisão) da correção é usada como injunção para os atrasos troposféricos no algoritmo de PPP-RTK.

Tabela 1 – Configurações do processamento GNSS para o servidor e para o usuário.

	Processamento GNSS da rede	**Processamento GNSS do usuário**
Modo	PPP estático (solução *float*)	PPP cinemático (solução *float*)
Órbitas e relógios	Produtos de relógios e orbitas do CNES RT	Produtos de relógios e orbitas do CNES RT
Ionosfera	*Ionospheric-free*	*Ionospheric-free*
Zenith Tropospheric delay	ZHD: (Saastamoinen, 1972)+ atmosfera padrão ZWD: estimado Mapping functions: (Niell, 1996)	ZHD: (Saastamoinen, 1972)+ atmosfera padrão ZWD: injuncionado (correção introduzida a cada *cold-start*) Mapping functions: (Niell, 1996)
Coordenadas	Injuncionadas (1 cm)	Estimadas
Máscara de elevação	10 graus	10 graus
Intervalo de observação	30 segundos	30 segundos
Processo Kalman	*Forward*	*Forward*
Demais parâmetros	*IERS Conventions 2010* (Petit and Luzum, 2010)	*IERS Conventions 2010* (Petit and Luzum, 2010)
Software	RTKLib 2.4.2 (Takasu, 2013)	RTKLib 2.4.2 (Takasu, 2013)

Para ajustar-se as condições de posicionamento em tempo real simulado, utiliza-se os produtos CNES para tempo real de órbita e relógio (Laurichesse et al., 2009). As medições GPS e GLONASS coletadas com intervalos de 30 segundos de amostragem são processadas considerando ângulo de elevação superior a 10 graus. Em tais condições, a adoção de um modelo troposférico padrão para ZHD (Saastamoinen, 1972) e da NMF (Niell, 1996) não apresenta tendências significativas em relação ao uso de modelos mais sofisticados como GPT2w (Böhm et al., 2015) e da GMF (Boehm et al., 2006) no posicionamento conforme verificado por Fund et al. (2011).

Modelagem Troposférica

Uma vez que os valores de ZWD em tempo real estejam estimados com o RTKLib para todas as estações de referência, o modelo troposférico de OFC pode ser gerado. O modelo aplicado de segunda ordem, adaptado de Shi et al. (2014).

$$ZWD_i = a_0 + a_1 x_i + a_2 y_i + a_3 z_i + a_4 x_i y_i + a_5 x_i z_i + a_6 y_i z_i + a_7 x_i^2 + a_8 y_i^2 + a_9 z_i^2 (i = 1, \dots n) \quad (1)$$

A equação (1) é usada com as seguintes injunções (2):

$$0 = \varphi_j a_j \tag{2}$$

com $\varphi_j = \{0,1\}$, $j = \{0, \ldots, 9\}$

Em (1), ZWD_i é o ZWD da estação de referência i, os termos (a_0, a_1, ..., a_9) representam os coeficientes do modelo, os quais são os parâmetros a serem estimados. x_i, y_ie z_i são as coordenadas geodésicas, j é o número do coeficiente. Diferentes conjuntos de coeficientes são estimados, em função da aplicação de injunções de modo gradativo aos coeficientes durante o ajuste por mínimos quadrados. O número de conjuntos de coeficientes a serem testados (c) é dado por (3):

$$c = \sum_{k=0}^{m} \frac{m!}{k!\,(m-k)!} \tag{3}$$

onde *m* é o número de coeficientes e *k* é o número de coeficientes injuncionados (a_j). Por exemplo, se o número de coeficientes for 4 (caso de primeira ordem), *c* é igual a 16. Mas, quando o número de coeficientes utilizados é 10 (caso de segunda ordem), o número de conjuntos de coeficientes testados aumenta para 1024. Em nosso estudo, foi implementada a modelagem de 2ª ordem, com algumas pequenas modificações para cobrir uma grande área.

O parâmetro de qualidade interna para o modelo OFC é o RMS dos resíduos (4) derivados da estimativa de coeficientes.

$$RMS_{Trop} = \sqrt{\frac{v_1^2 + v_2^2 + v_3^2 + \cdots + v_n^2}{n}} \tag{4}$$

Na equação (4), o RMS_{Trop} é o valor usado como informação de controle de qualidade para o aplicativo de correções troposféricas, *v* é a diferença entre o ZWD estimado no processamento RT-PPP com as observações da rede CORS e o valor ajustado na superfície troposférica.

A fim de detectar *outliers* nos ZWDs usados para estimar os coeficientes, é aplicado um método clássico de identificação de *outliers* (Leick, 2004), comparando os valores absolutos de cada resíduo de ZWD com o RMS residual global, se o resíduo individual exceder em 4 vezes o valor do resíduo de RMS, os coeficientes são estimados novamente com uma redução no peso da observação em questão.

Dados GNSS

As melhorias no tempo de convergência, obtidas com a injunção do ZWD a priori, foram avaliadas com o uso de correções provenientes de uma configuração de rede densa e esparsa (Figura 2), bem como apenas com o uso de dados GPS e com dados GPS+GLONASS.

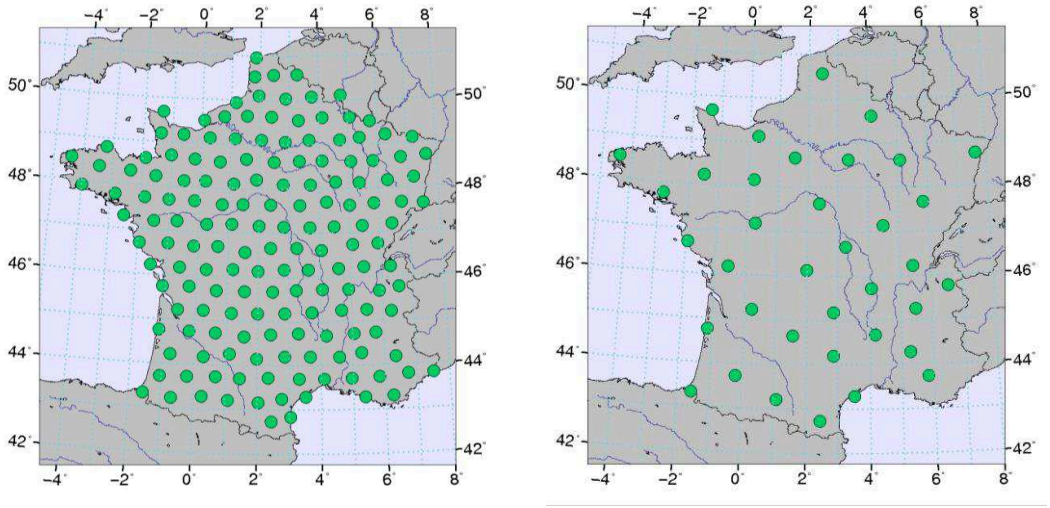

Figura 2 – Configurações densa (esquerda) e esparsa (direita) da rede GNSS Orphéon usadas para gerar correções troposféricas a partir do modelo OFC.

Foram selecionados 20 dias de dados distribuídos em quatro períodos principais ao longo do ano 2014 (Tabela 2). Estes períodos foram escolhidos de acordo com as estações do ano e as variações anuais de temperatura na França, conforme publicado pelo centro de meteorologia francês, Météo-France.

Tabela 2 – Períodos estudados

	Primavera	**Verão**	**Outono**	**Inverno**
Dias selecionados em 2014	121-126	205-210	289-294	357-362

Como referência externa independente para correções troposféricas, os produtos ZTD do IGN (*Institut National de l'Information Géographique et Forestière*) foram utilizados para avaliar o ZWD troposférico modelado por OFCs. Tal comparação mostrou que os valores de ZWD modelado apresentam uma precisão de cerca de 1,3 cm em relação aos produtos IGN de ZTDs. Além disso, foi verificada boa consistência entre o RMS dos resíduos

da modelagem OFC e as diferenças em relação aos produtos do IGN. Esse resultado é importante, uma vez que o RMS dos resíduos do modelo OFC é a quantidade utilizada como injunção às correções troposféricas, variando a maior parte do tempo entre 1 e 2 cm.

As reduções no tempo de convergência quando se utilizam correções troposféricas para o *float* PPP-RTK foram quantificadas. Para isso, foram selecionadas 22 estações RGP para simular usuários das correções SSR (Figura 3), distribuídas dentro da área de cobertura da rede Orphéon na França (território metropolitano).

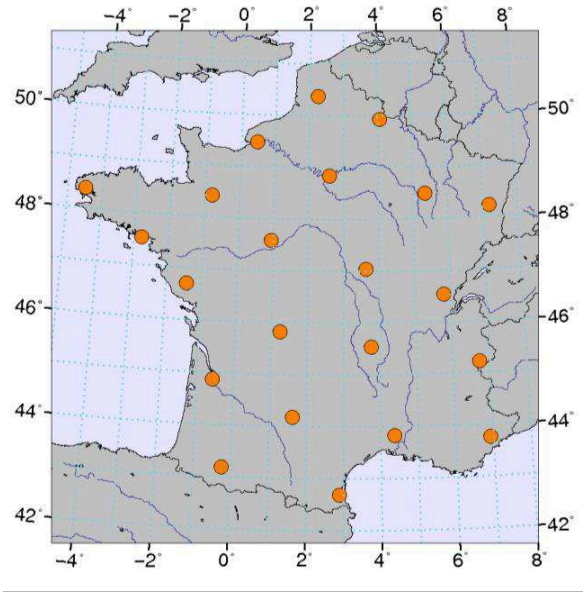

Figura 3 - Estações RGP selecionadas para simular usuários das correções SSR.

Resultados e análises

A Figura 4 mostra os resultados para o processamento GPS+GLONASS, considerando as médias e quantis à 68% de todos os *cold-starts* ou reinicializações (10 *cold-starts* por dia, durante 20 dias) para as 22 estações empregadas para simular usuários distribuídos dentro da área de cobertura da rede Orphéon na França. Foram avaliados quatro métodos: 1) uma solução padrão, ou seja, sem correções troposféricas (*Standard real-time* PPP), 2) o uso de produtos IGN, uma solução pós-processada com alta precisão usada como referência e o uso de correções externas geradas a partir de configurações de 3) rede Orphéon densa e 4) esparsa. As barras verticais na Figura 4 indicam quando o respectivo método atinge uma precisão alvo de 10 cm.

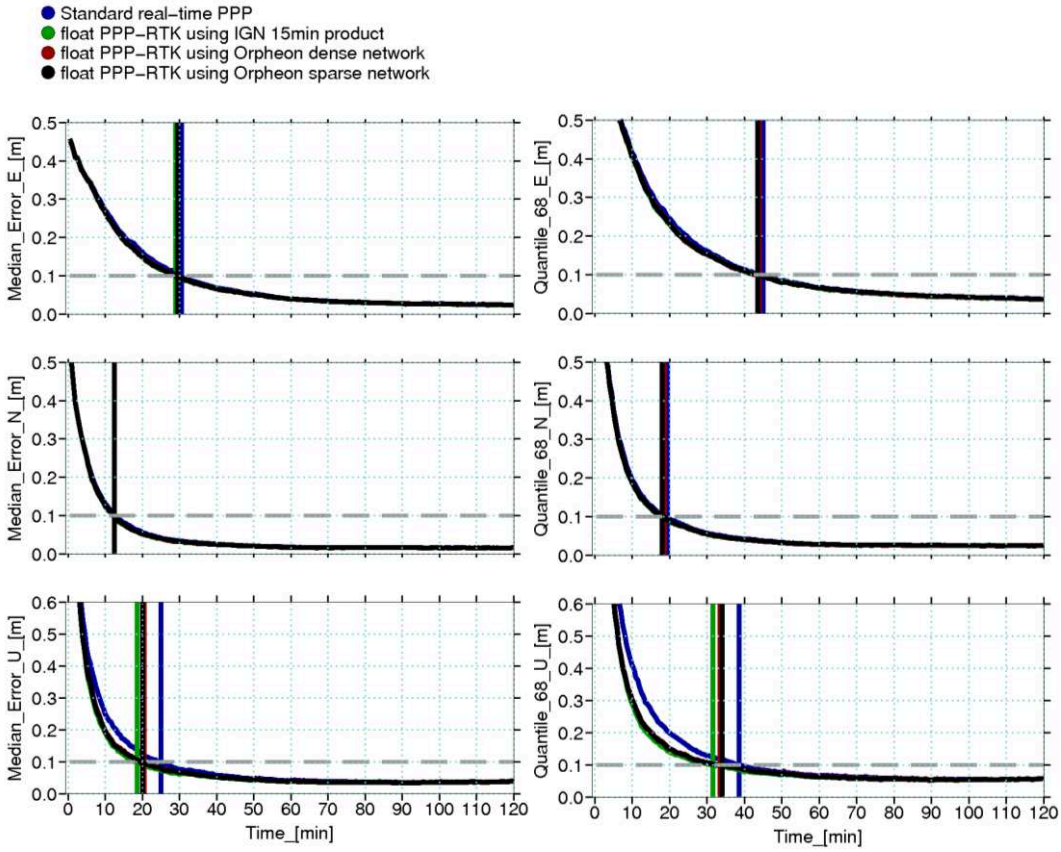

Figura 4 - Média (esquerda) e Quantis à 68% (direita) de erros no RT-PPP (GPS+GLONASS) cinemático por época ao longo do posicionamento, considerando-se as estações IGN utilizadas como *rover*.

Tabela 3 – Tempo de convergência (min) da solução de posicionamento com *float* PPP-RTK (GPS+GLONASS).

Tropospheric correction	Median Convergence time			68%-quantiles Convergence time		
	E	N	U	E	N	U
Standard (no correction)	30,5	12,5	25,0	45,0	19,5	38,5
IGN ZWD products	29,0	12,5	18,5	44,0	18,0	31,5
OFCs from dense network	29,5	12,5	20,5	44,0	18,5	33,5
OFCs from sparse network	29,5	12,5	20,0	43,5	18,0	34,0

Os ganhos médios observados no tempo de convergência usando os produtos de ZTD do IGN (solução de referência) são de cerca de 1,5 min (4,9%) e 6,5 min (26,0%) nas componentes Leste e Up, respectivamente. Ao aplicar os valores de ZWD obtidos com o modelo OFC usando configurações de rede densa ou esparsa, as mesmas melhorias são

encontradas na componente Este: 1 min (3,3%). Na componente altimétrica, o uso do modelo OFC derivado da rede esparsa proporcionou resultados ligeiramente melhores com um ganho de 5,0 min (20,0%) contra 4,5 min (18,0%) ao usar OFCs obtidos com a configuração de rede densa. Nenhum ganho na componente Norte foi verificado, com qualquer uma das correções troposféricas avaliadas. Uma vez que os impactos das correções troposféricas foram determinados, a adição de correções ionosféricas foi avaliada no segundo estágio deste estudo.

Segundo estágio: PPP-RTK com correções troposféricas e ionosféricas

Metodologia

Na segunda etapa, o software PPP-Wizard 1.3 é empregado para realizar o RT-IPPP (RT *Integer* PPP), o que corresponde ao PPP em tempo real com estimativa das ambiguidades inteiras. Esse método é utilizado para estimar atrasos ionosféricos e troposféricos usando dados GNSS das estações Orphéon. O atraso ionosférico é um parâmetro particularmente complexo, haja vista que seus valores são consideravelmente afetados pelas tendências ou *biases* de hardware do receptor e do satélite.

A Figura 5 mostra o esquema da estratégia aplicada para gerar e aplicar as correções atmosféricas SSR, respectivamente, no servidor da rede de referência quanto no posicionamento do usuário. Com relação à estratégia anteriormente utilizada no primeiro experimento, as principais diferenças são a adição da estimativa dos atrasos ionosféricos inclinados na rede de referência e o uso de algoritmo de interpolação, alinhado aos padrões RTCM para mensagens atmosféricas SSR.

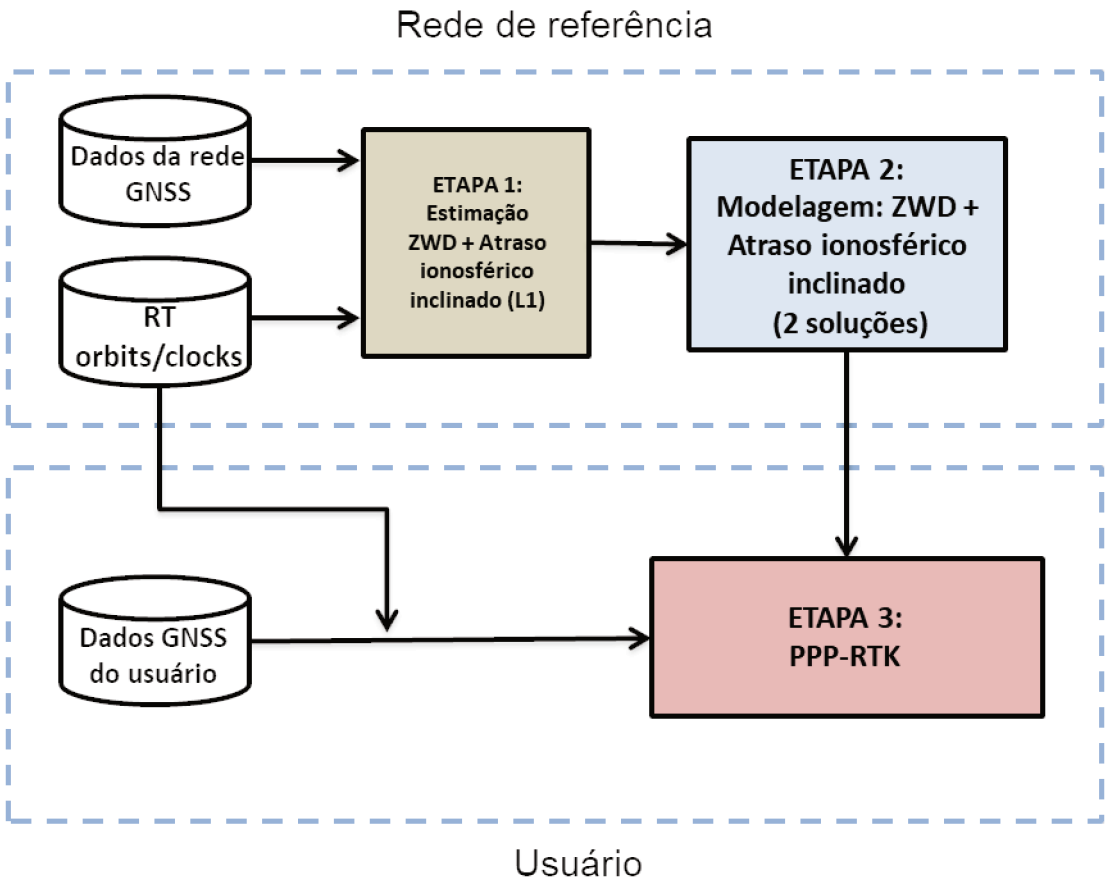

Figure 5 – Esquema para realização do PPP-RTK, com geração de correções atmosféricas SSR e aplicação das mesmas no posicionamento do usuário.

Ao estimar os atrasos atmosféricos da rede no servidor, as coordenadas da estação podem ser injuncionadas como valores precisos ou mesmo fixadas (isto é, sigma inicial de posições ajustadas para zero). Nesse segundo experimento, as coordenadas da estação são consideradas como parâmetros desconhecidos para que os erros do posicionamento sejam usados como um indicador de qualidade da computação atmosférica. As configurações de processamento PPP-Wizard 1.3 definidas no lado do servidor (rede Orphéon) são apresentadas na Tabela 4. As configurações sugeridas na documentação do PPP-Wizard 1.3 (Laurichesse, 2016) são usadas. A exceção de duas modificações: 1) limite aplicado ao desvio padrão pós-ajuste de ambiguidades, o qual é necessário para a função de decisão da fixação das ambiguidades (thrAmb) e 2) rejeição máxima de RAIM (maxReject).

Tabela 4 – Configurações do processamento GNSS no PPP-Wizard 1.3 para estimativa dos atrasos atmosféricos

Numero	Parâmetro	Tipo/Unidade	Descrição	Processamento GNSS no servidor
1	Mode	Enum	Modo de processamento: Mode_PPP_AR	Mode_PPP_AR
2	AntexFileName	String	Antex IGS file	igs08.atx
3	AR/JumpsIndicators	Boolean	Indicates ambiguities to be estimated. NL, WL and Extra WL. If 1: yes, 0: no.	1 1 0
4	useGPS	Boolean	Use GPS constellation. If 1: yes, 0: no.	1
5	useGLONASS	Boolean	Use GLONASS constellation. If 1: yes, 0: no.	1
6	sbasCorrection	Boolean	If 1: SBAS clock correction, otherwise 0: e.g. RTIGS or CNES clock correction	0
7	Reset	Int/sec	Time between consecutive reset (for convergence tests) 0 if no reset	0
8	OutputVerbose	Boolean	Verbose output	0
9	Step	Real/second	Measurement interval, i.e. the sampling interval of observations.	1
10	maxAge	Real/second	Maximum RTCM correction age	10
11	stepMin	Integer/S.U.	Minimum step before AR. Minimum number of epochs to start ambiguity fixing. If interval is 1 second, 3600 represents 1 hour.	3600
12	maxReject	Integer/S.U.	Maximum rejection RAIM (Receiver Autonomous Integrity Monitoring)	3
13	raim	Boolean	Advanced RAIM. Outlier detercion.	1
14	mapThr	Real/S.U.	Tropospheric mapping function threshold (1/sin(ele)). In this function (CNES mapping, 6 is equivalent to 10 degrees cutoff)	6
15	sigIniTro	Real/m	Tropo initial noise	0,5
16	sigModTro	Real/m	Tropo model noise	0,000005
17	nbSatFixAmb	Integer/S.U.	Minimum satellite for AR	0
18	thrAmb	Real/m	Ambiguity threshold for AR	0,25
19	sigIniBiasClk	Real/m	Initial clock bias noise	0
20	sigModBiasClk	Real/m	Model clock bias noise	0,001
21	sigIniIono	Real/m	Initial iono noise	10
22	sigModIono	Real/m	Model iono noise	0,002
23	sigMeasIono	Real/m	Iono measurement noise	1,0 1,0 1,0
24	IonoThr	Real/m	Iono measurement rejection threshold	5 0
25	sigMeasTropo	Real/m	Tropo measurement noise	0,1
26	tropoThr	Real/m	Tropo measurement rejection threshold	1
27	sigIniPos	Real/m	Initial position noise, 50 m position unknown or 0 (position fixed)	50
28	sigModPos	Real/m	Model position noise: 10 (mobile receiver), 0.02 (static receiver) or 0 (position fixed)	0,02
29	preDTMax	Real/sec	Maximum measurement gap	300
30	codeThr	Real/m	Code measurement rejection threshold	10
31	phaseThr	Real/m	Phase measurement rejection threshold	0,05
32	sigMeasCodeGps	Real/m	Code GPS measurement noise	1
33	sigMeasPhaseGps	Real/m	Phase GPS measurement noise	0,01
34	sigMeasCodeGlo	Real/m	Code GLONASS measurement noise	5
35	sigMeasPhaseGlo	Real/m	Phase GLONASS measurement noise	0,01

Para o parâmetro *thrAmb*, o valor sugerido no arquivo de configuração fornecido no software PPP-Wizard (0,25 ciclo) é usado em vez do sugerido na documentação do software (ciclo 0,01). Isso foi considerado, pois os testes iniciais mostraram que a precisão de posicionamento é reduzida, bem como o número de ambiguidades NL fixas ao usar o valor de

0,01 ciclo para *thrAmb*. No entanto, novas investigações para definir um limiar ideal devem ser realizadas. O parâmetro *maxReject* para RAIM foi aumentado para 3 satélites, em vez de 2. A configuração *maxReject* com 3 satélites proporcionou soluções ligeiramente melhores em testes iniciais, mas também devem ser realizadas investigações adicionais para definir a melhor configuração para este parâmetro.

Não é utilizada informação atmosférica a priori externa. Assim, um modelo empírico (Saastamoinen, 1972) é empregado para obter o atraso troposférico a priori inicial, que é injuncionado para 10 cm (*sigMeasTropo*). Os atrasos ionosféricos são inicializados em valores nulos e injuncionados com 1 m (*sigMeasIono*), conforme sugerido na configuração do manual do PPP-Wizard 1.3 (Laurichesse, 2016).

Os parâmetros ionosféricos podem exigir um tempo considerável para convergir adequadamente. Em Rovira-Garcia (2015), por exemplo, o processamento de estações de rede de referência (lado do servidor) é iniciado um dia antes do uso de parâmetros relacionados à ionosfera para garantir precisões e limites de confiança de 1 TECU (~16cm). Nestes experimentos de tese, o processamento no lado do servidor é iniciado a 0h00 min UTC de todos os dias e é contínuo durante todo o dia. Com o PPP-Wizard 1.3, a convergência pode demorar pelo menos 1h, conforme recomendado na documentação do PPP-Wizard 1.3 (Laurichesse, 2016) para iniciar a fixação das ambiguidades. Portanto, apenas as primeiras horas de processamento são impactadas pela convergência da solução. Para usar uma solução atmosférica convergente adequada, as primeiras 3h de processamento não são usadas para gerar correções de SSR. No entanto, ainda é necessário um estudo detalhado sobre a convergência de parâmetros atmosféricos com o PPP-Wizard 1.3.

Modelagem Atmosférica

Os atrasos ionosféricos e troposféricos estimados são então utilizados como entrada para o algoritmo de interpolação IDW (*Inverse Distance Weighting*) para gerar as correções de rede. São utilizadas pelo menos 3 estações de referência. Se o usuário estiver dentro da área da rede, as estações selecionadas cercam sua localização. Para os usuários localizados nas bordas da rede, o algoritmo IDW ainda funciona, mas a qualidade das correções pode ser menos efetiva devido à variabilidade espacial dos atrasos atmosféricos.

As correções ionosféricas geradas foram avaliadas por meio de comparação com os produtos GIM (*Global Ionospheric Maps*) do IGS. Também foi realizada comparação das correções ionosféricas com os atrasos ionosféricos estimados no próprio receptor do usuário, obtidas em processamento com o PPP-Wizard 1.3. Uma precisão de 20 ~ 40 cm foi encontrada na comparação com o produto ionosférico IGS, o que é coerente com a precisão nominal desse produto. Por outro lado, quando comparados aos atrasos ionosféricos estimados no próprio receptor *rover*, as correções ionosféricas implementadas apresentaram precisão entre 10 a 20 cm. Tais resultados indicaram que mesmo que as correções ionosféricas apresentem viés devidos as tendências de hardware do receptor, tais correções ainda mantiveram a precisão a aceitável, podendo ser empregadas como correções SSR nesse estudo. Finalmente, verificou-se que a precisão das correções ionosféricas é coerente com os valores de injunção aplicados às mesmas.

Uma vez geradas as correções ionosféricas e troposféricas, seus valores são introduzidos como informação a priori injuncionadas no processamento PPP do usuário. Para tanto, o PPP-Wizard 1.3 foi modificado para permitir mais flexibilidade na aplicação de injunções para as correções atmosféricas. Tais modificações possibilitaram a introdução de valores mais realísticos para os valores das injunções correspondentes às variações de precisão, no tempo e no espaço, sofridas pelas correções atmosféricas.

Dados GNSS

A topologia da rede com configuração densa e esparsa para gerar correções atmosféricas foi avaliada, tal como apresentado anteriormente pela Figura 2.

Com respeito aos usuários simulados, para aplicação das correções, nessa etapa, 63 estações IGN foram selecionadas de acordo com sua distribuição geográfica e disponibilidade de dados. Essas estações são distribuídas de tal forma que cobrem praticamente toda a área da rede de referência (Figura 6).

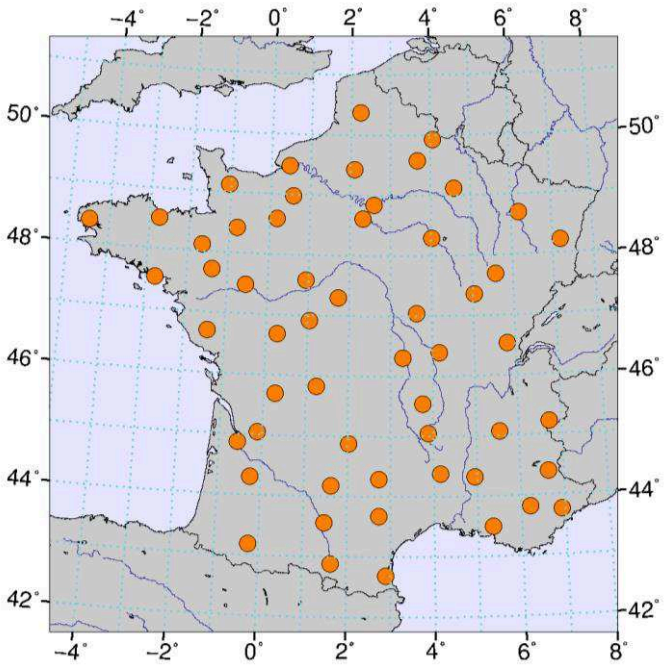

Figura 6 – Rede de estações *rover* utilizada para avaliar os impactos das correções ionosféricas e troposféricas SSR no PPP-RTK.

As reinicializações em estações utilizadas foram realizadas a cada 2 h durante 10 dias selecionados. Os dias desse experimento foram escolhidos de modo a assegurar uma amostragem representativa das condições ionosféricas, isto é, contendo dias de baixa, média e alta atividade ionosférica. Desse modo, tal seleção foi baseada em informações de TEC (*Total Electron Contents*) e do índice F10.7 oriundos do modelo IRI (*International Ionospheric Reference*).

Resultados e análises

A maior parte do *bias* presente nas correções ionosféricas é absorvida pelo parâmetro correspondente ao relógio do receptor. Isso pode ser verificado na Figura 7, através das estatísticas das diferenças entre o relógio do receptor estimado com e sem correções ionosféricas e o *bias* das correções ionosféricas com respeito ao atraso ionosférico estimado no próprio receptor. Nesta figura, cada ponto traçado corresponde às estatísticas para uma estação da rede de usuários simulados.

Esses resultados mostram uma anti-correlação bastante forte (maior que 99%) entre as médias das diferenças em questão. Contudo, é importante frisar que como os valores

dos *biases* podem atingir vários metros, o impacto da parte não absorvida pelo relógio sobre os demais parâmetros, como por exemplo as ambiguidades, deve ser melhor estudado.

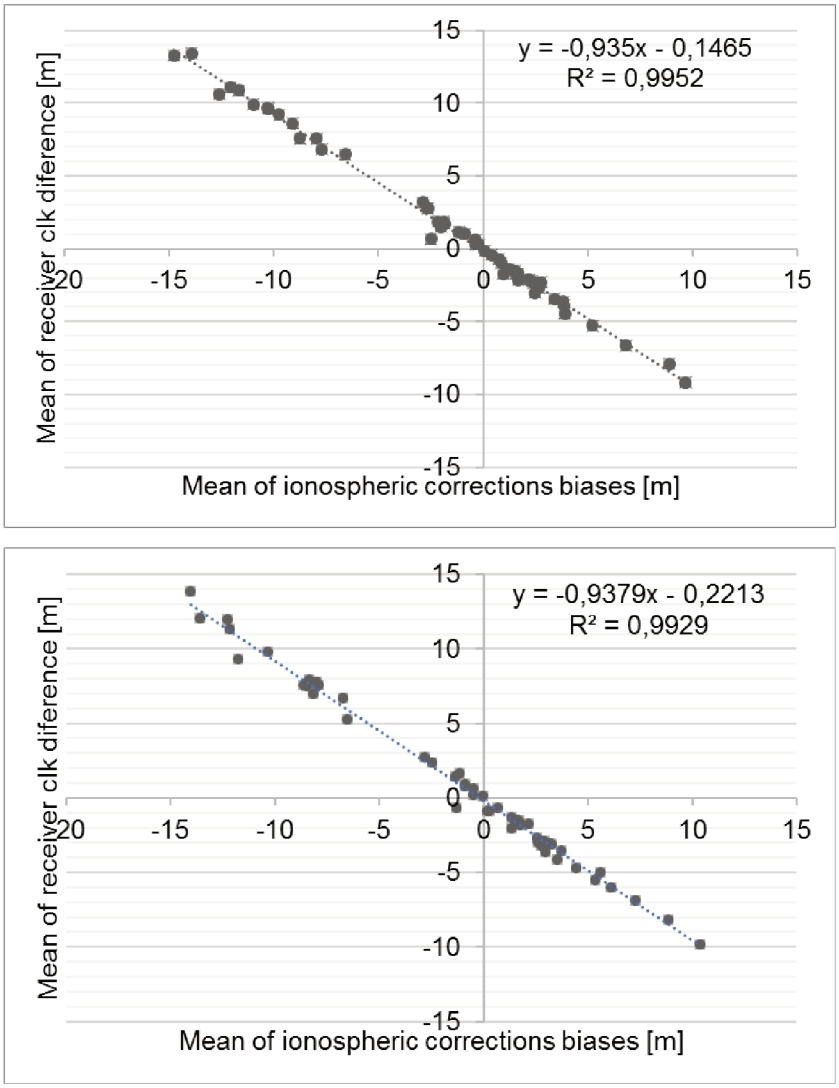

Figura 7 – Média das diferenças entre os parâmetros de *clock* do receptor estimados com e sem correções ionosféricas em relação às médias dos *biases* das correções ionosféricas, geradas com as configurações de rede densa (acima) e esparsa (abaixo).

O número de ambiguidades fixas com cada método avaliado também é analisado. A Figura 8 apresenta estatísticas em termos de desvio padrão e médio do número de ambiguidades de WL e NL fixadas nas estações *rover*.

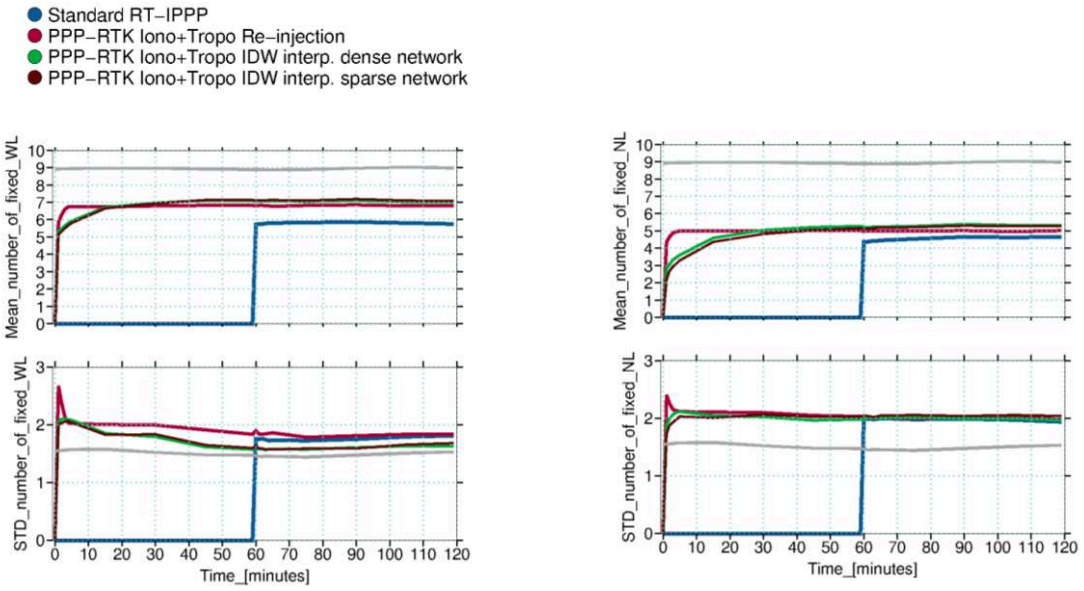

Figura 8 – Média (alto) e desvio padrão (baixo) do número de ambiguidades de WL (esquerda) e NL (direita) fixadas para valores inteiros; a linha cinza corresponde ao número de satélites GPS disponíveis.

Na Figura 8, os resultados mostram que a solução de re-injeção atinge uma média de aproximadamente 7 WL (77%) e 5 NL (54%) fixadas em 3 min. Os métodos que utilizam correções atmosféricas levam 12 minutos para alcançar os mesmos desempenhos. Um aspecto positivo é que nas soluções com correções atmosféricas mais ambiguidades são resolvidas do que na solução sem uso de correções atmosféricas, e esse número é estável, pois todos os métodos apresentam desvios padrão semelhantes sobre o número de ambiguidades fixas.

A Figura 9 mostra as medianas e os quantis à 68% considerando-se todas as reinicializações em todas as estações envolvidas no processamento. São ilustradas quatro soluções: 1) a solução padrão, ou seja, sem correções troposféricas (PPP Padrão em Tempo Real), 2) uma solução de referência, que é o uso de produtos troposféricos e ionosféricos re-injetados, os quais foram estimados com o PPP-Wizard 1.3 no próprio *rover*, e o uso de correções SSR externas geradas a partir de configurações Orphéon de 3) rede densa e 4) esparsa. Aqui novamente, as barras verticais indicam quando o respectivo método atinge a acurácia de 10 cm.

A partir da Figura 9 e da Tabela 5, pode-se concluir que a mediana dos erros no posicionamento usando correções atmosféricas de rede, densa e esparsa, apresenta convergência para 10 cm de acurácia na componente Leste de 6 min e 4 min, respectivamente.

Na componente Norte, esses valores são de 4,5 min e 5 min. Tais números representam ganhos em tempo de convergência horizontal de 58% com soluções de rede densa e 43% esparsa, em comparação com a solução RT-IPPP padrão. Para o método de referência (Re-injeção), esse ganho é de cerca de 95%. Somente o método chamado re-injeção (*Re-injection*) promoveu ganhos na componente Up (87%). Nas demais soluções o PPP-RTK usando correções atmosféricas externas apresenta degradação em Up, especialmente para a solução esparsa.

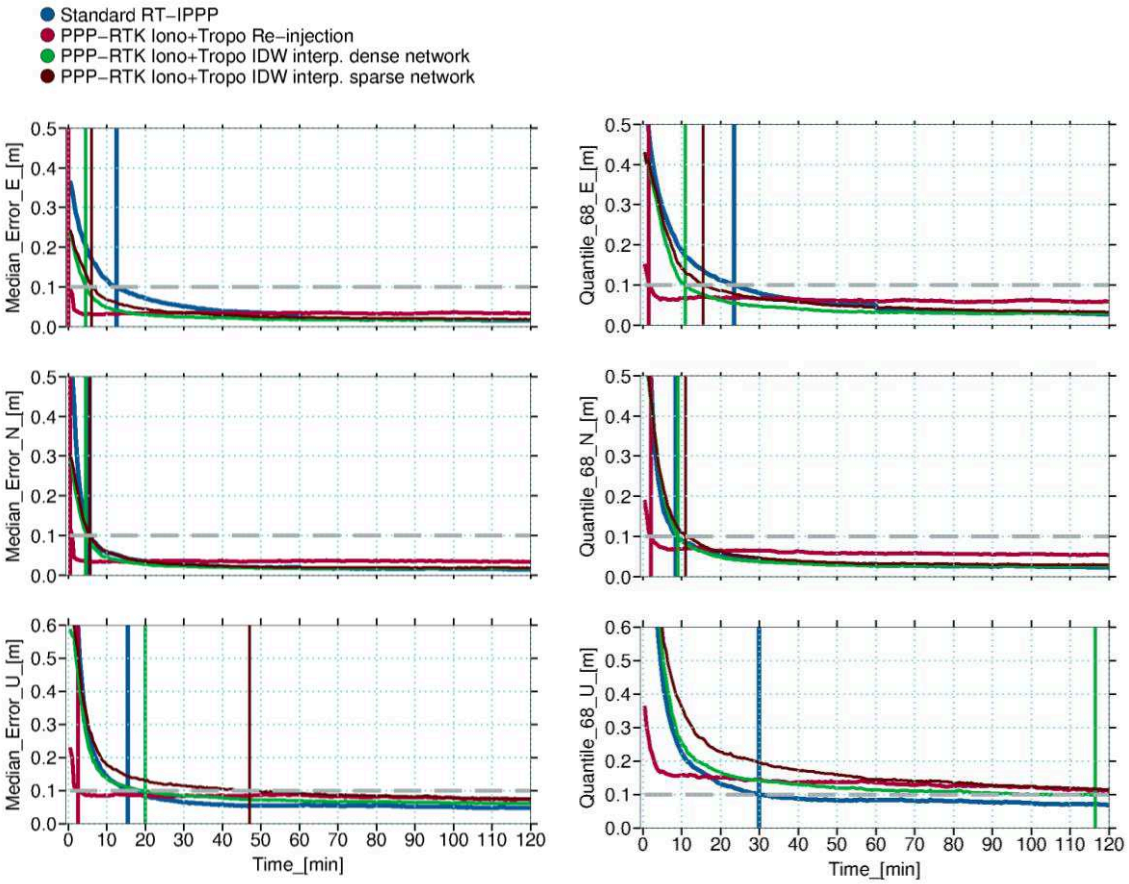

Figura 9 - Mediana (esquerda) e quantis à 68% (direita) dos erros absolutos de posicionamento obtidos com o PPP-RTK por época ao longo da convergência, em estações *rover* simuladas; As estatísticas envolvem todas as 63 Estações Rover, durante os 10 dias do experimento e com 10 *cold-starts* por dia.

Com relação aos quantis à 68%, as componentes Leste e Norte levam 24 min e 8,5 minutos para alcançar a convergência de 10 cm sem correções atmosféricas (RT-IPPP padrão). Ao usar correções de rede densa, Leste e Norte convergem dentro de 10,5 min e 9 min. Isso caracteriza um posicionamento horizontal 47% melhor que o padrão RT-IPPP. Com a rede esparsa, esse ganho no posicionamento horizontal em termos de quantis à 68% é equivalente à 24%, haja vista que as componentes Leste e Norte levam 16 minutos e 11

minutos para convergir. A estratégia de re-injeção promove um ganho de 85%, mostrando os desempenhos que uma modelagem perfeita pode alcançar. Mais uma vez, a degradação é verificada para o componente Up, e até mesmo a solução re-injeção não atinge 10 cm de precisão.

Tabela 5 - Tempo de convergência dos erros no PPP-RTK (GPS + GLONASS)

Método	Mediana Tempo de convergência [min]			Quantis à 68% Tempo de convergência [min]		
	E	N	U	E	N	U
RT-IPPP Padrão	13,5	5,0	16,5	24,0	8,5	30,0
PPP-RTK Re-injeção	0,5	0,5	2,0	2,0	3,0	Não conv.
PPP-RTK Rede densa	4,0	4,5	19,5	10,5	9,0	117,0
PPP-RTK Rede esparsa	6,0	5,5	47,0	16,0	11,0	Não conv.

As degradações provocadas na convergência da componente Up devem ser estudadas considerando-se a mitigação do viés de hardware do receptor, presente nas correções ionosféricas. Além disso, devem ser considerados maiores desenvolvimentos nos algoritmos implementados de interpolação/modelagem, especialmente para os atrasos ionosféricos.

Conclusões

A viabilidade de um serviço de posicionamento em tempo real com base no PPP e na modelagem SSR foi investigada. Os métodos e resultados obtidos foram apresentados em duas etapas que utilizaram diferentes soluções. A primeira etapa concentra os esforços nas correções troposféricas. Na segunda, são utilizadas correções troposféricas e ionosféricas.

As melhorias no tempo de convergência quando se utilizam correções troposféricas para o chamado *float* PPP-RTK foram quantificadas. Em termos de Quantis à 68%, os ganhos no tempo de convergência são de 1% em Leste, cerca de 20% em Norte e de 5% nas componentes Up, para o posicionamento GPS. A introdução de dados GLONASS reduz em cerca de 50% o tempo de convergência em todas as componentes. No entanto, adicionar correções troposféricas ao processar dados GPS+GLONASS melhora o

posicionamento horizontal em apenas cerca de 2% em Leste e 6% em Norte, porém Up é melhorada em cerca de 12%. A redução no número de estações de referência usando uma configuração de rede mais esparsa não degrada as correções troposféricas geradas derivadas de OFCs e performances similares são alcançadas entre as duas configurações.

Na segunda etapa, o PPP-RTK foi executado graças ao pacote CNES PPP-Wizard 1.3 bem como os produtos de órbita, *clock* e *biases* de fase do CNES. O processamento das observáveis foi realizado e os efeitos ionosféricos na direção inclinada foram estimados simultaneamente com os demais parâmetros. Portanto, nessa etapa, a modelagem de efeitos ionosféricos também foi aplicável. Assim, as correções ionosféricas e troposféricas foram introduzidas como parâmetros a priori injuncionados no posicionamento do usuário. Para produzir correções, foi escolhido um algoritmo padrão de interpolação de tipo IDW.

Os atrasos ionosféricos foram especialmente desafiadores para tratar, dado que eles são afetados pelo viés de hardware, tanto do receptor quanto do satélite. Esse desafio foi amplamente discutido na tese e os resultados mostram que o viés nas correções ionosféricas está altamente correlacionado com os deslocamentos do relógio do receptor, encontrados quando se aplica tais correções.

O software PPP-Wizard 1.3 foi aprimorado para permitir maior flexibilidade na aplicação de injunções para correções atmosféricas. Tais modificações possibilitaram a introdução de valores mais realistas para injuncionar as correções atmosféricas e considerar sua variação de acurácia ao longo do tempo.

A topologia da rede com configuração densa e dispersa usada para gerar correções atmosféricas foi avaliada novamente na segunda etapa. O RT-IPPP padrão leva ~ 25 min para alcançar acurácia horizontal de 10 cm, desta vez melhorado 46% (~ 14 min) com correções de rede densa e 24% (~ 19 min) com rede esparsa. Porém, o posicionamento vertical aumentou o seu tempo de convergência, especialmente quando se utilizam correções de solução de rede esparsa. Ainda assim, as melhorias no posicionamento horizontal do PPP-Wizard 1.3 com correções atmosféricas SSR externas de rede densa ou esparsa são promissoras e podem ser úteis para aplicações que dependem principalmente do posicionamento horizontal.

Trabalhos futuros

No que diz respeito à modelagem troposférica, devem ser considerados modelos empíricos mais recentes, como o GPT2w (Böhm et al., 2015; Kalita e Rzepecka, 2017), bem como modelos NWP (Böhm et al., 2011; Urquhart e Santos, 2011). A combinação dessas soluções com correções troposféricas de redes GNSS, como as implementadas nesta tese, pode melhorar substancialmente a qualidade das correções de SSR.

Em relação às correções ionosféricas, um dos principais desafios continua a ser a estratégia para tratar com o viés de hardware do receptor para modelar atrasos em uma escala de rede. As degradações encontradas na convergência de Up devem ser mais estudadas, considerando-se a mitigação do viés de hardware do receptor presente nas correções ionosféricas além de maiores desenvolvimentos nos algoritmos implementados de interpolação/modelagem. Além disso, as limitações das funções de mapeamento ionosférico também devem ser consideradas. Nesse sentido, o uso de funções de mapeamento ionosférico com base no campo de densidade eletrônica derivado do IRI pode ser uma alternativa interessante (Zus et al., 2017).

Melhorias na estratégia do controle de qualidade usado para seleção de atrasos ionosféricos e troposféricos empregados para o algoritmo de IDW devem ser melhoradas para permitir a fixação ou forte injunção das coordenadas nas estações de referência. Isso pode proporcionar uma convergência rápida dos parâmetros atmosféricos na rede de referência e aumentar sua qualidade.

O desempenho do método PPP melhorará significativamente com a disponibilidade de medidas GNSS mais precisas, bem como a adição de mais frequências portadoras, decorrente da modernização do GPS e demais GNSS. Tais aspectos devem ser fortemente explorados para alcançar o melhor do método. Dessa forma, é altamente recomendável estudar os benefícios do uso de correções atmosféricas com a adição de outras constelações GNSS, como o Galileo e o BDS (*BeiDou Navigation Satellite System*).

Contents

List of Tables

List of Figures

Abbreviations

ANTEX: ANTenna EXchange format 21

ARP: Antenna Reference Point 21

BDS: BeiDou Navigation Satellite System 9

BKG: *Bundesamt für Kartographie und Geodäsie* 36

BNC: BKG Ntrip Client 40

CLS: *Collecte Localisation Satellites* 49

CMC: Canadian Meteorological Centre 79

CODE: Center for Orbit Determination in Europe 31

CORS: Continuously Operating Reference Station 3

COSPAR: Committee on Space Research 95

Cospas: *Cosmicheskaya Sistyema Poiska Avariynich Sudow* 15

DC: Distinct Clock 50

DCB: Differential Code Biases 31

DoD: Department of Defense 10

DPSP: Direct Physical Statistical Prediction 71

DSC: Decoupled Satellite Clocks 49

ECMWF: European Centre for Medium-Range Weather Forecasts 76

EGNOS: European Geostationary Navigation Overlay Service 10

EKF: Extended Kalman Filter 31

ERA-Interim: European Centre for Weather Forecasts Re-Analysis 76

ESA: European Space Agency 9, 36

ESOC: European Space Operations Centre 36

EU: European Union 10

EW: Extra-Widelane 61

FCB: Fractional-Cycle Bias 44

FDMA: Frequency Division Multiple Access 13

GAGAN: GPS Aided Geo Augmented Navigation 10

GBAS: Ground-Based Augmentation System 10

GDGPS: Global Differential GPS 35

GDPS: Global Deterministic Prediction System 79

GeF: *Géomatique et Foncier* 4

INTRODUCTION

1. Context

Position information is a key value for the scientific development of our society. When its knowledge is provided with high accuracy (cm) and in real-time, its added-value significantly increases as well as the positioning applications. The GNSS (Global Navigation Satellite System) has proved to be a powerful technology for this task. One of the most remarkable methods to obtain user position by GNSS is PPP (Precise Point Positioning), thanks to several reasons that are discussed along this document.

PPP concept started to be properly researched by the scientific community at the end of the 90's, in the context of processing efficiently large data set from GPS (Global Positioning System) global network (Zumberge et al., 1997). Subsequently, PPP has been further developed and improved thanks to the availability of PPP products for satellite orbit and clock parameters destined for post-processing applications. Since many years, these products are generated and diffused by organizations such as NASA (National Aeronautics and Space Administration) JPL (Jet Propulsion Laboratory), IGS (International GNSS Service), NRCan (Natural Resources Canada), among others (Morel et al., 2014). Following studies found that PPP method is able to provide solutions at a centimeter-level accuracy (Kouba and Héroux, 2001) when using final orbit and clock products generated by IGS. After this, the number of applications using PPP has grown quickly. The method became essential, for example, in glacial or volcanology surveying, as well as at any place where baselines with respect to reference stations are too long for relative GNSS positioning (Morel, 2015).

Efforts of the geodetic community on PPP have since shifted to real-time or near real-time solutions. The IGS Real-Time Working Group (RTWG) has been established in 2001, to investigate precise products for real-time users (Caissy and Agrotis, 2011). Gao and Chen (2004) conducted analysis of PPP using real-time orbit and clock precise products and obtained promising results for positioning determination at a centimeter-level accuracy. Several sessions at ION (Institute of Navigation) GNSS annual event have been exclusively dedicated to PPP and most of works evidenced its potential for real-time applications (Laurichesse et al., 2009; Laurichesse and Mercier, 2007; Monico, 2008; Wübbena et al., 2005).

IGS started the Real-Time Pilot Project (RTPP) in 2007, using GNSS real-time observations from a global network. On April 2013, the Real Time Service (RTS) was officially launched. Its official products included only corrections to GPS satellite broadcast orbits and clocks (http://www.rtigs.net). The centimeter accuracy was achievable with real-time PPP based on products from global GNSS networks (Grinter and Roberts, 2013; Morel, 2015; Rizos et al., 2012).

The standard real-time PPP drawback is the time required for solution convergence. Actually, the standard PPP strategy needs to estimate state parameters (e.g. tropospheric delays) together with float ambiguities, that needs a considerable initialization time (at least 30 min) to achieve the proper convergence of the real-valued ambiguities, even with good satellites geometry and without important multipath effects (Ge et al., 2012; Rovira-Garcia et al., 2015). Therefore, for GNSS users requiring real-time centimeter-level accuracy, RTK (Real Time Kinematic) or NRTK (network RTK) methods were usually employed. RTK method requires at least two GNSS receivers connected by a communication link. In NRTK case, the user needs only one receiver but he also needs to have access to the OSR (Observation Space Representation) corrections from a dense local Continuously Operating Reference Station (CORS) network. Thus, NRTK positioning promoted an increasing number of CORS networks around the world (Grinter and Roberts, 2013).

The cost efficiency of PPP and the availability of precise products in real-time motivated several researches to improve the method to fix phase-ambiguity parameters to integer values (Collins et al., 2010; Ge et al., 2012; Laurichesse et al., 2010; Laurichesse and Mercier, 2007; Mervart et al., 2008). Significant achievements were obtained, when in addition to precise orbits and clock information, satellite phase biases products were provided allowing to fix phase ambiguities to integer values (Shi and Gao, 2014; Teunissen and Khodabandeh, 2015). This led to the concepts known as SSR (State Space Representation) with the aim to separate all physical errors affecting GNSS observables (Mervart et al., 2013; Wübbena et al., 2005).

Results including application of SSR corrections for atmospheric parameters, such as ionospheric and tropospheric delays, have demonstrated improvements with convergence at the centimeter level in first few minutes or even seconds (Leandro et al., 2011; Li et al., 2014b; Rovira-Garcia et al., 2015). In this case the improved solution convergence time is

promoted not only with the benefit of phase biases corrections, but also thanks to network augmentation providing atmospheric corrections, leading to the so-called PPP-RTK (Stürze et al., 2012; Wübbena et al., 2014, 2005). These studies revealed SSR based positioning, as a rival or complementary method to RTK or NRTK. This is the case if SSR atmospheric corrections can be generated from sparser networks than those required by OSR corrections, which means a less onerous infrastructure than that needed for NRTK. However, performances of atmospheric modeling for SSR corrections generation rely on network topology and atmospheric conditions.

In France, the Geodata Diffusion Company, subsidiary of the group Hexagon Geosystems, offers industrial services of GNSS network based positioning. Such services are available since 2004, using GNSS data from the Orphéon CORS network. In order to continue operating effectively and remain leader in its field, Geodata Diffusion needs to understand further technical details of PPP performances and the potential impacts of such method on GNSS industry. In such context, it was proposed the development of this thesis CIFRE-Brésil (*Convention Industrielle de Formation par la Recherche - Brésil*), under co-supervision of two research laboratories (GeF) (*Géomatique et Foncier*), and LGE (*Laboratório de Geodésia Espacial*).

2. Objectives

The primary objective of this thesis is to assess existing real-time PPP solutions enhanced with atmospheric SSR corrections, fitting in the industrial context of the project, as well as to improve employed solutions or models. Thus, the feasibility and demonstration of a new service for real-time precise GNSS positioning based on PPP method is achieved.

In order to achieve the above-mentioned objective, the following specific goals are accomplished:

- To review bibliography to understand the advances and the basic aspects of the subjects involved in this project,
- To ensure the cost-effective communication link bandwidth between user and server sides, as well as the alignment with standards defined for SSR corrections,
- To contribute with the modeling of the atmospheric variability, as well as the understanding of impacts of atmospheric corrections on GNSS processing parameters,
- To study the quality and reliability of user positioning with SSR atmospheric corrections,
- To assess the correlation between SSR based GNSS positioning performances with respect to the reference network topology used to generate the SSR atmospheric corrections.

3. Contributions

The contributions of this work are divided in two main stages: 1) use of network SSR tropospheric corrections and 2) corrections for tropospheric and ionospheric delays. Network topology is assessed in both stages, by reducing the number of reference stations up to 75%, thus using a sparser network configuration to perform the atmospheric modeling. Regarding this aspect, it is assessed the use of different configurations of a dense and regular GNSS network existing in France, the Orphéon network. This network has about 160 sites and it is owned by Geodata-Diffusion, subsidiary of the group Hexagon Geosystems and directly involved in this project.

Concerning the first stage, RTKLib 2.4.3-beta package (Takasu, 2013) is used but enhanced with modifications implemented to take into account the network SSR tropospheric corrections. Iono-free observations are used to mitigate the ionospheric contribution, and real-time PPP with troposphere augmentation is realized. Such positioning solution with float ambiguities is called here as “Float PPP-RTK”. The generation of tropospheric corrections is based on an adaptive polynomial modeling, Optimal Fitting Coefficients (OFC), which allows mono-directional link of communication between server and users, reducing required communication bandwidth (Shi et al., 2014). In this research, the second order degree of OFC method has been implemented and assessed, which was not realized in previous works, allowing the generation of tropospheric correction for larger areas.

In the second stage, CNES PPP-Wizard 1.3 package is used and ionospheric and tropospheric corrections are introduced as a priori parameters. In this PPP-RTK solution, uncombined observations are used and ambiguities fixing is performed, using CNES orbit, clock and phase biases products. The existing interface to apply atmospheric constraints in this software is improved to consider the variation of SSR atmospheric corrections accuracy (used as constraint) over the time. Generation of SSR tropospheric and ionospheric corrections is aligned with the RTCM (Real-Time Maritime Services) conventions, thanks to a conventional interpolation algorithm (Inverse Distance Interpolation) assuming that users would get access directly to information of ionospheric and tropospheric delays estimated at reference stations.

4. Contents

The chapters of this thesis are separated in five different groups. The manuscript is organized as follows:

- "INTRODUCTION", presents an overview of the thesis context as well as the main objectives,
- "PART I - REVIEW ON GNSS, REAL-TIME PPP AND ATMOSPHERIC EFFECTS", presents a theoretical overview and bibliography. An experimented reader does not need to read this part.
- "PART II - FLOAT PPP-RTK WITH TROPOSPHERIC MODELING" deals with results obtained in the first stage of researches which corresponds to the modeling of tropospheric effects for float PPP-RTK.
- "PART III - PPP-RTK WITH TROPOSPHERIC AND IONOSPHERIC MODELING" deals with results of the second step of researches where the tropospheric and also ionospheric effects are taken into account for ambiguity fixing at integer values.
- "CONCLUSIONS AND PROSPECTS" gives finding of the thesis. In this part several recommendations and challenges for future works are suggested.

PART I - REVIEW ON GNSS, REAL-TIME PPP AND ATMOSPHERIC EFFECTS

5. GNSS positioning and navigation

Satellite-based positioning consists of determining positions of observed sites on land, at sea, in the air or even in space by means of artificial satellites technology (Hofmann-Wellenhof et al., 2008). In this first chapter, the basic aspects of satellite-based positioning are presented together with a brief description of the main existing satellite systems.

5.1. Existing GNSS

The acronym GNSS refers to all global positioning systems by satellites such as GPS, GLONASS (*GLObal'naya NAvigatsionnaya Sputnikkovaya Sistema*), BDS (BeiDou Navigation Satellite System) and Galileo, besides the regional systems, and the regional augmentation systems (Hofmann-Wellenhof et al., 2008; Sanz Subirana et al., 2013).

A GNSS is composed by three segments: Spatial, Control and Users. The first one is associated with a satellites constellation and their signals, while the second is responsible for the control and maintenance of the system. The third segment is the User Segment and involves the civil and military communities, this segment is usually much bigger than the others and it is continuously increasing (Hofmann-Wellenhof et al., 2008; Monico, 2008).

GPS and GLONASS are the only fully deployed GNSS in operation and they are under the responsibility of the USA and Russian federation respectively. Both systems are under military control (Seeber, 2003). China is developing BDS which is also under military control. Galileo is the unique GNSS with a civil control, developed by ESA (European Space Agency) with the European Commission and the European Industry. Among the regional systems, which provide positioning services at regional scale, one can cites the Beidou-1 (predecessor of BDS), the QZSS (Quasi-Zenith Satellite System) (Japan), IRNSS (Indian Regional Navigation Satellite System), and also some initiatives in the private-sector, e.g. GEOSTAR , OmniTRACS (Hofmann-Wellenhof et al., 2008).

The regional augmentation systems refer to the provision of additional information to enhance the performances of space-based positioning. A regional augmentation system can be space-based (SBAS – Space-Based Augmentation System) or ground-based (GBAS – Ground-Based Augmentation System) (Hofmann-Wellenhof et al., 2008).

The most important SBAS are the American WAAS (Wide Area Augmentation System), EGNOS (European Geostationary Navigation Overlay Service) developed by the EU (European Union), MSAS (MTSAT Satellite Augmentation System) owned by Japan, and GAGAN (GPS Aided Geo Augmented Navigation) system (Indian government) (Hofmann-Wellenhof et al., 2008; Sanz Subirana et al., 2013).

5.1.1. GPS

GPS was developed by the DoD (Department of Defense) of the USA in order to be the main navigation system of the American army forces. Considering the previously mentioned GNSS systems, the GPS is actually the most used by the civil community.

GPS was declared operational on 17 July 1995 (Hofmann-Wellenhof et al., 2008). This system has been used as navigation system completely operational for more than two decades and it is still being modernized. During this period, several technological advances have occurred, besides the increasing demand for accuracy and applications by both military and civil users. Another pressure factor is the competition with other operational systems, e.g. GLONASS, or still in development, e. g. Galileo and BeiDou (Monico, 2008).

The GPS Space Segment was planned to have at least 24 MEO (Medium Earth Orbits) satellites distributed in six orbital planes. They are placed at around 20,200 km of altitude, with an orbital inclination of 55 degrees in relation to the equator, providing an orbital period of 11h58 (Monico, 2008). The Space Segment is responsible for the transmission of radio-navigation signals, the storage and retransmission of the navigation messages sent by the Control Segment (Sanz Subirana et al., 2013). The Control Segment (also referred as Ground Segment) is charged of the continuous monitoring and control of the satellites system. This segment is also responsible for the determination of orbital parameters, GPS Time System, prediction of satellites ephemerides and satellite clock corrections as well as the update of the navigation messages for every satellite (Monico, 2008). The Control

segment is currently composed by a Master Control Station (Colorado Springs), an alternate Master Control Station (Vandenberg), 11 control and command antennas and 16 monitoring ground stations which track GPS satellites and send them to the Master Control Station (www.gps.gov, access on 15/09/2017). At the Master Control Station, all the satellites parameters are computed and predicted. This configuration implies that every satellite can be observed from at least three monitor stations. GPS User Segment is represented by the civil and military user's communities (Duquenne et al., 2005; Sanz Subirana et al., 2013).

The GPS modernization involves the Control and Spatial segments and more specifically, the GPS signals (Hofmann-Wellenhof et al., 2008). The modernization process of the Spatial segment started in September 2005 with the launch of the first satellite of Block IIR-M (R for replenishment and M for modernized) and currently there are already satellites of Block IIF (F – follow on). The main characteristics of Block IIR-M satellites are the new civil code in the frequency L2 (L2C) and the new code M in the frequencies L1 and L2 which refers to the military code. The first satellite of the Block IIF was launched on May 2010. This class of satellites has the third-civil signal called L5C besides the military code (www.gps.gov, access on 15/09/2017). The active GPS satellites available in July 2017, as well as the corresponding blocks are showed in Table 1.

Block III will be the next generation of GPS satellites with significant enhancements in navigation capabilities by improving interoperability and jam resistance. They will provide a fourth civil signal called L1C (1575.42 MHz). This measurement was designed for interoperability with Galileo. It will be backward compatible with the current civil signal on L1. The first launch of a GPS block III satellite is expected for not earlier than 2018 (www.gps.gov, access on 15/09/2017).

The Control segment was composed by only 5 ground stations before the GPS modernization program: Hawaii, Colorado Springs (Colorado, US), Ascencion (South Atlantic), Diego Garcia (Indian Ocean) and Kwajalein (North Pacific). With the aim of providing greater visibility of the constellation, other 11 stations were incorporated, between 2001 and 2006 : Adelaide (Australia), Buenos Aires (Argentina), Hermitage (UK), Manama (Bahrain), Quito (Ecuador), Washington DC (USA), Fairbanks (Alaska), Osan (South korea), Papeete (Tahiti), Pretoria (South Africa), Wellington (New Zealand) (Sanz Subirana et al., 2013).

Table 1 – GPS constellation status in July 2017

Block (Launch order)	PRN	SVN	Launch date	Frequency Standard/Clock	Plane/Slot
IIR-2	13	43	23/07/1997	Rb	F6
IIR-3	11	46	07/10/1999	Rb	D5
IIR-4	20	51	11/05/2000	Rb	B6
IIR-5	28	44	16/07/2000	Rb	B3
IIR-6	14	41	10/11/2000	Rb	F1
IIR-7	18	54	30/01/2001	Rb	E4
IIR-8	16	56	29/01/2003	Rb	B1
IIR-9	21	45	31/03/2003	Rb	D3
IIR-10	22	47	21/12/2003	Rb	E2
IIR-11	19	59	20/03/2004	Rb	C3
IIR-12	23	60	23/06/2004	Rb	F4
IIR-13	2	61	06/11/2004	Rb	D1
IIR-14M	17	53	26/09/2005	Rb	C4
IIR-15M	31	52	25/09/2006	Rb	A2
IIR-16M	12	58	17/11/2006	Rb	B4
IIR-17M	15	55	17/10/2007	Rb	F2
IIR-18M	29	57	20/12/2007	Rb	C1
IIR-19M	7	48	15/03/2008	Rb	A4
IIR-20M	4	49	24/03/2009	Rb	
IIR-21M	5	50	17/08/2009	Rb	E3
IIF-1	25	62	28/05/2010	Rb	B2
IIF-2	1	63	16/07/2011	Rb	D2
IIF-3	24	65	04/10/2012	Cs	A1
IIF-4	27	66	15/05/2013	Rb	C2
IIF-5	30	64	21/02/2014	Rb	A3
IIF-6	6	67	17/05/2014	Rb	D4
IIF-7	9	68	02/08/2014	Rb	F3
IIF-8	3	69	29/10/2014	Rb	E1
IIF-9	26	71	25/03/2015	Rb	B5
IIF-10	8	72	15/07/2015	Cs	C5
IIF-11	10	73	31/10/2015	Rb	E6
IIF-12	32	70	05/02/2016	Rb	F5

Source: ftp://tycho.usno.navy.mil/pub/gps/gpsb2.txt (Access on Jul. 2017)

The modernization of the Control segment is related to the reduction of operational costs and improvement of system performances. These improvements also include more satellite activity without contact with the control segment, updates of the monitoring stations and new equipment, initiative to improve the accuracy of broadcast orbits and products related to GPS, among others (Hofmann-Wellenhof et al., 2008).

5.1.2. GLONASS

GLONASS started in the mid-1970s. The first GLONASS satellite was launched in 1982 together with two test satellites. GLONASS Space Segment also was planned to have at least 24 satellites in orbit, although differently from GPS, the nominal orbits of the satellites are distributed over three orbital planes separated by 120°. Satellites are equally spaced on each orbital plane with a nominal inclination of 64.8°. The nominal orbits are quasi-circular with approximated radius of 25,500 km, which provides an orbital period of around 11 h 15 min. In the end of 1995, GLONASS was declared fully operational with a constellation of 24 satellites (Hofmann-Wellenhof et al., 2008). However, due to the missing launch of new satellites to replace the older ones or those that presented problems, the number of satellites decreased dramatically and in the end of 2005 the constellation had only 12 satellites. With Russian economy recuperation, GLONASS received high priority and the constellation started to be recomposed (Monico, 2008). Firstly, with the launch of the modernized GLONASS-M satellites and later on with the launch of GLONASS-K satellites (Monico, 2008). The GLONASS constellation status on July 2017 is presented in Table 2.

An important difference between GLONASS and GPS is that every GLONASS satellite transmits on its own frequencies. This allows the identification of satellites by the signal's frequency, using a technique known as FDMA (Frequency Division Multiple Access). However, GLONASS system will also transmit data using the CDMA (Code Division Multiple Access) technique. It started with the launch of the satellites GLONASS-K in February 2011 and in December 2014. Some benefits of this transition have already been demonstrated (Zaminpardaz et al., 2016).

The GLONASS Control segment is responsible for the proper operation of the system with several activities like monitoring the status of satellites, determining ephemerides and clock corrections, as well as the upload of the navigation data to the satellites (Sanz Subirana et al., 2013). The terrestrial control center is located in Moscow and the monitoring stations are mainly distributed over the old USSR (Union of Soviet Socialist Republics) territory. The first GLONASS correction and monitoring station outside the former USSR territory was established in February 2013 in Brazil (Petrovski, 2014). Since then, more than 25 GLONASS monitoring stations were deployed abroad improving substantially the quality of ephemerides and clock offset corrections around the world (United Nations, 2016).

Table 2 – GLONASS constellation status in July 2017

Block /Version	GLONASS /number	Cosmos /number	Plane /slot	Frequ. chann.	Launch date	Intro date	Status	Outage date
M	730	2456	1/01	1	14/12/2009	30/01/2010	operating	-
M	747	2485	1/02	-4	26/04/2013	04/07/2013	operating	-
M	744	2476	1/03	5	04/11/2011	08/12/2011	operating	-
M	742	2474	1/04	6	02/10/2011	25/10/2011	operating	-
M	734	2458	1/05	1	14/12/2009	10/01/2010	operating	-
M	733	2457	1/06	-4	14/12/2009	24/01/2010	operating	-
M	745	2477	1/07	5	04/11/2011	18/12/2011	operating	-
M	743	2475	1/08	6	14/11/2011	25/12/2011	operating	-
K1	702	2501	2/09	-6	01/12/2014	25/12/2014	operating	-
M	717	2426	2/10	-7	25/12/2006	03/04/2007	operating	-
M	753	2516	2/11	0	29/05/2016	27/06/2016	operating	-
M	723	2436	2/12	-1	25/12/2007	22/01/2008	operating	-
M	721	2434	2/13	-2	25/12/2007	08/02/2008	operating	
M	715	2424	2/14	-7	25/12/2006	03/04/2007	unusable	26/06/2017
M	716	2425	2/15	0	25/12/2006	12/10/2007	operating	-
M	736	2464	2/16	-1	02/09/2010	01/10/2010	operating	-
M	751	2514	3/17	4	07/02/2016	24/02/2016	operating	-
M	754	2492	3/18	-3	24/03/2014	14/04/2014	operating	-
M	720	2433	3/19	3	26/10/2007	25/11/2007	operating	-
M	719	2432	3/20	2	26/10/2007	27/11/2007	operating	-
M	755	2500	3/21	4	14/06/2014	03/08/2014	operating	-
M	731	2459	3/22	-3	02/03/2010	28/03/2010	operating	-
M	732	2460	3/23	3	02/03/2010	28/03/2010	operating	-
M	735	2461	3/24	2	02/03/2010	28/03/2010	operating	-
K1	701	2471	3/(20)	-5	26/02/2011	-	fligh tests	-

Source: adapted from (www.GLONASS-iac.ru/en/CUSGLONASS/index.php) and (www.GLONASS-iac.ru/en/GLONASS) (Access in Jul. 2017)

In comparison to GPS only receivers, the number of GLONASS only receivers is considerably reduced. However the GLONASS users segment is directly involved with receivers industry and the number of GNSS receivers able to track several constellations is exponentially increasing (Duquenne et al., 2005; United Nations, 2016).

The GLONASS interface control document lists carrier frequencies as L1, L2 and L3 bands (Coordination Scientific Information Center, 2008). Hereafter, to differentiate from GPS, the GLONASS frequencies are denoted G instead of L. An open service for standard positioning is provided for users, without restriction using the three bands. However, for authorized users a secure service is provided, which uses precise positioning signals on the

GLONASS G1 and G2 bands modulated with a special code (Sanz Subirana et al., 2013; United Nations, 2016).

5.1.3. Galileo

As previously stated Galileo has civil control and interoperability with GPS and GLONASS. The Space Segment will be composed by 30 MEO satellites. The nominal constellation will be composed of 24 satellites, plus 6 actives in-orbit spares. The satellites are evenly spaced in three circular orbit planes with an inclination of 56 degrees relative to the equator. The nominal altitude is 23,000 km with an orbital period of about 14h.

The first Galileo satellite system was launched in December 2005 and called GIOVE-A (Galileo In-Orbit Validation Element-A). The second one, GIOVE-B, was launched in April 2008. These satellites are no longer included in Galileo system constellation status (Table 3).

In October 2011 happened the launch of the two first satellites designed to validate the Galileo orbits (IOV – In-Orbit Validation). Since these launches, the system has been continuously developed, and in December 2016 Galileo initial services provision started with 18 satellites, before the Galileo core infrastructure is fully deployed which requires only 6 additional satellites (ESA, 2016). Table 3 summarizes the constellation status in February 2017.

The Control segment controls and monitors the Galileo satellite constellation, provides satellite orbits, clock synchronization and continuously assesses the signal performances. There are two ground control centers, a global network of 16 Galileo Sensor Stations (GSS), 6 satellites tracking and command facilities and 5 mission Up-link Stations (ULS) (United Nations, 2016).

With regard to the Users segment, the open service of Galileo makes positioning, navigation and timing services widely available to all users free of charge. The User segment of Galileo is expected to benefit also to the search-and-rescue. It will complement the current international satellite system for search and rescue (Cospas-Sarsat: *Cosmicheskaya Sistyema Poiska Avariynich Sudow*- Search and Rescue Satellite-Aided Tracking) service by

performing detection and localization of Cospas-Sarsat distress beacons among other additional facilities. This service will be free of charge as well, and its accuracy performance is expected to be better than 100 m (95 % of time) for beacons fitted with Galileo receivers.

Table 3 – Galileo constellation status in February 2017

Satellite Name	SV-ID	PRN	Orbital Slot	Clock	Status	Launch Date	Mission name
GSAT0101	11	E11	B05	RAFS	Usable	21/10/2011	IOV-1
GSAT0102	12	E12	B06	PHM	Usable	21/10/2011	IOV-1
GSAT0103	19	E19	C04	PHM	Usable	12/10/2011	IOV-2
GSAT0104	20	E20	C05	RAFS	Not available	12/10/2011	IOV-2
GSAT0201	18	E18	Ext01	PHM	Testing	22/08/2014	Galileo Sat 5 & 6
GSAT0202	14	E14	Ext02	PHM	Testing	22/08/2014	Galileo Sat 5 & 6
GSAT0203	26	E26	B08	PHM	Usable	27/03/2015	Galileo Sat 7 & 8
GSAT0204	22	E22	B03	RAFS	Usable	27/03/2015	Galileo Sat 7 & 8
GSAT0205	24	E24	A08	PHM	Usable	11/09/2015	-
GSAT0206	30	E30	A05	PHM	Usable	11/09/2015	-
GSAT0208	08	E08	C07	PHM	Usable	17/12/2015	-
GSAT0209	09	E09	C02	PHM	Usable	17/12/2015	-
GSAT0210	01	E01	A02	PHM	Usable	24/05/2016	-
GSAT0211	02	E02	A06	PHM	Usable	24/05/2016	-
GSAT0207	07	-	C06	-	Under commissioning	17/11/2016	-
GSAT0212	03	-	C08	-	Under commissioning	17/11/2016	-
GSAT0213	04	-	C03	-	Under commissioning	17/11/2016	-
GSAT0214	05	-	C01	-	Under commissioning	17/11/2016	-

Source: https://www.gsc-europa.eu/system-status/Constellation-Information Access on 24/02/2017

The Galileo services will include commercial possibilities mostly to ensure integrity and reliability for secure applications. Such aspects are not necessarily aimed for civil users in the other systems and make Galileo very important for the GNSS positioning certification, especially, for civil aviation industry (United Nations, 2016).

A considerable number of guaranteed services to users equipped with Galileo-compatible receivers are envisaged and some of them are already opened (ESA, 2016). GNSS

markets are getting ready for Galileo constellation improvements and several multi-constellation receivers with the capability to track Galileo signals are already available (ESA, 2016; Sanz Subirana et al., 2013; United Nations, 2016).

5.1.4. BDS

The BDS also called BeiDou-2, is the China's second generation satellite navigation system, which is able to provide positioning navigation and timing services to worldwide users (Sanz Subirana et al., 2013).

The test phase finished in 2003. For the Space Segment more than 30 satellites in orbit transmitting data in three frequencies are expected. The whole system is intended to be complete by around 2020 (Li et al., 2015). BDS Space Segment consists of a constellation of 35 satellites, including 5 Geostationary Earth Orbit (GEO) satellites, 27 MEO satellites and 3 Inclined Geosynchronous Orbits (IGSO). With an inclination of 55 degrees the BDS satellites are evenly deployed in 3 orbital planes. (Sanz Subirana et al., 2013). BDS available satellites up to the redaction of this document are presented in Table 4.

Table 4 – BeiDou constellation status in February 2017

Satellite	NORAD ID	PRN	Launched	Orbit
M1	31115	C30	13/04/2007	MEO period 12.89 hours
G2	34779	N/A	14/04/2009	GEO drifting
G1	36287	C01	16/01/2010	GEO 140° E
G3	36590	C03	02/06/2010	GEO 110.5° E
IGS01	36828	C06	31/07/2010	IGS0 118° E, 55° Incl.
G4	37210	C04	31/10/2010	GEO 160° E
IGS02	37256	C07	17/12/2010	IGS0 118° E, 55° Incl.
IGS03	37784	C08	09/04/2011	IGS0 118° E, 55° Incl.
IGS04	37763	C09	26/07/2011	IGS0 95° E, 55° Incl.
IGS05	37948	C10	01/12/2011	IGS0 95° E, 55° Incl.
G5	38091	C05	24/02/2012	GEO 58.75° E
M3	38250	C11	29/04/2012	MEO slot 1-7
M4	38251	C12	29/04/2012	MEO slot 1-8
M5	38774	C13	18/09/2012	MEO slot 2-3
M6	38775	C14	18/09/2012	MEO slot 2-4
G6	38953	C02	25/10/2012	GEO 80° E
I1-S	40549	C31	30/03/2015	IGS0 95° E, 55° Incl.
M1-S	40748	C33	25/07/2015	MEO slot 1-6
M2-S	40749	C34	25/07/2015	MEO slot 1-1
I2-S	40938	C32	29/09/2015	IGS0 95° E, 55° Incl.
M3-S	41315	-	01/02/2016	MEO slot 2-1
IGS06	41434	C15	29/03/2016	IGS0 95° E, 55° Incl.
G7	41586	-	12/06/2016	GEO 144.5° E

Source: http://mgex.igs.org/IGS_MGEX_Status_BDS.html

The Control Segment consists of a master control station, two upload stations and 30 monitor stations. The Users Segment is expected to be very similar to all other GNSS for the open service. In December 2011, BDS was announced to provide initial operational services for the whole Asia-Pacific area.

5.2. GNSS basic observables

The basic GNSS observables are the pseudorange and phase measurements. The first one is basically a measure of time converted in distance between satellite and receiver, obtained without correction of the synchronization errors between their clocks, which justifies the nomenclature "pseudo". The pseudoranges commonly referred as code or even group measurements, in meters, at a given frequency *i* can be expressed as (1)

$$P_i = \rho + c[dt_r - dt^s] + T + I_i + M_{P_i} + b_{r,P_i} - b^s_{P_i} + \varepsilon_{P_i} \quad (1)$$

where:

- P_i is the pseudorange measurement at carrier frequency *i*,
- ρ is the geometric distance, in meters, between the satellite and receiver Antenna Phase Centers (APCs) at the emission and reception time, respectively, including the relativistic path corrections and Sagnac effect[1].
- c represents the speed of light in vacuum, in m/s,
- dt_r and dt^s are the receiver and satellite clock offsets, in seconds, from the GPS time scale, respectively, including the relativistic satellite clock correction,
- I_i is the slant ionospheric effect, in meters, at frequency i ,
- T is the slant tropospheric delay, in meters,
- M_{P_i} is the effect of multipath on pseudoranges, in meters, at frequency *i*,
- b_{r,P_i} is the receiver instrumental bias, in meters, for pseudoranges at frequency *i*,
- $b^s_{P_i}$ is the satellite instrumental bias, in meters, for pseudoranges at frequency *i*, and
- ε_{P_i} is the code measurement error, in meters.

Most of the errors present in the pseudorange measurements are illustrated in Figure 1 with an approximated order of magnitude (except the multipath effect).

[1] The Sagnac effect is a phenomenon provoked by rotation reference frames (e.g. Earth) in electromagnetic signals. For the case of the GNSS signals this effect is about 30 m (Sanz Subirana et al., 2013).

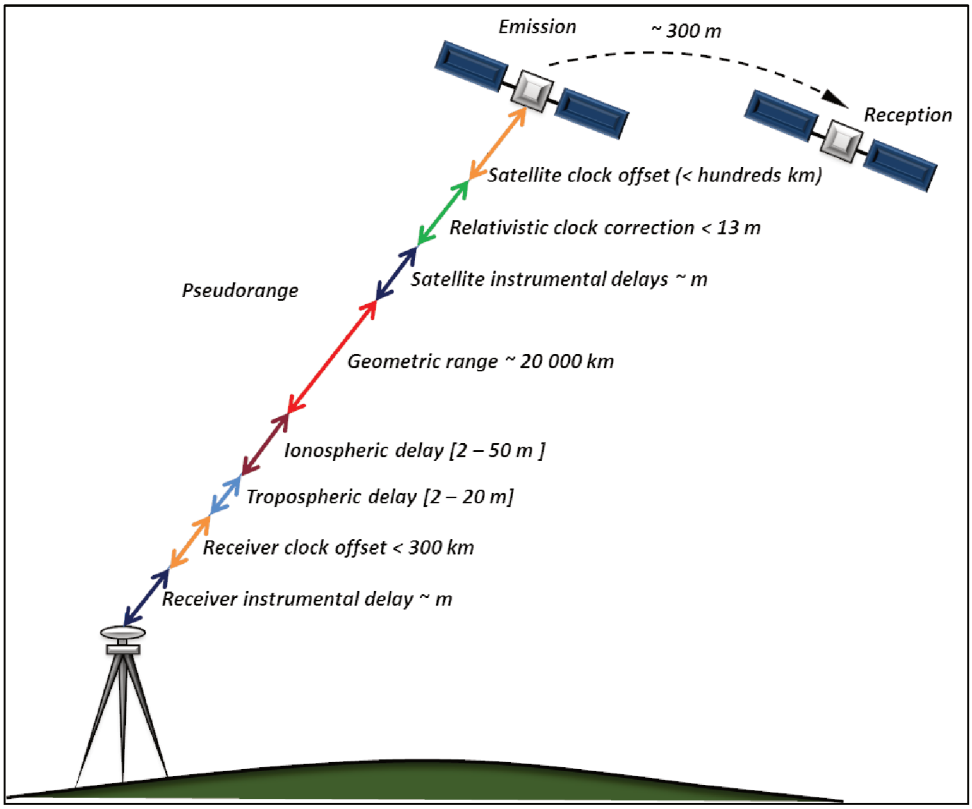

Figure 1 – GNSS Measurements Modelling
Source: adapted from (Sanz Subirana et al., 2013)

The second GNSS basic observable is the phase measurement, also known as carrier-phase which has much higher precision than pseudorange. Phase measurements have precision at the millimeter range while code ranges are at the meter level (Hofmann-Wellenhof et al., 2008). The phase (L_i) in meters can be given by the equation (2):

$$L_i = \rho + c[dt_r - dt^s] + T - I_i + M_{L_i} + \lambda_i W + \lambda_i N_i + b_{r,L_i} - b^s_{L_i} + \varepsilon_{L_i} \qquad (2)$$

where:

- λ_i is the signal frequency wavelength at the carrier frequency i, in meters, and $\lambda_i = c/f_i$,
- N_i is the phase ambiguity at frequency i (in number of cycles),
- M_{L_i} is multipath on phase observables, in meters, at frequency i ,
- W is the contribution of the wind-up effect (in number of cycles),
- b_{r,L_i} is the receiver instrumental bias for phase measurements, in meters, at frequency i,
- $b^s_{L_i}$ is the satellite instrumental bias for phase measurements, in meters, at frequency i,
- ε_{L_i} is the carrier phase measurement error, in meters.

It is important to state that the ambiguity parameter (N_i) infers a harder processing strategy for phase measurements due to the need of resolving that parameter.

The instrumental biases present in code ($b_{r,P_i}, b^s_{P_i}$) and phase ($b_{r,L_i}, b^s_{L_i}$) measurements are commonly referred in the literature as hardware delays, uncalibrated delays, uncalibrated biases, or simply biases.

The phase wind-up effect (W) is caused by the phase advance and delay provoked by the relative rotation between the receiver and satellite antennas. (Wu et al., 1992) presents the most known description on how to account for this effect.

For centimeter-level accuracy, code and carrier phase measurements need to take into account some additional quantities neglected in equations (1) and (2) for simplicity:

- The antenna PCO (Phase Center Offset), defined as the relative position of the antenna phase center with respect to the ARP (Antenna Reference Point), as well as the antenna PCV (Phase Center Variation), that is the excess phase delay of the antenna depending on the satellite elevation and azimuth angle. The PCO and PCV for several antenna types have been calibrated and provided by the IGS for user's community in standard formats (ANTEX – ANTenna EXchange format).

- All tides causing displacements of station antenna. Main ones are solid, ocean, and polar tides but they can be completed by the use of atmospheric tides. They are all documented in IERS conventions (Petit and Luzum, 2010).

Furthermore, the above described observables are employed in most of GNSS applications, according to the required accuracy and parameters to be estimated. Relying on the application context, they are modeled differently and often combinations between frequencies or observables are performed to achieve the expected outcomes. The combinations of interest in this work are detailed in next section.

.

5.3. Combinations between observables

Several combinations between the GNSS observables have been developed to minimize or better estimate specific quantities. Besides, GNSS processing using two or more frequencies is usually accomplished by using combined observables, with regard to the particular advantage or characteristic of each combination.

For all the combinations presented in this section, the reader can consider a single station and a single satellite tracked at a single epoch.

5.3.1. Ionospheric-free linear combination

One of the most important combinations is the ionospheric-free, commonly referred as iono-free. This combination considerably removes the first order ionospheric effect, up-to 99.9%, which is frequency dependent. The remaining 0.1% of ionospheric refraction affecting the measurements corresponds to only a few centimeters or even less. More details about first and higher order ionospheric effects are presented in section 7.2.1. Thanks to the mitigation of ionospheric effects, the ionospheric-free combination is commonly used for high precision positioning, like relative positioning with long baselines and PPP (Seeber, 2003).

In units of meters, the iono-free for code (P_{IF}) and phase (L_{IF}) observables, are given by equations (3) and (4), respectively (Sanz Subirana et al., 2013).

$$P_{IF} = \frac{f_1^2 P_1 - f_2^2 P_2}{f_1^2 - f_2^2} = \alpha_{IF} P_1 + \beta_{IF} P_2 \quad (3)$$

$$L_{IF} = \frac{f_1^2 L_1 - f_2^2 L_2}{f_1^2 - f_2^2} = \alpha_{IF} L_1 + \beta_{IF} L_2 \quad (4)$$

where $\alpha_{IF} = \frac{f_1^2}{f_1^2 - f_2^2}$ and $\beta_{IF} = -\frac{f_2^2}{f_1^2 - f_2^2}$.

It is important to state that for GNSS positioning using code and phase ionospheric free observables the so-called Timing Group Delays (TGDs) are also cancelled in the combination, and thus no longer needed, since the satellite clocks (by convention) refer to the L_1-L_2 iono-free combination (Laurichesse, 2008; Sanz Subirana et al., 2013).

5.3.2. Geometric-free linear combination

The geometric-free is another important combination. It is expressed by equation (5) for pseudorange measurement (P_{GF}), and by equation (6) for phase (L_{GF}), both in meters.

$$P_{GF} = P_2 - P_1 \tag{5}$$

$$L_{GF} = L_1 - L_2 \tag{6}$$

This combination removes geometry, including clocks, and all non-dispersive effects in the signal. It contains ionospheric delays and all kind of bias that are frequency-dependents (hardware biases, cycle slips, and ambiguities). Depending of ionospheric refraction, it can present small changes between close epochs. Thus, the geometry-free combination can be applied to realize analysis about the quality of the GNSS data, allowing reliable cycle slip and multipath detection (Hofmann-Wellenhof et al., 2008; Sanz Subirana et al., 2013).

5.3.3. Wide-lane and Narrow-lane linear combinations

The Wide-lane (WL) combinations, here given in meters, by equations (7) and (8), are used to create measurements with a significantly wide wavelength (λ_{WL} ≈86.2 cm).

$$P_{WL} = \frac{f_1 P_1 - f_2 P_2}{f_1 - f_2} = \alpha_{WL} P_1 + \beta_{WL} P_2 \tag{7}$$

$$L_{WL} = \frac{f_1 L_1 - f_2 L_2}{f_1 - f_2} = \alpha_{WL} L_1 + \beta_{WL} L_2 \tag{8}$$

Considering: $\alpha_{WL} = \frac{f_1}{f_1 - f_2}$ and $\beta_{WL} = -\frac{f_2}{f_1 - f_2}$, the WL wavelength is given by:

$$\lambda_{WL} = \frac{c}{f_1 - f_2} \tag{9}$$

The large wavelength of the Wide-lane combination is useful for ambiguity resolution algorithms, as well as cycle-slip and outliers detection. Although it is important to emphasize that errors present in the original observables are also amplified.

Equations (10) and (11) present the Narrow-lane (NL) combinations. In opposition to wide-lane combinations, this combination produces measurements with a narrow wavelength (λ_{NL} ≈10.7 cm) as its name suggests.

$$P_{NL} = \frac{f_1 P_1 + f_2 P_2}{f_1 + f_2} = \alpha_{NL} P_1 + \beta_{NL} P_2 \tag{10}$$

$$L_{NL} = \frac{f_1 L_1 + f_2 L_2}{f_1 + f_2} = \alpha_{NL} L_1 + \beta_{NL} L_2 \tag{11}$$

Considering $\alpha_{NL} = \frac{f_1}{f_1+f_2}$ and $\beta_{NL} = \frac{f_2}{f_1+f_2}$, NL wavelength is:

$$\lambda_{NL} = \frac{c}{f_1 + f_2} \tag{12}$$

The NL combinations have a lower error than the original observables used to generate them. Therefore, they can provide great accuracy-level results in GNSS processing, however the narrow wavelength turns ambiguity resolution harder in comparison to other combination. Further details about the use of Narrow-lane combinations for ambiguity resolution are discussed in chapter 6.

Considering the relevance of WL and NL combinations for the ambiguity resolution topic, their resulting wavelength are summarized in Table 5, for the GPS, GLONASS, Galileo and BDS systems, considering possibilities with three frequencies. The observables composing the combinations are assumed to be equally accurate and uncorrelated.

Table 5 – Wide-lane and Narrow-lane combinations of signals for different frequencies of GPS, GLONASS (channel k=0), Galileo (E5 and E6 signals not included for simplification purposes), and BDS.

System	Signal	Frequency (MHz)	Wavelength λ_i(m)	Signals combined	Wide-lane λ_W (m)	Narrow-lane λ_N (m)
	i	f_i	$\lambda_i = c/f_i$	ij	$c/(f_i - f_j)$	$c/(f_i + f_j)$
GPS	L_1	1575.420	0.190	L_1,L_2	0.862	0.107
	L_2	1227.600	0.244	L_1,L_5	0.751	0.109
	L_5	1176.450	0.255	L_2,L_5	5.861	0.125
GLONASS ($k = 0$)	G_1	1602.000	0.187	G_1,G_2	0.842	0.105
	G_2	1246.000	0.241	G_1,G_3	0.760	0.107
	G_3	1204.704	0.249	G_2,G_3	7.827	0.122
Galileo	E_1	1575.420	0.190	E_1,E_{5b}	0.814	0.108
	E_{5b}	1207.140	0.248	E_1,E_{5a}	0.751	0.109
	E_{5a}	1176.450	0.255	E_{5b},E_{5a}	9.768	0.126
BDS	B_1	1561.098	0.192	B_1B_3	1.024	0.105
	B_3	1268.520	0.236	B_1B_2	0.846	0.108
	B_2	1207.140	0.248	B_3B_2	4.884	0.121

Source: Adapted from Sanz Subirana et al. (2013).

5.3.4. Melbourne-Wübbena linear combination

Another very useful combination is the Melbourne-Wübbena (MW) combination, which is composed by phase and code measurements (Wübbena, 1985). The combination, in meters, can be expressed as:

$$L_{MW} = \frac{1}{f_1 - f_2}(f_1 L_1 - f_2 L_2) - \frac{1}{f_1 + f_2}(f_1 P_1 + f_2 P_2) = L_{WL} + P_{NL} \quad (13)$$

The MW combination mitigates ionospheric effects, geometry, clocks and tropospheric delays. This combination is very useful for cycle-slips detection and ambiguity resolution algorithms.

Many other combinations are described in GNSS literature, each one aiming the solution of a particular problem. Considering the modernization of some GNSS constellations with the third frequency, a large number of possible linear combinations become feasible, and

they will certainly improve GNSS data processing, especially ambiguity resolution (Liu and Gao, 2017).

5.4. Single station GNSS positioning

The basic principle of navigation by GNSS consists of measuring pseudo-distances between user and at least four satellites. With the knowledge of the satellite coordinates in a well-defined reference system, it is possible to compute the coordinates of the user antenna in the same system. From a geometrical point of view, only three satellites would be enough to determine the user position, however, the receiver clock is not synchronized with the satellites system clock (e.g. GPS time, GLONASS time, …), which requires a fourth observation to solve the equation system. Thus, the objective is to obtain the receiver coordinates $r = (x, y, z)$ and the receiver clock offset $\mathrm{dt_r}$ (Seeber, 2003).

Concerning the positioning methods, a user can have its coordinates determined by zero-difference or differential positioning methods. In the first case, coordinates are directly associated to the referential of satellite ephemerides, on the other hand, in relative positioning, coordinates are determined with respect to a referential materialized by one or more GNSS stations with known coordinates. In this thesis, we focus on zero-differential positioning approaches. Therefore, further details of the method are presented in the next sections.

5.4.1. Code based positioning

This is the method employed to get initial a priori positions at the meter or sub-meter level. Satellites coordinates are computed based on broadcasted satellite ephemerides and it can be performed the so-called point positioning. Positions are determined in the respective GNSS referential, e.g. WGS84 (World Geodetic System 1984) for GPS, PZ90 (*Parametry Zemli* – 1990) for GLONASS and GTRF (Galileo Terrestrial Reference Frame) for Galileo. In case of GPS positioning approach is known as Standard Positioning Service (SPS), which is basically the zero-difference positioning using only pseudorange or pseudorange smoothed by phase measurements (Duquenne et al., 2005; Monico, 2008;

Seeber, 2003). Considering the code pseudorange measurements, equation (1), geometric range between the satellite *s* and the receiver *r* can be expressed as (14) (Sanz Subirana et al., 2013):

$$\rho_r^s(x_r, y_r, z_r) = \sqrt{(x^s - x_r)^2 + (y^s - y_r)^2 + (z^s - z_r)^2} \tag{14}$$

grouping the modeled terms of the equation (1) in the term R_{mod}^s ,

$$R_{mod}^s = -cdt^s + T + \gamma_i I_1 + M_{P_i} + b_{r,P_i} - b_{P_i}^s + \varepsilon_{P_i} \tag{15}$$

every observation equation can be arranged in the form of the equation (16) to compose the equation system.

$$P_i^s - R_{mod}^s \cong \sqrt{(x^s - x_r)^2 + (y^s - y_r)^2 + (z^s - z_r)^2} + cdt_r, \tag{16}$$

where satellite index $s = 1, 2, \dots, n$ $(n \geq 4)$. The left side of equation (16) contains the code measurements (P_i^s) and the modeled terms (R_{mod}^s). However, some terms can be neglected in the modeling strategy regarding the code error. Relevant parameters to estimate are the four unknowns in the equation system, receiver coordinates (x_r, y_r, z_r) and receiver clock offsets (dt_r). Equation (16) defines a non-linear system, that can be solved by linearizing the geometric distance in equation (14), considering an initial approximate receiver position (x_0, y_0, z_0),

$$\rho_r^s(x_r, y_r, z_r) = \rho_0^s + \frac{x_0 - x^s}{\rho_0^s} dx + \frac{y_0 - y^s}{\rho_0^s} dy + \frac{z_0 - z^s}{\rho_0^s} dz \tag{17}$$

where: $dx = x_r - x_0$, $dy = y_r - y_0$ and $dz = z_r - z_0$.

The new linear system is obtained by substituting equation (17) into equation (16):

$$P_{i,r}^s - \rho_0^s - R_{mod}^s = \frac{x_0 - x^s}{\rho_0^s} dx + \frac{y_0 - y^s}{\rho_0^s} dy + \frac{z_0 - z^s}{\rho_0^j} dz + cdt_r \tag{18}$$

with: $s = 1,2, \dots, n$ $(n \geq 4)$

Thanks to an over-dimensioned number of observables ($n > 4$), the system can be solved using the Least Squares adjustment (Duquenne et al., 2005; Monico, 2008).

5.4.2. Precise Point Positioning

PPP is the zero-difference positioning when both pseudorange and phase measurements are employed together with precise information on orbit and satellite clocks information (precise ephemerides) (Zumberge et al., 1997). Currently, the IGS (International GNSS Service) and its analyses centers provide these products for worldwide users free of charge. According to the IGS web-page, the quality of the precise ephemeris, as well as the satellite clock corrections are those presented in Table 6.

Table 6 – Properties of IGS GPS and GLONASS products

Product	Accuracy Position/Clock	Latency	Interval Position/Clock
Ultra-rapid (predicted)	~5 cm / ~3ns	Real-time	15 min
Ultra-rapid (observed)	~3 cm / ~150ps	6 h	15 min
Rapid	~2.5 cm / 75ps	24 h	15 min / 5 min
Final	~2.5 cm / 75ps	12 to 18 days	15 min / 30 s
Final for GLONASS	~3 cm	12 to 18 days	15 min

(Source: http://igscb.jpl.nasa.gov/components/prods.html - access in 15 January of 2017)

A key point is the infrastructure needed to produce precise ephemerides and satellite clock corrections. A global GNSS network used as reference must be available. Therefore, PPP can be considered as a combination of “natural” zero-difference positioning and differential positioning methods, given that PPP uses phase observations data of a single receiver and additionally state information on individual GNSS errors derived from the global GNSS network (Wübbena et al., 2005).

5.4.2.1. PPP observation model

PPP can use dual-frequency data and single frequency as well. For dual-frequency data, ionospheric-free observables are frequently used in the literature, mainly because ionospheric effects are mitigated and because satellite clocks are by convention consistent

with iono-free code measurements. Detailed iono-free combinations are presented in equations (19) and (20).

$$P_{IF} = \rho + c[dt_r - dt^s] + T_0 + T_c + M_{P_{IF}} + b_{r,P_{IF}} - b^s_{P_{IF}} + \varepsilon_{P_{IF}} \quad (19)$$

$$L_{IF} = \rho + c[dt_r - dt^s] + T_0 + T_c + M_{L_{IF}} + \lambda_{IF} N_{IF} + b_{r,L_{IF}} - b^s_{L_{IF}} + \varepsilon_{L_{IF}} \quad (20)$$

where:

- N_{IF} is the ambiguity of the observable ionospheric-free (real number),
- T_0 is the tropospheric delay (a priori) computed by an available tropospheric model,
- T_c represents residual correction for the a priori tropospheric delay (T_0) to be estimated,
- $M_{P_{IF}}$ and $M_{L_{IF}}$ are the multipath effect resultant for the ionospheric-free combinations at code and phase observables,
- λ_{IF} is the ionospheric-free wave-length,
- $b_{r,P_{IF}}$ and $b^s_{P_{IF}}$ are the ionospheric-free code biases, for receiver and satellite, respectively,
- $b_{r,L_{IF}}$ and $b^s_{L_{IF}}$ are the ionospheric-free phase biases, for receiver and satellite, respectively,
- $\varepsilon_{P_{IF}}$ and $\varepsilon_{L_{IF}}$ are code and phase measurement error.

Based on the model presented by equations (19) and (20), it is possible to observe that the parameters to be estimated involve the station coordinates, receiver clock offsets, residuals of tropospheric delays (T_c), which have several possibilities for modeling, and the ambiguities vector composed by the parameters N_{IF} (1 per satellite). When all the errors affecting the GNSS measurements are properly taken into account, it is possible to obtain high accuracy level.

For single frequency PPP (based on L1 observable), it is necessary to input an appropriate ionospheric model. The accuracy of the final results in this case will rely on the ionospheric modeling quality, especially the vertical component (Seeber, 2003). More details

about ionospheric effects are presented in chapter 7.2, and the potential of ionospheric corrections is exploited later in Part III.

5.4.2.2. PPP corrections

In addition to GNSS measurement corrections cited in section 5.2 for the basic GNSS observables, there are other important effects to correct in order to allow PPP method achieving centimeter accuracy, such as the tidal effects and the instrumental inter-frequency biases. Both are briefly described in this section.

5.4.2.2.1. Tidal effects

The Earth is subjected to gravitational forces (mainly Sun and Moon), which involve crustal displacements. These displacements can reach up to some decimeters and are referred as the effect of Solid earth tide. Simultaneously, water masses are also affected by gravitational forces, thus oceans produce loading on the crust as well. This effect also must be accounted and is called Ocean Tide Loading (OTL) effect. It varies from one area to another being the highest in coastal areas ,especially in Brittany (Fund, 2009).

According to accuracy level desired, GNSS processing can require corrections for atmospheric tidal loading. These tidal effects are well-known and are routinely taken into account in precise GNSS data analysis (Ferenc, 2014). More details about the modeling of these effects can be found in IERS (International Earth Rotation and Reference System) Conventions (Petit and Luzum, 2010). About OTL, a service widely used by the geodetic community to compute displacements induced by the 11 main loading waves at a specific location is available at http://www.oso.chalmers.se/~loading/.

5.4.2.2.2. Satellite code biases

Another essential aspect is the correction of inter-frequency instrumental biases, affecting code and phase measurements. These biases have satellite and receiver contributions. Satellite component of code biases is calibrated during the satellite's phase tests

and transmitted in the broadcast messages. These biases are referenced, by definition, to the iono-free pseudorange observable (Wilson et al., 1999). Therefore, the code biases corrections suppose combined observations compatible with iono-free based PPP. A possible transition to an uncombined model is presented in section 6.2.3.

Historically, it was observed discrepancies between broadcasted and estimated values of satellite code biases, indicating that instrumental biases change with time. This fact motivated organizations such as IGS and its analysis centers (e.g. JPL and CODE - Center for Orbit Determination in Europe) to generate and deliver estimated code biases. Satellite Differential Code Biases (DCBs) estimations are routinely realized, as a by-product of mapping the ionosphere using data from global IGS network (Wilson et al., 1999). Once satellite component of code biases is corrected using DCBs, the receiver contribution still remains. This contribution can be estimated or corrected; otherwise it will be absorbed by other parameters such as receiver clock (Hofmann-Wellenhof et al., 2008).

No corrections for phase biases are broadcast nor delivered by IGS. Under the assumption they are not null, they are absorbed by the iono-free ambiguity parameter. Further discussions about existing phase biases products as well as methods to solve ambiguities to integer values are presented in chapter 6.

5.4.2.3. PPP parameters estimation

The previously mentioned PPP parameters may be estimated by least squares adjustment, since it assumed redundancy of observations in the equations system. One possibility is the EKF (Extended Kalman Filter) also known as nonlinear version of the Kalman filter (Gelb, 1974; Kalman, 1960). Indeed the EKF has been considered one standard in navigation systems theory estimation (Fund et al., 2013; Julier and Uhlmann, 2004; Marques, 2012). Thus the explanation here will focus on EKF application in order to estimate the PPP parameters. In such a case, considering the observation of m satellites at the receiver r, the unknown state vector (X), when using undifferenced iono-free measurements, can be settled as:

$$X = \begin{bmatrix} dx \\ dy \\ dz \\ cdt \\ T_c \\ N_{IF}^1 \\ N_{IF}^2 \\ \vdots \\ N_{IF}^m \end{bmatrix} \tag{21}$$

The measurement vector (Y), considering phase and pseudorange observables is given by:

$$Y = \begin{bmatrix} L_{IF}^1 \\ L_{IF}^2 \\ \vdots \\ L_{IF}^m \\ P_{IF}^1 \\ P_{IF}^2 \\ \vdots \\ P_{IF}^m \end{bmatrix} \tag{22}$$

Since the measurement errors ($\varepsilon_{L_{IF}}$ and $\varepsilon_{P_{IF}}$), multipath effects ($M_{P_{IF}}$ and $M_{P_{IF}}$), as well as the measurement biases are not taken into account in the model, they will not be included in the measurement model vector $h(x)$, which can be expressed as:

$$h(x) = \begin{bmatrix} \rho + c[dt_r - dt^{s_1}] + T_c^1 + \lambda_{IF} N_{IF}^1 \\ \rho + c[dt_r - dt^{s_2}] + T_c^2 + \lambda_{IF} N_{IF}^2 \\ \vdots \\ \rho + c[dt_r - dt^{s_m}] + T_c^m + \lambda_{IF} N_{IF}^m \\ \rho + c[dt_r - dt^{s_1}] + T_c^1 \\ \rho + c[dt_r - dt^{s_2}] + T_c^2 \\ \vdots \\ \rho + c[dt_r - dt^{s_m}] + T_c^m \end{bmatrix} \tag{23}$$

Other parameters (e.g. tropospheric gradients) can also be added to the model of equation (23), depending on desired user's application. If GPS+GLONASS observations are included, for example, two parameters corresponding to receiver clock offsets will be estimated, since there are as many receiver clock offsets, as GNSS systems included in observation equations. Ambiguities expressed in (23) are affected by remaining biases not

included in the present modeling, so ambiguities estimated with that equations have a real-nature. PPP enabling solving integer ambiguities is the subject of next chapter.

The design matrix, $A(x)$, also known as matrix of partial derivatives or Jacobian matrix is given by:

$$A(x) = \begin{bmatrix} \frac{\partial L_{IF}^1}{\partial X_r} & \frac{\partial L_{IF}^1}{\partial Y_r} & \frac{\partial L_{IF}^1}{\partial Z_r} & \frac{\partial L_{IF}^1}{\partial dt_r} & \frac{\partial L_{IF}^1}{\partial T_c^1} & \frac{\partial L_{IF}^1}{\partial N_{IF}} & 0 & 0 & \cdots & 0 \\ \frac{\partial L_{IF}^2}{\partial X_r} & \frac{\partial L_{IF}^2}{\partial Y_r} & \frac{\partial L_{IF}^2}{\partial Z_r} & \frac{\partial L_{IF}^2}{\partial dt_r} & \frac{\partial L_{IF}^2}{\partial T_c^2} & 0 & \frac{\partial L_{IF}^2}{\partial N_{IF}} & 0 & \cdots & 0 \\ \vdots & \vdots & \vdots & \vdots & \vdots & \vdots & \vdots & \vdots & \ddots & 0 \\ \frac{\partial L_{IF}^m}{\partial X_r} & \frac{\partial L_{IF}^m}{\partial Y_r} & \frac{\partial L_{IF}^m}{\partial Z_r} & \frac{\partial L_{IF}^m}{\partial dt_r} & \frac{\partial L_{IF}^m}{\partial T_c^m} & 0 & 0 & 0 & \cdots & \frac{\partial L_{IF}^m}{\partial N_{IF}} \\ \frac{\partial P_{IF}^1}{\partial X_r} & \frac{\partial P_{IF}^1}{\partial Y_r} & \frac{\partial P_{IF}^1}{\partial Z_r} & \frac{\partial P_{IF}^1}{\partial dt_r} & \frac{\partial P_{IF}^1}{\partial T_c^1} & 0 & 0 & 0 & \cdots & 0 \\ \frac{\partial P_{IF}^2}{\partial X_r} & \frac{\partial P_{IF}^2}{\partial Y_r} & \frac{\partial P_{IF}^2}{\partial Z_r} & \frac{\partial P_{IF}^2}{\partial dt_r} & \frac{\partial P_{IF}^2}{\partial T_c^2} & 0 & 0 & 0 & \cdots & 0 \\ \vdots & \vdots & \vdots & \vdots & \vdots & \vdots & \vdots & \vdots & \ddots & 0 \\ \frac{\partial P_{IF}^m}{\partial X_r} & \frac{\partial P_{IF}^m}{\partial Y_r} & \frac{\partial P_{IF}^m}{\partial Z_r} & \frac{\partial P_{IF}^m}{\partial dt_r} & \frac{\partial P_{IF}^m}{\partial T_c^{1m}} & 0 & 0 & 0 & \cdots & 0 \end{bmatrix} \quad (24)$$

PPP functional model can also use between-satellite Single-Differences (SDs) as input observations, by setting a pivot satellite. Such algorithms can select the satellite with maximum elevation angle as pivot. The between-satellite SDs cancel out some receiver-related biases, including receiver clock offsets (dt_r).

Matrix of observations variances/covariances (Σ_{Y_k}) is built with the measurements variances. Since the observables are iono-free combinations, their covariances can be computed thanks to the propagation of variances.

$$\Sigma_{Y_k} = \begin{bmatrix} {\sigma_{L_{IF}^1}}^2 & & & & & & & \\ & {\sigma_{L_{IF}^2}}^2 & & & & & \mathbf{0} & \\ & & \ddots & & & & & \\ & & & {\sigma_{L_{IF}^m}}^2 & & & & \\ & & & & {\sigma_{P_{IF}^1}}^2 & & & \\ & & & & & {\sigma_{P_{IF}^2}}^2 & & \\ & \mathbf{0} & & & & & \ddots & \\ & & & & & & & {\sigma_{P_{IF}^m}}^2 \end{bmatrix} \quad (25)$$

The Kalman filter consists of a combination between prediction and filtering (Gelb, 1974; Kalman, 1960). The filtering step is commonly referred as correction or update step.

In the filtering step, the updated state vector at epoch k ($\hat{X}_{k(+)}$) and its covariance matrix ($\Sigma_{\hat{X}_{k(+)}}$) can be obtained as follows:

$$\hat{X}_{k(+)} = \hat{X}_{k(-)} + K_k \left(Y_k - h_{\hat{X}_{k(-)}} \right) \tag{26}$$

$$\Sigma_{\hat{X}_{k(+)}} = \left(I_n - K_k A_{\hat{X}_{k(-)}} \right) \Sigma_{k(-)} \tag{27}$$

The symbols $(-)$ and $(+)$ indicate if matrix are predicted and or updated. K_k is the Kalman gain matrix, which can be computed by:

$$K_k = \Sigma_{\hat{X}_{k(-)}} A^T_{\hat{X}_{k(-)}} \left(A_{\hat{X}_{k(-)}} \Sigma_{\hat{X}_{k(-)}} A^T_{\hat{X}_{k(-)}} + \Sigma_{Y_k} \right)^{-1} \tag{28}$$

Prediction (or propagation) step of state vector and its covariance matrix at previous epoch are expressed, respectively, as:

$$\hat{X}_{k+1(-)} = F_k^{k+1} \hat{X}_{k(+)} \tag{29}$$

$$\Sigma_{\hat{X}_{k+1(-)}} = F_k^{k+1} \Sigma_{\hat{X}_{k(+)}} \left[F_k^{(k+1)} \right]^T + \Sigma_{W_k}^{k+1} \tag{30}$$

In these equations, F_k^{k+1}stands for the transition matrix and $\Sigma_{W_k}^{k+1}$ is the covariance matrix of the system error.

According to the positioning mode established (e.g. kinematic or static), the EKF Time Update must be settled differently. Indeed, in RTKLIB package (section 5.4.5.1) one of engines used in this thesis, when kinematic positioning is performed the transition matrix ($\mathrm{F_k^{k+1}}$) and the covariance matrix of the system noise ($\Sigma_{W_k}^{k+1}$) from epoch time $\mathrm{t_k}$ to $\mathrm{t_{k+1}}$ are given by:

$$F_k^{k+1} = \begin{bmatrix} I_{n_{(3\times3)}} & & & \mathbf{0} \\ & 1 & & \\ & & 1 & \\ \mathbf{0} & & & I_{n\,(m\times m)} \end{bmatrix} \tag{31}$$

and:

$$\Sigma_{W_k}^{k+1} = \begin{bmatrix} \infty_{(3\times3)} & & \mathbf{0} \\ & 0 & \\ & & 0 \\ \mathbf{0} & & 0_{(m\times m)} \end{bmatrix} \quad (32)$$

To avoid numerical instability when adding infinite process noises to positions variances for kinematic positioning, receiver position states are reset every epoch to the initial guess values (derived from SPS section 5.4.1) and larger process noises (e.g. $10^4 m^2$) are added to the variance instead of $\infty_{(3\times3)}$. On the other hand, if static positioning is realized the infinite process noises of the matrix presented in (32) are set to $0_{(3\times3)}$.

Once the presented sequence is finished, an estimation of PPP parameters is available. In case of post processing, EKF can be conducted in forward and backward pass directions. This characterizes a smoothing process to extend accurate results to all epochs processed. The forward pass is the regular EKF presented above. In the backward pass, the smoothed states estimation based on all the measurements, is computed starting from the last time step and following backwards in time using recursive equations. Further explanations on backward pass can be found in (Gelb, 1974). Since the main interest in this thesis is real-time positioning, only forward passes are considered.

5.4.3. Real-Time PPP

Historically, JPL has delivered a real-time PPP service since the beginning of the last decade (Gao and Chen, 2004). Even if that service is nominated GDGPS (Global Differential GPS), data processing is accomplished as point positioning. Accuracy of such service is announced to be 10 cm after solution convergence, which takes more than 30 min depending on satellites geometry and site conditions.

Nowadays, there are several private and public initiatives to support real-time PPP. The most important public effort is the IGS Real-time Service (RTS). Through a subscription, users have access to RTS as a public service. At a worldwide scale, RTS provides GNSS orbit and clock corrections enabling PPP and related applications (e.g. synchronization and disaster monitoring) in real-time. The service uses the IGS global

network of stations, data and analysis centers. Currently GPS-only corrections are officially available. However experimental products including GLONASS are already provided as well. Other GNSS constellations will be added as soon as they become available.

Main actors of RTS are NRCan (Natural Resources Canada), BKG (*Bundesamt für Kartographie und Geodäsie* - German Federal Agency for Cartography and Geodesy) and ESA/ESOC (European Space Agency/European Space Operations Centre). Approximately 160 stations operators around the world, together with 10 IGS analysis centers, are fundamental for the RTS continuity as well.

Aside from the RTS, other initiatives for demonstration or didactic purposes have been freely available for real-time PPP users. The CNES real-time analysis center, throughout the PPP-Wizard project broadcasts phase biases on the CLK93 stream since 2014/09/14. These biases are compatible with the PPP ambiguity resolution method described in section 6.2.3. Most of these corrections/products are integrated in the RTCM standards for SSR corrections (c.f. section 5.5.2).

The private supports for real-time PPP are increasing considerably. There are several commercial services providing differential GPS/GNSS corrections, also referred as GPS/GNSS augmentation, with complementary real-time PPP solutions. Target markets are industries of precise agriculture, exploration, production of hydrocarbons, and many other real-time applications that require centimeter or decimeter accuracy. For instance, we can mention important available services (Morel, 2015; Morel et al., 2014) :

- Omnistar XP and G2 (http://www.omnistar.com/),
- C-Nav (1 e 2) of C&C Technology (http://cnavgnss.com/site.php),
- Starfire of Navcom (http://www.navcomtech.com),
- Starfix of Fugro (http://starfix.com),
- PPP-RTK of Nexteq Navigation (http://www.nexteqnav.com),
- Trimble CenterPointRTX (https://www.trimble.com/positioning-services),
- Apex2 and Ultra2 from Veripos (http:// www.veripos.com),
- TerraStar correction services (www.terrastar.net) from NovAtel.

These services are based on global permanent networks they own or not. Announced horizontal accuracies are under decimeter or centimeter. For centimeter accuracy-level, the time required for solution's convergence is at least 5 min.

In particular, the Trimble's CenterPointRTX service counts with global and also regional networks augmentation in USA and many European countries, including France. Thus, this service offers a considerably improved convergence up to 1 ~ 2 min, in such regions depending on observing conditions.

5.4.4. PPP with integer ambiguity resolution and PPP-RTK: definitions considered in this work

In GNSS literature, PPP method with integer ambiguity resolution has been referred with different acronyms. Most current ones are 'PPP-AR' for 'PPP with Ambiguity Resolution' (Collins et al., 2010; Laurichesse, 2008; Mervart et al., 2013); 'IPPP' referring to 'Integer PPP' (Fund et al., 2013; Perosanz et al., 2016; Petit et al., 2014) and 'PPP-RTK' (Geng et al., 2011; Teunissen and Khodabandeh, 2015). The lack of standard terms can, sometimes, make the reading difficult.

An excellent theoretical description and comparison of various integer ambiguity resolution methods for PPP is presented by Khodabandeh and Teunissen, 2016. In this contribution the authors consider PPP-RTK as PPP with integer ambiguity resolution enabled thanks to satellite phase biases, which allow recovering the integerness of ambiguities, thus reducing solution convergence time in comparison with standard PPP. However, Wübbena et al. (2005) is, in our knowledge, the first work using PPP-RTK term to describe the method as PPP with centimeter-level accuracy and fast convergence through integer ambiguity resolution and atmospheric corrections from RTK networks. In this case, improved convergence time is promoted not only with the benefit of phase biases corrections, but also thanks to RTK networks providing atmospheric corrections, leading to the so-called PPP-RTK (Stürze et al., 2012; Wübbena et al., 2014).

Mervart et al. (2013) call PPP with integer ambiguity resolution improved with atmospheric corrections as 'PPPFAR' (PPP with Fast Ambiguity Resolution). Li et al (2014) propose also a strategy to perform PPP with fast ambiguity fixing using regional atmospheric

corrections based on GNSS data. It is called “PPP-RA” (PPP-Regional Augmentation). Rovira-Garcia et al. (2015) use ‘Fast-PPP’ when referring to PPP with integer ambiguity resolution, and improved convergence time using ionospheric corrections.

In this work, we denote post-processing PPP with integer ambiguity resolution enabled by phase biases products as ‘IPPP’. For Real-Time Integer PPP, the acronym ‘RT-IPPP’ is used. Additionally, we use ‘PPP-RTK’ for integer PPP improved by atmospheric corrections from local/regional RTK networks, as in Wübbena et al. (2005). However, when ambiguities are not fixed, and atmospheric corrections are still used to improve float PPP, we employ the acronym “float PPP-RTK”. The Table 7 summarizes the meanings of the acronyms adopted in this thesis.

Table 7 – Meanings corresponding to acronyms adopted in this thesis report in order to distinguish the different PPP approaches.

Acronym/Term	Meaning
PPP	Post-processing PPP with float ambiguities
RT-PPP	Real-time PPP with float ambiguities
IPPP	Post-processing PPP with integer ambiguities
RT-IPPP	Real-time PPP with integer ambiguities
float PPP-RTK	Real-time PPP with float ambiguities and atmospheric corrections from RTK networks
PPP-RTK	Real-time PPP with integer ambiguities and atmospheric corrections from RTK networks

A discussion about RT-IPPP models is presented in chapter 6. Methodology and results for float PPP-RTK, as well as PPP-RTK enabled by atmospheric corrections implemented in this work are described in Part II and III, respectively.

5.4.5. Open source solutions available for RT-PPP and RT-IPPP

Computer software with its source code available is considered Open-source software. In general, a software is available with a license in which the copyright owner provides the rights for studies, changes and even to distribute under specific conditions (St. Laurent, 2008).

In this research two main Open-source initiatives involving real-time PPP have been exploited. First one is the RTKLIB (www.RTKLib.com), which is an open source program package for GNSS positioning. Second one is the PPP-Wizard (Precise Point Positioning With Integer and Zero-difference Ambiguity Resolution Demonstrator) a demonstrator 'proof of concept' dedicated to zero-difference ambiguity resolution method developed in the orbit determination service at CNES (www.ppp-wizard.net). Further details about both programs are discussed in the following sections.

5.4.5.1. RTKLIB

The purpose of the RTKLIB package is to perform standard and precise GNSS positioning. It can be used in real-time and post-processing and allows either relative or absolute positioning. RTKLIB package runs with a GUI on Windows and some modules run with command lines on both Windows and Linux. With geodetic receivers and antennas, centimeter accuracy is achievable (Takasu, 2013).

One interesting point of RTKLIB package is its license. It is distributed under the BSD 2-clause license with some additional clauses (Annex 1). In this case, users are permitted to develop, produce and even sell their own non-commercial or commercial products utilizing, linking or including RTKLIB. More details about the BSD style license can be found in (St. Laurent, 2008).

Source code is in C/C++ language, it is quite well commented allowing easy changes. This software can be found in a Version Control Repository, which allows downloading binary files, source files, as well as the complete package to be compiled by developers (https://github.com/tomojitakasu/RTKLIB/tree/RTKLib_2.4.3).

Currently the last available official version of the software is 2.4.2, but in this work we use the RTKLib 2.4.3 beta version because it has substantial improvements and also the corrections of small bugs. IPPP using CNES 'GRG' product is available in this version as well. However, RT-IPPP is not available yet. In this work, RT-PPP with RTKLIB is modified to allow the use of tropospheric corrections, as a priori tropospheric delays. Details about such modifications and achievements are presented in Part II.

5.4.5.2. PPP-Wizard

The PPP software package provided by CNES under the PPP-Wizard project contains the PPP implementation with integer ambiguity resolution at the user side (RT-IPPP). More details are explained in section 6.2.3. Some information about concepts, models as well as the internal structure of the package can be found in (Laurichesse and Privat, 2015). This open-source implementation is provided by the on-line PPP-Wizard demonstrator (http://www.ppp-wizard.net/). This online engine shows real-time results for a couple of stations worldwide, demonstrating centimeter accuracy-level performances.

The demonstrator has three main parts. The first part is the SSR parameters computation (orbit, clock and biases). To generate such products, a global network of real-time GNSS stations is used. This is by far the most complex part of the whole system. The second part is the transmission of the network SSR parameters, which are provided freely by CNES for non-commercial purposes. This part employs the IGS RTS caster. The third part, named PPP monitoring, performs RT-IPPP and compares the results to absolute reference positions. The open-source PPP package is the third part, which is the user side.

Source codes are implemented in C++ language, and use BNC (BKG Ntrip Client) and RTKLIB libraries. Use and modifications are authorized, however only for educational purposes. The terms of the license distributed with the PPP-Wizard version 1.3 are presented in Annex 2.

In the context of this thesis, one interesting feature is the compatibility with regional augmentation, thanks to the use of a specific atmospheric interface. This interface includes tropospheric and ionospheric delays (Laurichesse and Privat, 2015). Here, such

interface was explored and improved to use the tropospheric and ionospheric corrections that we generated (Part III).

At the time of our studies, only GPS and GLONASS data could be processed. Since then, PPP-Wizard has become 'Full-GNSS', because it is able to process GPS, GLONASS, Galileo, and BDS data. It is also able to process L5 GPS signals. The use of new signals is left as prospects.

5.5. State Space Representation

In traditional RTK or NRTK systems, the main errors affecting the GNSS measurements are monitored thanks to a GNSS reference station or a CORS dense network, and provided to the users as range corrections. This OSR (Observation-Space-Representation) approach characterizes the RTK/NRTK corrections services like Orphéon. This approach is used in most of NRTK corrections algorithms such as the widely employed VRS (Virtual Reference Station). However, OSR is not able to dissociate the different errors impacting GNSS measurements (Wübbena et al., 2005).

The State-Space-Modeling (SSM) approach is the representation of all relevant physical effects by a mathematical modeling with parameters that are estimated in real-time using CORS network GNSS observations. With a proper knowledge of temporal and spatial behavior of these effects, it is possible to optimize the use of all observations coming from the CORS network. The state vector of such State-Space-Representation (SSR) is provided by the integrated and optimized SSM. This representation is applicable to PPP-RTK (Wübbena et al., 2014, 2005).

5.5.1. SSR highlights

It is interesting to observe that SSM approach can also provide solutions for classical OSR concept, by converting corrections from SSR to OSR for conventional. Minimized bandwidth, reduced infrastructure requirements are some of advantages of SSM for SSR approach and even for conventional NRTK (Wübbena et al., 2005).

Since different error sources have different behaviors, it is possible to apply separate updating rate for different parameters. For example, the satellite clock offset must be updated every few seconds to ensure centimeter accuracy, whilst the satellite orbits and even the tropospheric and ionospheric delays may vary on longer periods and can be updated with a lower rate. Thus, the SSR based service can improve the transmission rate and resolution in function of the parameter to be modeled, requiring less stream bandwidth (Wübbena et al., 2014, 2005).

Regarding the low-cost industry, it is possible to achieve single frequency users, because the ionospheric effects can be modeled and taken into account by the SSM (Rovira-Garcia et al., 2015; Wübbena et al., 2005).

Thanks to the modeling improvements the inter-distances between reference stations can be increased in comparison to traditional NRTK systems. Another interesting point is that reference stations that do not track all available GNSS signals can still contribute to the final atmospheric modeling (Wübbena et al., 2014, 2005).

5.5.2. RTCM State Space Parameters

The RTCM has established in 2007 a working group in the context of the RTCM's Special Committee 104 (SC104) to develop RTCM-SSR messages to exchange GNSS error states for RT-PPP and RTK (Wübbena et al., 2014). In the development of RTCM-SSR messages, Wübbena et al. 2014 emphasizes three major steps or stages:

- 1st stage, standards for transmission of orbits, satellite clocks and satellite code biases together with quality information. This first step must ensure compatibility with the standard PPP enabled by IGS products, allowing RT-PPP for dual frequency receivers. Since May 2007 such corrections are standardized for GPS and GLONASS.

- 2nd stage enables code-based RT- PPP for single frequency users. Additionally it is intended ambiguity resolution (i.e. RT-IPPP) for dual frequency users by including satellite phase bias information.

- 3rd stage, enables PPP-RTK with the addition of ionospheric slant TEC (Total Electron Contents) and tropospheric messages.

The need for an additional Stage 4 regarding the compression of messages and therefore reducing minimum required bandwidth will also take place (Wübbena et al., 2014).

The Table 23, presented in Annex 3, summarizes the different messages currently standardized, as well as experimental or planed SSR messages in the context of the RTCM's SC104. Important to keep in mind, that such corrections must be applied together with broadcast ephemerides of the respective GNSS constellation (Stürze et al., 2012).

6. Integer ambiguity resolution for PPP

6.1. Phase biases influence

The discussion about instrumental or hardware biases affecting the code and phase observables are presented in section 5.4.2.2.2. Now efforts are concentrated in understanding how phase biases impact integer ambiguity resolution.

When a receiver starts to track a GNSS satellite, it computes the difference between the phase emitted by the satellite, and the one generated in the receiver, at transmission and reception time, respectively. This difference results in the fractional-cycle part, which composes the phase measurement. Then, the receiver starts to count the next phase cycles. However, the initial integer number of cycles between satellite and receiver remains unknown, and must be estimated as a parameter called ambiguity (N) (equation (2)).

Integer ambiguity resolution has been extensively investigated in GNSS literature (Blewitt, 1989; Collins et al., 2010; Geng et al., 2011; Laurichesse, 2008; Teunissen, 1995). Studies show that phase biases are absorbed by phase ambiguities, destroying their integer property (Blewitt, 1989). Thus, phase biases are considered as key parameter to recover integer ambiguities.

Figure 2 illustrates the geometric interpretation of the ambiguity parameter and the phase bias at the initial tracking epoch t_0 and a further one t_1, over a GNSS satellite pass. It is important to keep in mind that phase biases represented in this figure are real-valued, therefore the sum $(N + \text{phase bias})$, is also real-valued. This leads to float ambiguities, if such biases are not properly corrected. The fractional part of this sum $(N + \text{phase bias})$ is also known as Fractional-Cycle Bias (FCB) (Geng et al., 2012), and it is basically the fractional part of the bias, which makes the sum to be real-valued.

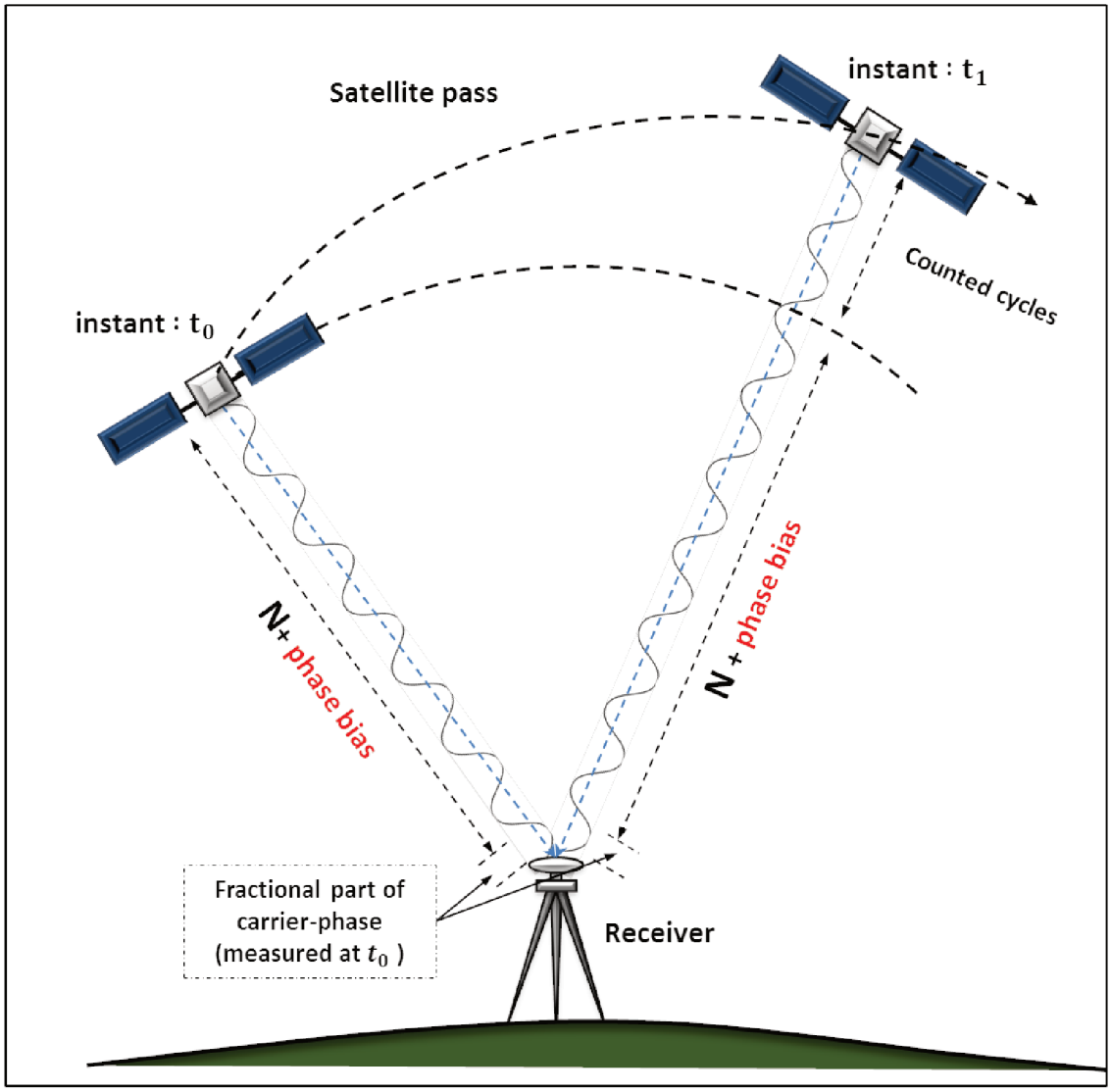

Figure 2 – Geometric interpretation of ambiguities and phase biases in phase measurements over a GNSS satellite pass.
Source: adapted from Alves (2015)

As code biases, phase biases also have satellite and receiver components (Figure 3), differing according to measurement's frequency (i). In phase measurement model, in equation (2) (chapter 5) receiver and satellite phase biases correspond to instrumental delays, b_{r,L_i} and $b^s_{L_i}$.

Since biases are frequency dependents, when performing combinations between phase measurements at different frequencies, the combined biases are proper of the resulting combination. The ionospheric-free phase is affected by the resulting iono-free receiver and satellite phase biases $b_{r,L_{IF}}$ and $b^s_{L_{IF}}$ as showed in equation (20). Any other phase

combination, e.g. Wide-lane and Narrow-lane, will also have their specific receiver and satellite biases.

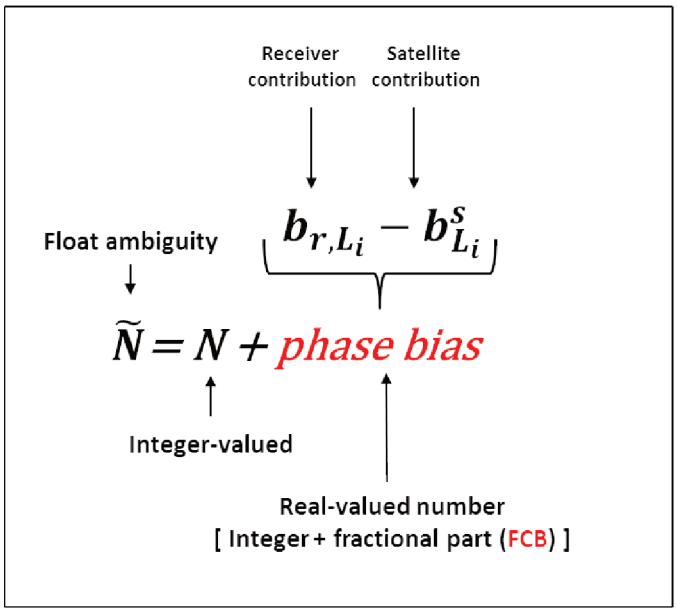

Figure 3 – Receiver and satellite phase bias components.

Phase biases are different for each receiver, and they are also different for each individual GNSS satellite. As a consequence, between-satellites SDs may eliminate receiver bias, however it will still be affected by satellites SD phase biases of a specific observable (e.g. uncombined phase or Wide lane, Narrow lane phase combination) (Ge et al., 2008).

Considering the ambiguities and phase biases present in phase measurements of two GNSS satellites (s_i) and (s_j) observed at a single receiver (r), Figure 4 clarifies the different possibilities for phase biases (in red) assuming dual frequency measurements. These biases refer to their respective ambiguity parameters at different levels: undifferenced and uncombined, combined, and as single differences. Table 8 summarizes such information and introduces the acronyms corresponding to each combination level, description and symbols considered along this work. In Figure 4 and Table 8, there are just some representative examples for the possible phase biases. Many other possibilities exist depending on the combinations and differences realized, especially if we include the third frequency observables (L5) (Liu and Gao, 2017).

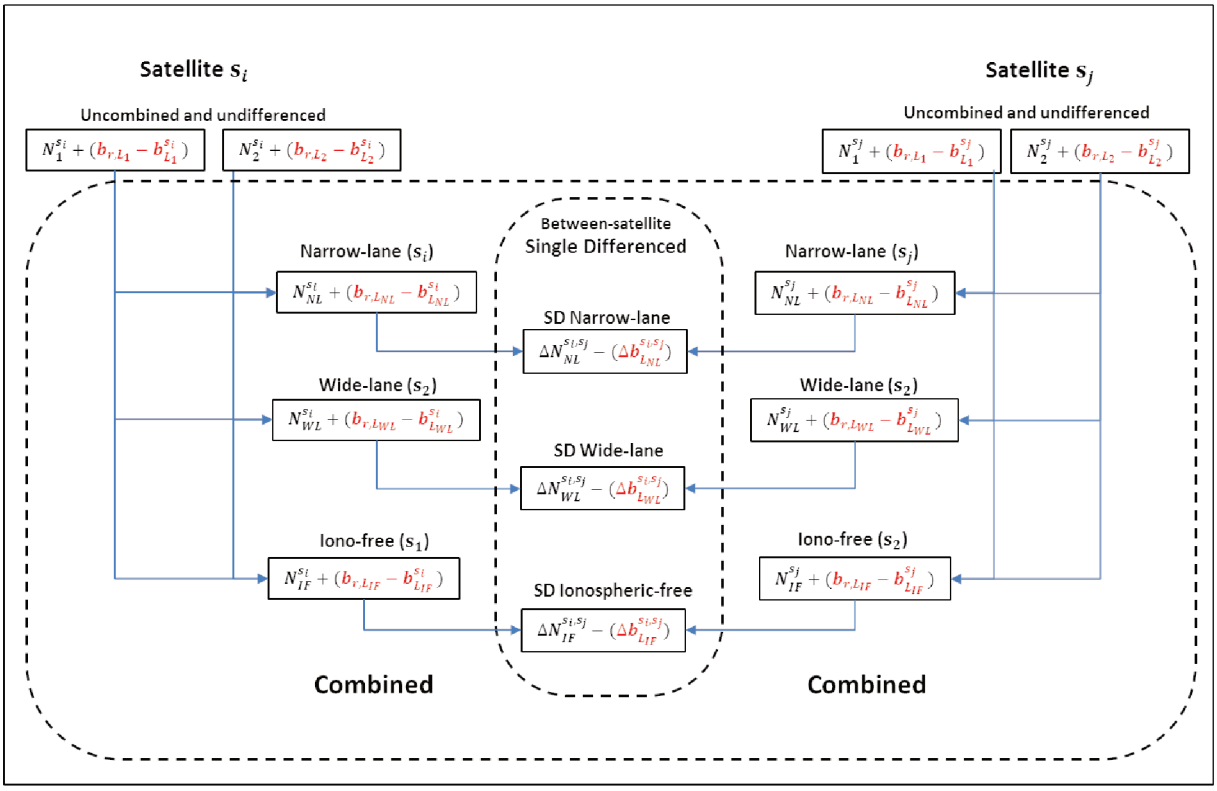

Figure 4 – Dual-frequency case of phase biases (red) affecting the corresponding ambiguity parameter at different levels: undifferenced and uncombined, combined, and between-satellites single-differences.

Table 8 – Description of different phase biases, for dual-frequency measurements, affecting ambiguities parameter at different levels: undifferenced and uncombined, combined, and between-satellites single-differences.

Combination level	Acronym	Bias description	Symbol
Uncombined and undifferenced	L_1SB	L_1 Satellite phase Bias	$b_{L_1}^{s}$
	L_1RB	L_1 Receiver phase Bias	b_{r,L_1}
	L_2SB	L_2 Satellite phase Bias	$b_{L_2}^{s}$
	L_2RB	L_2 Receiver phase Bias	b_{r,L_2}
Combined	NSB	Narrow-lane Satellite phase Bias	$b_{L_{NL}}^{s}$
	NRB	Narrow-lane Receiver phase Bias	$b_{r,L_{NL}}$
	WSB	Wide-lane Satellite phase Bias	$b_{L_{WL}}^{s}$
	WRB	Wide-lane Receiver phase Bias	$b_{r,L_{WL}}$
	ISB	Iono-free Satellite phase Bias	$b_{L_{IF}}^{s}$
	IRB	Iono-free Receiver phase Bias	$b_{r,L_{IF}}$
Single Differenced	SD-NSB	Single Differenced Narrow-lane Satellite phase Bias	$b_{L_{NL}}^{s_i,s_j}$
	SD-WSB	Single Differenced Wide-lane Satellite phase Bias	$b_{L_{WL}}^{s_i,s_j}$
	SD-ISB	Single Differenced Iono-free Satellite phase Bias	$b_{L_{IF}}^{s_i,s_j}$

About biases presented in Figure 4 and Table 8, it would be convenient to add that the MW combination is affected by the WL biases, since this combination depends on the WL combination (cf. section 5.3.4).

It is of interest to state as well, that the iono-free observable can be written in function of other ambiguities, e.g. the WL and NL combinations, which implies that the iono-free biases can also be written in function of the WL and NL biases, equation (33) (Ge et al., 2008):

$$N_{IF} = \frac{f_1}{f_1 + f_2}\left[N_{NL} + \left(b_{r,L_{NL}} - b^s_{L_{NL}}\right)\right] + \frac{f_1 f_2}{f_1^2 - f_2^2}\left[N_{WL} + \left(b_{r,L_{WL}} - b^s_{L_{WL}}\right)\right]. \quad (33)$$

The satellite phase biases have small variation over short term periods. This is usually true for geodetic receivers in good operating conditions, e.g. IGS receivers (Laurichesse et al., 2009). Such characteristic have been explored to provide by-products allowing the corrections of satellite biases, or their fractional part (i.e. the FCB), thus the sum ($N + phase\ bias$) could take only the integer part of the $phase\ bias$, becoming integer (Geng et al., 2012; Laurichesse, 2008). These methods are discussed in next section. They explore different levels of combinations and differentiations of phase biases, but always with the same objective: estimate integer ambiguities.

6.2. Models for PPP integer ambiguity resolution

In order to allow PPP ambiguities fixing, Leandro and Santos (2006) proposed an approach based on the determination of fractional part of the satellite phase biases using a network of receivers. Experiments are realized and satellite phase biases estimates presented as possible by-products to further enable IPPP (Leandro and Santos, 2006).

Other advances dealing with phase biases are achieved in studies conducted by Blewitt (2006), where PPP ambiguities of GPS reference network stations are fixed to integer values, by eliminating phase biases with Double Difference combination of PPP ambiguities between reference stations. This method was applied for IPPP for GPS networks using 24 hours data processing (Blewitt, 2006). Later on, several studies introduce IPPP for isolated receivers, based in the iono-free combination. However, all methods still require the use of

reference GNSS networks to provide precise information about satellite clocks and satellite phase biases (Bertiger et al., 2010; Collins, 2008; Ge et al., 2008; Laurichesse and Mercier, 2007).

Laurichesse and Mercier (2007) introduce a new method to perform zero-difference IPPP. This model employs WSB (Wide-Lane Satellite Biases) corrections, together with clock products, which have the property of preserving the integer nature of ambiguities, the so-called 'phase clocks' (Laurichesse et al., 2009; Mercier and Laurichesse, 2008). These clock solutions are available within the CNES/CLS (*Collecte Localisation Satellites*) IGS analysis center solution since 2009 ('GRG' products). Hereafter this model is denoted as Integer Recovery Clock (IRC) model, since one of its main feature are the phase clocks. The use of GRG products to accomplish the IRC model is feasible with the CNES software GINS (Géodésie par Intégrations Numériques Simultanées) (Fund et al., 2013; Morel et al., 2014; Perosanz et al., 2016).

Collins (2008) propose a model characterized by different clock parameters for phase and code. This model is known as the Decoupled Satellite Clocks (DSC) model. By applying the satellite decoupled integer clock and phase biases corrections, estimated thanks to a GNSS reference network, it is possible to estimate the receiver decoupled clock parameters and undifferenced ambiguities (Collins et al., 2010). According to Shi and Gao (2013), the only difference between the IRC-model and the DSC-model is the approach for fixing the WL ambiguity. The IRC model uses WSB corrections and MW averaging process to estimate WRB (Wide-Lane Receiver Biases) and integer WL ambiguities while the DSC model directly estimates WL ambiguity with other parameters. Teunissen and Khodabandeh (2014) shows that IRC and DSC models are equivalent.

Ge et al. (2008) propose a method based on the estimation of SD-WSBs and SD-NSBs over a GNSS reference network. The fractional part of these estimated satellite biases could be used as by-product to allow IPPP for single stations that are not part of the reference network (e.g. IPPP users). These products are successfully assessed for IPPP with daily (Ge et al., 2008) and hourly (Geng et al., 2009) GNSS data. The method is also called as SD-UPD (Uncalibrated Phase Delay, i.e. phase bias)/FCB model (Teunissen and Khodabandeh, 2015) or even SD between-satellites Model (Shi and Gao, 2014). The IPPP SD-UPD/FCB model is implemented for RT-IPPP at FCT/Unesp (Lima, 2015). This approach based in SD-WSB and

SD-NSB is also used by Bertiger et al. (2010), however without the use of the fractional operator (Teunissen and Khodabandeh, 2015). The method developed by Bertiger et al. (2010), denoted as SD-UPD model, is implemented into the JPL's GIPSY-OASIS (GNSS Inferred Positioning System-Orbit Analysis Simulation) software package (Bertiger et al., 2010).

The above methods of IPPP (SD-UPD/FCB, SD-UPD, IRC and DSC model), based on iono-free combination, could make the inclusion of triple frequency observations to be cumbersome, since many possible dual-combinations exist (Laurichesse, 2008).

In order to provide a suitable representation for triple frequency receivers, Laurichesse (2008) presents an uncombined phase biases model compatible with the RTCM SSR framework. The model is based on uncombined satellite biases (e.g. L_1SB, L_2SB and L_5SB) corrections. These corrections are available in real-time (product prefix CLK9x) by the CNES IGS RTS analysis center (cf. section 5.4.3). Actually, this is the solution implemented in PPP-Wizard (section 5.4.5.2) software package (http://ppp-wizard.net/). A particular advantage is that the uncombined approach is easily compatible with regional atmospheric augmentation (i.e. PPP-RTK) (Laurichesse and Blot, 2016; Laurichesse and Privat, 2015). This is one of the main reasons for the adoption of this RT-IPPP solution in the second step on this thesis work (c.f. Part III).

Two other uncombined IPPP models enabling PPP-RTK can be found in the literature. One of them considers a common clock for code observables and two different clocks for the two different phase observables (L_1 and L_2). This model is known as Distinct Clock (DC) model and it is used in Teunissen et al. (2010) to assess PPP-RTK. The second uncombined model is the method based on Common Clock (CC) parameters for code and phase observables, which is also considered as an undifferenced solution (Odijk et al., 2014; Zhang et al., 2011).

Table 9 lists the above cited IPPP methods according to their satellite clock characteristics (common or decoupled), and functional model (combined or uncombined).

Table 9 – IPPP methods with respective clock nature (common or decoupled), as well as required corrections to allow ambiguity fixing to integer values.

IPPP method	Nature of satellite clocks	Functional model
Decoupled Satellite Clock (DSC) (Collins, 2008; Collins et al., 2010)	Decoupled	Combined
Integer Recovery Clock (IRC) (Laurichesse et al., 2009; Laurichesse and Mercier, 2007; Loyer et al., 2012)	Decoupled	Combined
Uncombined phase biases model (Laurichesse, 2008; Laurichesse and Blot, 2016; Laurichesse and Privat, 2015)	Common	Uncombined
SD-UPD/FCB (Ge et al., 2008; Geng et al., 2009)	Common	Combined
SD-UPD (Bertiger et al., 2010)	Common	Combined
Distinct Clocks (DC) (De Jonge, 1998; Teunissen et al., 2010)	Decoupled	Uncombined
Uncombined-Common Clock (CC) (Zhang et al., 2011)	Common	Uncombined

Next sections describe three representative IPPP methods included in Table 9: 1) the SD-UPD/FCB method, 2) the IRC method, and 3) the uncombined phase biases method. These methods are further described in more details considering they are able to provide an overview about the diversity of IPPP. Since, as already stated, the SD-UPD/FCB has small differences wrt SD-UPD model, and the IRC method is even sometimes described as equivalent to DSC method (Teunissen and Khodabandeh, 2015). Finally, the uncombined phase biases method is representative of the uncombined and undifferenced IPPP methods and is the solution used to enable PPP-RTK in this work. The reader interested in remaining IPPP methods not described in more details here can find valuable information in the references listed in Table 9.

6.2.1. SD-UPD/FCB method

As already stated, this method is based on iono-free combination for phase and code observables, equations (3) and (4), together with the MW combination (cf. section 5.3.4). The following sections present overall strategy proposed by (Ge et al., 2008).

6.2.1.1. Network corrections

In this method, IPPP corrections are the fractional part of the satellite biases (i.e. FCBs), affecting the between-satellites SD-WL and SD-NL combinations (Ge et al., 2008). IGS satellite code clocks are employed, for code and phase measurements, and no-additional satellite clock corrections are required. Therefore the UPD/FCB model is considered as a common clock model (Teunissen and Khodabandeh, 2015) and as presented in Table 9, it is not the only model with such property.

Initially, the between-satellites (s_i, and s_j) SD of WL ambiguities affecting the SD of MW (SD-MW) combination $\Delta L_{MW}^{s_i s_j}$ for all stations of the global or regional reference network are constructed, as presented in equation (34), in cycles.

$$\frac{\Delta L_{MW}^{s_i s_j}}{\lambda_{WL}} = \frac{L_{MW}^{s_i} - L_{MW}^{s_j}}{\lambda_{WL}} = \Delta N_{WL}^{s_i s_j} - \Delta b_{L_{WL}}^{s_i s_j} = \Delta \widetilde{N}_{WL}^{s_i s_j}, \tag{34}$$

where :

- Δ represents the differentiation operator, for this case, between-satellites (s_i, s_j),
- λ_{WL} is the WL wavelength (~0.862 m, cf. 5.3.3), in meters,
- $\Delta b_{L_{WL}}^{s_i s_j}$ and $\Delta N_{WL}^{s_i s_j}$, in WL cycles, are respectively, the between-satellites SD-WSB and the integer SD-WL ambiguities. Their sum is real,
- $\Delta \widetilde{N}_{WL}^{s_i s_j}$ is the float SD-WL ambiguities, in WL cycles, and its float nature is indicated by "$\sim$".

Thus, WRBs are canceled and once the solution has converged, the integer value for the ambiguity of between-satellites SD-WL $\overline{\Delta N}_{WL}^{s_i s_j}$ is determined by rounding the real-valued ambiguity (Ge et al., 2008), as presented in equation (35), in WL cycles.

$$\overline{\Delta N}_{WL}^{s_i,s_j} = \left\langle \frac{\Delta L_{MW}^{s_i,s_j}}{\lambda_{WL}} \right\rangle. \tag{35}$$

In equation (35), the operand $\langle\ \rangle$ denotes the rounding procedure to the nearest integer value and the symbol "$\bar{}$" indicates that the associated parameter is rounded to the integer.

After solution convergence in previous step, i.e. good integer estimation for $\Delta\widetilde{N}_{WL}^{s_i s_j}$, FCB of SD-WSB (FCB-SD-WSB) $\hat{\Delta}b_{L_{WL}}^{s_i s_j}$, in WL cycles, for each pair of satellites can be computed as:

$$\hat{\Delta}b_{L_{WL}}^{s_i s_j} = frac\left(\widetilde{N}_{WL}^{s_i} - \widetilde{N}_{WL}^{s_j}\right). \tag{36}$$

According to Ge et al. (2008), *frac*(.) is a function to return the positive fractional part of the input variable. The by-product solution for the FCB-SD-WSB can be generated by averaging the FCB-SD-WSBs for each pair of satellites observed at every station of the network. Considering a network composed by *n* stations, each FCB-SD-WSB correction of the set is given by:

$$\hat{\Delta}b_{L_{WL}}^{s_i s_j} = \frac{1}{n}\sum_{station=1}^{n}\left[frac\left(\widetilde{N}_{WL}^{s_i} - \widetilde{N}_{WL}^{s_j}\right)\right]. \tag{37}$$

As stated before, two biases corrections are necessary, the FCB-SD-WSBs corrections obtained in equation (36) and the FCB corrections for the SD-NL (FCB-SD-NSB). Thus, NL ambiguities must be fixed and this is possible thanks to WL ambiguities fixed in (35).

The NL ambiguity fixing can be performed considering the iono-free ambiguity as a function of NL and WL ambiguities (cf. equation (33)), which can be developed as (Ge et al., 2008):

$$\begin{aligned} N_{NL} + \left(b_{r,L_{NL}} - b_{L_{NL}}^{s}\right) &= \frac{f_1 + f_2}{f_1}\left[N_{IF} + \left(b_{r,L_{IF}} - b_{L_{IF}}^{s}\right)\right] \\ &- \frac{f_2}{f_1 - f_2}\left[N_{WL} + \left(b_{r,L_{WL}} - b_{L_{WL}}^{s}\right)\right] \end{aligned} \tag{38}$$

after, by applying the between-satellites SDs, the receiver biases are removed:

$$\Delta N_{NL}^{s_i s_j} + \Delta b_{L_{NL}}^{s_i s_j} = \frac{f_1 + f_2}{f_1}\left(\Delta N_{IF}^{s_i s_j} - \Delta b_{L_{IF}}^{s_i s_j}\right) - \frac{f_2}{f_1 - f_2}\left(\Delta N_{WL}^{s_i s_j} - \Delta b_{L_{WL}}^{s_i s_j}\right) \quad (39)$$

Subtracting the fixed SD-WL ambiguities $\overline{\Delta N}_{WL}^{s_i,s_j}$ from the real-valued SD-WL term $\left(\Delta N_{WL}^{s_i s_j} - \Delta b_{L_{WL}}^{s_i s_j}\right)$ in equation (39), thus resulting in:

$$\Delta N_{NL}^{s_i s_j} - \Delta b_{L_{NL}}^{s_i s_j} = \frac{f_1 + f_2}{f_1}\left(\Delta N_{IF}^{s_i s_j} - \Delta b_{L_{IF}}^{s_i s_j}\right) - \frac{f_2}{f_1 - f_2}\left(\Delta N_{WL}^{s_i s_j} - \overline{\Delta N}_{WL}^{s_i,s_j} - \Delta b_{L_{WL}}^{s_i s_j}\right) \quad (40)$$

The term $\left(\Delta N_{WL}^{s_i s_j} - \overline{\Delta N}_{WL}^{s_i,s_j} - \Delta b_{L_{WL}}^{s_i s_j}\right)$ in (40) can be assumed as constant over the pass for the considered satellites SD. Additionally, it is important to keep in mind that the term $\left(\Delta N_{IF}^{s_i s_j} - \Delta b_{L_{IF}}^{s_i s_j}\right)$ can be considered as the real-valued iono-free SD ambiguity (sum of ambiguity and its biases) (Ge et al., 2008; Shi and Gao, 2014).

After convergence of the real-valued SD-NL ambiguity, i.e. the term ($\Delta N_{NL}^{s_i s_j} - \Delta b_{L_{NL}}^{s_i s_j}$), the integer ambiguity $\overline{\Delta N}_{NL}^{s_i s_j}$ can be obtained by rounding the real-valued one (equation 41), which is consistent with the use of the FCB-SD-WSB corrections, since the fixed SD-WL ambiguities are employed in equation (40).

$$\overline{\Delta N}_{NL}^{s_i s_j} = \left\langle \Delta N_{NL}^{s_i s_j} - \Delta b_{L_{NL}}^{s_i s_j} \right\rangle \quad (41)$$

The FCB-SD-NSB corrections $\hat{\Delta} b_{L_{NL}}^{s_i s_j}$ for a pair of satellites can be obtained as:

$$\hat{\Delta} b_{L_{NL}}^{s_i s_j} = frac\left(\widetilde{N}_{NL}^{s_i} - \widetilde{N}_{NL}^{s_j}\right) \quad (42)$$

High precision corrections can be generated by averaging the fractional FCB-SD-NSB corrections over the receivers of the network as did for the FCB-SD-WSB corrections in equation (37). These FCB-SD-NSB corrections, together with FCB-SD-WSB corrections computed in the previous step are then broadcasted to the users over network area.

Quality of corrections relies mainly on the precision of WL estimated ambiguities and on the quality of pseudorange measurements used to form the MW combination. Additionally, corrections for NL phase bias must be determined in shorter intervals, assuming variations in a few hours, than those for WL phase biases which can be determined with daily interval (Ge et al., 2008; Lima, 2015; Teunissen and Khodabandeh, 2015).

6.2.1.2. User solution

A between-satellites SD for same pair (s_i, and s_j) of equation (34) is also performed at the user side. Applying the appropriated FCB-SD-WSB corrections $\hat{\Delta}b_{L_{WL}}^{s_i s_j}$ one can obtain the integer WL user solution, $\overline{\Delta N}_{WL}^{s_i s_j}$, in cycles:

$$\left\langle \frac{\Delta L_{MW}^{s_i s_j}}{\lambda_{WL}} - \hat{\Delta}b_{L_{WL}}^{s_i s_j} \right\rangle = \overline{\Delta N}_{WL}^{s_i s_j} \tag{43}$$

Therefore, the integer property of the user SD-WL ambiguity $\Delta N_{WL}^{s_i s_j}$ can be recovered. In order to resolve the user NL ambiguities to integer values $\overline{\Delta N}_{NL}^{s_i s_j}$, considering units of cycles, the same principle is employed to equation (40) leading to equation (44):

$$\left\langle \left(\Delta N_{NL}^{s_i s_j} - \Delta b_{L_{NL}}^{s_i s_j} \right) + \hat{\Delta}b_{L_{NL}}^{s_i s_j} \right\rangle = \overline{\Delta N}_{NL}^{s_i s_j} \tag{44}$$

The implementation algorithm for IPPP ambiguities resolution must consider the precision of the corrections, that is also provided (Ge et al., 2008). Frequency of the update is very important for RT-IPPP applications, especially about the corrections of NL biases (Lima, 2015).

6.2.2. IRC Model

The IPPP method introduced by Mercier and Laurichesse (2007) is usually called Integer Recovery Clock model, because together with the phase biases corrections an additional satellite phase-clock correction is required to solve ambiguities (Shi and Gao, 2014; Teunissen and Khodabandeh, 2015). It is also an IPPP model based on iono-free and MW undifferenced combinations (section 5.3.4). Indeed, between-satellites SD are not realized, and thus receiver biases must be taken into account (Laurichesse et al., 2009; Loyer et al., 2012).

6.2.2.1. Network corrections

Firstly, FCB-WSBs are estimated for all satellite observed thanks to MW computed on a global network of stations. As between satellites SD are not realized, MW combination depends on both satellite and receiver hardware biases:

$$\frac{L_{MW}}{\lambda_{WL}} = N_{WL} + (b_{r,WL} - b^{s}_{L_{WL}}) \tag{45}$$

Without any additional information the system with observation equation (45) is singular, only the differences: $(b_{r,L_{WL}} - b^{s}_{L_{WL}})$ can be observed. Therefore, in order to fix WL and estimate FCB-WSBs, a stable geodetic receiver from the reference network is selected as reference. The WRB of the MW combination ($b_{r,MW}$) for this reference receiver is set to zero. When the solution of reference receiver achieves convergence, the integer part of the estimated float WL ambiguities from the MW combination, is assumed to be the integer WL:

$$\overline{N}_{WL} = \langle \frac{L_{MW}}{\lambda_{WL}} \rangle \tag{46}$$

Consequently, in WL cycle units, the fractional part is attributed to the WSBs as:

$$\hat{b}^{s}_{L_{WL}} = \frac{L_{MW}}{\lambda_{WL}} - \overline{N}_{WL} \tag{47}$$

These estimated WSBs are employed to obtain WRBs $b_{r,MW}$ in the data processing of other stations involved in the network solution. Since the WSBs are known, the estimation of their WRB becomes feasible. However, their WRBs will be implicitly relative to the WRB of the reference receiver.

WSB corrections $\hat{b}^{s}_{L_{WL}}$ that can be broadcast to the users are obtained. However, the phase-clock corrections are also necessary to the IRC model, and they are computed together with the N_1 fixing. Code and phase iono-free combinations, equations (3) (4), are involved in this manipulation.

Assuming that the N_{WL} is known, the iono-free combination can be expressed in function of the remaining unknown ambiguity N_1 as follows (Laurichesse et al., 2009; Loyer et al., 2012):

$$L_{IF} = \frac{\gamma L_1 - (L_2 - \lambda_2 N_{WL})}{\gamma - 1} - \rho = c(dt_r - dt^s) + T_c - \lambda_{NL} N_1 \quad (48)$$

with $\gamma = \lambda_2^2/\lambda_1^2$.

The terms ρ is the geometric distance corrected of systematic errors (e.g. relativistic effects). This quantity is known using coordinates of reference network. The respective iono-free for pseudorange equations, is the classical P_{IF}, however, it is referred to code-clocks and can be arranged as (Laurichesse et al., 2009; Loyer et al., 2012):

$$P_{IF} = \frac{\gamma P_1 - \lambda_2 P_1}{\gamma - 1} - \rho = (dt_r - dt^s) + T_c \quad (49)$$

Equation (48) can be simplified as following with a good knowledge of tropospheric delays:

$$R_c = cdt_{r,L_{IF}} - cdt^s - \lambda_{NL} N_1 \quad (50)$$

The term R_c can be determined with good precision, remaining the need for estimating the phase-clocks and N_1 ambiguities (Mercier and Laurichesse, 2008). However, this solution is singular in two points. Only the difference $\left(dt_{r,P_{IF}} - dt^s_{P_{IF}}\right)$ is estimable, thus a receiver clock of the network must be constrained to zero. Second singularity deals with clocks which values can change by an integer number 'k' multiple of the NL wavelength λ_{NL}. Therefore, sets of clock values cannot be connected with overlapping satellite passes (Laurichesse et al., 2009).

Other receivers of the network are iteratively added to the process until a complete set of the satellite phase-clocks $cdt^s_{L_F}$ and $\overline{N}_1$are obtained. Applying rounding operator to N_1 is assumed to be its integer value and its fractional part to be the receiver phase-clock cdt_r:

$$\overline{N}_1 = -\left\langle \frac{R_c - c(dt_r - cdt^s)}{\lambda_{NL}} \right\rangle \quad (51)$$

As satellite-phase clocks are estimated simultaneously with integer ambiguities, they keep the integer nature of ambiguities. That's why such clocks are often called in the literature 'Integer Satellite Phase-Clocks'.

The complete set of satellite phase clocks cdt^s is broadcasted to users together with the WSB $b^s_{L_{WL}}$ corrections. These corrections are currently available for zero-differenced

IPPP applications, by the CNES-CLS IGS Analysis Center (GRG products), where this methodology is efficiently implemented (Loyer et al., 2012).

6.2.2.2. User solution

At the user side, as indicated previously, WSBs and satellite phase-clock are required.

In the first step, in order to resolve integer WL ambiguities the WSB corrections are applied to MW combinations:

$$\frac{L_{MW}}{\lambda_{WL}} + \hat{b}^{s}_{L_{WL}} = N_{WL} + \left(b_{r,MW} - b^{s}_{L_{WL}}\right) + \hat{b}^{s}_{L_{WL}} = N_{WL} + b_{r,MW} \tag{52}$$

with $\hat{b}^{s}_{L_{WL}}$ representing the WSB correction. Considering that WRB is the same for all satellites, it can be obtained by averaging the fractional parts of the real valued WL ambiguities for all "*m"* observed satellites as follows (Shi and Gao, 2014):

$$b_{r,L_{WL}} = \frac{1}{m}\sum_{satellite=1}^{m}\left[\frac{L_{MW} + \hat{b}^{s}_{L_{WL}}}{\lambda_{WL}} - \left\langle\frac{(L_{MW} + \hat{b}^{s}_{L_{WL}})}{\lambda_{WL}}\right\rangle\right] \tag{53}$$

Finally, integer WL ambiguity resolution can be achieved by substituting the WRB from equation (53) into equation (52). Once N_{WL} has its integer property recovered, the N_1 ambiguity resolution is realized. Similar to the network side, by manipulating iono-free equations to have iono-free ambiguity replaced by N_1 and N_{WL}. Assuming that WL ambiguity is known, iono-free phase combination, in meters, becomes (Laurichesse et al., 2009):

$$L_{IF} = \frac{\gamma L_1 - (L_2 - \lambda_2 N_{WL})}{\gamma - 1} = \rho + c(dt_r - dt^s) + T_c + \lambda_{NL} N_1 \tag{54}$$

Equation (54) and code iono-free equation (49) are used to perform user positioning. In these equations, the phase-clocks corrections cdt^s are employed. IGS satellite code-clocks are not necessary, since phase-clocks are assumed to be aligned, by more or less 'k' integers, to phase-clocks. Tropospheric delays, receiver clock offsets, N_1 ambiguities, and positions become estimable.

6.2.3. Uncombined phase biases model

The IPPP methods presented in sections 6.2.1 and 6.2.2 are based on combined phase biases products, thus their current formulation leads to the presence of some drawbacks. Laurichesse (2008) evokes that such representation makes difficult the standardization of the biases messages on the RTCM context, since its representation depends on the IPPP method adopted. Two points are highlighted 1) the requirement for users is to employ the same method used at the network side and 2) biases representation for triple frequency observations could be heavy, since a non-exhaustive list of combinations exist.

In order to overcome such limitations, Laurichesse (2008) developed a method based on uncombined GNSS measurements, which is briefly presented in the next sections. This method is implemented in PPP-Wizard software package (Laurichesse and Blot, 2016; Laurichesse and Privat, 2015). As previously stated the source codes of the PPP-Wizard (for user side) are available for didactic purposes (cf. section 5.4.5.2).

6.2.3.1. Network corrections

For the triple-frequency case, the corrections provided by this method are the uncombined satellite phase biases: b_{L_1}, b_{L_2},b_{L_5} and satellite phase-clocks According to (Laurichesse and Langley, 2015), each independent phase bias could be directly estimated in a filter. Although, in order to maintain compatibility with the dual-frequency case during the establishment of the modernized satellites (i.e. 3rd frequency) the uncombined biases are obtained in the old framework, which means working with combinations, but considering some modifications.

Concerning the bias estimation for the dual frequency case, there are only two biases to provide: L_1SB ($b^s_{L_1}$) and L_2SB ($b^s_{L_2}$). The estimation of the uncombined biases can be obtained using the corrections provided by the IRC model, b^s_{WL} and dt^s, thus the network solution can be the same as presented in the previous section. The remaining problem to be solved is a transformation that provides uncombined biases to be broadcasted at the user side (Figure 5).

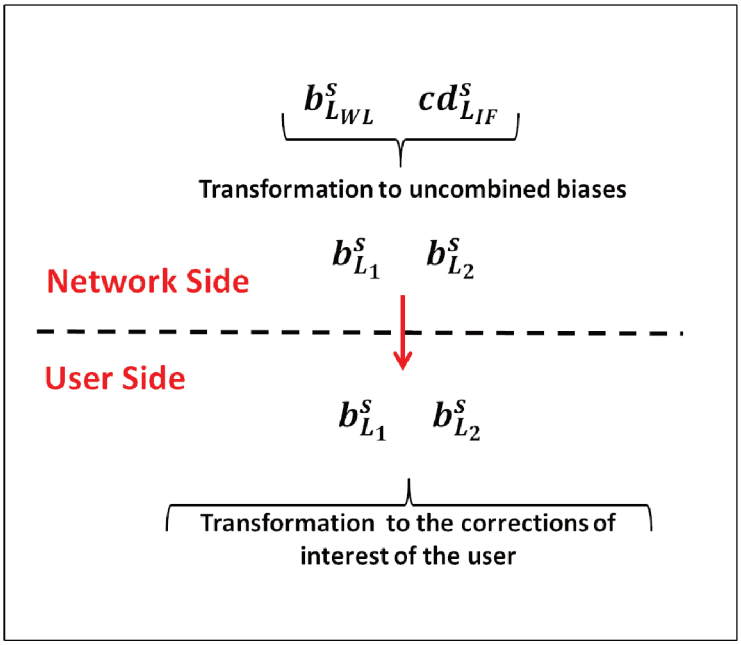

Figure 5 – Combined to uncombined satellite phase biases in the dual-frequency case. Source: adapted from (Laurichesse, 2008)

Laurichesse and Langley (2015) present the transformation between the uncombined biases b_{L_1} and b_{L_2} and both WSBs and satellite phase-clock cdt^s_{IRC} from the IRC model (section 6.2.2). The problem can be solved as follows:

$$\begin{pmatrix} b^s_{L_1} \\ b^s_{L_2} \end{pmatrix} = \frac{1}{\gamma_2\lambda_1 - \lambda_2} \begin{pmatrix} -\lambda_2 & 1 \\ -\gamma_2\lambda_1 & 1 \end{pmatrix} \begin{pmatrix} b^s_{L_{WL}} - \alpha_{21} b^s_{P_1} - \alpha_{22} b^s_{P_2} \\ (\gamma_2 - 1)(cdt^s - cdt^s_{IRC}) \end{pmatrix} \tag{55}$$

with $\alpha_{21} = \frac{\lambda_1 - \lambda_2}{\lambda_1 + \lambda_2} / \lambda_1$ and $\alpha_{22} = \frac{\lambda_1 - \lambda_2}{\lambda_1 + \lambda_2} / \lambda_2$.

This system comes from both iono-free phase and MW combinations. On iono-free phase combination, it is assumed that satellite clocks refer to phase clocks. IGS provides, conventionally, satellite code-clocks on which IRC phase clocks are aligned more or less 'k' integers. To make phase clocks compatible to IGS clocks, the difference $(cdt^s - cdt^s_{IRC})$ must be introduced on the iono-free phase combination.

The transformation in equation (55) can be applied at the network side to generate the uncombined biases, which is the representation defined as standard for the SSR RTCM framework (Laurichesse, 2008).

The solution above is an option for the dual-frequency approach. If the generation of triple-frequency biases is aimed, the bias estimation is more complicated.

First, WL biases $b^s_{L_{WL}}$ and $b^s_{L_{WL_{2,5}}}$ are estimated thanks to the two possible MW combinations using L_1,L_2 (i.e. classical MW) and the MW using L_2,L_5. The estimation of these biases can be realized together with another phase bias. This phase bias is given by the triple-frequency iono-free phase combination L_{IF_3} given as (Liu and Gao, 2017):

$$L_{IF_3} = \frac{f_1}{f_1 - f_5} L_{WL} - \frac{f_5}{f_1 - f_5} L_{WL_{2,5}} \tag{56}$$

where:

- $L_{WL_{2,5}}$ is the WL combination between L_2 and L_5, also known as Extra-Widelane (EW) combination (Sanz Subirana et al., 2013),
- L_{IF_3} is the triple-frequency iono-free phase combination, in units of meters.

The triple-frequency iono-free phase combination is more accurate than MW functions, since only phase measurements are involved.

The system to be solved is redundant, however according to Laurichesse (2008), the noise of the different equations (the two MWs and the IF triple-frequency) must be chosen carefully.

b_{L_1} which is the remaining bias to be estimated can be obtained using the traditional iono-free phase combination of the dual frequency case (L_1 and L_2).

This network solution is implemented in the CNES real-time analysis center software and nowadays CNES broadcasts phase biases compatible with this triple-frequency concept (Laurichesse and Blot, 2016).

6.2.3.2. User solution

The functional model can be based on uncombined measurement equations. Laurichesse and Langley (2013) proposed the following GPS measurement equations, which can be duplicated for all GNSS constellations involved in the processing :

$$P_1 = \rho + c(dt_r - dt^s) + T_c + I_1 + (b_{r,P_1} - b^s_{P_1}) \quad (57)$$

$$P_2 = \rho + c(dt_r - dt^s) + T_c + \gamma_2 I_1 + (b_{r,P_2} - b^s_{P_2}) \quad (58)$$

$$C_5 = \rho + c(dt_r - dt^s) + T_c + \gamma_5 I_1 + (b_{r,C_5} - b^s_{C_5}) \quad (59)$$

$$L_1 = \rho + c(dt_r - dt^s) + T_c - I_1 + \left(b_{r,L_1} - b^s_{L_1}\right) - \lambda_1 N'_1 \quad (60)$$

$$L_2 = \rho + c(dt_r - dt^s) + T_c - \gamma_2 I_1 + \left(b_{r,L_2} - b^s_{L_2}\right) - \lambda_2 (N'_W + N'_1) \quad (61)$$

$$L_5 = \rho + c(dt_r - dt^s) + T_c - \gamma_5 I_1 + \left(b_{r,L_5} - b^s_{L_5}\right) - \lambda_5 (N'_E + N'_W + N'_1) \quad (62)$$

With:

$$N'_1 = N_1 + \delta N_1$$
$$N'_W = N_W + \delta N_W$$
$$N'_E = N_E + \delta N_E$$

$$\gamma_2 = \frac{f_1^2}{f_2^2},\ \gamma_5 = \frac{f_1^2}{f_5^2}, \lambda_1 = \frac{c}{f_1}, \lambda_2 = \frac{c}{f_2}, \lambda_5 = \frac{c}{f_5}$$

All the satellite elements, i.e.: positions, clock dt^s and biases $(b^s_{P1}, b^s_{P2}, b^s_{C5}, b^s_{L1}, b^s_{L2}, b^s_{L5})$ in the functional model are assumed to be known. Satellite clock dt^s is arbitrary. This means that any definition can be followed, if the code and phase biases are consistent. For convenience IGS convention is adopted. Thus, these clocks are referenced to the iono-free P1-P2 combination (cf. DCB correction in section 5.4.2.2.2).

Parameters N'_1, N'_W and N'_E are the integer values for N_1, WL and Extra-WL (WL using L_2 and L_5) phase ambiguities, respectively. The terms $\delta N'_1$, $\delta N'_W$ and $\delta N'_E$, also represent integer quantities introduced to allow gap-bridging and cycle slips detection capabilities.

The uncombined satellite phase biases recover the integer nature of ambiguities. Then, ambiguities can be fixed in a cascading scheme: initially the Extra-WL N_E, then the WL N_W, and finally N_1. Further details about the implementation of this method are presented in next section.

6.2.3.3. Details on PPP-Wizard 1.3 implementation

Implementation of the uncombined phase biases model in PPP-Wizard 1.3 uses a bootstrap estimator to recover integer ambiguities. This estimator takes correlations between ambiguities into account. However, it also makes use of integer rounding. Therefore, the bootstrap estimator is a more advanced but still relatively simple integer ambiguity estimator. Considering that a set of n real ambiguities are available at one epoch, a sequential process is performed as follows (Teunissen, 2001; Teunissen et al., 2002):

1) A first selected ambiguity ($\hat{a}_1$) has its value rounded to the nearest integer, recursively for WL and NL ambiguities. Only NL for which corresponding WL is fixed to its integer value is rounded,

2) All parameters of the filter (positions, atmospheric delays, receiver clocks offsets, hardware biases and ambiguities) are re-estimated using the previous integer ambiguity $\hat{a}_1$. In that case, variance of hardware biases are set to infinite values in order to make their estimates compatible with the integer nature of $\hat{a}_1$.

3) Step 1) and step 2) are repeated for the remaining $(n-1)$ real-valued ambiguities,

4) Step 1) to 3) are repeated at the following epoch.

It is important to underline that changing the order of ambiguities in the ambiguities vector ($\hat{a}_1, \hat{a}_2 \dots \hat{a}_n$), will produce a different set of ambiguities. Indeed, remaining $(n-1)$ ambiguities always refer to the first integer ambiguity $\hat{a}_1$. That is why the corresponding satellite can be pointed out as a '*pivot satellite'*. However, whatever the pivot satellite, estimates of the ambiguities vector ($\hat{a}_1, \hat{a}_2 \dots \hat{a}_n$) are consistent at '$k$' integer values. The integer 'k' value is 'absorbed' by hardware phase delays b_{L_1} and b_{L_2}.

So with the bootstrapped estimator, after one initial ambiguity is a priori fixed the remaining ambiguities are fixed iteratively. This strategy allows partial ambiguity fixing, and this can be an interesting point for PPP-RTK applications where SSR atmospheric corrections may not be available for all satellites.

Especially for real-time applications the bad fixed ambiguity values can be very frequent, thus in order to avoid staying on a wrong ambiguity solution during several epochs, a new set of integer ambiguity is estimated at each epoch (step 4)).

With regards to the Kalman filter, the following formulation is applied (Kalman, 1960; Laurichesse and Privat, 2015) (section 5.4.2.3) :

$$P = UDU^T \tag{63}$$

where:

- P is the a priori covariance matrix,
- U is the unit upper triangular matrix and,
- D is a squared diagonal matrix $D = diag(d_1, \dots, d_n)$.

Update of the solution matrix uses the Bierman algorithm (Bierman, 1975) and the propagation uses the Thornton algorithm (Thornton and Bierman, 1975). In this algorithm, the *U* updating has been arranged to minimize computation. Bierman (1975) explains that the main motivation for introducing the '*U-D'* covariance factorization is computational. Besides, the factorization is a valuable tool to analyze the parameter estimation problem. In the case of the Kalman filter, the gain is an auxiliary result of the update computation.

PPP-Wizard filter settings are presented in Table 10, for kinematic positioning of an unknown station. The GPS+GLONASS case is considered, however it is possible to generalize for other constellations (Laurichesse and Privat, 2015). Another important detail to clarify is that hardware bias b_{P_1} is estimated as a unique parameter with receiver clock offset dt_r, for practical purposes. Thus, resulting parameter corresponds to the sum $h_{r_{P_1}} = (cdt_r + b_{r_{P_1}})$, estimated on P1 measurement.

Table 10 – State vector and setting of the Kalman filter

Parameter	Unit	Quantity	Typical initial covariance	Typical model noise (1 s)
Position (X_r, Y_r, Z_r)	m	3	50 m	10 m
Clock GPS (P1) $(h_{r_{P_{1,GPS}}})$	m	1	Inf	Inf
Bias P2 GPS $(b_{r_{P_{2,GPS}}})$	m	1	0	1 mm
Bias C5 GPS $(b_{r_{C_{5,GPS}}})$	m	1	0	1 mm
Bias L1 GPS $(b_{r_{L_{1,GPS}}})$	m	1	0	1 mm
Bias L2 GPS $(b_{r_{L_{2,GPS}}})$	m	1	0	1 mm
Bias L5 GPS $(b_{r_{L_{5,GPS}}})$	m	1	0	1 mm
Clock GLONASS (P1) $(h_{r_{P_{1,GLO}}})$	m	1	inf	inf
Bias P2 GLONASS $(b_{r_{P_{2,GLO}}})$	m	1	0	1 mm
Bias L1 GLONASS $(b_{r_{L_{1,GLO}}})$	m	1	0	1 mm
Bias L2 GLONASS $(b_{r_{L_{2,GLO}}})$	m	1	0	1 mm
Zenith Wet delay (ZWD) (see chapter 6)	m	1	0.5 m	0.005 mm
Slant ionospheric delay at frequency 1 (I_1)	m	1 per satellite	10 m	2 mm
Phase ambiguity (N_E)	Cycle	1 per satellite	inf	0
Phase ambiguity (N_W)	Cycle	1 per satellite	inf	0
Phase ambiguity (N_1)	Cycle	1 per satellite	inf	0
Phase ambiguity (δN_E)	Cycle	1 per satellite	inf for gap-bridging otherwise 0	0
Phase ambiguity (δN_W)	Cycle	1 per satellite	inf for gap-bridging otherwise 0	0
Phase ambiguity (δN_1)	Cycle	1 per satellite	inf for gap-bridging otherwise 0	0

Source: adapted from Laurichesse and Privat (2015)

To achieve a target accuracy of 5 mm, the terms and models listed in IERS Conventions 2010 are applied in the Kalman filter. An example of PPP-Wizard 1.3 positioning performances is illustrated in Figure 6. Simulated RT-IPPP is realized at station RENN, day 208/2014. The recommended minimum number of epochs to start the ambiguity fixing trials is used (3600). Figure 6 shows slight changes in precision when ambiguity fixing

is accomplished after 1h of processing. However, by this time and in this particular case, the float solution has already achieved a centimeter quality level in terms of accuracy and precision before the ambiguity fixing. In other cases, under poor satellite geometry the solution may require more time to converge.

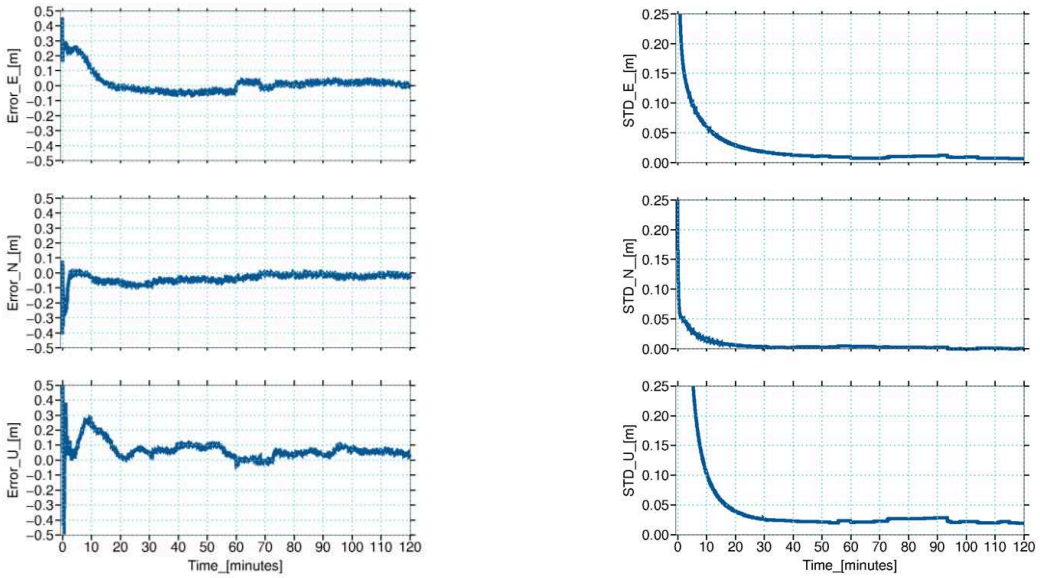

Positioning errors | Post-fit standard deviations

Figure 6 – Positioning performance in terms of accuracy (left) and post-fit standard deviations (right) of RGP station RENN during day 208/2014

Tropospheric and ionospheric parameters estimated together with receiver coordinates are illustrated in Figure 7. It is possible to appreciate the convergence of both parameters. Tropospheric delay takes less than 10 min to converge after cold start. About ionospheric delays, a parameter is estimated for every satellite, therefore when a new satellite is included in the processing, a new parameter as well as a new convergence is observed.

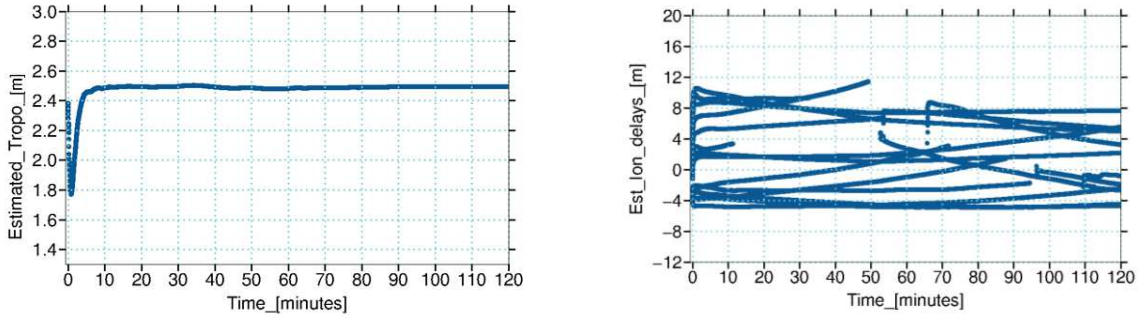

Tropospheric delay | Slant ionospheric delays

Figure 7 – Tropospheric (left) and ionospheric (right) delays estimated at RGP station RENN during day 208/2014

The ionospheric and tropospheric delays presented in Figure 7 are the parameters for which atmospheric SSR corrections are provided. With such corrections the PPP-Wizard 1.3 solution convergence time can be improved (Part III). The chapter 7 presents a brief review about atmospheric effects on GNSS signals.

Receiver clock offsets with respect to GPS and GLONASS are illustrated in Figure 8. As previously stated, such parameters are in practice the sum $h_{r_{P_1}} = (cdt_r + b_{r_{P_1}})$. Hardware biases on other measurements are estimated with respect to $h_{r_{P_1}}$. Their estimation is illustrated in Figure 9.

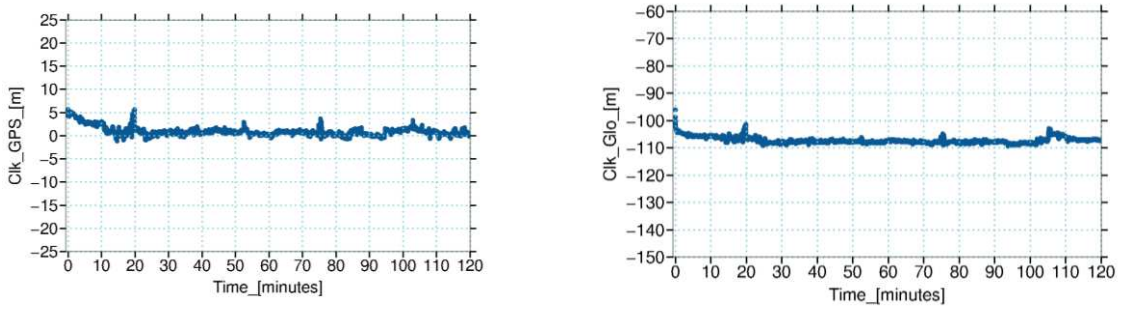

GPS receiver clock GLONASS receiver clock

Figure 8 – GPS (left) and GLONASS (right) receiver clock offsets estimated at RGP station RENN during day 208/2014.

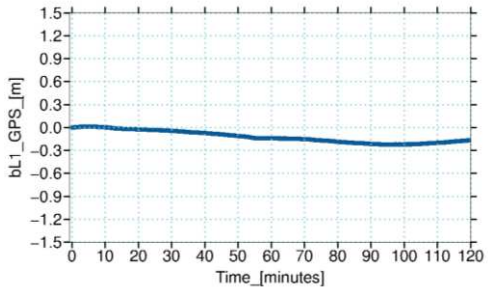

GPS L1 receiver bias

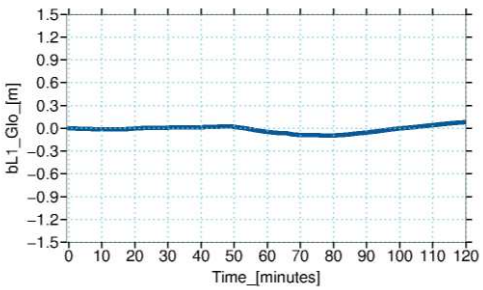

GLONASS L1 receiver bias

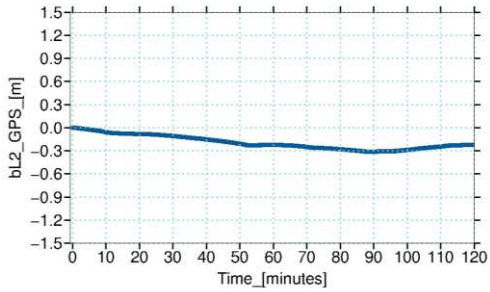

GPS L2 receiver bias

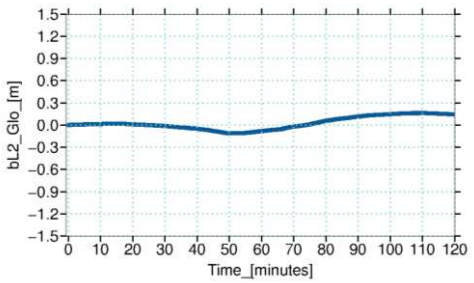

GLONASS L2 receiver bias

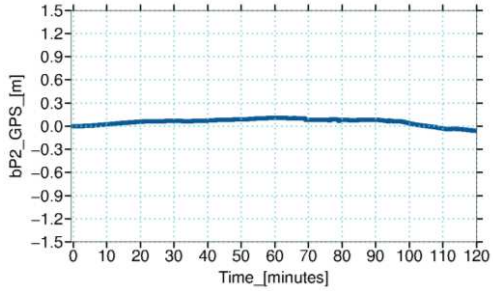

GPS P2 receiver bias

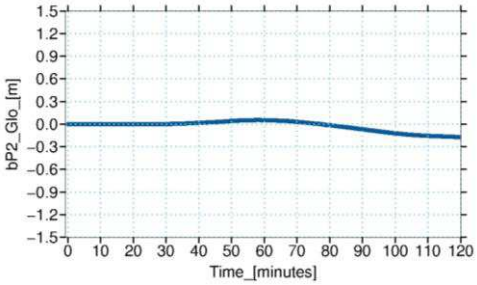

GLONASS P2 receiver bias

Figure 9 – GPS (left) and GLONASS (right) hardware biases estimated at RGP station RENN during day 208/2014.

Receiver clock offsets present metric variations while hardware biases present smaller values with smoothed variations during the process.

Finally, WL and NL ambiguities estimates are presented in Figure 10. Integer-valued ambiguities are plotted in dark blue. After 60 min, most of ambiguities are fixed to integer values.

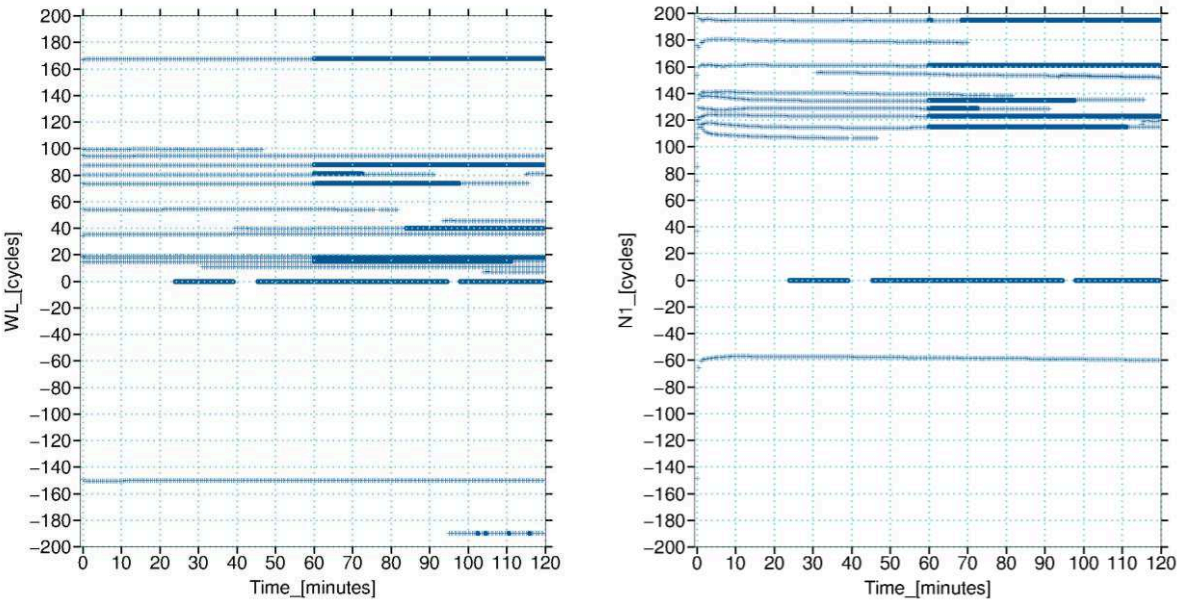

WL ambiguities NL ambiguities

Figure 10 – WL (left) and NL (right) ambiguities estimated at RGP station RENN during day 208/2014; integer values are plotted in dark blue.

7. Atmospheric effects on GNSS signals

Satellite signals propagate throughout the dynamic atmosphere, crossing layers of different natures and variable states. Therefore, the signals suffer different influences that affect propagation direction, propagation speed, polarization and signal power (Monico, 2008; Seeber, 2003).

Considering the propagation of electromagnetic signals, atmosphere is composed by two distinct layers, troposphere and ionosphere. This corresponds to the atmospheric division in function of ionization and it is the one considered in Geodesy, with a neutral and ionized atmospheric part. However, the meteorology sciences usually consider another division in function of temperature. Thus, in this division the tropospheric layer is presented with a different extension (Figure 11).

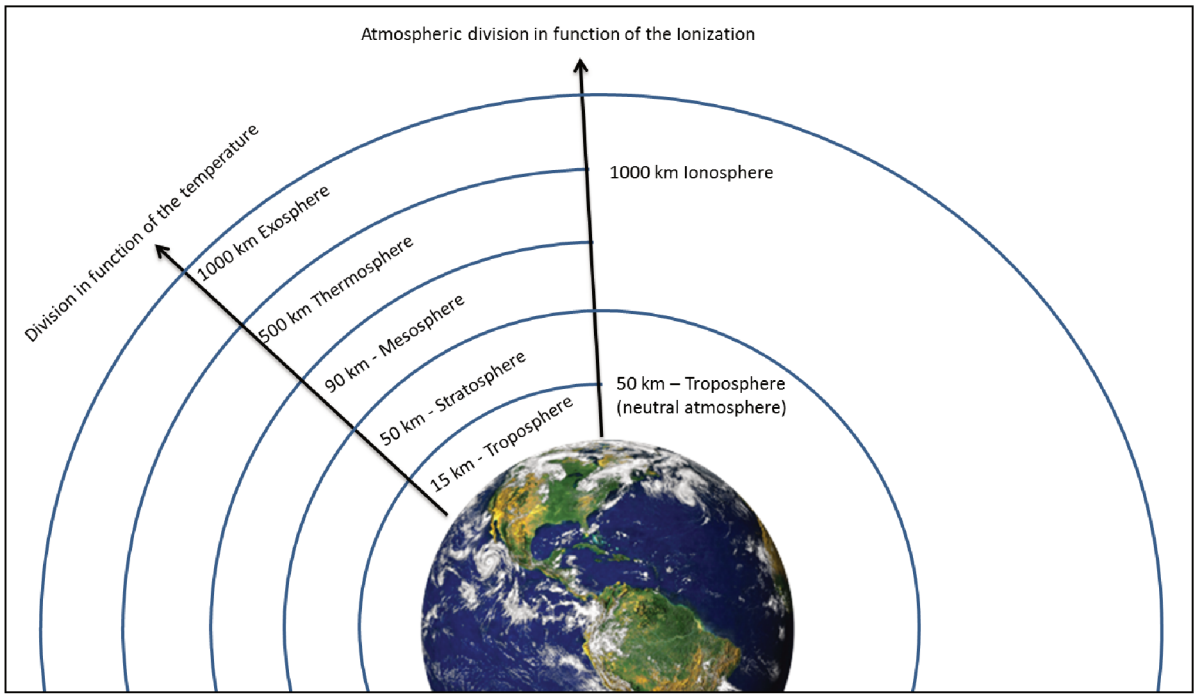

Figure 11 – Atmospheric division in function of temperature (Meteorology) and in function of electrical ionization (Geodesy).

In this work we consider the division in function of ionization and the next sections will detail the effects in GNSS signals caused by the tropospheric and ionospheric layers, respectively.

7.1. Tropospheric effects

The troposphere is the atmospheric layer between Earth surface and an altitude of approximately 50 km. It is a non-dispersive medium for frequencies lower than 30 GHz, e.g. the refraction does not depend on the signal frequency (Seeber, 2003).

Many effects of the terrestrial troposphere on GNSS signals are known, and the most important are the atmospheric attenuation, the tropospheric scintillation and the tropospheric delay (Sapucci, 2001). We briefly describe these three phenomenons in this part.

The atmospheric attenuation is a reduction of the electromagnetic wave power performed by one of the atmospheric elements, and it is different for each frequency. For bands between 1 and 2 GHz, which is the GNSS case, the attenuation is mainly due to the oxygen gas. These effects certainly affect L1 and L2 GNSS frequencies, which are 1575.42 and 1227.6 MHz, respectively.

Moreover, the scintillation is an oscillation in amplitude on the electromagnetic wave caused by irregularities and fast variations of the tropospheric refractive index. For small elevation angles and short fractions of time, the attenuation and tropospheric scintillation can be significant.

There are several tropospheric scintillation prediction models described in the literature, such as the Karasawa, ITU-R, designated by the international telecommunication union recommendations), Otung, DPSP (Direct Physical Statistical Prediction), STH2 (Statistical Temperature and Humidity 2), STN2 (Statistical Temperature and refractivity 2), Ortgies-N (Ortgies model based on component of the surface refractivity), Ortgies-T (Ortgies model based on component of the temperature), and Van de Kamp models. A detailed review and evaluation of these currently existing tropospheric scintillation prediction models have been presented in (Chen and Singh, 2014). The results confirmed that the ITU-R model gives the best scintillation intensity predictions for countries that have tropical climates, where this effect is usually stronger.

With regard to the tropospheric attenuation error, various mathematical models on millimeter wave propagation are derived in (Park et al., 2016). In such study, the recommended model is the ITU-R, also considered as good solution.

Nevertheless for elevation angles greater than ten degrees and relatively long periods, both effects (tropospheric attenuation and scintillation) are very small, and can often be neglected. However, these effects will get more attention since for next GNSS generation, new carrier frequencies in Ku/V band are expected to emerge as a promising alternative to the current frequency windows in L band as they get severely congestive. In the case of higher frequency bands, signal attenuation phenomenon through the atmosphere is significantly different from the L band signal propagation (Park et al., 2016).

The tropospheric delay is very well known in the space Geodesy literature. It generates larger errors than tropospheric scintillation and attenuation effects, even for traditional GNSS L band frequencies, and thus must be treated appropriately (Fund, 2009; Morel, 2015; Parkinson and Spilker, 1996). Following sections describe further details about the tropospheric delays, as well as some of its modeling approaches.

7.1.1. Tropospheric delay

The total tropospheric delay in zenith direction is usually referred as ZTD (Zenith Total Delay) and it has two main contributions, the so-called ZHD (Zenith Hydrostatic Delay) and the ZWD (Zenith Wet Delay) from hydrostatic and wet atmosphere, respectively. The ZHD varies mainly in function of temperature, latitude and atmospheric pressure and usually present values of up to about 2.3 m in zenith direction (Parkinson and Spilker, 1996). This delay can be estimated or predicted with good accuracy because its variation is small (~1 cm) over about 6 hours. On the other hand, ZWD relies on total atmospheric water vapor and its variation is much bigger, about 20% in a few hours. Such variations can represent up to ~35 cm in zenith direction. Consequently, its accurate prediction is difficult, even when in situ measurements are available. The above mentioned hydrostatic and wet delays can significantly increase when considering low elevation angles (Seeber, 2003).

In general, the models that estimate the tropospheric delay (T) can be written as (Seeber, 2003):

$$T = \int (n-1)dl = (10^{-6}) \int N_T ds, \tag{64}$$

where n represents the refractive index of air and the term $N_T = 10^6(n-1)$ is the tropospheric refractivity. The integral along the signal path is solved when the value of N_T is known.

Further in this discussion, it is showed as well, that the term N_T, can be spread into wet and hydrostatic parameters, which implies that the integral of (64) can be also presented as the sum of two integrals (Fund, 2009; Morel, 2015; Rüeger, 2002).

The tropospheric delay is estimated with an appropriated mapping function, which provides the relation between the zenith delay and other elevation angles. Since tropospheric delay can be approximated as the sum of the hydrostatic and wet delays affecting the signal along the path between satellite and receiver antennas, the tropospheric delay can be expressed as:

$$T = ZHD.m_h(E) + ZWD.m_w(E) \tag{65}$$

where:

- ZHD is the zenith hydrostatic delay,
- ZWD is the zenith wet delay,
- $m_h(E)$ and $m_w(E)$ are, respectively, the mapping functions that relate the hydrostatic and wet delay to the elevation angle (E).

For all troposphere related parameters, *h* and *w*, denote the hydrostatic component and wet, respectively. In order to better understand the tropospheric delay (T), it is necessary first to understand the tropospheric refractivity, to determine the terms ZHD and ZWD, as well as the models to be used as mapping functions $m_h(E)$ and $m_w(E)$.

The empirical expression for the tropospheric refractivity of a gas not ideal, including the water vapor, is given by equation (66) (Davis et al., 1985; Parkinson and Spilker, 1996):

$$N_T = k_1.\left(\frac{P_h}{T_K}\right).Z_H^{-1} + k_2\left(\frac{e}{T_K}\right).Z_W^{-1} + k_3.\left(\frac{e}{{T_K}^2}\right).Z_W^{-1} \tag{66}$$

where:

- P_h is the partial pressure mainly due to the dry air (in millibars),
- e is the partial pressure of the water vapor (in millibars),

- T_K is the temperature in Kelvin degrees,
- Z_H and Z_W are the factors of compressibility for the hydrostatic and wet components respectively,
- $k_1 = 77.604 \pm 0.0124, k_2 = 64.79 \pm 10$ and $k_3 = 377600 \pm 3000$ are constant values determined experimentally.

It must be modeled the relation between pressure and temperature with respect to the altitude, producing proper models for refractivity (N_T) with respect to the altitude using the equation (66). By applying the gazes law, the following equation is obtained (Davis et al., 1985):

$$N_T = k_1 . \frac{R . d}{M_H} + \left(k_2 - k_1 \frac{M_W}{M_H}\right) . \frac{e}{T_K} . Z_W^{-1} + k_3 . \frac{e}{T_K^2} . Z_W^{-1} \quad (67)$$

where:

- R is universal constant of the gazes,
- d is the total air density,
- M_H and M_W are the molar masses of the dry part of the air and the water vapor, in this order.

If we assume that $M_W = 18.0145\ kg/kmol$, $M_H = 28.9644\ kg/kmol$ and $R = 8.31434\ kJ/kmol\ °K$, it is possible to obtain (Parkinson and Spilker, 1996):

$$N_T = 22.276d + (16.5 \pm 10) . \frac{e}{T_K} . Z_W^{-1} + 377600 . \frac{e}{T_K^2} . Z_W^{-1} \quad (68)$$

The first term of equation (68), which refers to the hydrostatic refractivity, has a small imprecision ($\pm 0.014\%$), depending only on the total atmospheric density. Consequently, it can be determined with good precision. The remaining terms in equation (68) refer to the wet refractivity and possess considerable imprecision, relying on parameters with high variability (~20%) such as temperature and water vapor pressure.

In summary, equation (68) can be written as (Monico, 2008; Sanz Subirana et al., 2013):

$$N_T = N_H + N_W \quad (69)$$

with:

$$N_H = \left(\frac{k_1 R}{M_H}\right) d = 22.276d \tag{70}$$

and:

$$N_W = \left(k_2 - k_1.\frac{M_W}{M_H}\right).\frac{e}{T_K}.Z_W^{-1} + k_3.\frac{e}{T_K^2}.Z_W^{-1} \tag{71}$$

Since the determination of the wet refractivity is very complicated, several models were developed to describe the behavior of this variable. These models are employed to determine a priori corrections for the tropospheric delay and additional parameters can be estimated in the adjustment.

7.1.2. Models for tropospheric delay

The Saastamoinen model is one of the most used existing models for tropospheric delay. It is based on the assumption of linear decrease of temperature up to a medium altitude of about 12 km (tropopause). For altitudes higher than this limit a constant value characterizes the stratosphere as an isothermal model. It is also considered that the atmosphere is in hydrostatic equilibrium and all water vapor is concentrated in the troposphere, with the behavior of an ideal gaz.

With respect to the partial pressure of dry air and water vapor, exponential equations were adopted, because the values increase together with the total tropospheric pressure, although much faster. The model proposed by Saastamoinen with some refinements is presented in equation (72) (Hofmann-Wellenhof et al., 2008; Saastamoinen, 1972):

$$ZTD = 0{,}002277(1 + D)^{-1} \sec z \left[P_t + \left(\frac{1255}{T_K} + 0{,}05\right).e - B.tan^2 z\right] + \partial_R \tag{72}$$

where:

- ZTD is the zenith total tropospheric delay,
- P_t is the total barometric pressure in millibars,
- B, e and ∂_R are correction factors depending on the station altitude and the zenith angle (Hofmann-Wellenhof et al., 2008),

- z is the zenith angle.

The zenith angle (z) and the value for the term D can be obtained from the equations (73) and (74).

$$z = 90° - E \quad (73)$$

$$D = 0{,}0026 \cdot \cos 2\phi + 0{,}00028.H \quad (74)$$

where H is the station orthometric altitude and ϕ is the latitude.

It is important to underline that equation (72) can be manipulated to obtain only the dry tropospheric delay contribution. This can be achieved by setting the partial pressure of the water vapor (e) with null values.

In tropospheric modeling, the choices of the a priori ZHD model as well as the mapping functions (section 7.1.3), are very relevant aspects for centimeter accuracy-level applications. When using a good priori value for ZHD, the residual part of the ZTD, estimated in GNSS processing, corresponds to the ZWD.

About the a priori ZHD, the IERS 2010 conventions (Petit and Luzum, 2010) advise the use of the Saastamoinen model with measured pressure values at the stations, empirical models, as well results of NWP (Numerical Weather Prediction) based models.

For the empirical models, the GPT (Global Pressure and Temperature) is commonly used. This model corresponds to an expansion in spherical harmonics series up to degree and order 9. In this expansion are employed the mean values and mean amplitudes of pressure and temperature parameters from ECMWF (Boehm et al., 2007). More recently, improved empirical models have been used such as the GPT2w (Global Pressure and Temperature 2 wet) (Böhm et al., 2015; Kalita and Rzepecka, 2017). This model provides the mean values plus annual and semiannual amplitudes of pressure, temperature water vapor pressure and all climatological parameters are derived from monthly mean pressure level data of ERA-Interim (European Centre for Medium-Range Weather Forecasts Re-Analysis) fields (Böhm et al., 2015).

With the considerable availability of meteorological data, NWP models are also becoming commonly used in GNSS processing (Morel, 2015). With regards to these NWP models, one can use the values of ZHD calculated by the University of Vienna ZHD model (VZHD) derived from the ECMWF (European Centre for Medium-Range Weather Forecasts)

data (Böhm et al., 2011; Fund et al., 2011). Fund et al. (2011) illustrates the difference between these different choices and explain the advantage of using VZHDs, which have better spatial and temporal resolutions. Another option for a priori ZHD values based on NWP models, are those provided by University of New Brunswick (UNB) service, based on NCEP (National Center of Environmental Prediction) data (Böhm et al., 2011; Urquhart and Santos, 2011). The recent models based on NWP were not used in this thesis, however their importance is considered and the application of NWP based solutions is aimed for future works.

7.1.3. Mapping functions

A mapping function is a mathematical model for the elevation dependence of the respective delays. As previously mentioned, the tropospheric delay increases when the elevation angle of the GNSS satellite decreases. This occurs mainly because the signal crosses a longer path in the Earth troposphere. The curvature of the Earth and the curvature of the path of the satellite signal propagating through the atmosphere also contributes to this increased delay (Parkinson and Spilker, 1996). Figure 12 illustrates this situation.

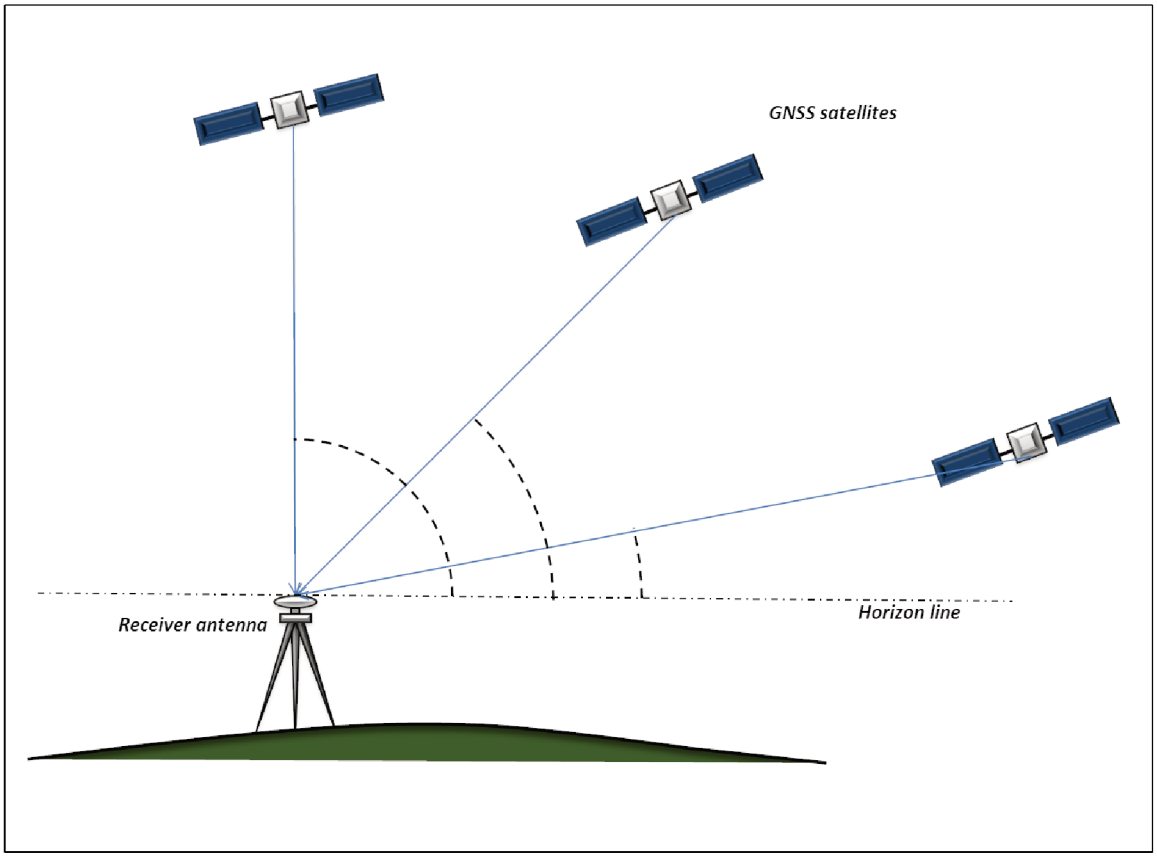

Figure 12 – GNSS satellites at several elevation angles

Thus, to obtain the values of delay in slant direction it is necessary to use a mapping function. In general, these functions are based on continued fractions as a function of the sine of the elevation angle, and the coefficients (a, b, and c) associated with tropospheric delay variations (Marini,1972):

$$m(E,a,b,c) = \frac{1+\dfrac{a}{1+\dfrac{b}{1+c}}}{\sin(E)\dfrac{a}{\sin(E)+\dfrac{b}{\sin(E)+c}}} \tag{75}$$

As tropospheric delay is divided in hydrostatic and wet delays, two groups of coefficients (a_h, b_h, c_h) and (a_w, b_w, c_w) are required. So, the tropospheric delay is given by equation (76):

$$ZTD(E) = m_h(E, a_h, b_h, c_h).ZHD + m_w(E, a_w, b_w, c_w).ZWD \tag{76}$$

Some of the most popular mapping functions are Marini (Marini, 1972), Lanyi (Lanyi, 1984), and Davis (Davis et al., 1993). Such functions have a limited accuracy due to the temperature dependence of the Earth surface. The Niell Mapping Function (NMF) does not have this problem. But, the NMF was derived from 2 years of radiosonde measurements. In these functions, spatial and temporal variability only depend on latitude and seasons of the year. Such mapping functions have as considerable advantage the independence from surface meteorology, thus they are particularly valuable for those situations where such input are not available (Niell, 1996). Besides Fund et al. (2011) verified that, for 10 degrees elevation cut-off, the NMFs does not introduce significant errors, in comparison to the usage of the more sophisticated mapping functions.

The meteorological contribution is exploited for mapping functions based on data from NWP model. Coefficients (a, b, c) are computed by ray-tracing. Through a specified NWP model data, the hydrostatic and wet delays are retrieved at a certain elevation angle. Then the hydrostatic and wet slant coefficients are estimated by least squares fitting of the fraction form (Marini, 1972) normalized to yield unity at zenith direction (Herring, 1992).

The main example of these MFs are the Isobaric (IMF – Isobaric Mapping Function) (Niell and Petrov, 2003), the VMF (Vienna Mapping Function) (Boehm and Schuh, 2004), the VMF1, an update of the VMF, and the GMF (Global Mapping Function) (Boehm et al., 2006). Table 11 summarizes some additional information about the mapping functions mostly adopted by the IGS analysis centers and their respective models (Urquhart et al., 2014).

Table 11 - Mapping functions

Mapping Function	Resolution	ZHD Model
NMF	Annual resolution, derived from radiosonde data	SPT
VMF1	6h resolution, integration of data from ECMWF	VZHD
GMF	Annual resolution, spherical harmonics of VMF1 data	GPT

The spatial resolution of the NWP itself, directly impacts the ability to model atmospheric conditions effectively. Thus at the UNB the UNB-VMF1 service was developed using the high resolution model from the CMC (Canadian Meteorological Center) based on GDPS (Global Deterministic Prediction System). Using ray-tracing algorithms developed by

Nievinski (2009), the differences between VMF1 and UNB-VMF1 were assessed. The results between the 2 MF were almost identical except in certain conditions.

7.2. Ionospheric effects

Ionosphere is the atmospheric layer situated, approximately, between 50 km and 1000 km altitude from the Earth surface as illustrated in the beginning of this chapter by Figure 11.

The ionosphere is formed because the Sun ultra-violet rays ionize a portion of gaz molecules, increasing the number of free-electrons. These free-electrons affect the radio signal waves, and so the GNSS satellite signals. The ionospheric effect is very significant (1-2 ppm or more) even under moderate ionospheric conditions at mid-latitudes, with minimal presence of sunspots. Such effects vary in time and space, influenced by geographical location, geomagnetic activity, solar cycle, season of the year, time of day, among other anomalies and irregularities, such as the equatorial anomaly and the ionospheric scintillation (Camargo et al., 2000; Leick, 2004; McNamara, 1991; Seeber, 2003). Such irregularities, especially the ionospheric scintillation can even provoke a loss of tuning between the receiver and satellite (Kintner et al., 2007; Sreeja et al., 2011).

Differently of the troposphere, the ionosphere is a dispersive medium wich means that its effect is frequency dependent, and can be quite well mitigated by interfrequency combinations. Historically, the possibility to remove the ionospheric effect is the main reason that different frequencies were implemented in GNSS (Hofmann-Wellenhof et al., 2008).

7.2.1. Ionospheric refraction

In terms of geodetic positioning, the ionospheric parameter that produces the major part of the effects in GNSS signals is the total number of electrons in the signal path throughout the ionosphere, which is usually called TEC (Total Electron Contents). Therefore, the magnitude of the systematic error due to ionospheric refraction is directly proportional to the TEC in the ionospheric layer and inversely proportional to the square of the carrier wave

frequency. Thus, in the course of this section it is developed this relationship between the TEC and the ionospheric refraction for phase and pseudorange measurements.

For the propagation of a single electromagnetic wave in space, the phase velocity (v_{ph}) can be expressed as a function of its corresponding wavelength (λ) and frequency (f) (Hofmann-Wellenhof et al., 2008):

$$v_{ph} = \lambda f \tag{77}$$

Considering a group of waves, i.e. the codes modulated on phase observable, the propagation of the resultant energy is defined by group velocity (v_{gr}):

$$v_{gr} = -\frac{df}{d\lambda}\lambda^2 \tag{78}$$

This velocity has to be considered for GNSS pseudorange measurements. Thus, the relationship between phase and group can be established by forming the total differential of phase velocity in equation (77):

$$dv_{ph} = fd\lambda + \lambda df \tag{79}$$

By rearranging the previous equation one can obtain:

$$\frac{df}{d\lambda} = \frac{1}{\lambda}\frac{dv_{ph}}{d\lambda} - \frac{f}{\lambda} \tag{80}$$

With the substitution of (80) in the (78):

$$v_{gr} = -\lambda\frac{dv_{ph}}{d\lambda} + f\lambda, \tag{81}$$

the Rayleigh equation can be found by subtituting equation (77) into equation (81):

$$v_{gr} = v_{ph} - \lambda\frac{dv_{ph}}{d\lambda} \tag{82}$$

The wave progation in a medium depends on the refractive index. Considering the respectives phase and group refractive indices (n_{ph}, n_{gr}), the phase and group velocities can be represented as:

$$v_{ph} = \frac{c}{n_{ph}}, \qquad v_{ph} = \frac{c}{n_{gr}} \tag{83}$$

By performing the derivatives of the phase velocity with respect to the wavelengh term (λ):

$$\frac{dv_{ph}}{d\lambda} = -\frac{c}{n_{ph}^2}\frac{dn_{ph}}{d\lambda} \tag{84}$$

and substituting the equation (83) into equation (84) into Rayleigh equation (82) yields:

$$\frac{c}{n_{gr}} = \frac{c}{n_{ph}} + \lambda\frac{c}{n_{ph}^2}\frac{dn_{ph}}{d\lambda} \tag{85}$$

which may be presented as:

$$\frac{1}{n_{gr}} = \frac{1}{n_{ph}}\left(1 + \lambda\frac{1}{n_{ph}^2}\frac{dn_{ph}}{d\lambda}\right) \tag{86}$$

Inverting the equation (86) and applying the approximation: $(1+\varepsilon)^{-1} \cong (1-\varepsilon)$:

$$n_{gr} = n_{ph}\left(1 - \lambda\frac{1}{n_{ph}}\frac{dn_{ph}}{d\lambda}\right) \tag{87}$$

The previous equation leads to the modified Rayleigh equation (88) (Hofmann-Wellenhof et al., 2008; Monico, 2008):

$$n_{gr} = n_{ph} - \lambda\frac{dn_{ph}}{d\lambda} \tag{88}$$

By differentiating the relation $c = \lambda f$ with respect to wavelength (λ) and frequency parameters f:

$$\frac{d\lambda}{\lambda} = -\frac{df}{f} \tag{89}$$

and substituting it into (88), a slightly different form is achieved:

$$n_{gr} = n_{ph} + f\frac{dn_{ph}}{df} \tag{90}$$

Concerning, the ionosphere refractive index for phase n_{ph}, an approximation can be obtained by (Seeber, 2003):

$$n_{ph} = 1 + \frac{c_2}{f^2} + \frac{c_3}{f^3} + \frac{c_4}{f^4} + \cdots \tag{91}$$

The coefficients: c_2, c_3, c_4 rely only on the electrons density n_e (i.e. electrons per

cubic meter) along the signal propagation path. Considering only the effects of the first order, by cutting off the series expansion after the quadratic term:

$$n_{ph} = 1 + \frac{c_2}{f^2} \tag{92}$$

the total differential of this equation yields:

$$dn_{ph} = -\frac{2c_2}{f^3} df \tag{93}$$

Replacing the two last equations in the modified Rayleigh equation (90) we have:

$$n_{gr} = 1 + \frac{c_2}{f^2} - f\frac{2c_2}{f^3} = 1 - \frac{c_2}{f^2} \tag{94}$$

Thus, the group and phase refractive indexes differ only in the sign of the c_2 coefficient. As clarified previously, such coefficient depends of the electrons density (n_e). Thus, considering an estimate for the coefficient c_2 (Davies, 1990; Seeber, 2003):

$$c_2 = -40.3\, n_e$$

In units of the International System of Units (*Système International d'unités,*in French and traditionally abbreviated as SI), the constant 40.3 is given in $[mHz^2(el/m^2)^{-1}]$ and the n_e in $[el/m^3]$. Thus:

$$n_{ph} = 1 - \frac{40.3 n_e}{f^2}, \qquad n_{ph} = 1 + \frac{40.3 n_e}{f^2}, \tag{95}$$

Since the electrons density is always positive group and phase will have always different velocities. Thus, is not difficult to verify that group is delayed and phase is advanced. As a consequence, GNSS code ranges are increased and phase ranges are reduced of the same quantity.

The optical distance (S_r) between the satellite *s* and the receiver *r*, regardless of the other systematic errors, following the principle of Fermat, can be defined as:

$$S_r = \int_r^s n dS \tag{96}$$

By setting $n = 1$, the geometric distance (S_0) along a straight line between the

satellite and the receiver may be achieved:

$$S_0 = \int_r^s dS_0 \tag{97}$$

The difference between the two last equations can provide the ionospheric refraction, neglecting the other systematic errors:

$$I = \int_r^s nds - \int_r^s ds_0 \tag{98}$$

The equivalent ionospheric refraction for code and phase measurements can be expressed by substituting the appropriated refractive index in equation (98):

$$I_{L_i} = \int_r^s \left(1 + \frac{c_2}{f^2}\right) ds - \int_r^s ds_0 \tag{99}$$

$$I_{P_i} = \int_r^s \left(1 - \frac{c_2}{f^2}\right) ds - \int_r^s ds_0 \tag{100}$$

When approximating the integration for the first term along the geometric range, a simplification of equations (99) and (98) can be obtained as follows:

$$I_{L_i} = -\int_r^s \frac{c_2}{f^2} ds_0, \qquad I_{P_i} = \int_r^s \frac{c_2}{f^2} ds_0 \tag{101}$$

result that can be also written:

$$I_{L_i} = -\frac{40.3}{f^2} \int n_e ds_0\,, \qquad I_{P_i} = \frac{40.3}{f^2} \int n_e ds_0 \tag{102}$$

By definition, the TEC is the number of electrons in a column with a crossed section of one square meter along all the GNSS signal path up to the receiver's antenna. The TEC itself can be expressed as (Davies, 1990):

$$TEC = \int n_e ds_0 \tag{103}$$

A unit of TEC corresponds to 10^{16} electrons/m^2 and is usually referred as TECU (TEC-Unit). The extreme values of TEC observed on the Earth ionosphere are situated

between 10^{16} to 10^{19}el/m^2 (Parkinson and Spilker, 1996).

Therefore, the ionospheric delay as function of the TEC can be expressed as (Sanz Subirana et al., 2013):

$$I_{L_i} = -\frac{40.3}{f^2}TEC, \qquad I_{P_i} = \frac{40.3}{f^2}TEC \tag{104}$$

Since the phase measurements are advanced on crossing the ionosphere, this observable presents negative ionospheric delays ($-I_i$). On the other hand, the code measurements undergo a positive delay ($+I_i$).

Equations (104) represent 99.9% of the ionospheric effect. This is the first order of the total delay caused by ionosphere disturbances. The higher order magnitude errors of ionospheric effects can achieve a few centimeters and they can be relevant for high accuracy applications, e.g. geophysical studies (Petrie et al., 2010). Seeber (1993) summarizes the magnitude of the first, second and third order of the ionospheric effect over each GPS frequency as presented in Table 12.

Table 12 - Maximum systematic vertical effect due to the ionosphere

Frequency	1st order ($1/f^2$)	2nd order ($1/f^3$)	3rd order ($1/f^4$)
L_1	32.5 m	0.036 m	0.002 m
L_2	53.5 m	0.076 m	0.007 m
L_0	0.0 m	0.026 m	0.006 m

Source: Seeber (1993).

7.2.2. Standard geometric mapping function

In order to obtain TEC values in the vertical direction, the so called VTEC (Vertical TEC), a standard geometric mapping function is usually employed, such projection is given by the equation (105) (Liu, 2001).

$$VTEC = \cos(z')\,TEC \tag{105}$$

with

$$\sin(z') = \frac{r_m}{r_m + h_m} sin(z) \tag{106}$$

Therefore, the slant ionospheric delays in (104) can be expressed now as vertical ionospheric delays:

$$I_{L_i} = -\frac{1}{\cos z'}\frac{40.3}{f^2}VTEC, \qquad I_{P_i} = \frac{1}{\cos z'}\frac{40.3}{f^2}VTEC \tag{107}$$

In these equations, z and z' represent the satellite zenith angle of the signal path over an ionospheric point, placed over a plane at medium height in the ionosphere (h_m), respectively, and r_m is the medium radius of the Earth ($r_m \cong 6371km$). Figure 13 illustrates the geometric quantities related in equations (105) and (106). In this figure it is important to highlight that the vertical quantity produced (VTEC), by using the standard geometric mapping function, does not have its position at the station location as for the tropospheric mapping function. Thus, the VTEC is not projected in the zenith of the station, as clarified in Figure 13. Every GNSS satellite has a different value of VTEC.

The ionospheric models that usually consider this approach define the ionosphere as a thin shell layer. This assumption is possible thanks to the electrons concentration at certain levels in the ionosphere (section 7.2.4). Therefore, the VTEC position is determined at the intersection between the receiver-satellite vector and this infinitesimal layer, which has pre-established altitude. This altitude is where the ionospheric profile presents its strongest values (c.f. Figure 15) and represents the ionosphere.

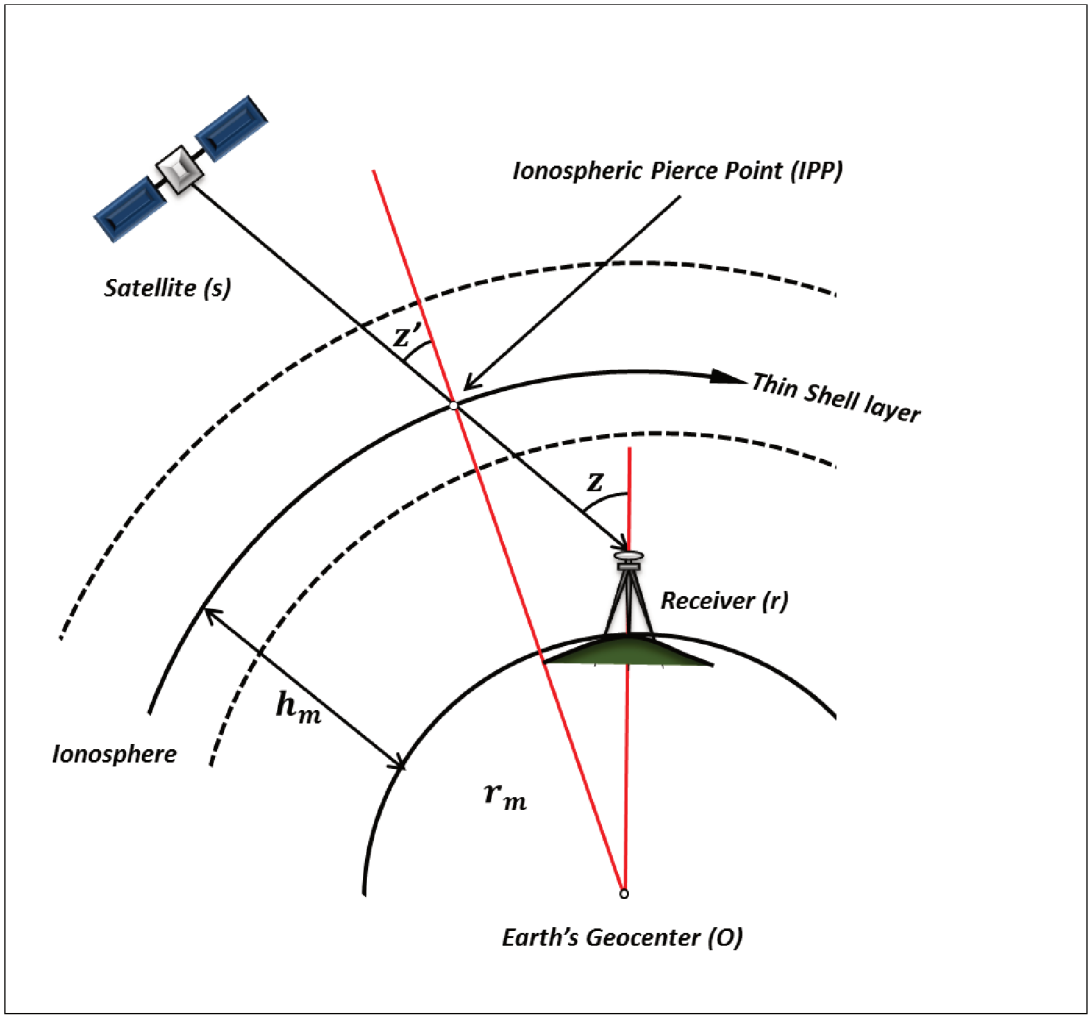

Figure 13 – geometric trajectory of the satellite signal
Source: adapted from Camargo (1999)

7.2.3. Ionospheric Piercing Points

It is possible to determine the position of the IPPs (Ionospheric Piercing Points) in function of the station geographic coordinates. Moreover, to know the satellite azimuth and elevation angle is necessary. Thus, the geographic latitude and longitude of the IPP can be obtained by the following expressions (El-Gizawy, 2003)

$$\phi_{PI} = sin^{-1}[sin\phi_r cos\psi + cos\phi_r sin\psi cosAz] \tag{108}$$

$$\lambda_{PI} = \lambda_r + sin^{-1}\left(\frac{sin\psi sinAz}{cos\phi_{PI}}\right) \tag{109}$$

with:

$$\psi = \frac{\pi}{2} - E - sin^{-1}\left(\frac{r_m}{r_m + h_m}\cos(E)\right) \quad (110)$$

where:

- ϕ_{PI} and λ_{PI} represent the IPP latitude and longitude, respectively,
- ϕ_r and λ_r are the receiver latitude and longitude GNSS,
- Az is the satellite azimuth angle,
- r_m is mean Earth ratio,
- h_m is the mean altitude of the ionospheric layer.

Figure 14 shows the IPPs at a given epoch determined for GNSS stations over France considering an ionospheric layer altitude (h_m) of 400 km.

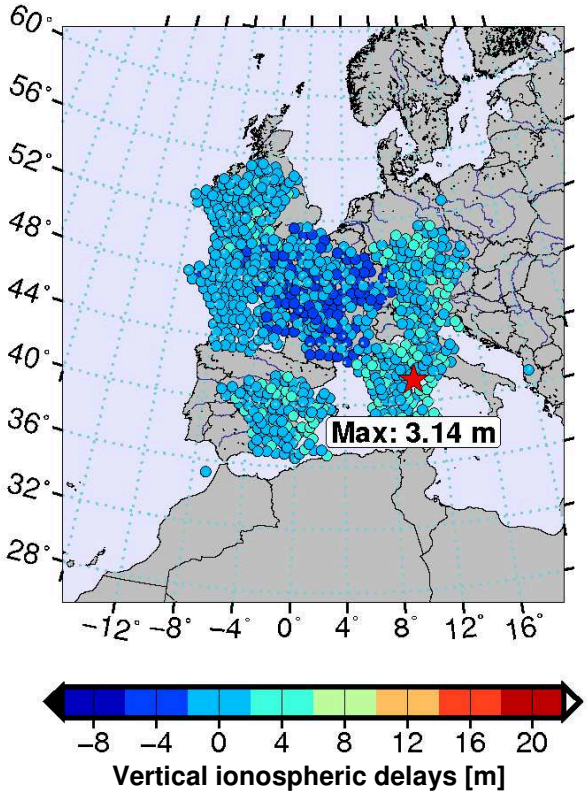

Figure 14 – Ionospheric Pierce Points colored in function of corresponding vertical ionospheric delays [m], over Orphéon network stations.

The IPP position determination is a very important step of ionospheric modeling, as well as for the use of the generated models. Given that, commonly used ionospheric models provide ionospheric grids of IPP with the respective vertical ionospheric delay or even the VTEC values.

7.2.4. Ionospheric divisions

The ionization of gazes occurs gradually and during the process, a molecular gaz dissociates first into an atomic gaz that ionizes with the increasing temperature. The resulting plasma is composed by a mix of neutral particles, positive ions and negative electrons (Kaplan and Hegarty, 2006). Due to the different molecules and atoms present in the atmosphere and their different rates of absorption, different ionospheric regions are formed.

When the ionosphere was discovered, the first ionospheric regions were called E and F, respectively for Electric and Field with the idea that less dense layers with previous alphabet letters could appear latter (Parkinson and Spilker, 1996).

The D layer stays in the lower part of the ionospheric layer between 60 and 90 km from the Earth surface (c.f. Figure 15). The atmosphere in this region is not very dense and the atoms divided in ions recombine quickly. The level of ionization is directly related with the solar electromagnetic radiation that starts with the Sunrise and reduces drastically or even disappears during the night (Leick, 2004).

The E layer extends, approximately, from 90 to 140 km of altitude considering the Earth's surface and its primary source of ionization is the solar electromagnetic radiation in the X-ray range. This layer is also composed by a fine layer designed 'E-sporadic', due to variations in the electrons density close to the region between 90 and 130 km (McNamara, 1991).

The F layer is placed between the altitudes of 140 km and 1000 km and is subdivided in F1 and F2 layers that surge during the day. In this layer, the electrons and ions recombine slowly due to the low pressure. The effects due to the solar radiation in this layer develop slowly and peaks of electrons density are observed after midday.

The ionospheric regions with their diurnal differences are represented in Figure 15.

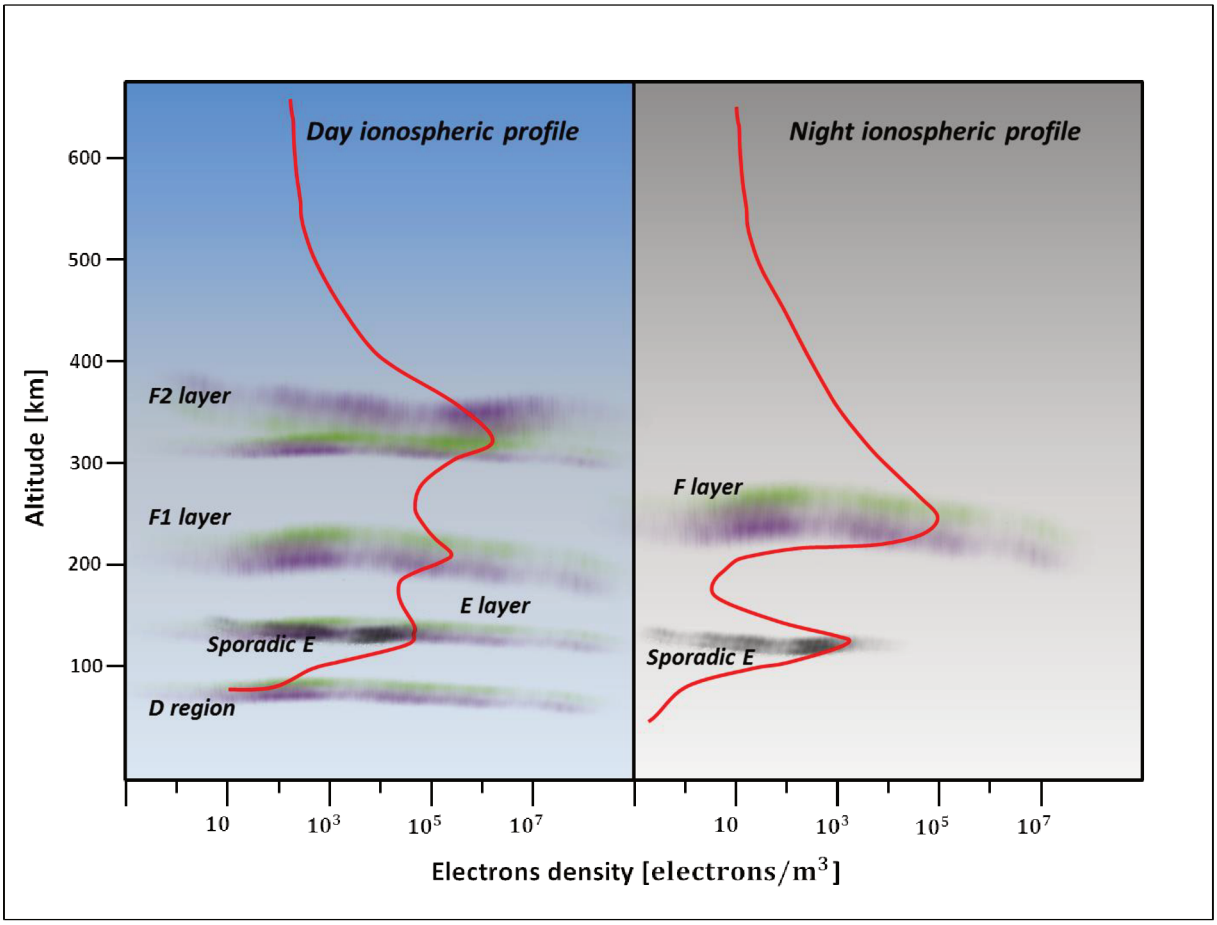

Figure 15 – Subdivisions of Ionosphere
Source: adapted from <http://www.sws.bom.gov.au/Educational/1/2/5>, access in 02/02/2017

The F1 layer is formed between the altitudes of 140 and 200 km and the layer F2 between 200 and 1000 km. The F1 layer together with E layer is responsible for up to 10% of delay impacting GNSS signals. The F2 layer is more dense and presents much more variability, causing the most important effects for the radio waves propagation at the range of GNSS signals frequency. The altitude of the peak of electrons density at the F2 layer varies between 250 and 400 km, but can be higher or sometimes lower under extreme atmospheric conditions (Parkinson and Spilker, 1996).

7.2.5. Ionospheric variations

The temporal variations of the ionosphere comprises the diurnal and seasonal variations as well as cycles of long periods. They influence directly the changes of electrons in the atmosphere (Parkinson and Spilker, 1996).

The diurnal variations are caused by the alterations that occur in certain regions of the ionosphere, and disappear at night due to the recombination and junction of the electrons and ions. The main reason for the existence of the diurnal variations is due to the illumination of the Sun, which means the solar radiation.

The ionospheric seasonal variations occur along the year due to the variations of the Sun zenith angle as well as to intrinsic changes in the ionosphere. Such variations are expected to be different according to the ionospheric region (section 7.2.6). In general, in the equinoxes the ionospheric effects are considerably higher, while the minimum values are verified around solstices.

The long cycle variations, in the electrons density, have periods of about 11 years. They are directly associated to the occurrence of sunspots, which corresponds to the periods of solar high activity. An increase of sunspots number increases the solar radiation and generates a change of electrons density in the ionosphere (Leick, 2004). A white image of the Sun with some spots is shown by Figure 16, where one can observe some grouped dark spots over the solar surface.

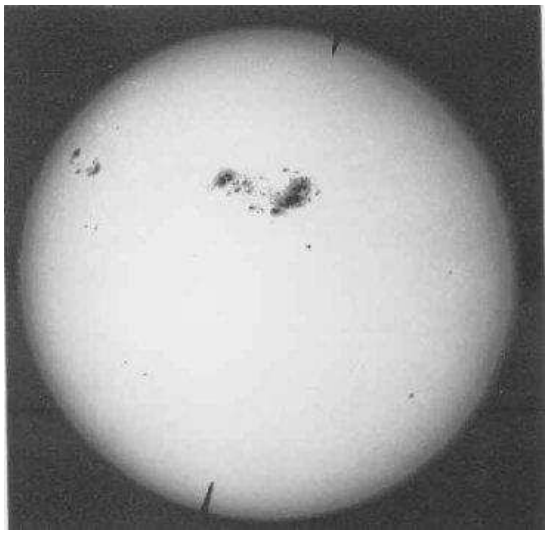

Figure 16 – White image of the Sun's surface showing some sunspots.
Source: http://www.crh.noaa.gov/fsd/?n=sunspots

The sunspots are colder regions and thus the darkest ones in the Sun surfaces. They are surrounded by more brilliant regions that produce high level of ultraviolet radiation. Therefore, an increase in the sunspots number directly provokes changes in the electrons density in the ionosphere. The sunspots generally appear in groups and are associated to intense magnetic fiels in the Sun. Some of them remain only for a few days, while others can

continue during several solar rotations. The period of a solar rotation correspond to about 27 terrestrial days (Leick, 2004).

Figure 17 shows the history of solar cycles (averaged number of sunspots) since 1700 up to nowadays. Concerning the information in this figure, it is important to emphazise that, from the year 1700 up to 1750, the mean of solar sunspots number where computed yearly (grey part of the graph), while from year 1750 up to nowadays, aproximately, this mean is computed monthly (blue part of the graph).

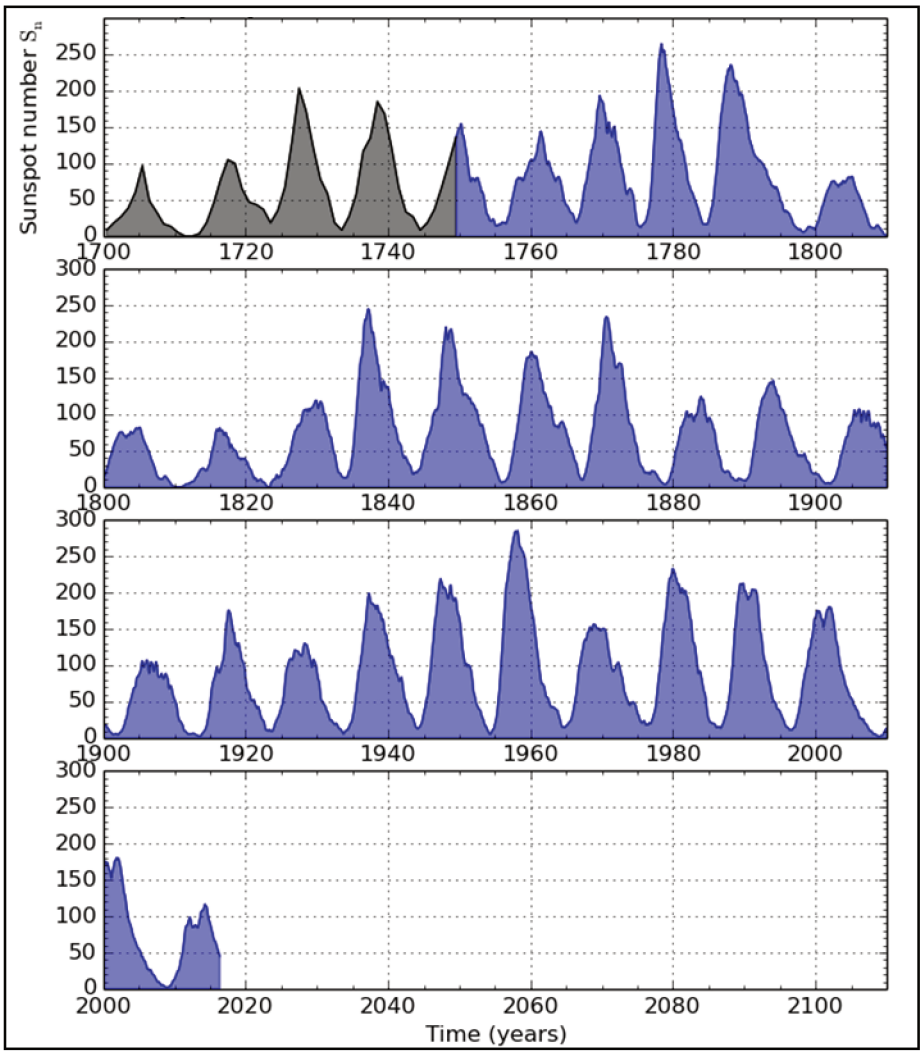

Figure 17 – Historic of sunspots number (solar cycles).
Source : http://sidc.oma.be/html/wolfaml.html. Access at 27/12/2016

Besides the cycles of 11 years, there are also longer cycles which can have period of about 80 years. According to Leick (2004), such cycles are not symmetric as we can verify in Figure 17.

The prediction of the solar cycle behavior becomes reliable only after about 3 years the minimal number of sunspots number (Matsuoka, 2007). Figure 18 presents the prediction made by NASA up to 2020. The last peak of sunspot numbers was for the sun solar cycle 24 and occurred in 2014. Since the current cycle has began several year ago, the current predictions are very reliable.

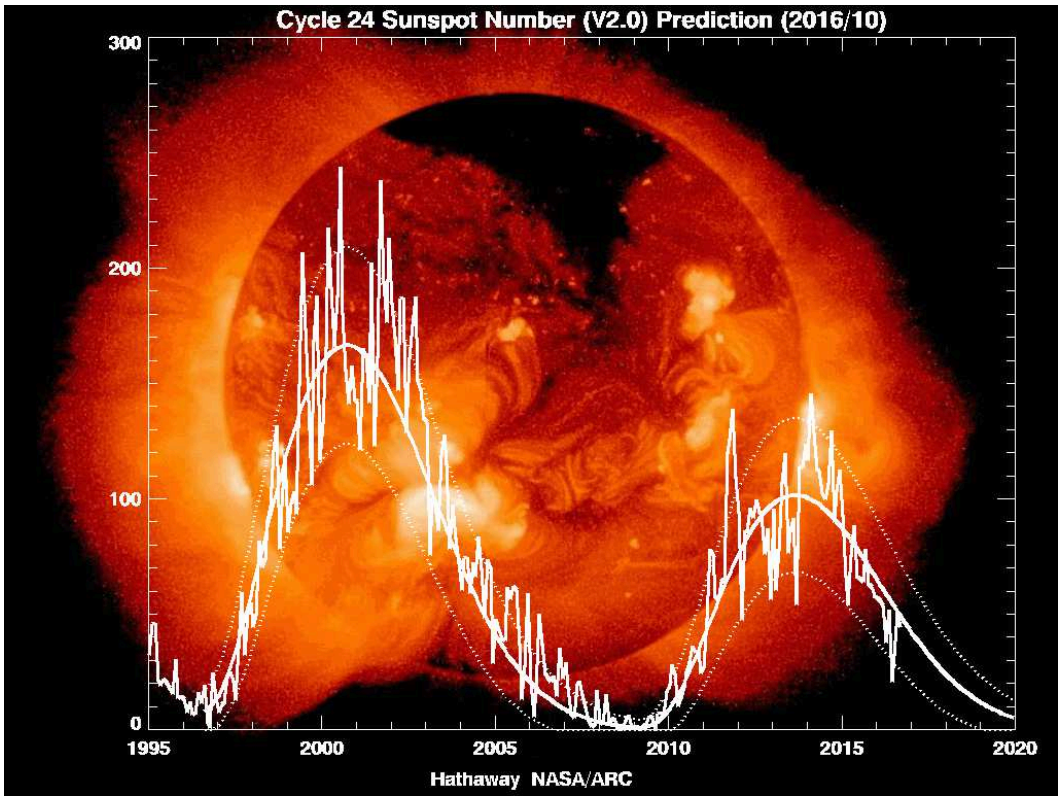

Figure 18 – Prediction of sunspots number (solar cycle 24)
Source: https://solarscience.msfc.nasa.gov/images/ssn_predict_l.gif
Access on 27/12/2016

Regarding Figure 18, we could say that nowadays the number of sunspots could be considered low, especially in comparison to the high values observed around 2003, which was the maximum period of sunspots number of previous solar cycle.

7.2.6. Geographic ionospheric regions

Over the globe, the ionospheric structure is not homogeneous. There are three major geographic ionospheric regions. They are known as high and medium latitudes and also equatorial regions.

Even though amplitude of the geographic ionospheric regions cannot be exactly established, when projected in the Earth surface, it is convenient to indicate, approximately, their localization. Therefore, Figure 19 shows the geographic localization of such regions in the global map.

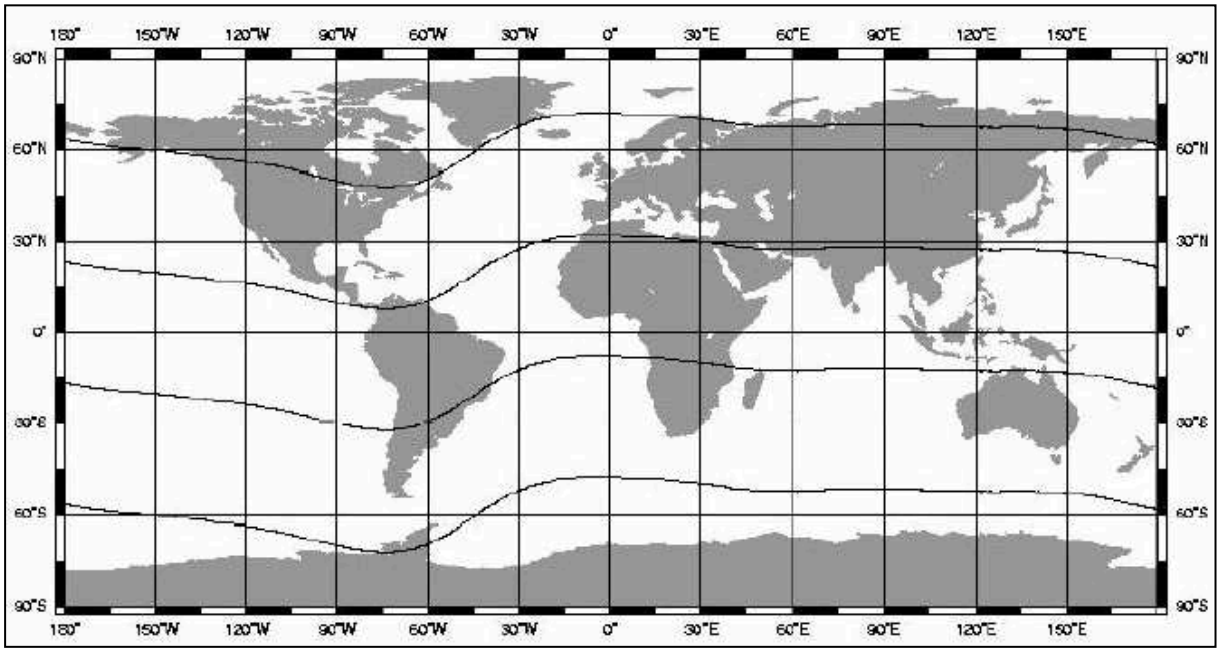

Figure 19 - Geographic regions of the ionosphere
Source: adapted from Seeber (2003)

The ionosphere over the poles, usually called polar ionosphere or high latitude ionospheric regions, is extremely instable. The equatorial region is characterized by a high level of electrons density, and several ionospheric particularities occur in this region. On the other hand, the medium latitude ionospheric regions are considered relatively free from ionospheric anomalies (Marques, 2012; Seeber, 2003).

7.2.7. International Reference Ionosphere

IRI (International Ionosphere Reference) is a model for ionosphere activity parameters based on data sources such as: ionosondes networks; incoherent scatter radars (Jicamarca, Arecibo, Millstone Hill, Malvern, St. Santin), ISIS (International Satellites for Ionospheric Studies) and Alouette topside sounders, besides of ionospheric sensors in several satellites and rockets. IRI model is a result of efforts realized by an International project with

supports from COSPAR (Committee on Space Research) and URSI (International Union of Radio Science) (Bilitza et al., 2012).

An online tool for IRI users is available at (omniweb.gsfc.nasa.gov). Many ionosphere activity indicators can be obtained, considering a profile between 50 km to 2000 km altitude. Users can set a specific location, time and date. One of the most representative indicators provided by IRI is the F10.7, because it is highly correlated with sunspots (Tapping, 2013). This index characterizes solar radio flux at 10.7 cm (2800 MHz). It is reported in s.f.u (solar flux units) and varies between 50 and 300 s.f.u. during a solar cycle (NOAA, 2017). IRI model products, such as F10.7 index and TEC are employed in our study to obtain information about ionospheric activity for experiments realized in Part III.

PART II - FLOAT PPP-RTK WITH TROPOSPHERIC MODELING

8. Introduction to Part II

Part II, focuses on tropospheric SSR corrections. The findings presented in this part are published in de Oliveira et al. (2017):

Figure 20 – Publication of the discussions and results presented in Part II

It is also important to underline that in Part II, ionospheric SSR corrections are not considered yet, as well as ambiguity resolution. However, they are taken into account in Part III. So Float PPP-RTK is processed.

The use of external tropospheric information in GNSS processing could reduce high correlations between estimated parameters and so reduce the convergence time of the position. This motivated several studies to generate tropospheric models to produce corrections for positioning applications. These corrections can be generated by means of empirical models, meteorological data, NWP, or directly from modeling the ZTD estimates over a GNSS reference network.

Böhm et al. (2015) introduced the empirical GPT2W (Global Pressure and Temperature 2 Wet) model to derive a priori ZWDs from mean values, annual and semi-annual terms for water vapor pressure, weighted average temperature, and the water vapor decay factor. The comparison of this model with the delays estimated by IGS for 341 stations during the year of 2012 presented an average RMS (Root Mean Square) of 3.6 cm.

Ibrahim and El-Rabbany (2011) analyzed the impacts of using the NWP-based tropospheric corrections of NOAA (National Oceanic and Atmospheric Administration) on ionospheric-free PPP solutions. They concluded that the performance of the model is a function of the season of the year and geographical location. The NWP model improved the PPP solution convergence by respectively 1%, 10% and 15% for the latitude, longitude and height components. In recent works, conducted at GFZ (German Research Center for Geosciences), it was studied the delivery of real-time tropospheric products (e.g. STDs, tropospheric gradients, and mapping functions using NWP models) with high speed and precision (Zus et al., 2014). Dousa and Elias (2014) described a new concept to derive ZWD using the model of Askne and Nordius (1987) with external meteorological data from numerical weather models. Their approach was superior to existing methods by a factor of 2 to 3. The impact of the initial tropospheric delays on PPP during active tropospheric conditions has been assessed using combined NWP and GNSS modeling, and improvements by up to 30% have been obtained for the convergence of the height component (Kalita and Rzepecka, 2017).

Hadas et al. (2013) discussed the impacts of two a priori tropospheric models on simulated float PPP-RTK. The first one was derived from near real-time ZTD estimates on a real-time GNSS network data. The second one was derived from meteorological parameters, such as temperature, pressure, and humidity. The positive impact of tropospheric model application to positioning on convergence time is evidenced but not quantified. Li et al. (2014a) presented regional atmospheric augmentation results for the PPP-RTK system in development at the GFZ. Comparable accuracy and convergence time with NRTK were obtained. Although, even if the proposed approach uses a sparse network, the solution presented by Li et al. (2014b) still requires a bidirectional link of communication. Shi et al. (2014) introduced a strategy to overcome this limitation with local troposphere corrections. It consists of modeling ZWD estimates inside a real-time GNSS reference network thanks to OFC (Optimal Fitting Coefficients). This method does not require the a priori knowledge of the user location, since the coefficients can be broadcasted to unlimited number of users. It is quiet similar to the low order surface model also known as partial derivative algorithm presented by (Wübbena et al., 1996) and studied by Fotopoulos and Cannon (2001). However, the method described in Shi et al. (2014) can test up to several sets of coefficients by applying different constraints and choosing the optimal set, which makes the method more adaptive.

Concerning PPP in general, the above mentioned research only indicates that tropospheric corrections can improve its performances, especially the convergence time. However, the use of tropospheric corrections for PPP still needs to be assessed and quantified with a significant amount of data.

In this research, special attention is given to methods that need a mono-directional communication link. So, the assessment is dedicated to the use of tropospheric modeling by OFCs in float PPP-RTK. In comparison with Shi et al. (2014), this study is done on a larger area that requires one to go further by using the second order degree of their mathematical model, what has not been presented before. Another positive point is that GNSS data of a real-time reference network well densified over France (160 stations) with a regular distribution (sites inter-distances of 60 km) are used and the effect of reducing up to 75% its density is assessed. In order to consider the weather variability, periods over the four seasons of year 2014, with different meteorological conditions are selected to be analyzed in the experiments. There is an additional consideration to the impact of adding GLONASS data to float PPP-RTK processing.

The next sections describe the overall strategy employed and the GNSS data used. The assessment and outcomes of the strategies adopted are then discussed, while conclusive considerations are presented in the summary section.

9. Method, data and processing

The products and the processing parameters used to estimate the real time ZWDs at the reference network, as well as the methods employed to obtain ZWDs corrections are described in this section.

9.1. Methodology

The main inputs as well as the strategy used to accomplish the tropospheric modeling are presented in Figure 21. In the first step, ZWDs are estimated in real-time over a reference GNSS network with station positions strongly constrained (1 cm). In the second step, ZWD estimates are used to generate a model for ZWDs usable at any location in the network area. During this process quality control parameters are checked to eliminate outliers. At this step, the modeling must be low bandwidth consuming, and allow omnidirectional link of communication with users. The alternative here is to estimate coefficient which could be broadcast to users instead of the ZWD of every station of the network. Finally, this ZWD model is transmitted to rovers to derive a priori ZWDs values used as constraints in the float PPP-RTK algorithm.

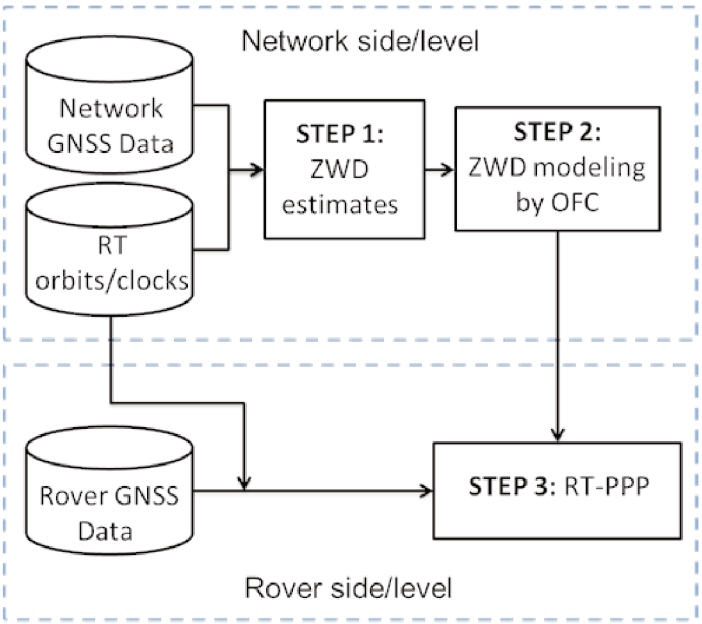

Figure 21 - Overall strategy to generate and use tropospheric corrections for float PPP-RTK

In order to perform float PPP-RTK we use the RTKLib 2.4.2 software (Takasu, 2013) modified in this research to have an option to introduce constrained a priori values for the ZWD parameter. Strategies used to estimate ZWDs in the reference GNSS network (step 1) and to perform float PPP-RTK at the rover level (step 3) are summarized in Table 13. The main differences between them are the positioning mode, static or kinematic, and the constrained parameters. During step 1, reference stations coordinates are well known (1 cm), so they are strongly constrained while ZWDs are estimated. At the rover, the receiver coordinates are estimated during step 3 while ZWDs are constrained with a priori ZWD values, every cold-start (i.e it is provided the initial value at the first epoch), coming from the tropospheric modeling. Its accuracy is used to constrain tropospheric delays in the PPP-RTK algorithm.

Table 13 - GNSS processing parameters used at both reference network and rover levels.

	GNSS Network Processing	**GNSS Rover Processing**
Mode	PPP static (float solution)	PPP kinematic (float solution)
Orbits and clocks	CNES RT orbit and clock products	CNES RT orbit and clock products
Ionosphere	Ionospheric-free	Ionospheric-free
Zenith Tropospheric delay	ZHD: (Saastamoinen, 1972)+ standard atmosphere ZWD: estimated Mapping functions: (Niell, 1996)	ZHD: (Saastamoinen, 1972)+ standard atmosphere ZWD: constrained (correction introduced every cold-start) Mapping functions: (Niell, 1996)
Coordinates	Constrained (1 cm)	Estimated
Elevation mask	10 degrees	10 degrees
Sampling data	30 seconds	30 seconds
Kalman process	Forward	Forward
Other parameters	IERS Conventions 2010 (Petit and Luzum, 2010)	IERS Conventions 2010 (Petit and Luzum, 2010)
Software	RTKLib 2.4.2 (Takasu, 2013)	RTKLib 2.4.2 (Takasu, 2013)

In order to fit conditions of simulated real-time positioning, CNES real-time orbit and clock products are used (Laurichesse et al., 2009). 30s-sampling GPS and GLONASS measurements are processed with a cutoff angle of 10 degrees. In such conditions the adoption of

a standard tropospheric model for ZHD (Saastamoinen, 1972) and the NMF (Niell, 1996) does not introduce significant biases with respect to the use of more sophisticated models like GPT2w (Böhm et al., 2015) and GMF (Boehm et al., 2006) in positioning as verified by Fund et al.(2011).

9.2. Tropospheric modeling

Once real-time ZWDs at all reference stations are estimated with RTKLib, the OFC for tropospheric modeling are generated. The model applied is a second-order fitting model adapted from Shi et al. (2014).

$$ZWD_i = a_0 + a_1 x_i + a_2 y_i + a_3 z_i + a_4 x_i y_i + a_5 x_i z_i + a_6 y_i z_i + a_7 x_i^2 + a_8 y_i^2 + a_9 z_i^2 (i = 1, \dots n) \quad (111)$$

Equation (111) is used with the following constraints (112):

$$0 = \varphi_j a_j \quad (112)$$

with $\varphi_j = \{0,1\}$, $j = \{0, \dots, 9\}$

In (111), ZWD_i is the ZWD from the reference station i, the terms $(a_0, a_1, \dots, a_9)$ represent the fitting coefficients; which are the parameters to be estimated. x_i, y_i and z_i are the geodetic coordinates, j is the coefficient number. Different coefficient sets are estimated by increasing the number of constrained coefficients during the least squares adjustment. The number of coefficient sets to be tested (c) is given by (113):

$$c = \sum_{k=0}^{m} \frac{m!}{k!\,(m-k)!} \quad (113)$$

where m is the number of coefficients and k is the number of constrained coefficients (a_j). For example, if the number of coefficients is 4 (first-order case), c is equal to 16. But, when the number of coefficients used is 10 (second-order case), the number of coefficient sets tested increases to 1024. In our study, it was implemented the 2nd order modeling, with some small modifications to cover a large area.

The internal quality parameter for the OFC model is the RMS of the residuals (114) derived from the coefficients estimation.

$$RMS_{Trop} = \sqrt{\frac{v_1^2 + v_2^2 + v_3^2 + \cdots + v_n^2}{n}} \quad (114)$$

In the equation (114), the RMS_{Trop} is the value used as quality control information to the tropospheric corrections application, v is the difference between the ZWD estimated in the RT-PPP processing with the CORS network observations and the adjusted value in the tropospheric surface.

In order to detect outliers in the ZWD used to estimate the coefficients, it is applied a classical method of outliers identification (Leick, 2004) by comparing the absolute values of each ZWD residual with the global RMS residual, if the individual residual exceeds 4 times the size of the RMS residual the coefficients are estimated again with a reduction in the weight of the observation.

9.3. GNSS data

The area studied is continental France and GNSS data from two different reference networks in this country are used: 1) the Orphéon GNSS network (Figure 22) to estimate ZWDs, while 2) the Réseau GNSS Permanent (RGP) is used to assess tropospheric OFCs (Figure 23, left) impacts on float PPP-RTK (Figure 23, right).

Periods of the experiment consider the four seasons of the year 2014: 20 days of data distributed over the year (Table 14). Days of each period were chosen taking into account the evolution of daily mean temperatures in France during 2014, published by the official French meteorology agency Météo France (http://www.meteofrance.fr) in the climate summary for that year.

Table 14 - Periods studied

	Spring	Summer	Autumn	Winter
Days of 2014	121-126	205-210	289-294	357-362

9.3.1. The Orphéon network

The Orphéon network (http://reseau-orpheon.fr) is composed of 160 stations, regularly distributed over France, with baselines of about 60 kilometers long. All the stations have antennas and receivers of the same brand and model (Leica GRX1200+GNSS or GRX1200GGPRO receivers and Leica AS10 or 1202GG antennas) to guaranty homogeneity of electronic biases. This network is managed by the Geodata Diffusion Company to provide NRTK services in the country.

Two configurations of this network are assessed, 1) a dense network (Figure 22, left) taking into account the observations from all reference stations and 2) a sparse network (Figure 22, right) composed of only 37 stations, which represents a reduction of about 75%. Similar relief variations are considered for both network configurations, with a difference of 1651 m between the highest site elevation (1707 m) and the lowest one (56 m).

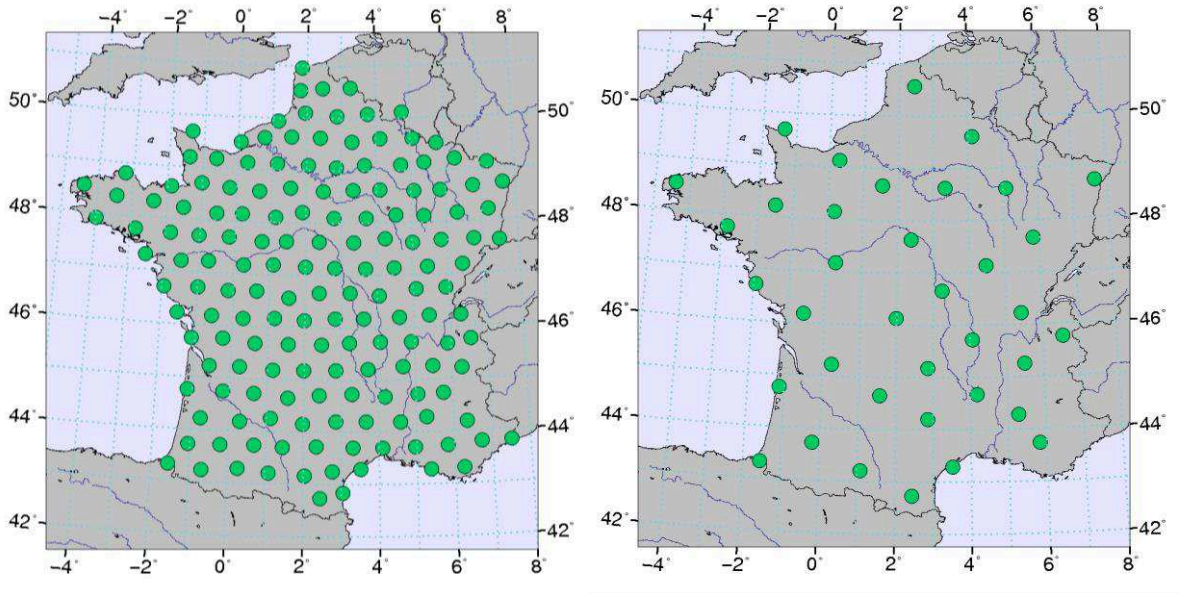

Figure 22 - The Orphéon GNSS networks used to derive tropospheric OFCs: dense (left) and sparse (right)

9.3.2. The *Réseau* GNSS *Permanent*

The RGP (*Réseau* GNSS *Permanent*) is the GNSS network managed by IGN (*Institut National de l'Information Géographique et Forestière*) which publishes tropospheric ZTDs estimated with the Bernese 5.2 software (Dach et al., 2015). Figure 23 (left) presents all RGP stations that have final ZTD products available (ftp://rgpdata.ign.fr/pub/products) during the tested periods. First these products for all stations, delivered every 15 min, are used as external reference to assess the quality of tropospheric OFCs derived from the Orphéon network. Secondly only 22 RGP stations regularly distributed over the French territory are used to perform float PPP-RTK at the rover level Figure 23 (right). This network takes into account as much as possible the geographical conditions in France. These stations were chosen considering the quality of their observations in order to avoid multipath effects and noisy measurements.

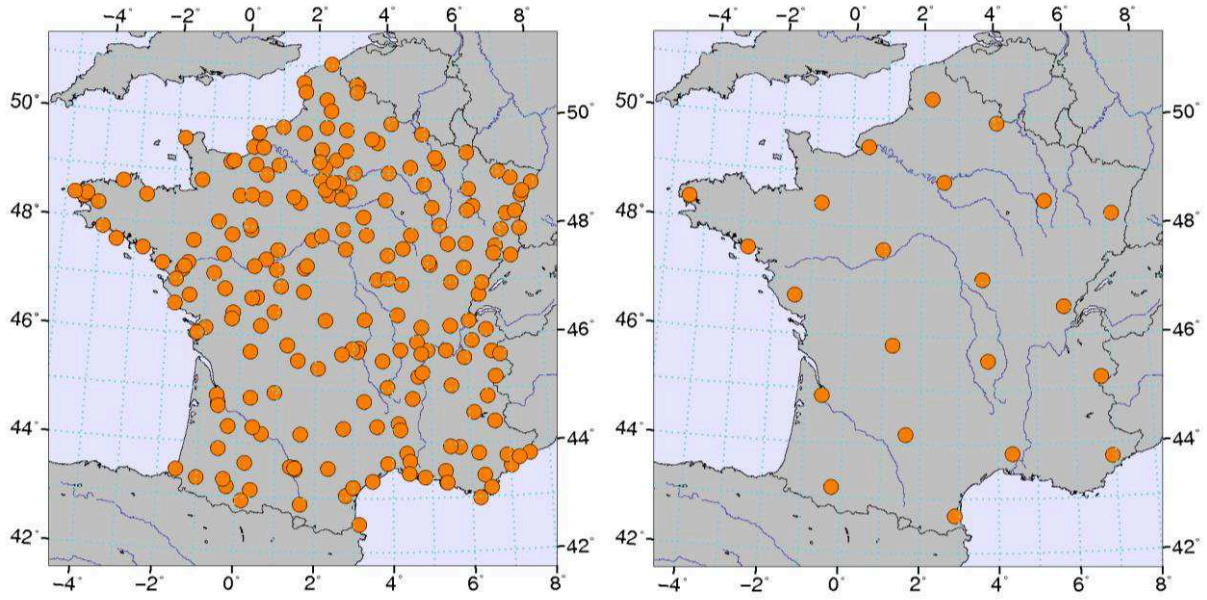

Figure 23 - The RGP GNSS Networks used to assess tropospheric OFCs derived from Orphéon networks (left) and to assess rover positioning (right).

10. Results and analysis

This section presents the results and analysis performed to assess the quality of tropospheric corrections and their impacts on positioning. As stated previously, all results presented here consider simulated real-time positioning conditions.

10.1. Internal quality control

The OFC modeling is performed every hour during the 20 days presented in Table 14. It uses a server model Quad-Core AMD Opteron (tm), Processor 8380 with 2.2 GHz and 40 GB RAM (Random Access Memory). In such conditions, the computer time to test the 1024 coefficient sets and choose the optimal fitting coefficient set is less than 2 or 3 seconds. The RMS of residuals calculated with the dense and sparse network configurations are presented in Figure 24 and Figure 25 respectively.

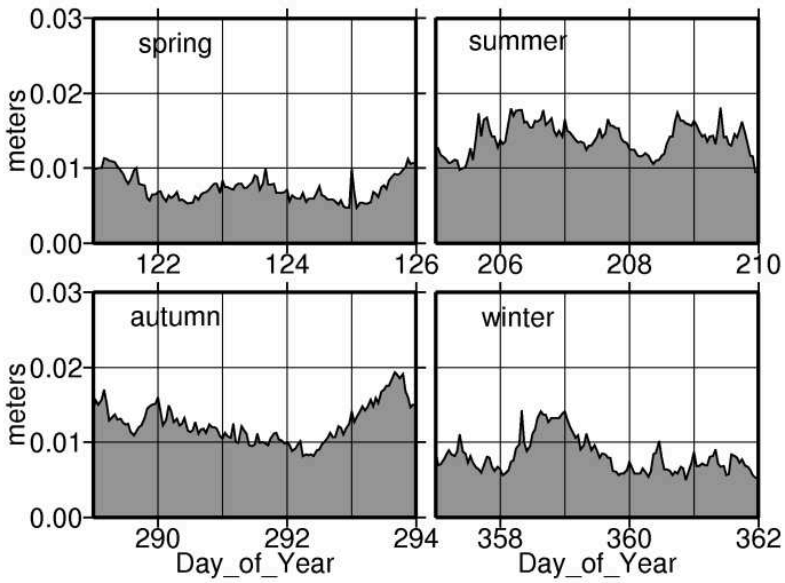

Figure 24 - RMS of OFC estimates using a dense network

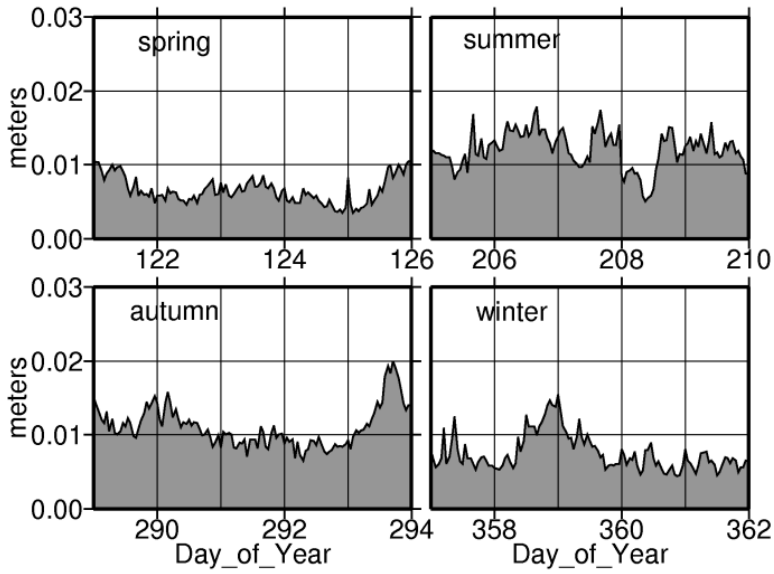

Figure 25 - RMS of OFC estimates using a sparse network

In Figure 24 we observe that RMS reaches values between 0.6 cm and 1.8 cm. The highest values appear in summer and autumn. With the sparse network (Figure 25) values are between 0.6 cm and 2 cm, so that RMS residuals are quite similar for both network configurations. However, a slightly degradation (about 2 mm) is observed with the dense network.

10.2. External validation

As independent external reference, the 15 min-IGN ZTD products estimated using a cutoff angle of 10 degrees are used to assess tropospheric OFCs. For consistency, ZHDs are computed and subtracted from IGN ZTDs using the parameters described in Table 13.

All stations with ZTD products available (172 stations) are used. A typical IGN-ZWD product is showed in Figure 26 (right). The middle and left panels present tropospheric OFCs derived from dense and sparse reference networks calculated at IGN station locations, respectively.

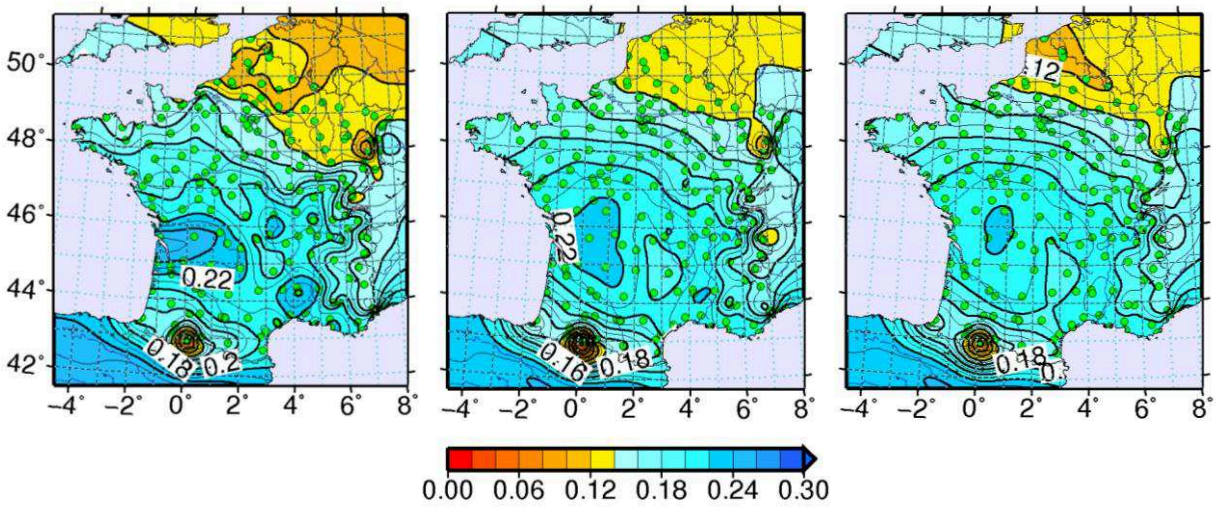

Figure 26 - Examples of tropospheric ZWD (m) surfaces (day 289/2014 – 15 h~16 h): obtained with IGN ZWD products (right), OFCs modeling coefficient generated from Orphéon dense (middle) and sparse (left) network configurations.

ZWDs coming from IGN products present values of about 22 cm in the southwestern France, except for a station which is the highest site in France (in the Pyrenees mountain), and consequently located in a drier environment implying ZWD of about 12-14 cm. Since the OFC modeling takes into account height variations, it is possible to reconstruct ZWD values for this station with quite good accuracy. In the northern France, ZWD are also less significant, about 12-16 cm. This is quite expected considering the latitudinal and relief variations of the French territory. ZWDs modeled from OFCs using dense or sparse reference network configurations present a similar tropospheric surface, but quite less detailed.

The corresponding ZWD differences between IGN products and those from OFCs at IGN station locations are presented in Figure 27. This example in Figure 27 shows that the ZWDs derived from OFCs are consistent with IGN products. It means that three solutions plotted in Figure 26 present similar spatial distributions. Results using the dense configuration present a maximum difference of 4 cm, versus -3.7 cm with those using the sparse network. For this example the hourly mean and standard deviation differences calculated over the whole network are 0.4 cm ± 1.3 cm and -0.5 cm ± 1.4 cm for the dense and sparse network configurations respectively.

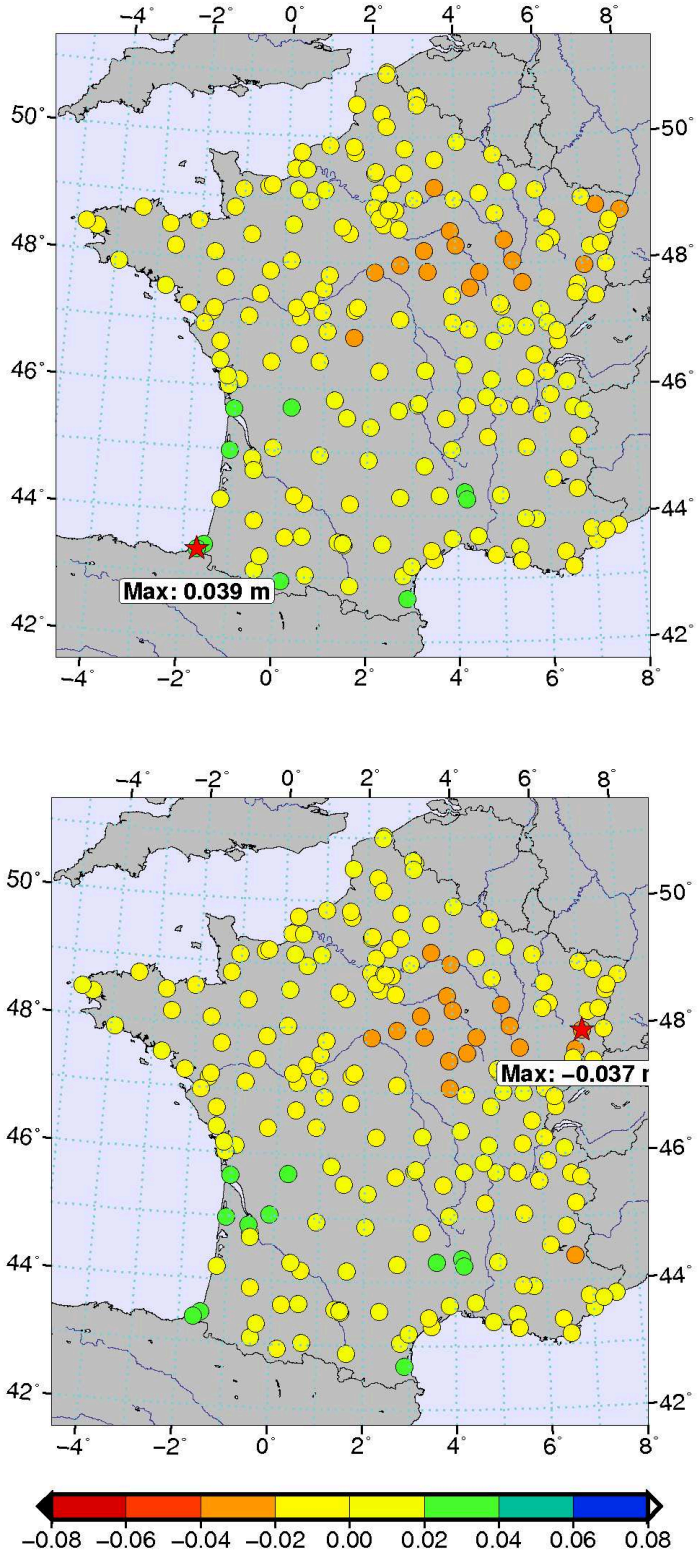

Figure 27 - Differences (m) between ZWDs provided by IGN and OFCs calculated at RGP site locations using a dense network (top) and OFCs calculated at RGP site locations using a sparse network (bottom) for the day 289/2014 between 15 h and 16 h

For all the periods assessed, time series of mean differences over the whole network are presented in Figure 28 and Figure 29 for dense and sparse network corrections, respectively. The corresponding standard deviations for these results are presented in Figure 30 and Figure 31. Unfortunately, IGN products were not available for day 124. The mean differences with respect to IGN ZWDs for all days assessed in 2014 present a mean bias of -4.0 mm for both network configurations. However, mean differences can reach values up to 4 cm.

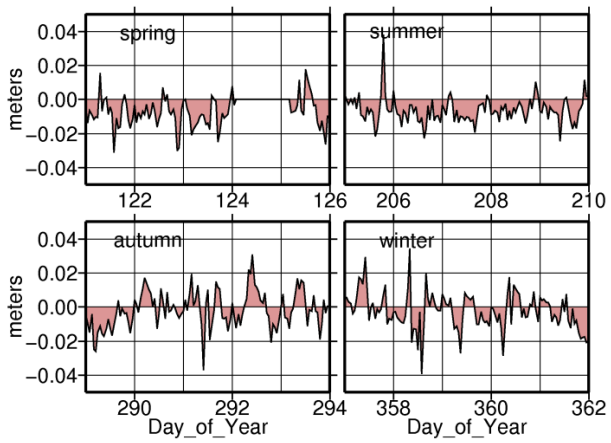

Figure 28 **-** Means of the differences between ZWDs provided by IGN and OFCs using a dense network

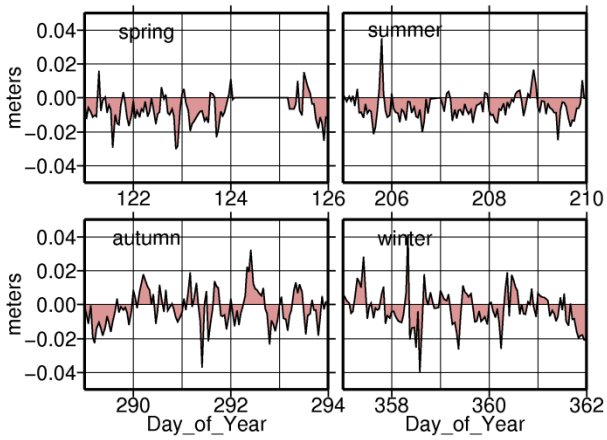

Figure 29 - Means of the differences between ZWDs provided by IGN and OFCs using a sparse network

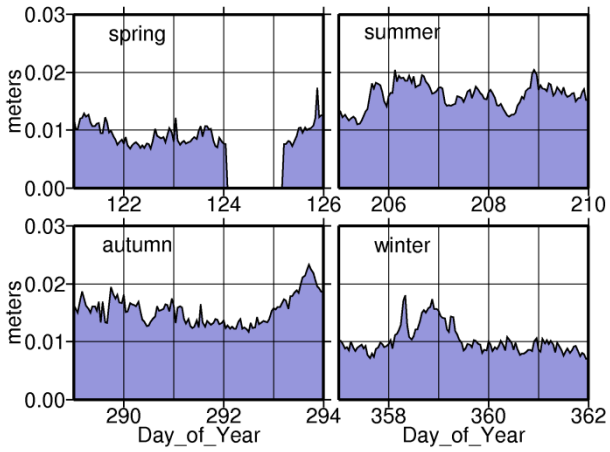

Figure 30 - STD of the differences between ZWDs provided by IGN and OFCs using a dense network

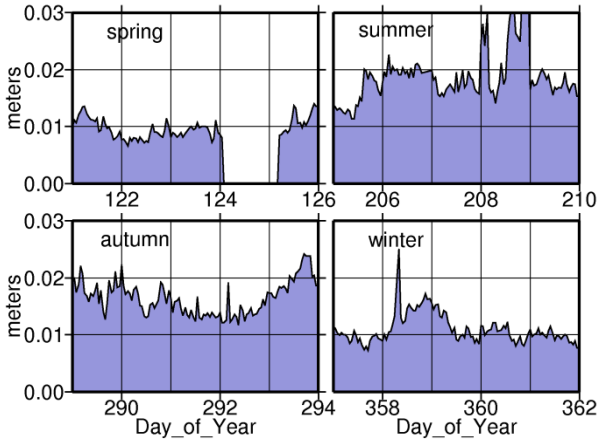

Figure 31 - STD of the differences between ZWDs provided by IGN and OFCs using a sparse network

In Figure 30 and Figure 31, the mean STD for all assessed days is 1.2 cm for both dense and sparse network configurations. Worst results are obtained in summer and autumn, especially for the sparse network. It can be due to higher spatial tropospheric gradients that OFCs cannot fit as well as in winter. On the other hand, it shows a good coherence between internal (Figure 24 and Figure 25) and external RMS, which means that the internal quality control is realistic and the residuals RMS is an appropriate parameter to be used as a quality indicator of OFC estimates as well as a constraint for the ZWD at the rover side.

10.3. Impact of tropospheric OFCs on float PPP-RTK

In order to quantify the impacts of using OFCs on positioning, data of IGN stations plotted in Figure 23 (bottom) are processed in float PPP-RTK over the 20 days of 2014. Processing is re-initialized (cold start) six times per day to assess the impact on convergence time. A time window of four hours is chosen in order to ensure enough time for convergence to 10 cm accuracy in almost all the cases. Considering the entire experiment over all IGN stations it gives 2640 cold starts (22 stations x 20 days x 6 initializations).

The statistics of positioning errors with respect to the positions in ITRF2008 analyzed are median and 68% - quantile. These statistical parameters are chosen instead of mean and standard deviation due to possible remaining biases that might cause results that do not follow a Gaussian distribution. Figure 32 presents results (absolute position errors) performed using GPS CNES orbit and clock products on East, North, and Up components, respectively. The blue curve represents the results of standard kinematic PPP with ZWD estimation. About the use of OFCs as a priori ZWDs, two possibilities are also plotted on Figure 32: 1) OFCs derived from the dense network (violet) and 2) OFCs derived from the sparse network (black). Finally, as a reference solution the float PPP-RTK results with constrained ZWDs provided by IGN over the RGP network (green) are plotted too. The times required for medians and 68%-quantiles to reach 10 cm accuracy is emphasized by vertical bars. It is considered that the solution has converged at this time.

10.3.1. GPS Only

The results presented in Figure 32 indicate that OFCs can reduce the convergence time up to 15 min between standard kinematic PPP and PPP-RTK using accurate a priori ZWDs, especially for the Up component. However, the gain on the Up component is more important for median errors while the gain on the North component is more important for 68%-quantile errors. The East component presents the slowest convergence, especially because ambiguities are kept float. Introducing OFCs has only a small impact on convergence time for that component. Detailed results are listed in Table 15.

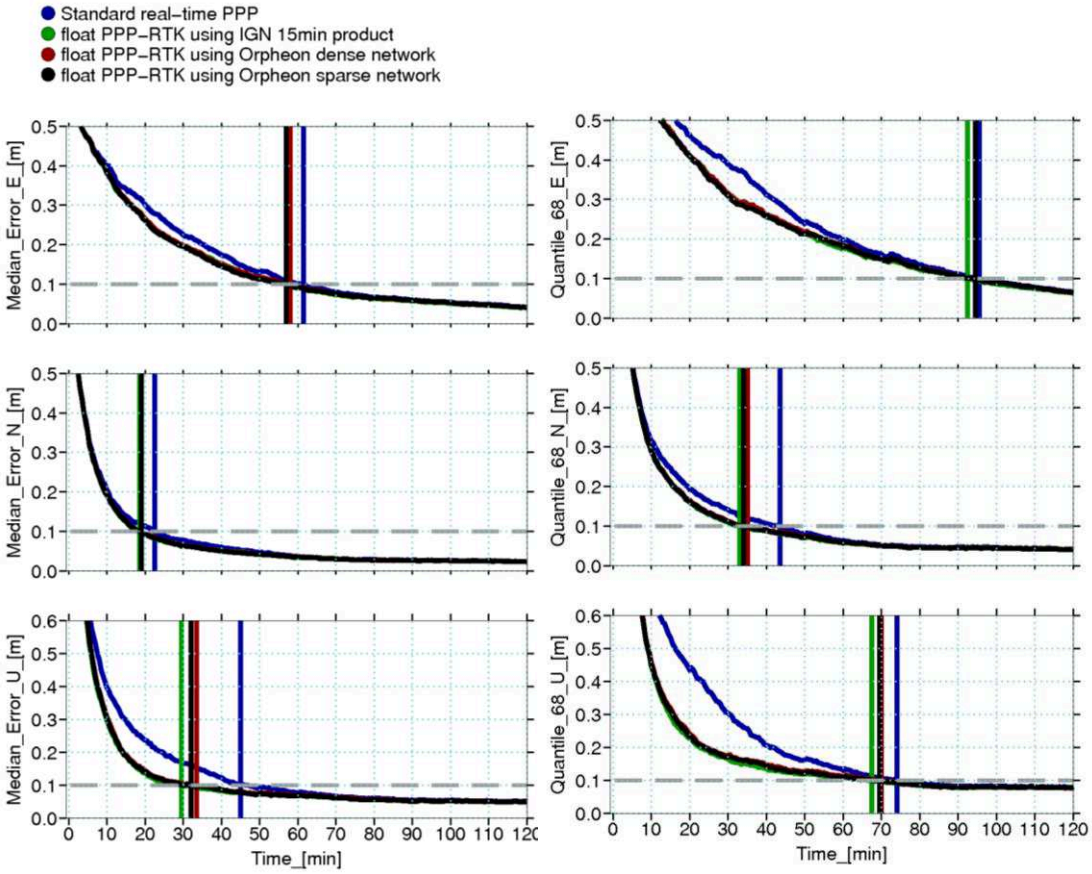

Figure 32 - Medians (left) and 68% quantiles (right) of kinematic RT-PPP positioning errors (GPS-only) per epoch at RGP stations plotted on Figure 23 (right).

Table 15 - Convergence times (min) of PPP-RTK positioning errors (GPS-only)

Tropospheric correction	Median Convergence time			68%-quantiles Convergence time		
	E	N	U	E	N	U
Standard (no correction)	61.5	22.5	45.0	95.5	43.5	74.0
IGN ZWD products	57.0	18.5	29.5	92.5	33.0	67.5
OFCs from dense network	58.0	19.0	33.5	94.5	35.0	70.5
OFCs from sparse network	57.0	19.0	32.0	94.5	34.0	69.5

Concerning median results, using IGN ZWD products perform the shortest time convergence for the Up component: 29.5 min. This represents a gain of 15.5 min (34.4%) against the standard kinematic PPP (convergence time of 45 min). On that component, positioning using OFC derived from dense and sparse Orphéon configurations show similar

performances. The gains with respect to standard kinematic PPP are 11.5 min (25.6%; with dense network) and 13 min (28.9%; with sparse network). The East presents gains of 4.5 min (7.3%) using IGN ZWDs products, 3.5 min (5.7 %) using OFCs derived from dense network and 4.5 min (7.3%) using OFCs derived from sparse network. In North component these gains are equivalent to 4.0 min (17.8%) using IGN ZWDs products and 3.5 min (15.6%) with OFC modeling obtained from dense or sparse network.

About 68%-quantile results for the Up component, the positioning converged around 74 min. The use of IGN ZWD products decreases the convergence time by 6.5 min, which represents an improvement of 8.8%. When OFCs derived from dense and sparse networks are used, improvements are 3.5 min (4.7%) and 4.5 min (6.1%), respectively. The gain in convergence time on the North component with respect to standard kinematic PPP is 10.5 min (24.1%) when using IGN ZWD products, 8.5 min (19.5%) when using OFCs derived from dense network and 9.5 min (21.8%) when using OFCs derived from sparse network. For the East component, gains are less important since the convergence is much slower than the other components. Indeed, standard kinematic PPP achieved the convergence in 95.5 min and using IGN ZWDs products has an impact of only 3 min (3.1%). Using OFCs derived from dense and sparse network has no significant impact 1 min (about 1%).

10.3.2. GPS+GLONASS

Using OFCs as a priori ZWDs with GPS+GLONASS observations is also evaluated. Medians and 68%- quantiles of positioning errors are presented in Figure 33. Detailed results are listed in Table 16. When observations from GLONASS constellation are added to the processing there is a significant reduction in convergence time with respect to results obtained with GPS-only processing. It shows that the estimation of tropospheric ZWDs (standard kinematic PPP) is less problematic when the positioning geometry is augmented. More satellites help to decorrelate ZWD and height estimates.

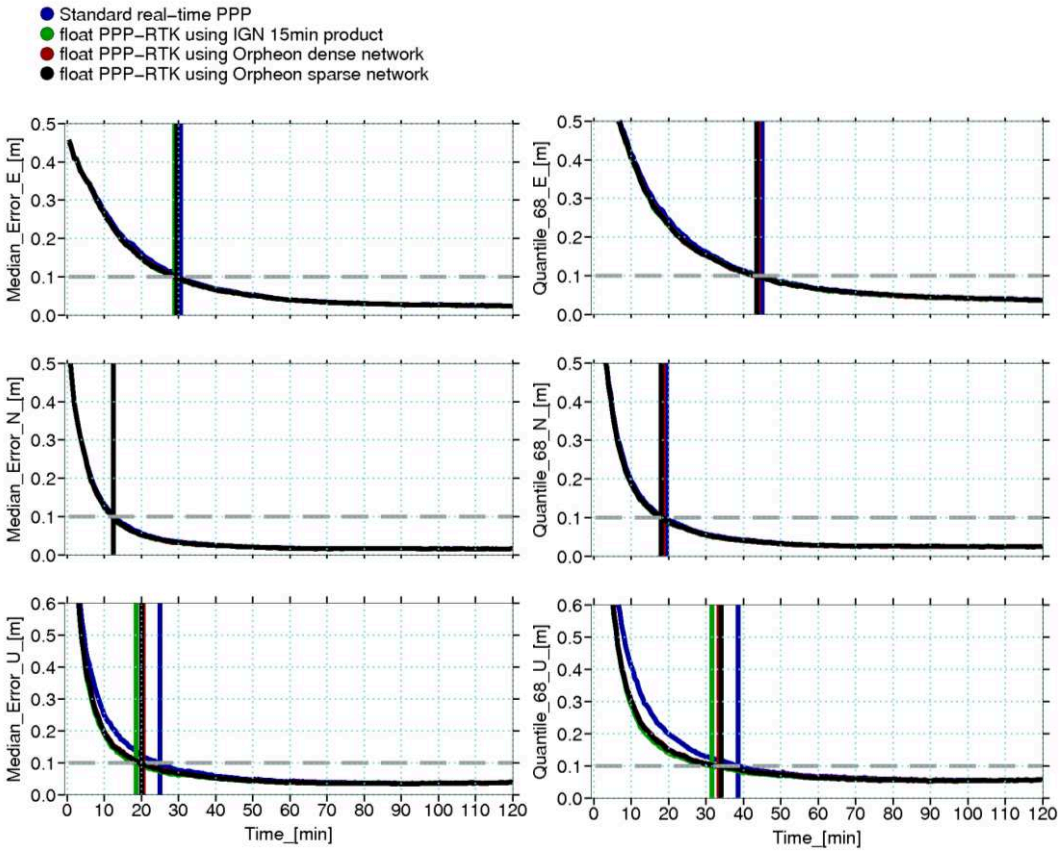

Figure 33 **-** Medians (left) and 68% quantiles (right) of kinematic RT-PPP positioning errors (GPS+GLONASS) per epoch at RGP stations plotted on Figure 23 (right).

Table 16 - Convergence times (min) of PPP-RTK positioning errors (GPS+GLONASS).

Tropospheric correction	Median Convergence time			68%-quantiles Convergence time		
	E	N	U	E	N	U
Standard (no correction)	30.5	12.5	25.0	45.0	19.5	38.5
IGN ZWD products	29.0	12.5	18.5	44.0	18.0	31.5
OFCs from dense network	29.5	12.5	20.5	44.0	18.5	33.5
OFCs from sparse network	29.5	12.5	20.0	43.5	18.0	34.0

For GPS+GLONASS processing, the median gains observed in convergence time using IGN ZWD products are around 1.5 min (4.9%) and 6.5 min (26.0%) on East and Up components, respectively. When applying ZWDs from OFC modeling using dense or sparse network configurations, the same improvements are found on the East component: 1 min (3.3%). On the height, using OFCs derived from sparse network performed slightly better

results with a gain of 5.0 min (20.0%) against 4.5 min (18.0%) when using OFCs from dense network configuration. No gain on North component is found with any of the assessed tropospheric corrections.

Results in terms of 68%-quantiles are quite different. Using ZWDs derived from IGN products performs gains of 1 min (2.2%) on East, 1.5 min (7.7%) on North, and 7 min (18.2%) on Up. Again, the gains achieved using OFC derived from both dense or sparse networks are similar. Indeed, the use of a dense network provides gains of 1.0 min (2.2%) on East, 1.0 min (5.1%) on North, and 5.0 min (13.0%) on Up component, while using a sparse network improves by 1.5 min (3.3%) on East, 1.5 min (7.7%) on North, and 4.5 min (11.7%) on Up. These improvements in 68% quantiles are comparable to those presented by Ibrahim and El-Rabbany (2011) on ionospheric-free based PPP with tropospheric corrections derived from NWP modeling in North America. Besides, the relative gains when applying tropospheric corrections in GPS+GLONASS processing are quite comparable with those found in GPS-only results, especially for median.

10.3.3. Seasonal Studies

In order to assess the impact of tropospheric corrections over 2014, Table 17 presents 68%-quantiles of positioning errors over the four periods assessed (spring, summer, autumn and winter). The most significant achievements with tropospheric corrections are observed in summer but the convergence time is also the largest among the four periods of the experiment. For GPS-only results using IGN ZWD products, convergence times are improved by 3 min (2.4%; East), 20 min (42.5%; North), and 19.5 min (14.0%; Up). When adding GLONASS data, these improvements become 6 min (9.3%; East), 2.5 min (12.8%; North), and 8.5 min (21.5%; Up). Gains of horizontal components using OFC modeling are quite similar to those using IGN products. However, it is not the case for the Up component whose convergence time is enhanced, up to 13.5 min (34.2%) and 12.5 min (31.6%), with dense and sparse network configurations.

Table 17 - 68%-quantile of convergence times (min) over 2014

		GPS only Convergence time to 10 cm accuracy			GPS+GLONASS Convergence time to 10 cm accuracy		
	Tropospheric corrections	E	N	U	E	N	U
Spring	Standard (no correction)	84.5	34.0	49.5	33.0	20.5	37.5
	IGN ZWD products	82.0	29.0	40.0	31.0	20.0	25.5
	OFCs from dense network	83.0	29.0	40.0	31.5	19.5	29.0
	OFCs from sparse network	82.0	30.0	40.5	31.5	19.5	29.0
Summer	Standard (no correction)	124.5	47.0	139.5	64.5	19.5	39.5
	IGN ZWD products	121.5	27.0	120.0	58.5	17.0	31.0
	OFCs from dense network	121.5	29.0	120.0	64.5	17.0	26.0
	OFCs from sparse network	121.5	29.5	123.0	58.5	17.0	27.0
Autumn	Standard (no correction)	72.5	51.5	72.5	45.0	18.5	38.0
	IGN ZWD products	67.0	43.5	64.5	44.0	18.0	38.0
	OFCs from dense network	68.5	47.0	69.5	44.0	18.5	39.0
	OFCs from sparse network	68.0	45.0	67.0	44.0	18.0	39.0
Winter	Standard (no correction)	104.5	26.5	61.5	46.5	17.5	41.0
	IGN ZWD products	104.5	31.0	45.0	46.5	17.0	33.0
	OFCs from dense network	106.0	31.0	47.5	46.5	18.0	36.0
	OFCs from sparse network	106.0	31.0	48.0	46.5	18.0	38.5

During spring and for GPS-only results, the gains achieved with IGN ZWD products are about 2.5 min (3%; East), 5.0 min (15%; North), and 9.5 min (19%; Up). When GPS+GLONASS positioning is performed these gains are 2.0 min (6%; East), 0.5 min (2%; North), and 12 min (32%; Up). The use of OFC modeling presents very close performances for this period, using GPS-only or GPS+GLONASS, except for the Up component of GPS+GLONASS results where the improvement is 22.7% with both network configurations.

During autumn the gains achieved with IGN ZWD products are 5.5 min (7.6%; East), 8 min (15.5%; North), and 8 min (11%; Up) for only GPS results. Performances using the OFC modeling are about 4 min (6%; East), 5 min (10%; North), and 4 min (6%; Up). For GPS+GLONASS results, only small improvements are verified even if some small negative impacts are observed for the Up component.

During winter the tropospheric corrections improve only the convergence of the Up component with GPS and GPS+GLONASS. On the other hand, the horizontal convergence time is even slightly degraded.

11. Summary of Part II

From the results and discussions presented in Part II, it is possible to conclude that the atmospheric effects have to be considered carefully. One of these effects is the tropospheric ZTD, which has a residual component (ZWD) that must be estimated as an additional parameter in GNSS processing. However, the use of accurate a priori ZWDs helps to reduce the convergence time of the position.

In order to reduce the time required for PPP-RTK to converge to 10 cm accuracy, the strategy presented in Part II has focused on two points: 1) tropospheric modeling to provide network based ZWD corrections and 2) the impacts of using such a model to constrain a priori ZWDs in float PPP-RTK processing. The OFC modeling technique (Shi et al., 2014) is used because it requires only a mono-directional communication link. Improvements of constraining a priori ZWDs on convergence time have been assessed with dense and sparse networks as well as with GPS only and with GPS+GLONASS data. 20 days distributed in four main periods along the year 2014 are selected. These periods were chosen according to the seasons of the year and the annual temperature variations in France as published by Météo-France.

As an independent external reference, the IGN ZTD products are used to assess tropospheric ZWD modeled by OFCs. The modeled ZWDs present an accuracy of around 1.3 cm with respect to IGN ZTDs. In addition a good consistency between the RMS of residuals and the differences with respect to the IGN products is found.

Improvements of convergence time when using tropospheric corrections for PPP-RTK are quantified. In terms of 68%-quantiles, gains on convergence time are 1% on East, about 20% on North, and about 5% on Up when using GPS only. Introducing GLONASS data shortens by about 50% the convergence time of all components. However, adding tropospheric corrections when processing GPS+GLONASS data only improves horizontal positioning by about 2% on East and about 6% North but height is improved by about 12% Up. In summer and autumn due to more relevant tropospheric activity, the positions convergence takes more time. Even if ZWD modeling does not fit tropospheric delays as well as in winter, using a priori ZWDs derived from dense or sparse networks improves the

convergence time. Finally, a reduction in the number of reference stations by using a sparser network configuration does not degrade the generated tropospheric corrections derived from OFCs, and similar performances are achieved between the two configurations.

PART III - PPP-RTK WITH TROPOSPHERIC AND IONOSPHERIC MODELING

12. Introduction to Part III

In this part, PPP-RTK is performed thanks to the CNES PPP-Wizard 1.3 package as well as the use of CNES orbit, clock and uncombined phase biases products. As already stated, this software allows the estimation of slant ionospheric effects in GNSS data processing. Therefore, unlike GNSS processing in Part II, both tropospheric and ionospheric effects are here considered. Thus, a C/C++ library dedicated to ionospheric corrections generation was implemented in CNES PPP-Wizard 1.3 package to generate atmospheric corrections from data of a reference station network.

The modeling of ionospheric effects is a challenge for most of GNSS SSR based positioning methods, when iono-free combination is not used to mitigate the ionospheric refraction on GNSS signals. There are several alternatives for ionospheric modeling, relying on the scale: global, regional or even local. The IGS GIMs (Global Ionospheric Maps) are an example of global model for ionosphere (Zhang et al., 2013). For regional or local modeling it is possible to interpolate directly the STEC (Slant TEC) values estimated on a CORS network to the user positions (Li et al., 2014c).

The IGS GIMs have a vertical accuracy of 2-8 TECU (TEC Units). Considering that 1 TECU corresponds to 16.24 centimeters in the L1 band, this accuracy can limit PPP-RTK performances (Rovira-Garcia et al., 2015). Zhang et al (2013) present an assessment of PPP convergence when using alternatively IGS GIM and ionospheric corrections model obtained from a regional GNSS reference network. Results show that ionospheric model derived from a regional network provide horizontal convergence time (to 10 cm accuracy) of 11 to 5 min better than using IGS GIM. In this work, the authors also state that receiver biases are correlated with solution's convergence time and neglecting them could introduce significant biases (2~3 m) on height component when performing ionospheric constrained PPP. The height biases decrease to 0.2 m ~ 0.4 m when receiver biases are included in the modeling.

Li et al (2014) present a multilayer processing scheme for PPP-RTK, considering a regional augmentation for large GPS reference networks in Germany, providing among

other corrections, the tropospheric and ionospheric information as SSR corrections. User performs L1+L2 positioning and estimates the atmospheric delays which are further constrained to the values derived from a reference network processing. The results indicate that PPP-RTK performances are similar to the traditional relative RTK.

As alternative, for global-scale PPP, Rovira-Garcia et al (2015) use a real-time ionospheric model with accuracy better than 1 TECU, considering directly STEC values. The convergence is assumed at accuracies of 20 cm. Their ionospheric model allows PPP-RTK with results evidencing convergence time significantly shortened for horizontal (40% ~ 90%), and height (20% ~ 60%) components compared to iono-free based PPP of four simulated rovers processing with a reset every 2 h along day 150 of 2011. These analyses, focused on a short data sampling (one day), may not represent properly the critical variability of ionospheric effects on GNSS signals.

In this thesis, modeling of ionospheric effects uses a method aligned with the RTCM conventions for the transmission of SSR ionospheric parameters (cf. section 5.5.2), and is based in IDW (Inverse Distance Weighting) interpolation algorithm. The implementation makes use of a refined quality control with regard to the precision of ionospheric delays estimated at the reference network side, which are used as input for the corrections generation. Impacts of generated corrections on PPP-RTK performances are assessed during selected days distributed along the last years. These days are selected in function of ionospheric activity. Atmospheric corrections are compared to IGS IONEX (IONosphere map EXchange format) for ionospheric corrections and IGN tropospheric products for tropospheric corrections. The assessment of such corrections using different reference network topologies (dense and sparse) are performed in this step as well. Results evidencing the achievements on simulated user positioning and impacts on PPP-RTK performances are quantified on several parameters: positions accuracy, required convergence to achieve the target accuracy and ambiguity fixing.

Chapter 13 presents the experiment data, the PPP-Wizard processing strategies at the server and rover sides, as well as the algorithms employed to model and apply the atmospheric corrections. Chapter 14 shows the assessment of atmospheric SSR corrections and the impacts of such corrections on PPP-RTK. Finally, Chapter 15 summarizes the outcomes presented in Part III.

13. Method, data and processing

Methodology as well as GNSS data and products adopted for the generation and application of SSR atmospheric corrections are described in this chapter.

13.1. Days of experiment

Days selected in this experiment aim to represent as good as possible the ionospheric activity over the time window: January/2014 to April/2016. Therefore, TEC and F10.7 index using IRI model (cf. section 7.2.7) are generated for that period. As location, the coordinates of the area covered by Orphéon network is used. Figure 34 presents the ionospheric activity based on these two parameters and Table 18 shows the extreme values as well as the statistics (mean/standard deviation) during that period.

10 days with different ionospheric characterizations are selected. Table 19 shows the days selected and the corresponding ionospheric activity in the settled time window. Most of these days describe high, medium, and low ionospheric activities. Some days with geomagnetic anomalies are also included, such as day 173 and day 174 of 2015. All these days are plotted with red bars in time series of Figure 34.

Table 18 – Statistics of TEC and F10.7 indicators on selected days of experiment

	2014		2015		2016	
Information	F10.7	TEC	F10.7	TEC	F10.7	TEC
Maximum observed value	253,3	36,1	255,0	28,0	119,8	18,0
Minimum observed value	88,9	16,5	79,5	12,7	77,5	14,5
Mean	145,9	25,4	118,1	20,0	96,4	16,4
Standard deviation	27,0	4,4	21,1	4,1	9,6	0,7

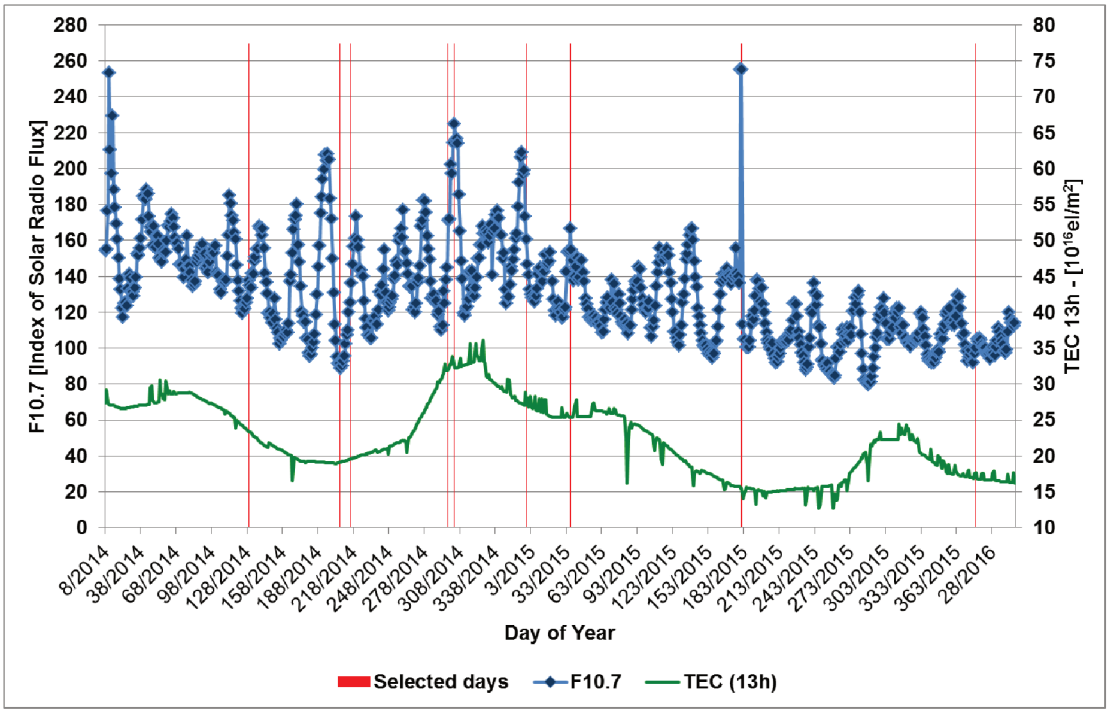

Figure 34 – Ionospheric activity given by IRI from January 2014 to April 2016; TEC and F10.7 indicators are represented.

Table 19 – Ionospheric activity characterized by TEC and F10.7 solar flux index based on IRI, in France (central point coordinates) for the selected days of the experiment.

Day of Year	TEC (TECU)	F10.7	Ionospheric Activity
122 / 2014	137.6	23.4	Medium
199 / 2014	91.4	19.1	Low
208 / 2014	125.2	19.6	Low
290 / 2014	144.8	31.9	High
296 / 2014	224.8	32.2	High
357 / 2014	160.5	27.0	High
029 / 2015	166.7	25.4	Medium
173 / 2015	255.0	15.5	Geomagnetic Storm
174 / 2015	255.0	15.5	Geomagnetic Storm
007 / 2016	99.9	17.7	Low

13.2. Overall strategy

The idea considered in Part II of working with a reference network and with another different network to simulate rover is also used in Part III. Thus, GNSS data come from two different networks. A reference network at the server side is used to generate SSR atmospheric corrections and another GNSS network is used to perform/simulate rover processing using the previous SSR atmospheric corrections as users. Both networks are presented in next section.

Figure 35 shows the workflow applied to generate SSR atmospheric corrections at the server side and their assessment at the user side. With respect to the strategy previously used in Part II, the main differences are the addition of the Slant Ionospheric Delays at the reference network level and the assessment of an interpolation algorithm method aligned with the RTCM standards for SSR atmospheric messages.

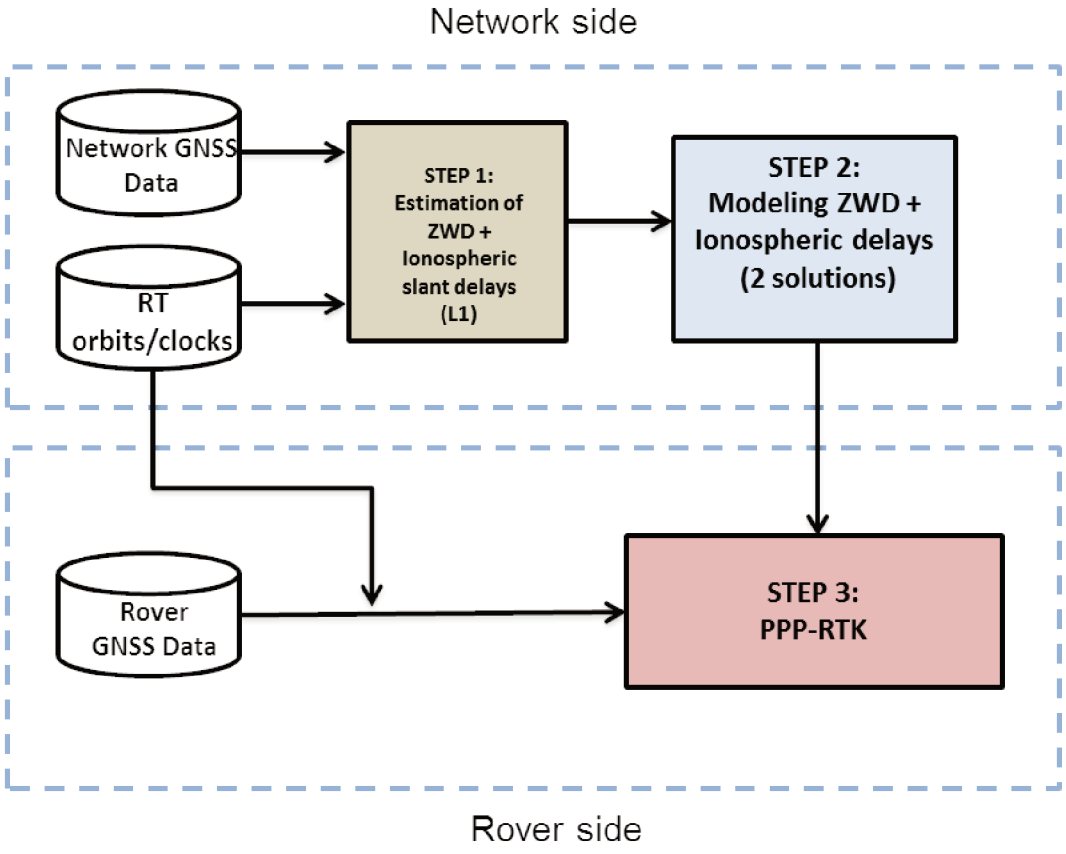

Figure 35 - PPP-RTK workflow to generate SSR atmospheric corrections and assess them at user side.

13.3. GNSS Data Set

At the server side, the Orphéon reference network, presented in section 5.3.1, is used with its previously defined dense (160 stations) and sparse (37 stations) configurations. These configurations are presented in Figure 22 of section 9.3.1.

In order to assess PPP-RTK performances at the user side, stations from the IGN network are again used to simulate rovers, as in Part II. The difference now is the number of simulated rovers, which was increased with respect to the experiments of Part II. This increase is motivated by the fact that ionospheric parameters have high spatial variability (Ge et al., 2012; Leandro et al., 2011). Now 63 IGN stations are selected according to their geographic distribution and data availability. Such stations are distributed in such a way that they cover practically the whole reference network area. Figure 36 presents the rover network considered in this study.

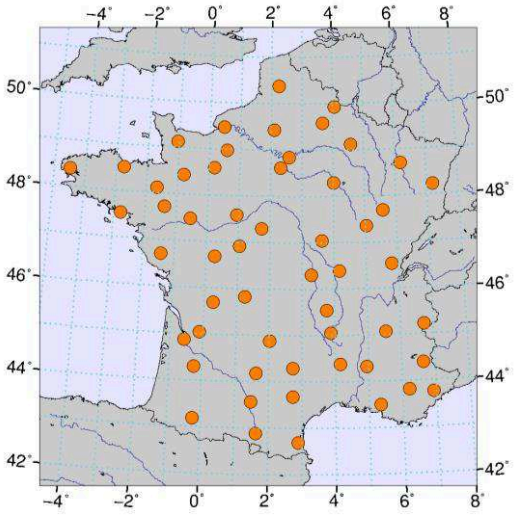

Figure 36 – Rover stations Network used to assess impacts of SSR ionospheric and tropospheric corrections in PPP-RTK.

13.4. Step 1: GNSS data processing at the server side

While estimating atmospheric delays at the server side, station coordinates can be constrained to accurate values or even fixed (i.e. initial sigma of positions set to zero). Here, station coordinates are considered as unknown parameters so that positioning errors are used as a quality indicator of atmospheric computation. PPP-Wizard 1.3 processing configurations

defined at server side (Orphéon network) are presented on Table 20. All parameters suggested in PPP-Wizard 1.3 documentation (Laurichesse, 2016) are used. Therefore, coordinates are estimated together with ZTDs and slant ionospheric delays. Only two are modified: 1) threshold applied to the post-fit standard deviation of ambiguities, that is needed for the decision function of ambiguity fixing (thrAmb) and 2) RAIM maximum rejection (maxReject).

Table 20 – PPP-Wizard 1.3 configurations set at the network side in order to estimate atmospheric parameters.

Number	Parameter	Type/Unit	Description	Value adopted at server processing
1	Mode	Enum	Processing mode: Mode_PPP_AR	Mode_PPP_AR
2	AntexFileName	String	Antex IGS file	igs08.atx
3	AR/JumpsIndicators	Boolean	Indicates ambiguities to be estimated. NL, WL and Extra WL. If 1: yes, 0: no.	1 1 0
4	useGPS	Boolean	Use GPS constellation. If 1: yes, 0: no.	1
5	useGLONASS	Boolean	Use GLONASS constellation. If 1: yes, 0: no.	1
6	sbasCorrection	Boolean	If 1: SBAS clock correction, otherwise 0: e.g. RTIGS or CNES clock correction	0
7	Reset	Int/sec	Time between consecutive reset (for convergence tests) 0 if no reset	0
8	OutputVerbose	Boolean	Verbose output	0
9	Step	Real/second	Measurement interval, i.e. the sampling interval of observations.	1
10	maxAge	Real/second	Maximum RTCM correction age	10
11	stepMin	Integer/S.U.	Minimum step before AR. Minimum number of epochs to start ambiguity fixing. If interval is 1 second, 3600 represents 1 hour.	3600
12	maxReject	Integer/S.U.	Maximum rejection RAIM (Receiver Autonomous Integrity Monitoring)	3
13	raim	Boolean	Advanced RAIM. Outlier detercion.	1
14	mapThr	Real/S.U.	Tropospheric mapping function threshold (1/sin(ele)). In this function (CNES mapping, 6 is equivalent to 10 degrees cutoff)	6
15	sigIniTro	Real/m	Tropo initial noise	0. 5
16	sigModTro	Real/m	Tropo model noise	0.000005
17	nbSatFixAmb	Integer/S.U.	Minimum satellite for AR	0
18	thrAmb	Real/m	Ambiguity threshold for AR	0.25
19	sigIniBiasClk	Real/m	Initial clock bias noise	0
20	sigModBiasClk	Real/m	Model clock bias noise	0.001
21	sigIniIono	Real/m	Initial iono noise	10
22	sigModIono	Real/m	Model iono noise	0.002
23	sigMeasIono	Real/m	Iono measurement noise	1.0 1.0 1.0
24	IonoThr	Real/m	Iono measurement rejection threshold	5 0
25	sigMeasTropo	Real/m	Tropo measurement noise	0.1
26	tropoThr	Real/m	Tropo measurement rejection threshold	1
27	sigIniPos	Real/m	Initial position noise, 50 m position unknown or 0 (position fixed)	50
28	sigModPos	Real/m	Model position noise: 10 (mobile receiver), 0.02 (static receiver) or 0 (position fixed)	0.02
29	preDTMax	Real/sec	Maximum measurement gap	300
30	codeThr	Real/m	Code measurement rejection threshold	10
31	phaseThr	Real/m	Phase measurement rejection threshold	0.05
32	sigMeasCodeGps	Real/m	Code GPS measurement noise	1
33	sigMeasPhaseGps	Real/m	Phase GPS measurement noise	0.01
34	sigMeasCodeGlo	Real/m	Code GLONASS measurement noise	5
35	sigMeasPhaseGlo	Real/m	Phase GLONASS measurement noise	0.01

For thrAmb, the value suggested in the configuration file provided within PPP-Wizard package (0.25 cycle) is used instead of the one suggested in the PPP-Wizard

documentation (0.01 cycle). Indeed, initial tests showed that positioning accuracy is reduced as well as the number of fixed NL ambiguities when using 0.01 cycle for thrAmb. However, further investigations to define an ideal threshold must be carried out. maxReject parameter for RAIM is increased to 3 satellites, instead of 2. Setting maxReject to 3 satellites also performs slightly better solutions in initial tests, but further investigations to define the best configuration for this parameter also must be carried out.

No external a priori atmospheric information is used. Thus, an empirical model (Saastamoinen, 1972) is employed to obtain the initial a priori tropospheric delay, which is constrained to 10 cm (sigMeasTropo). Ionospheric delays are initialized to null values and constrained with 1 m (sigMeasIono), as suggested in the typical configuration of PPP-Wizard 1.3 (Laurichesse, 2016).

Ionospheric parameters may require considerable time to converge properly. In Rovira-Garcia (2015), for example, processing of reference network stations (server side) is started a day before the use of ionospheric related parameters in order to ensure accuracies and confidence bounds of 1 TECU (~16 cm). In this thesis experiments, processing at the server side is initiated at 0 h 00 min UTC of every day and is continuous all-day long. With PPP-Wizard 1.3, the convergence can take at least 1h, as recommended in PPP-Wizard 1.3 documentation (Laurichesse, 2016) to start ambiguity fixing. Therefore, only first hours of processing are impacted by solution convergence. In order to use a proper converged atmospheric solution, first 3h of processing are not used to generate SSR corrections. However, a detailed study about atmospheric parameters convergence with PPP-Wizard 1.3 is still necessary.

13.5. Step 2: Generation of SSR atmospheric corrections

13.5.1. Ionospheric delays

IDW interpolation is chosen because this method is consistent with stage 3 of RTCM standards evolution to send ionospheric estimates from reference stations (Wübbena et al., 2014). In this case, undifferenced corrections can be generated and broadcasted station by

station, enabling the user to employ a distance based algorithm to choose the nearby reference stations for interpolating corrections. Therefore the bidirectional communication burden of the traditional NRTK methods can be reduced (Li et al., 2014b).

First, reference stations are ordered in function of their distances to rover's location obtained from its approximate positions. Then, the four closest references stations are selected. Besides, results from GNSS data processing for at least 3 of the 4 selected reference stations must fit some quality indicators, mostly defined according to isolated tests. The thresholds are chosen in order to reach the best cost-benefit value in term of SSR corrections:

- Post-fit standard deviation of slant ionospheric delays estimates not higher than 0.1m.
- Post-fit standard deviations of zenith tropospheric delays estimates not higher than 0.01m.
- Post-fit standard deviations of positions estimates (3D) not higher than 0.05m.
- 3D positioning error with respect to the reference coordinates not higher than 0.18 m. This value corresponds is about 2 times the final 68%-quantiles of 3D positioning errors after convergence. (see section 14.1). So, 0.18 m is close to 90%-quantiles of 3D positioning errors. It is a loose threshold defined only to avoid significant errors provoked by data gaps or bad fixes at reference stations.

Considering the four closest stations initially selected, atmospheric delays of only one station can be rejected from IDW solution. When more than one station is rejected, another set of 4 closest stations is selected excluding reference stations whose results do not fit the above thresholds.

Throughout IDW algorithm, slant ionospheric delay (I_{user}^{s}) of a satellite (s) visible by one user is interpolated from n reference stations and weighted by inverse distances (D_j) between reference station and user's location. Equation (115), considering such weights (w_j), is presented as follows (Mitas and Mitasova, 1999):

$$I_{user}^{s} = \sum_{j=1}^{n} w_j I_j^s = \frac{\sum_{j=1}^{n} I_j^s / D_j}{\sum_{j=1}^{n} 1/D_j} \tag{115}$$

where stations j is the reference station number and ($j = 1,..n$).

Standard deviations of interpolated ionospheric delays ($\sigma_{I_{user}}^{s}$), are estimated from post-fit standard deviations of slant ionospheric delays at the reference stations ($\sigma_{I_j}^{s}$):

$$\sigma_{I_{user}}^{s} = \sum_{j=1}^{n} w_j \sigma_{I_j}^{s} = \frac{\sum_{j=1}^{n} \sigma_{I_j}^{s} / D_j}{\sum_{j=1}^{n} \sigma_{I_j}^{s} D_j} \tag{116}$$

The error associated to the ionospheric correction ($err_{I_{user}^{s}}$) is obtained in function of the distance of the closest station (D_1):

$$err_{I_{user}^{s}} = \sigma_{I_{user}}^{s} + 2ppm(D_1) \tag{117}$$

The value of 2 ppm is introduced to mitigate spatial ionospheric variability (Lejeune et al., 2012; Tregoning and Rizos, 2008). Of course, this approximation can lead to incoherencies and must be improved. Said that, the resulting ionospheric error obtained ($\mathrm{err}_{\mathrm{I}_{\mathrm{user}}^{\mathrm{s}}}$) is our alternative to be used as constraint in the application of the SSR ionospheric correction ($\mathrm{I}_{\mathrm{user}}^{\mathrm{s}}$). However, ionospheric delays interpolated from satellites for which the ambiguities are not fixed to integer values at reference stations, the constraint value ($\mathrm{err}_{\mathrm{I}_{\mathrm{user}}^{\mathrm{s}}}$) is multiplied by a factor of 2 to reduce the weight of their constraints.

As illustrated in Figure 37, at least 3 reference stations are used. If the user is inside the network area, selected stations surround its location. For users located at network borders, IDW algorithm still works but the quality of corrections can be less effective due to spatial variability of atmospheric delays.

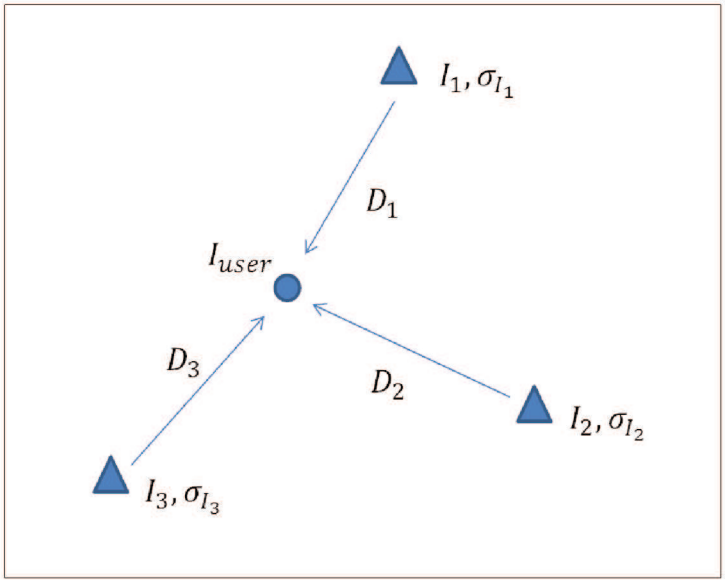

Figure 37 - Inverse Distance Weighting Interpolation.

Actually, the distances: D_1, D_2 and D_3, are horizontal distances, since they are computed considering the IPPs locations. Figure 39 illustrates the geometry.

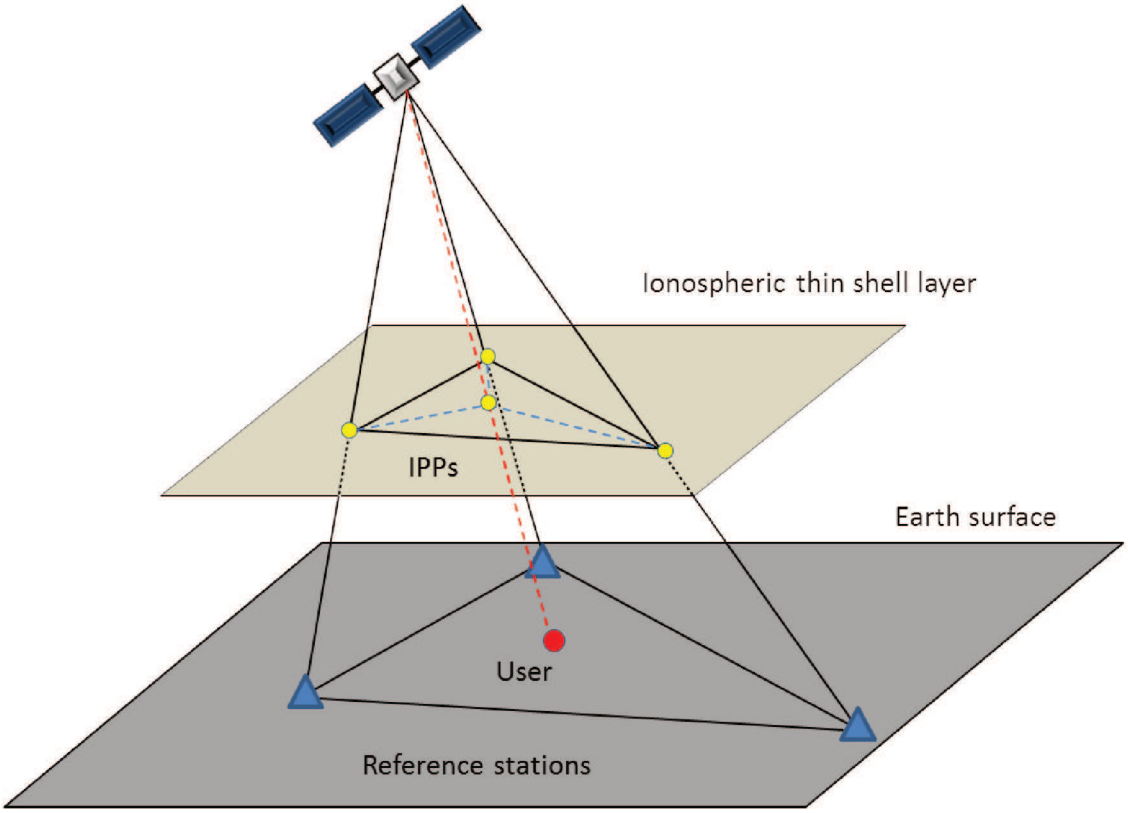

Figure 38 - IDW interpolation geometry
Source: adapted from (Zhang et al., 2013)

Two points about IDW interpolation for ionospheric corrections must be underlined to make its process clear:

1) Interpolation uses directly slant ionospheric delays estimates at reference stations as input. These delays are interpolated satellite per satellite. This solution is retained to minimize mismodeling of ionospheric mapping functions. Even if elevation angles of a satellite in view at several reference stations are similar at first order, a little elevation angle difference is amplified when delays are mapped to the vertical, especially for satellites close to horizon.

2) Distances are calculated from IPPs locations because Zhang et al. (2013) demonstrate that using inter-station distances derived from IPPs-locations do not introduce significant differences in interpolated ionospheric delays.

In Figure 39, vertical ionospheric delays for all stations are plotted at the ionospheric IPPs locations considering an infinitesimal layer of 400 km height. IPPs are colored according to the magnitude of vertical ionospheric delays

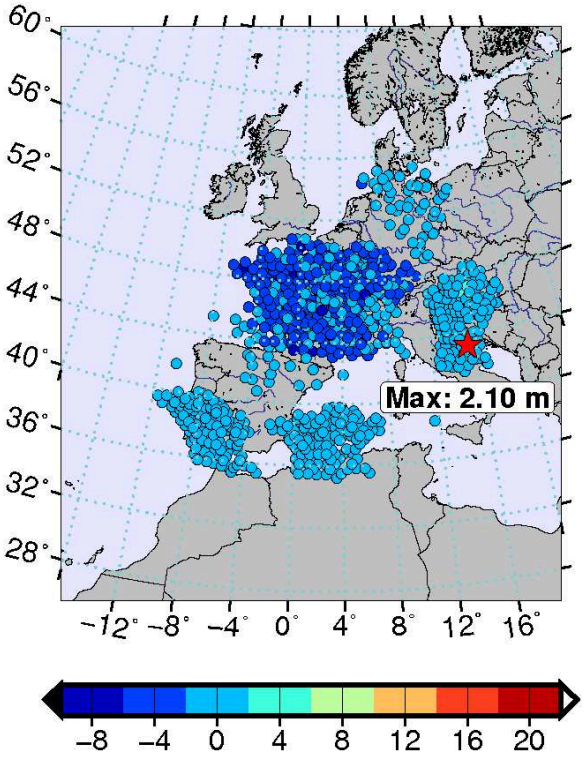

Figure 39 – Vertical Ionospheric Delays (m) at IPPs (6 h 30 min/290-2014).

In this example, 898 ionospheric delays (GPS-Only) are available. Each group of IPPs represents a common tracked satellite by reference stations. Here, 117 reference stations are used and only satellites with ambiguities fixed to integer values are showed. One can see the re-projection of the network stations at the ionospheric thin shell layer. For satellites with low elevation angles only part of the network is available.

13.5.2. Tropospheric delays

To interpolate tropospheric delays, IDW algorithm is applied using ZWD delays from reference stations and 3D distances, since tropospheric delays are function of station height:

$$ZWD_{user} = \sum_{j=1}^{n} w_j ZWD_j = \frac{\sum_{j=1}^{n} ZWD_j/D_j}{\sum_{j=1}^{n} 1/D_j} \quad (118)$$

The constraint for tropospheric correction is obtained in the same way as for ionospheric corrections. First, the precision is interpolated:

$$\sigma_{ZWD_{user}} = \sum_{j=1}^{n} w_j \sigma_{ZWD_j} = \frac{\sum_{j=1}^{n} \sigma_{ZWD_j}/D_j}{\sum_{j=1}^{n} \sigma_{ZWD_j} D_j} \tag{119}$$

The considered final tropospheric error, i.e. the constraint to be applied is given as:

$$err_{ZWD_{user}} = \sigma_{ZWD_{user}} + 0.5ppm(D_1) \tag{120}$$

0.5 ppm is based on the residual tropospheric biases on relative positioning (Gupta, 2011). This value is an approximation and can obviously lead to the same problem as for ionospheric constraints.

Figure 40 brings an illustrative example of ZWDs estimated at reference stations using PPP-Wizard 1.3. The overall magnitude of these ZWDs is between 13 to 23 cm. The amplitudes fit to expected values for such parameter.

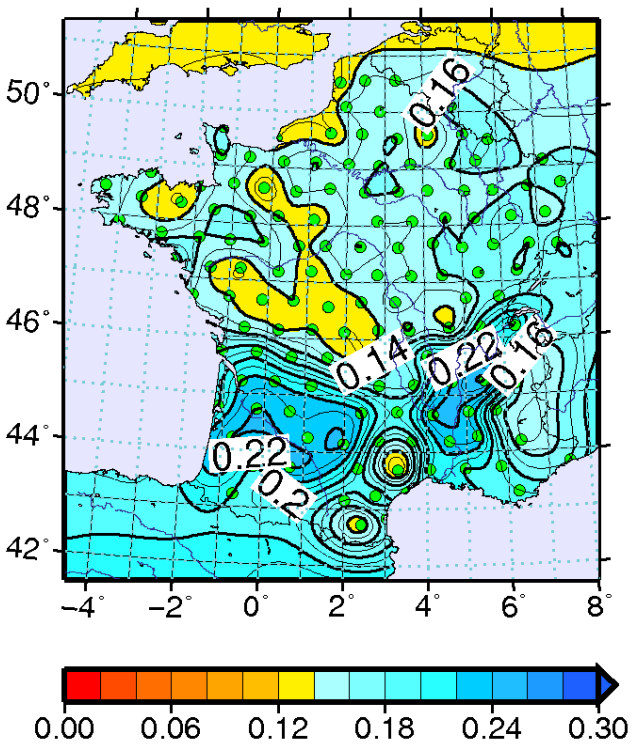

Figure 40 – ZWDs (m) at Orphéon reference stations at 6 h 30 min, day 290/2014.

A detailed flowchart of atmospheric delays interpolation method (step 2 of Figure 35) is presented in Figure 41.

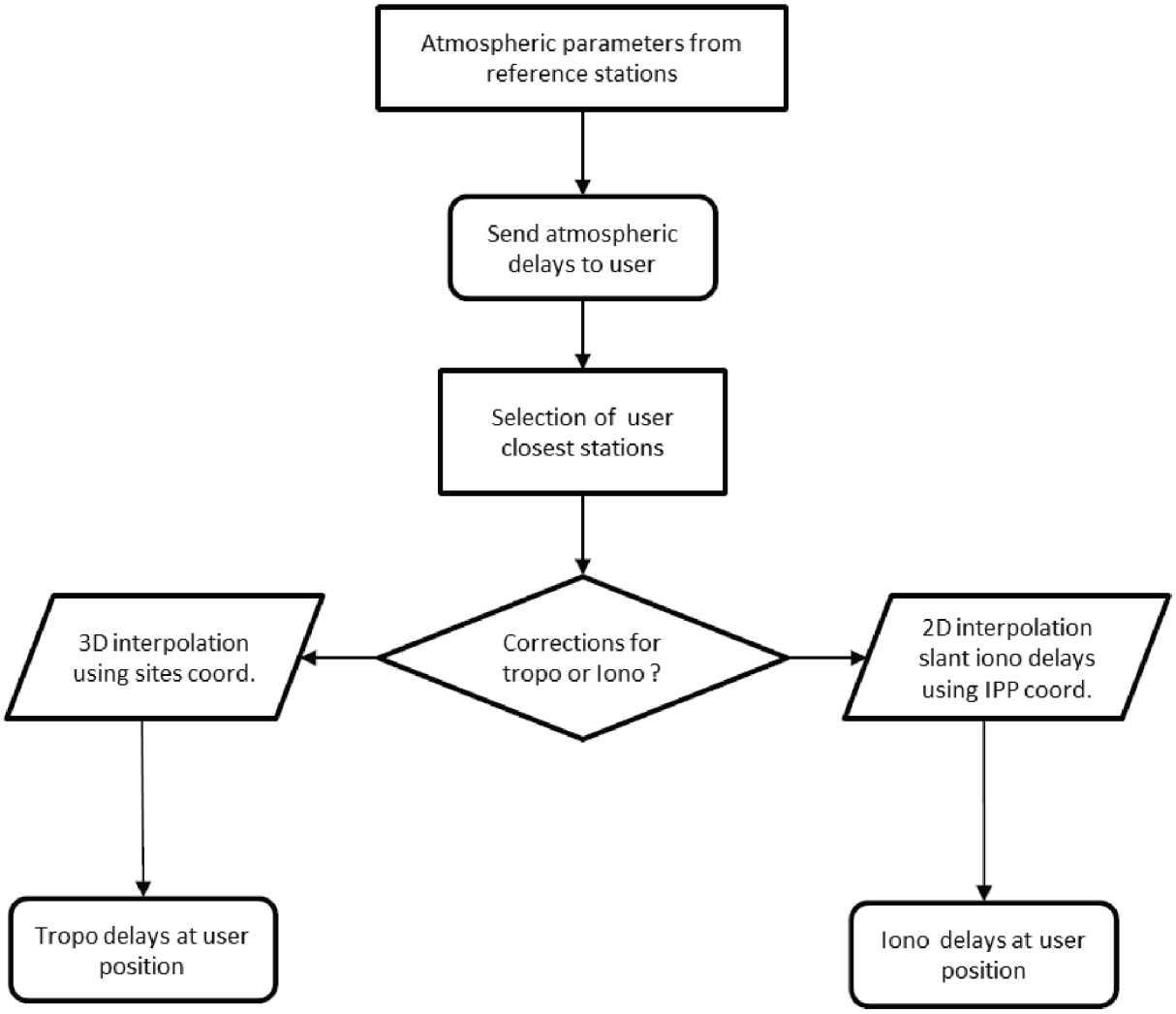

Figure 41 – Flowchart of atmospheric delays interpolation method.

Once SSR ionospheric and tropospheric corrections are generated (value and constraint), they are provided to users and taken into account as described in next section.

13.6. Step 3: GNSS data processing at the user side

At rover side, PPP-Wizard processing is focused on its positions and how they benefit from SSR atmospheric corrections. Ionospheric and tropospheric corrections are introduced as a priori information not only for the first epoch, as realized in Part II, but for every new epoch and used as a priori constrained parameter. PPP-Wizard 1.3 has already implemented an interface to use such corrections (Laurichesse, 2016). A single tropospheric correction is applied to all satellites, thus one constraint is needed. On the other hand, there are three different levels of accuracy for ionospheric corrections. Therefore, instead of using a

specific constraint value for each individual ionospheric correction, it is possible to simplify to a global level (1, 2 or 3) of accuracy for all satellites. Thus, the predefined constraint from the configuration file could be used. However, even thought that such predefinition is very useful, it is also a small limitation, since only 3 levels of corrections may not represent the different accuracies of ionospheric SSR corrections of each satellite with different satellites geometries. Another important point to consider is that accuracies of tropospheric and ionospheric SSR corrections can change during time and the constraint values set in the configuration do not allow updates overtime.

In order to improve PPP-Wizard 1.3 interface for atmospheric SSR corrections, some modifications are implemented with two goals:

1) to introduce a specific SSR ionospheric constraint value for each individual ionospheric SSR correction,

2) to consider the time variation of constraints for both SSR tropospheric and ionospheric corrections, i.e. to update the constraint value at every epoch.

There are four distinct GNSS data processing strategies considered at the rover side. Such strategies differ in the use of SSR atmospheric corrections and are defined as follows:

1. **Standard RT-IPPP**: processing with no atmospheric SSR corrections, i.e. PPP with ambiguity fixing, simulating nominal real-time conditions. Actually, this strategy uses almost the same processing configurations settled for the strategy at server side. However, the rover is considered as a mobile receiver (i.e. sigModPos is defined as 10 m) and processing is re-initialized every 2 hours, because this session time can be enough to observe the positioning convergence. This processing is conducted to assess typical RT-IPPP with PPP-Wizard 1.3.

2. **PPP-RTK Iono+Tropo re-injection**: refers to processing strategy using as SSR corrections the atmospheric delays estimated in GNSS data processing of the rover station itself, which are re-injected constrained in a re-run of the GNSS data processing. In this case standard RT-IPPP processing is realized, starting 2 hours before the first epoch atmospheric estimates are used as a priori SSR corrections. An example of this solution is presented in Laurichesse and Privat (2015) and is also available at PPP-

Wizard project web page. This solution is assumed as the reference one, since the best SSR correction that can be provided is the truly estimated atmospheric delays using own GNSS station data. Atmospheric corrections are assumed to have high quality, thus constraint values for ionospheric and tropospheric delays are quite strong. 1 cm is used for tropospheric delay and two levels: 1) 5 cm and 2) 10 cm are used for ionospheric delays. The choice of Level (5 cm or 10 cm) for the ionospheric constraints relies on ambiguity parameter for the corresponding satellite. If ambiguity satellite is fixed to integer in previous processing, the constraint for ionospheric delay is set to 5 cm (level 1), otherwise it is set to 10 cm (level 2).

3. **PPP-RTK Iono+Tropo IDW interpolation using dense network:** this processing solution uses SSR atmospheric corrections coming from IDW interpolation algorithm using Orphéon dense network configuration. Corrections are constrained according to the correction accuracy provided by IDW interpolation (section 13.5). Such accuracies vary over the time. This is possible thanks to the modifications implemented in PPP-Wizard 1.3.

4. **PPP-RTK Iono+Tropo IDW interpolation using sparse network**: this processing is similar to strategy 3, but Orphéon sparse network configuration is used.

When atmospheric SSR corrections are used, ambiguity fixing to integer values starts after 60 seconds (60 epochs). Besides all rover solutions are processed in kinematic mode. Session duration is 2h. Considering the 10 selected days, cold-starts begin at 03, 05, 07, 09, 11, 13, 15, 17, 19 and 21 UTC, which means that there are 10 re-initializations per stations for every day. The total of re-initializations performed is ~ 6600.

Table 21 summarizes configurations applied at the user side for each strategy. In this table, only parameters that differ from those used at network side (Table 20) are listed.

Table 21 – PPP-Wizard 1.3 configurations at user side that differ from those used at the network side.

Number	Strategy	Number of epochs to start ambiguity fixing (stepMin)	Iono constraint (sigMeasIono)	Tropo constraint (sigMeasTropo)	sigModPos
1	Standard RT-IPPP	3600 epochs	1.0 m	0.1 m	10 m (kinematic)
2	PPP-RTK Iono+Tropo Re-injection	60 epochs	Level 1: 5 cm Level 2: 10 cm	2 cm	
3	PPP-RTK Iono+Tropo IDW interp. dense network	60 epochs	Coming from IDW interpolation (1 per satellite)	Coming from IDW interpolation	
4	PPP-RTK Iono+Tropo IDW interp. sparse network	60 epochs	Coming from IDW interpolation (one per satellite)	Coming from IDW interpolation	

13.7. Awareness of receiver biases

Ionospheric delays are frequency dependent, which is not the case for tropospheric delays. Therefore, ionospheric delays suffer from receiver and satellite's hardware inter-frequency biases. Taking into account hardware biases present on GNSS measurements is an important aspect when modeling ionosphere effects (Camargo, 2009; Ma and Maruyama, 2003).

Figure 42 shows an example of estimated ionospheric delays at reference station CORB along day of year 007/2016. In this figure, ionospheric delays from GLONASS satellites (R01, R02, …, R27) are plotted in grey and ionospheric delays from GPS satellites (G01, G02, …, G27) are plotted with different colors.

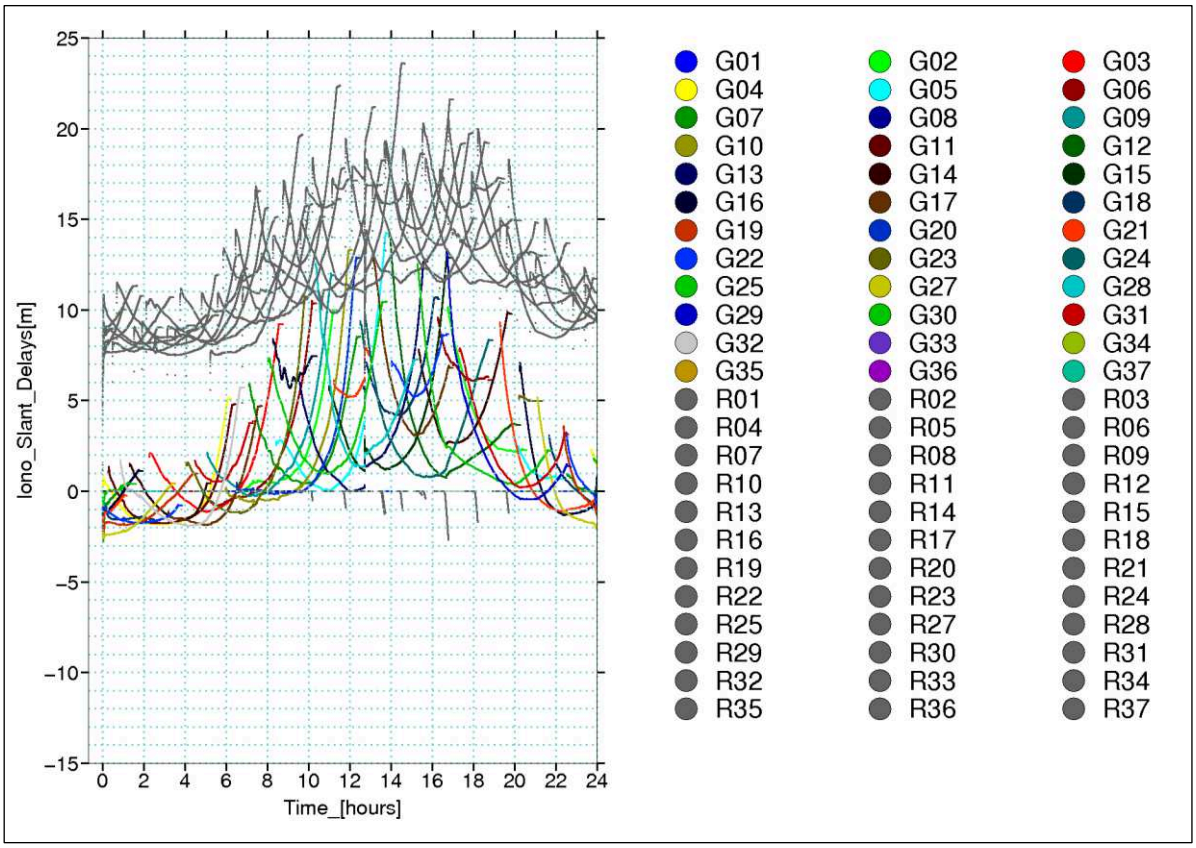

Figure 42 - Example of slant ionospheric delays for GLONASS (R**) and GPS (G**) estimated at station CORB during day 007/2016.

In Figure 42, ionospheric delays increase at the beginning and at the end of satellite passes, when satellites have the lowest elevation angles and when signals cross a thicker portion of ionosphere. Strongest values are observed in the afternoon at 14 h ~ 15 h before decreasing in the evening. Ionospheric delays around zero values at the beginning of the passes for some satellites are due to the convergence of ionospheric delays estimates, since ionospheric delays are initially set to zero (cf. processing configurations in section 13.4). This convergence is longer for some satellites. In this figure, two points are visible: 1) an inter-system offset between GPS and GLONASS ionospheric delays and 2) negative values for GPS ionospheric delays, which is physically not possible. The inter-system ionospheric biases (offsets) are potentially due to the inter-system bias between different GNSS constellations (Khodabandeh and Teunissen, 2016).

It is still necessary to think about inter-frequency hardware biases between different satellites of the same constellation, as well as the biases between different receivers of the reference network. Even, supposing receivers have same brand and model, they can use cables with different length and they can be subject to different temperature conditions.

Changes, in antenna and receiver model have also to be considered. Such aspects can explain different hardware biases for different receivers. These biases affect both, code and phase measurements as discussed in Part I, sections 5.4.2.2.2 and 6.1, respectively. In PPP-Wizard 1.3, uncombined satellite biases are corrected for code and phase measurements thanks to CNES orbital products. The PPP-Wizard 1.3 engine, estimates simultaneously uncombined receiver hardware biases together with positions, receiver clock offsets, atmospheric delays and phase ambiguities (see section 6.2.3). Considering the correlations existing among such parameters, ionospheric delays may absorb part of receiver hardware bias. Understanding how such bias can affect the ionospheric corrections is crucial for a successful ionospheric correction.

According to Rovira-Garcia (2015), an ionospheric model can be biased. The biases present in the model would be absorbed by parameters such as receiver clock offsets. For that, the receiver's bias contribution must be the same for ionospheric delays of all satellites, i.e. characterizing a unique bias that could be absorbed by clock parameter. This is true for implemented IDW interpolation because:

- IDW interpolation is realized individually satellite per satellite, i.e. biases between different satellites or biases related to different constellation would keep the same relationship, since they are not mixed in each individual correction computation;

- Concerning influence of receiver biases from reference network stations, for all satellites, IDW interpolation results in a unique combined receiver bias of stations used in the algorithm.

Thus, interpolated hardware biases, affecting ionospheric corrections are assumed to be the same for all satellites and can be absorbed by receiver clock offsets of users. Therefore, the final positions estimates of user do not suffer from the biases in ionospheric corrections. However, it is possible that such biases in ionospheric corrections reduce its effectiveness for a fast solution convergence. Ideally, hardware biases of reference stations can be estimated as parameters of a polynomial modeling for ionospheric delays as realized, for example, by Camargo (1999), but this has not been studied in this work and left as prospect.

Instead, just to have a better idea of the magnitude of hardware biases affecting ionospheric delays estimated at the reference network, some analysis on behavior of minimal ionospheric delays are carried out. Normally, ionospheric delays have minimal values in the first hours of the day as showed in Figure 42. This information can be used to get an approximate value for receiver hardware biases. Following this assumption, the mean of ionospheric delays estimated between 3 h and 5 h are computed as they can be considered to be close to receiver hardware biases. For this analysis, vertical ionospheric delays of all GPS satellites are used at every epoch. Only satellites with ambiguities fixed to integer values are used, in order to get the most precise ionospheric delays. In addition, only satellites with elevation angle higher than 40 degrees are used to reduce impacts of mapping function. All stations of the reference network are used every day of the experiment. Figure 43 shows such mean of vertical ionospheric delays for 130 reference stations (those with less availability discontinuities).

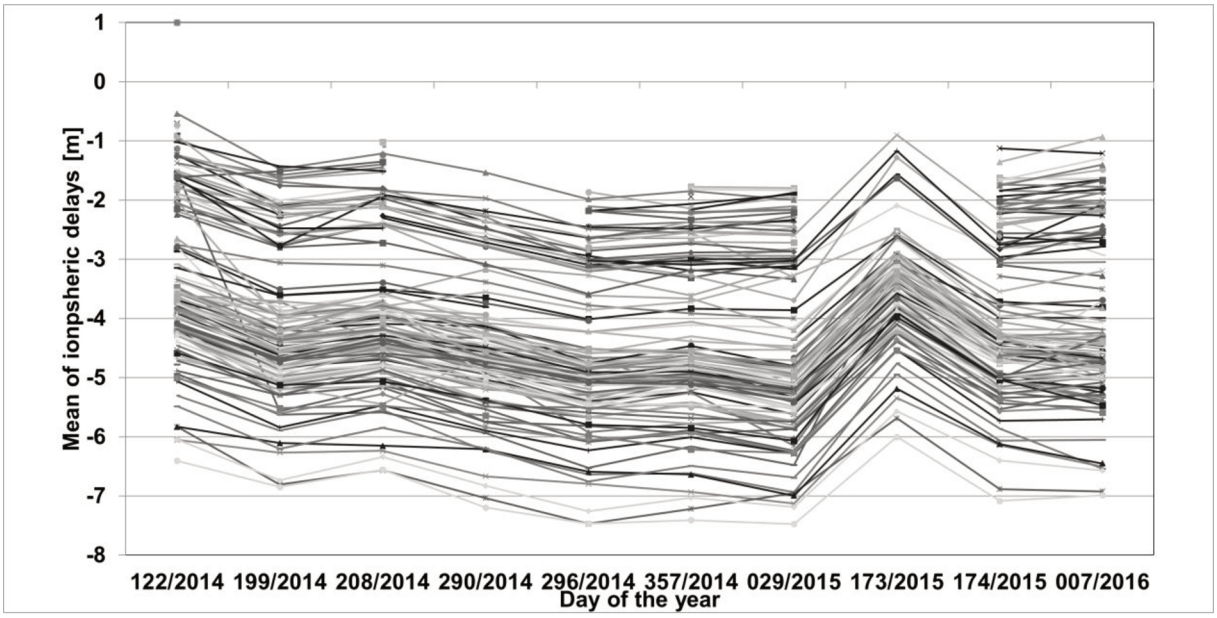

Figure 43 – Mean of ionospheric delays estimated with PPP-Wizard 1.3 at the Orphéon reference stations during low ionospheric activity hours (3 h to 5 h) of days involved in the experiment.

Two different groups of values appear. The first one is around -2 m and the second one is around -4m. As already stated, Orphéon reference network is composed by two different receiver models, Leica GRX1200+GNSS and Leica GRX1200GGPRO, equipped with three different antenna models, Leica AS10, Leica 1202GG, and Leica 1203GG. Stations whose mean ionospheric delays roughly around -2 m are equipped with Leica receivers

GRX1200GGPRO while the values roughly around -4 m corresponds to stations equipped with Leica receiver GRX1200+GNSS.

However, these results must be taken with caution. Even if means of ionospheric delays in Figure 43 are computed over low activity hours, they are still affected by seasonal variations of ionosphere activity (section 7.2.5), which make difficult to conclude about the magnitude of hardware biases of the reference stations. For example, means of ionospheric delays of day 173/2015 present higher values with respect to other days, which is a potential consequence of the geomagnetic storm that happened on that day, as verified with index F10.7 (section 13.1).

These results indicate that hardware biases affecting ionospheric delays depend on receiver model. It means that GNSS networks equipped with similar receiver models can improve the modeling of ionospheric delays as for the method described in Camargo (1999). In the case of interpolation, that method gets around hardware delays because hardware delays of reference stations are mixed and the resulting bias can be absorbed by receiver clock offset of receiver user.

14. Results and analysis

Results are described separated with respect to both, server and user sides. First the results at the reference network are analyzed in terms of positioning performances and estimated atmospheric delays. This is required to verify GNSS processing quality at this step. Next, atmospheric corrections and user positioning are assessed. Concerning this last part, user positioning is analyzed in more details, including the study of some examples, followed by a statistic generalization.

14.1. Server side: reference network results

14.1.1. Positioning performances

As previously stated, positioning of Orphéon reference stations is done using parameters defined in Table 20. Figure 44 presents typical positions errors on horizontal (E, N) and vertical (U) components for results of CORB reference station belonging to Orphéon network, and computed over 24 h of days 199/2014, 208/2014 and 173/2015. Ambiguity fixing starts 1 h after the cold-start, and once the solution has converged, it preserves its accuracy most of the time. However, epochs with large data gaps, bad fixed ambiguities and cycle-slips can happen even after the ambiguity fixing. It leads to significant positioning errors and a new cold-start. Such event is observed at 14 h of day 199/2014 (Figure 44 - left). This induces a full reset of ambiguities parameters. This is the reason why coordinates are estimated at reference stations and positioning errors are used as a quality indicator to decide if atmospheric delays estimated at a specific reference station can be included in SSR corrections generation. Improvements in such strategy are aimed for next studies in order to allow fixing or at least strongly constraint coordinates of reference stations.

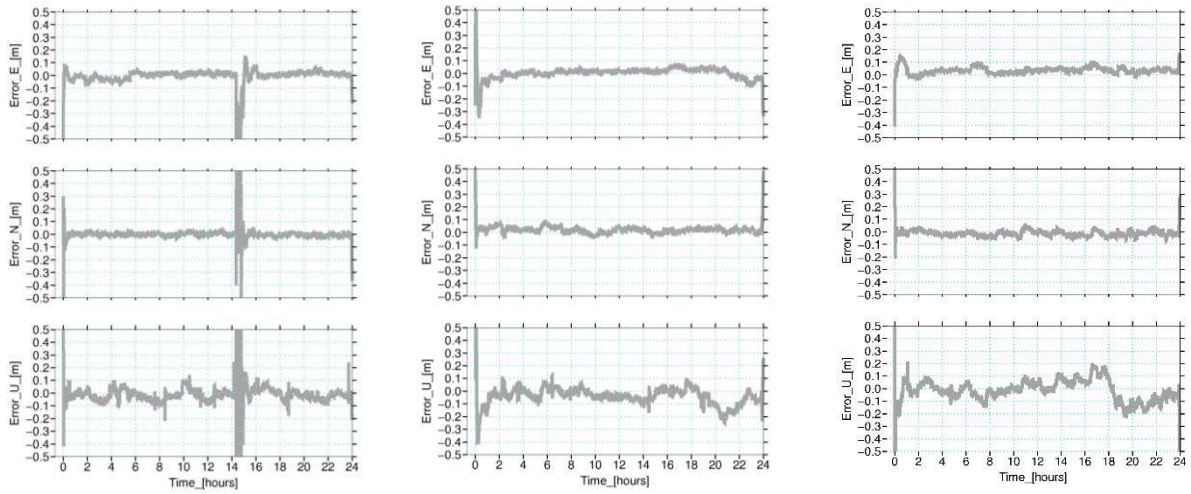

Day 199/2014 Day 208/2014 Day 173/2015

Figure 44 – Typical positions errors at reference station CORB over 24 h (server side).

To ensure that RT-IPPP solutions at server side converge properly and are able to provide atmospheric delays for SSR corrections, first two hours of RT-IPPP processing at network side are assessed statistically. Figure 45 shows Medians (left) and 68%-quantiles (right) of positions errors computed during the first two hours of all days of the experiment and over the whole Orphéon network. Each day includes about 150 cold-starts.

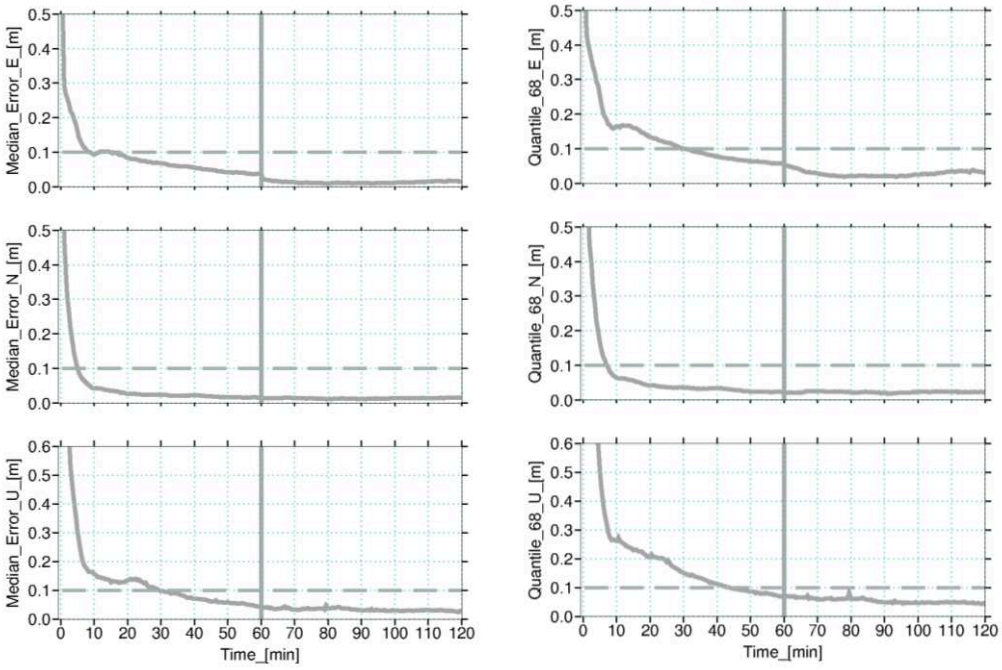

Figure 45 – Medians (left) and 68%-quantiles (right) of positions errors computed during the first two hours of all days of the experiment and over the whole Orpheon network; the vertical bar indicates the time ambiguity fixing starts.

In Figure 45, once ambiguity fixing started, 68%-quantiles of positions errors (absolute) have a mean of ~3 cm on East and ~2 cm north components respectively. The vertical component is less accurate with a mean of absolute error of ~7 cm. This represents a mean 3D error of ~8 cm, that is lower than the 18 cm threshold, used to select/reject stations into the SSR atmospheric corrections engine. For future studies, the adoption of more rigorous threshold is something to think about. Besides, the possibility of fixing reference stations coordinates can improve the estimation of atmospheric parameters.

14.1.2. Ionospheric Delays

Analysis on ionospheric SSR corrections are carried out in section 14.3 (user side). Although, a few results and comments on PPP-Wizard 1.3 estimates are presented in next paragraphs to better visualize the ionospheric delays that are used as input for SSR corrections engine.

In Figure 46, GPS ionospheric delays estimated at the Orphéon reference station CORB are presented for some days involved in the experiment. Ionospheric delays from GLONASS satellites are not included as ambiguity fixing is only done on GPS phase measurements. Daily variability of minimum ionospheric activity around 3 h is visible. Some days minimum is about -5 m (e.g. day 122/2014), while other days it is about -2 m (e.g. day 199/2014). Maximum values of ionospheric delays vary between 0 and 15m, and are achieved in the afternoon between 12 h and 15 h, except for day 174/2015. Indeed, on that day the maximum values are verified at night. This anomaly is provoked by the geomagnetic storm that occurred on this day (section 13.1), which also affected the beginning of day 173/2015, as observed in Figure 46. These results evidence that PPP-Wizard 1.3 estimated ionospheric delays were physically coherent.

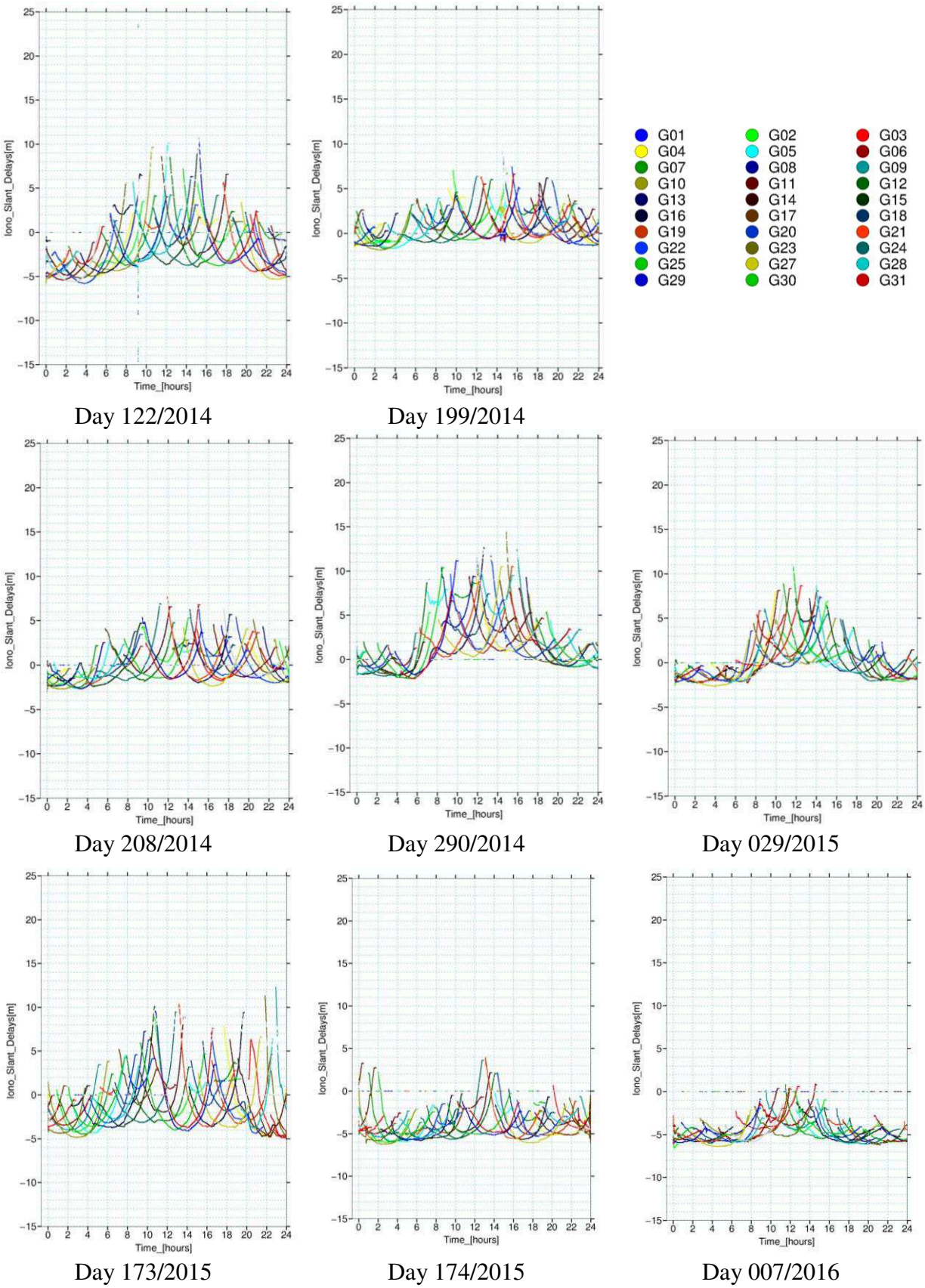

Day 122/2014 Day 199/2014

Day 208/2014 Day 290/2014 Day 029/2015

Day 173/2015 Day 174/2015 Day 007/2016

Figure 46 – GPS slant ionospheric delays estimates at reference station CORB.

In order to have a look at the spatial variability of ionospheric delays over the network, charts of vertical ionospheric delays at IPP locations during day 290/2014, are presented in Figure 47. Vertical ionospheric delays are obtained with the standard geometric mapping function described in section 7.2.2. It is important to keep in mind, that these vertical values are showed here only for visualization purposes, since the input for IDW interpolation are the slant ionospheric delays. As explained in section 13.5.1, this choice was motivated by the limitations of such mapping.

In Figure 47, network maximum values of vertical ionospheric delays are verified in the afternoon, as in results presented for station CORB (Figure 46). Indeed, vertical ionospheric delays over the network at 15 h present a mean value of 4.2 m and a standard deviation of 1.7m. Smallest values correspond to satellites with the highest elevation angles and whose IPPs are located above the network. Strongest values are outside the network area, corresponding to satellites with the lowest elevation angles. Ionospheric mapping functions should be able to remove such impact of satellite elevation angle. To overcome this limitation, recent studies have proposed the use of ionospheric mapping functions based on the electron density field derived from IRI (Zus et al., 2017). The use of improved mapping functions for atmospheric corrections must be seriously considered for future works.

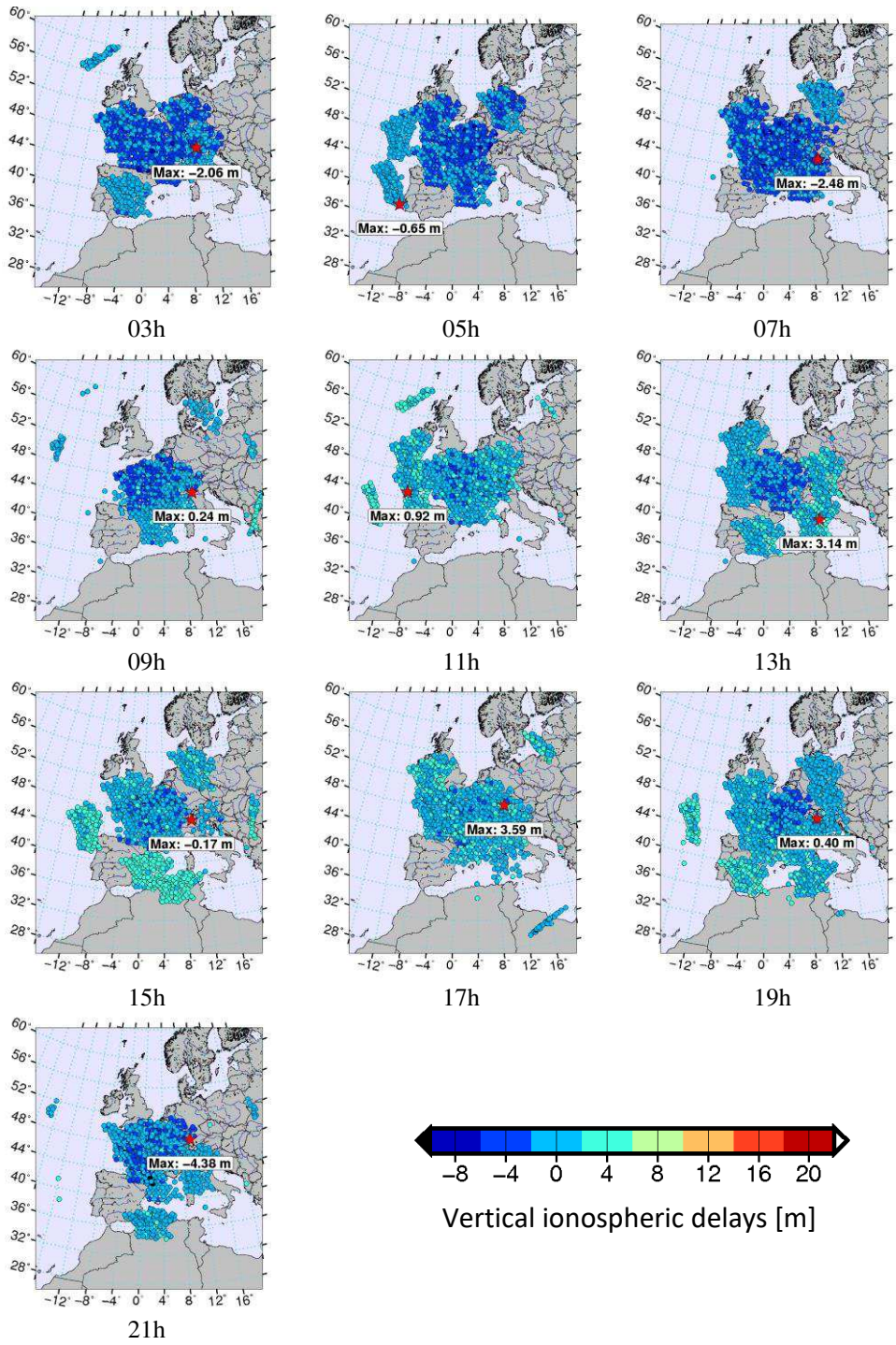

Figure 47 - Vertical ionospheric delays at IPPs estimated over Orphéon network at different times of day 290/2014.

14.2. User side: SSR tropospheric corrections

As explained in section 13.5, SSR tropospheric corrections are a priori tropospheric delays that user must use with a constraint value representing its accuracy. Such

strategy is assessed considering the corrections generated at locations of Rover Network stations (Figure 36). As done in Part II, tropospheric delays estimates are assessed thanks to IGN products (section 10.2).

Figure 48 presents typical differences between tropospheric delays corrections (IDW interpolation) and IGN products at station VFCH on day 007/2016. Differences are computed every hour.

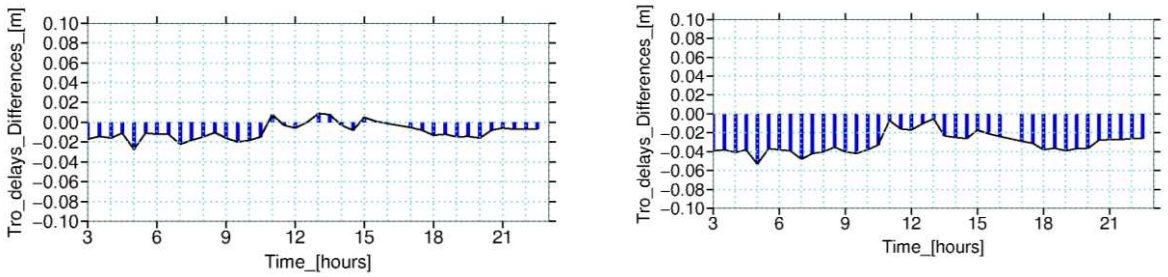

IDW from dense network IDW from sparse network

Figure 48 – Differences between tropospheric delays estimates interpolated from dense (left) and sparse (right) networks and IGN products at VFCH station on day 007/2016.

The differences with respect to IGN products using dense network achieve a maximum of around 3 cm, but they are better than 2 cm most of time. These differences increase by ~2 cm when using the sparse network, in this case. Such performances are comparable to those of tropospheric corrections using OFC model (Part II). However, statistical validation is required to confirm these results.

In order to assess accuracies of SSR tropospheric corrections statistically, the comparison with IGN products is accomplished for all the three solutions: 1) tropospheric corrections from interpolation with dense network, 2) from interpolation with sparse network as well as those of the reference solution, (re-injection), i.e. tropospheric delays estimated at the own simulated user stations. Differences between corrections coming from these solutions are computed on the whole Rover Network and on all the days of the experiment. Results are plotted in Figure 49.

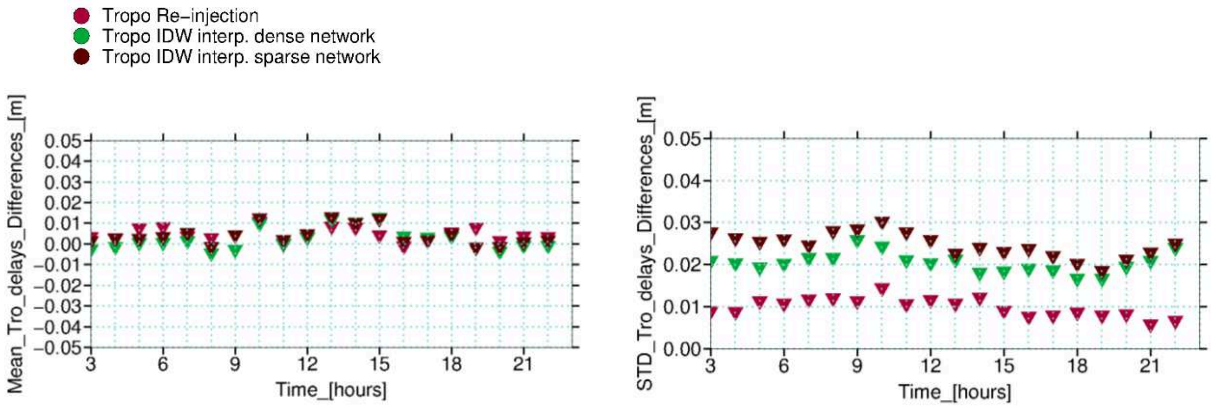

Figure 49 - Hourly means and standard deviations of differences between tropospheric delays corrections and IGN products computed over Orphéon network.

Mean values are very similar whatever the type of SSR corrections, about 1 cm. Lowest standard deviations are obtained with SSR corrections coming from Re-injection. They are very close to 1 cm. This is an indicator of the best performances SSR tropospheric corrections can achieve. Standard deviations computed with SSR corrections coming from interpolation decrease with network density. With our sparse network, they reach about 3 cm.

14.3. User side: SSR ionospheric corrections

To analyze ionospheric SSR corrections, two reference methods are considered: IGS IONEX and ionospheric delays estimates at the stations. The latter are obtained thanks to Standard RT-IPPP processing of PPP Wizard 1.3, that is those used in Re-injection method. IONEX products are based on GNSS observables and resulting ionospheric delays are globally modeled together with satellites and receivers DCBs (see section 5.4.2.2.2). Such products are used because they are an external reference of ionospheric products and provide valuable information on ionosphere behavior.

Figure 50 shows an example for both IONEX and ionospheric delays estimates. Ionospheric delays estimates present negative values. As such parameter must be always positive, these negative values can be caused by hardware biases. Even though, there is a bias between IGS IONEX and ionospheric delays estimates Figure 50 shows that both have similar behavior over the day.

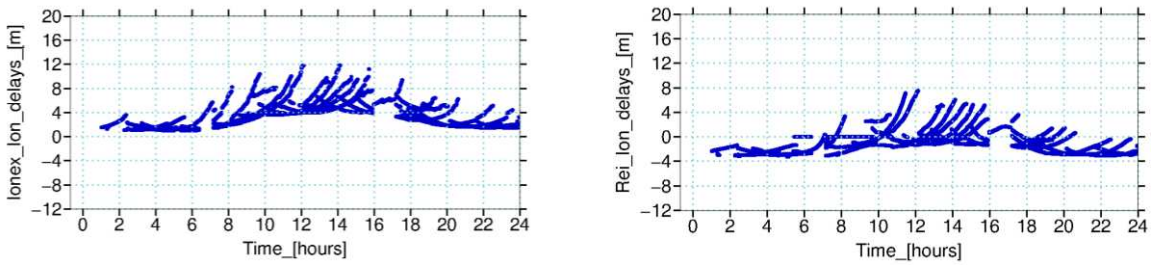

Ionospheric delays from IONEX PPP-Wizard 1.3 estimated ionospheric delays

Figure 50 – Slant ionospheric delays coming from IONEX (left) and Standard RT-IPPP (right) at BRST station on day 007/2016.

Section 14.3.1 presents the comparison of ionospheric corrections obtained using dense or sparse networks to IGS IONEX products. In section 14.3.2, such comparison is realized with respect to ionospheric delays estimated at the rover itself. Besides, two additional analyzes are presented: 1) the correlation between estimated receiver clock and biases present in ionospheric corrections (section 14.3.3) and 2) the assessment of the constraints calculated at the server side to represent the quality of ionospheric corrections (section 14.3.4). These analyzes are necessary to understand the ionospheric solutions generated. For every study results are presented for two stations followed by statistic results considering relevant data set.

14.3.1. Comparison with IGS IONEX products

Differences between interpolated GPS slant ionospheric delays and IONEX products at stations VFCH and BRST are plotted in Figure 51. Differences are computed every 30 min over a 2 h sliding window. Results using dense and sparse networks ionospheric corrections are presented.

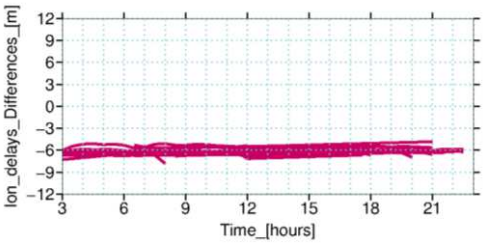

Dense network configuration
station VFCH
(Mean: -6.11 m, Standard deviation: 0.42 m)

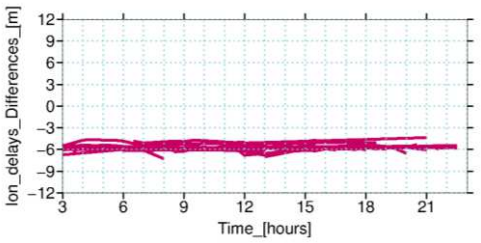

Sparse network configuration
station VFCH
(Mean: -3.57 m, Standard deviation: 0.44 m)

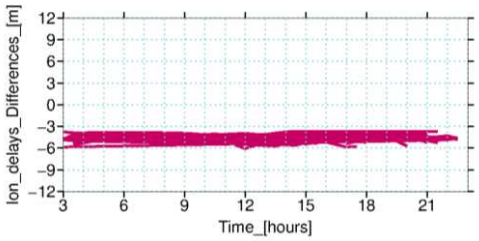

Dense network configuration
station BRST
(Mean: -4.72 m, Standard deviation: 0.45 m)

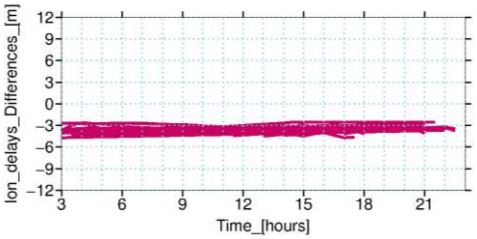

Sparse network configuration
station BRST
(Mean: -5.66m, Standard deviation: 0.42 m)

Figure 51 – Differences between interpolated GPS slant ionospheric delays from dense (left) and sparse (right) networks and IGS IONEX at VFCH and BRST stations on day 007/2014.

At BRST station, and using the dense network, mean of differences is -4.72 m, with a standard deviation of 0.45 m. At VFCH station, mean and standard deviation are -6.11 m and 0.42 m, respectively. When the sparse network is used, the biases change, since different set of stations are used to generate the ionospheric delays, but standard deviations remain similar to those obtained with the dense network. These results reveal biases with metric amplitudes, and a decimeter accuracy. The latter is consistent with IONEX nominal precision, claimed to be between 2 and 8 TECU (1 TECU~16 cm on L1 ; (Rovira-Garcia et al., 2015)).

In order to validate the precision of ionospheric corrections, i.e. the repeatability of differences, the same computations presented in Figure 51 are repeated on the whole Rover Network and on all days of the experiment. Mean standard deviations of the differences with respect to IONEX are computed. Results for several stations are plotted in Figure 55 for dense and sparse network configurations.

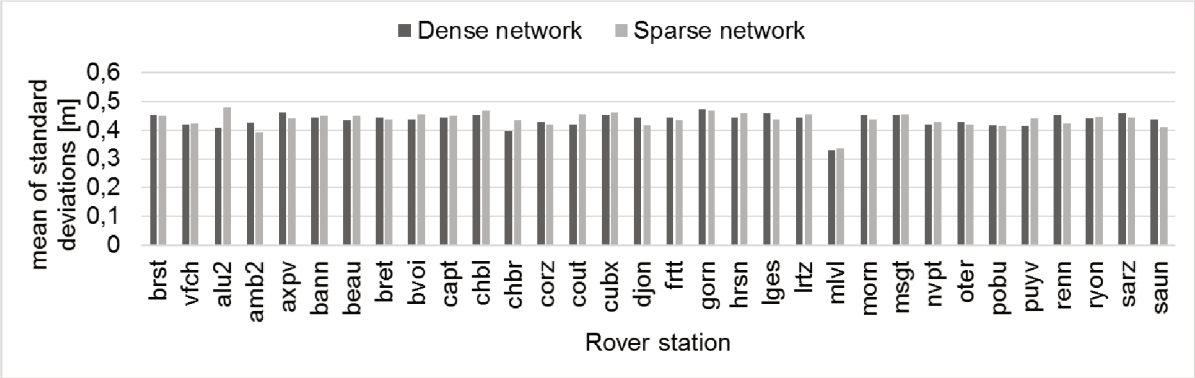

Figure 52 – Mean standard deviations of differences between interpolated ionospheric delays and IONEX products computed over stations from Rover Network considering all days of the experiment.

Using sparse and dense network provide similar results at each station. Differences induced by network density is about 0.02m. On the whole Rover Network, the standard deviation of these differences is about 0.43m. These standard deviations over the network fit with those plotted in Figure 51, and are also coherent with the precision of IGS IONEX products.

14.3.2. Comparison with ionospheric delays estimated at the rover

Figure 53 present differences between interpolated GPS ionospheric delays and ionospheric delays estimated at rover station thanks to Standard RT-IPPP processing, for VFCH and BRST. Differences are computed every 30 min over a 2 h sliding window. Results using dense and sparse networks are presented. In these results, biases show metric amplitudes, however better repeatability is found than with IONEX products (Figure 51), since here standard deviations of differences are about 20 cm.

Computations whose results are plotted in Figure 53 are repeated on the whole Rover Network. Interpolated ionospheric delays are compared to those estimated at the Rover itself with RT-IPPP (Re-injection). This is a more precise reference, but also biased as verified on results of Figure 53. Figure 54 shows the results. Here, more differences from a station to another appear but differences induced by network density are still at the centimeter level.

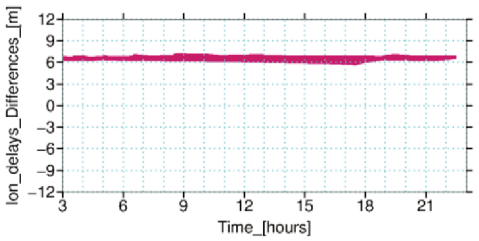

Dense network configuration
station VFCH
(Mean: 6.59m, Standard deviation: 0.20 m)

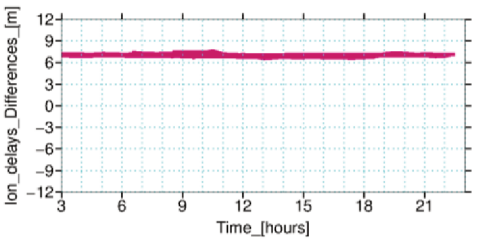

Sparse network configuration
station VFCH
(Mean: 7.06 m, Standard deviation: 0.19 m)

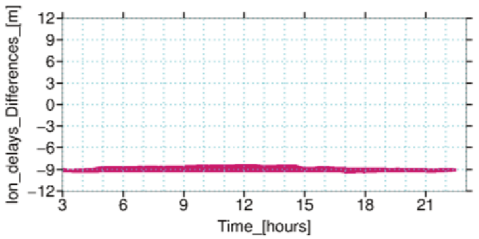

Dense network configuration
station BRST
(Mean: -8.95 m, Standard deviation: 0.21 m)

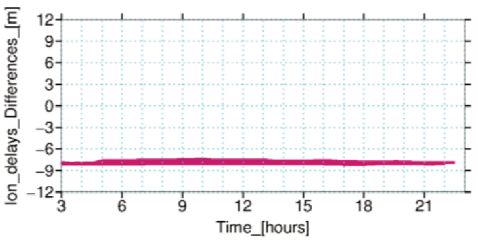

Sparse network configuration
station BRST
(Mean: -7.84 m, Standard deviation: 0.19 m)

Figure 53 – Differences between interpolated GPS slant ionospheric delays from dense (left) and sparse (right) networks and delays coming from RT-IPPP at VFCH and BRST stations on day 007/2014.

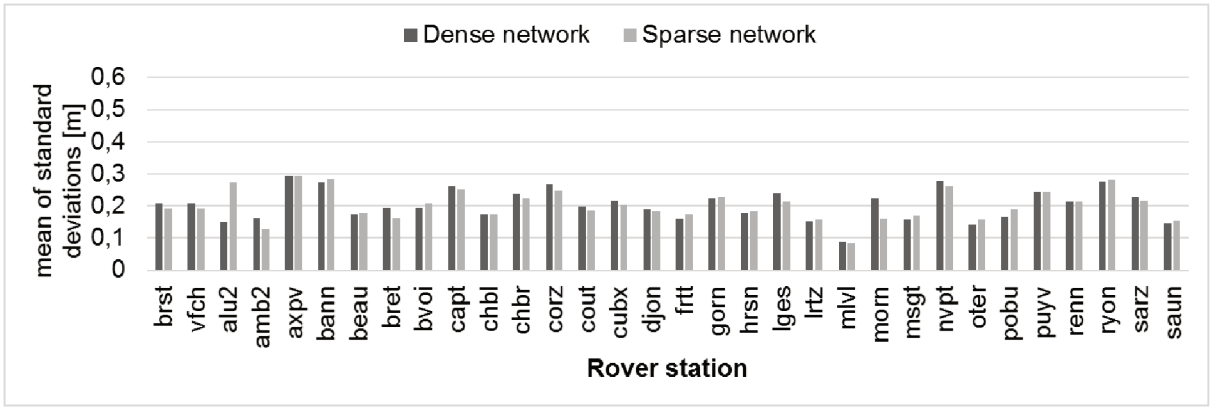

Figure 54 - Mean of standard deviation of differences between interpolated ionospheric delays estimates and delays previously estimated at stations.

Figure 53 shows that precision of ionospheric corrections provided by both sparse of dense network is around 20 cm and can reach up to 30 cm for some stations. Though ionospheric corrections have quite good repeatability (i.e. precise), it is necessary to understand the effects of the biases. Next section brings some results on receiver clock estimated using such corrections.

14.3.3. Correlation between bias in ionospheric corrections and estimated receiver clock offset

While processing positions using atmospheric corrections, ionospheric errors can be absorbed by other parameters due to correlations in the filter. It can be shown that main correlated parameter with ionospheric delays is receiver clock offset. Figure 55 shows the differences of GPS receiver clocks estimates computed using Standard RT-IPPP and PPP-RTK using a priori interpolated ionospheric corrections calculated with sparse and dense networks, respectively.

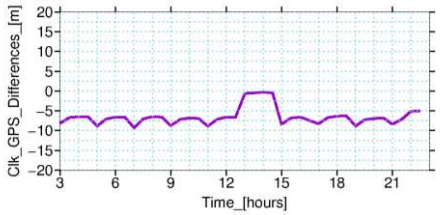

Dense network configuration
station VFCH
(Mean: -6.4 m, Standard deviation: 2.2 m)

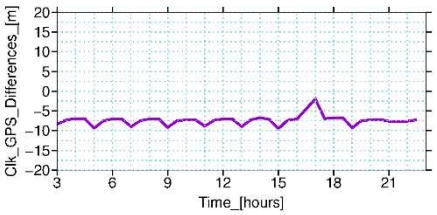

Sparse network configuration
station VFCH
(Mean: -7.4 m, Standard deviation: 1.2 m)

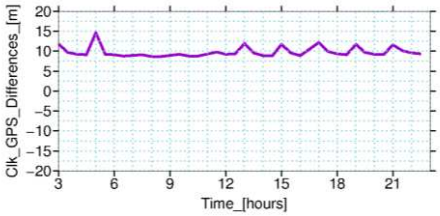

Dense network configuration
station BRST
(Mean: 9.8 m, Standard deviation: 1.3 m)

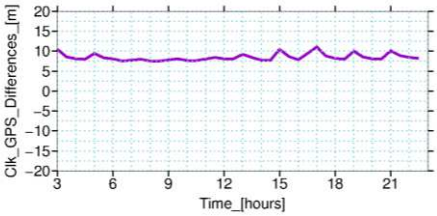

Sparse network configuration
station BRST
(Mean: 8.5 m, Standard deviation: 0.9 m)

Figure 55 – Differences of GPS receiver clock offsets of VFCH and BRST stations on 007/2014 between Standard RT-IPPP and PPP-RTK using ionospheric delays computed from dense (left) and sparse (right) networks.

Mean differences between GPS receiver clock offsets have similar magnitude but with an opposite value as those found for ionospheric delays plotted in Figure 53.

Figure 56 presents differences between receiver clock offsets with respect to ionospheric delays differences computed over the whole Rover Network. Results show that receiver clocks offsets and ionospheric delays are close to be anti-correlated. Because vertical component and receiver clocks offsets are also correlated, errors on ionospheric delays impact positions. The next chapter assesses these impacts.

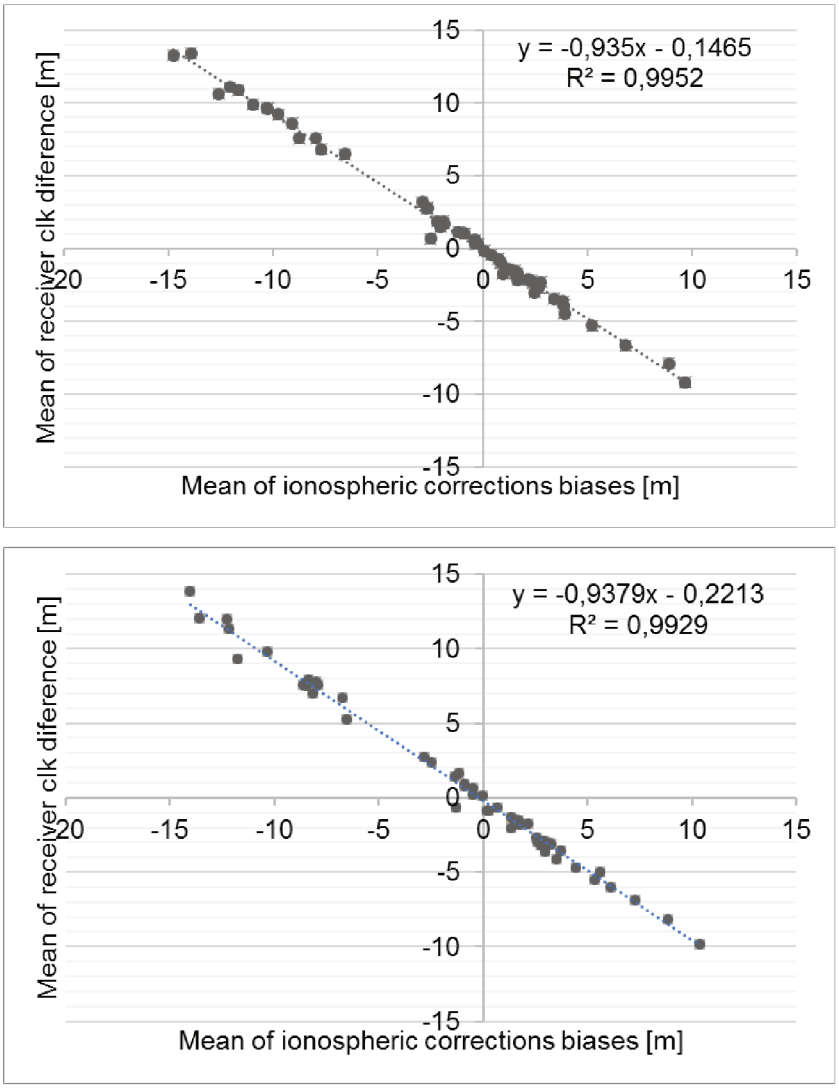

Figure 56 – Differences between receiver clock offsets with respect to ionospheric delays differences generated with dense (top) and sparse network (bottom).

14.3.4. Constraints applied to ionospheric corrections

Accuracy of ionospheric delays is calculated using information from reference stations processing, e.g. ambiguity fixing, as well as distances with respect to user (c.f section 13.5.1). During processing, different constraints are applied to ionospheric delays when ambiguities are kept float or integer. Figure 57 shows values of ionospheric constraints used over the time. They are calculated as defined in section 13.5, and provided to users together with atmospheric corrections.

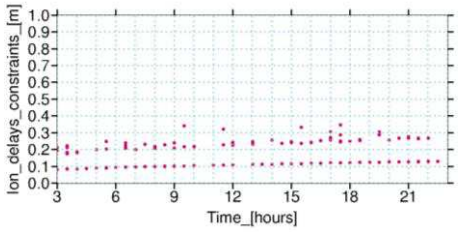

Dense network configuration
station VFCH
(Mean: 0.13 m, Standard deviation: 0.05 m)

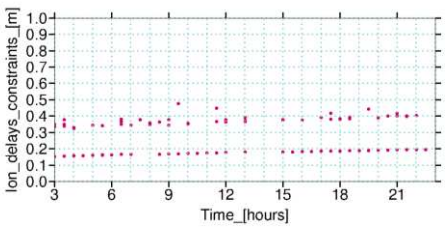

Sparse network configuration
station VFCH
(Mean: 0.21 m, Standard deviation: 0.08 m)

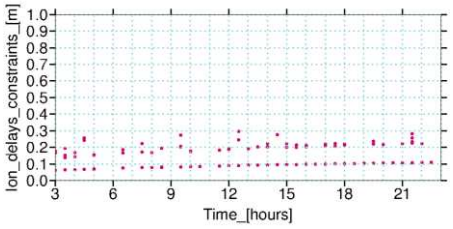

Dense network configuration
station BRST
(Mean: 0.11 m, Standard deviation: 0.05 m)

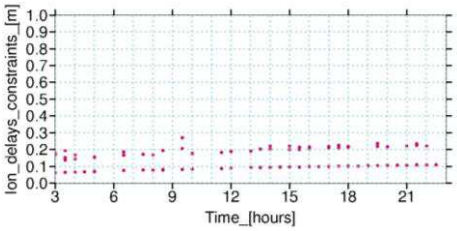

Sparse network configuration
station BRST
(Mean: 0.11 m, Standard deviation: 0.04 m)

Figure 57 – Constraints for SSR GPS ionospheric corrections at VFCH and BRST stations on day 007/2014 for dense (left) and sparse (right) networks.

In Figure 57, every plot presents two groups of constraints. The first one, better than 10 cm, corresponds to ionospheric corrections for satellites whose phase ambiguities are fixed at the reference stations used to compute the correction. The second one, between 15 cm and 45 cm, is calculated with phase measurements whose ambiguities are not all integer. These constraints can represent the precision of the ionospheric corrections achieved in results of comparison with respect to the ionospheric delays estimated at the station itself Figure 54. At BRST station, ionospheric constraints are similar whatever the network density. Constraints are 11 cm in mean, with standard deviation of ~5 cm. These results are due to dense and sparse network topologies which are similar in BRST area. At VFCH station, constraints differ following the network density because topology of both networks are significantly different. Mean values are 13 cm 21 cm with dense and sparse network respectively. Standard deviations are also different. They increase up to 8 cm with the sparse network.

Figure 58 presents mean and standard deviations of constraints provided with SSR ionospheric corrections for PPP-RTK. The mean of precisions showed in Figure 54, considers all GPS ionospheric delays.

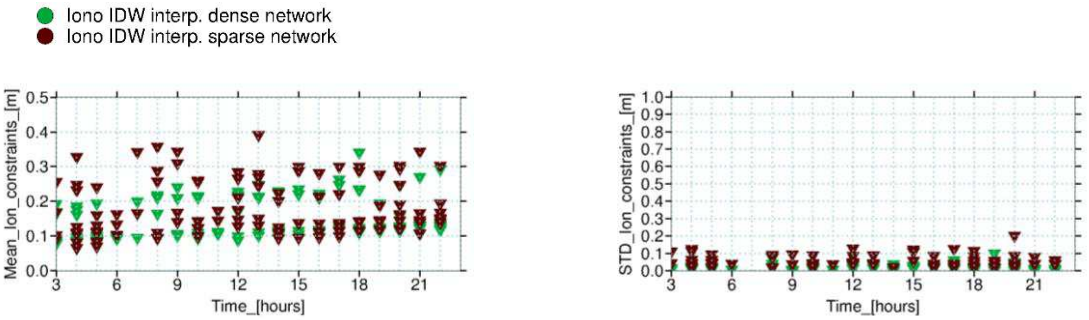

Figure 58 – Mean and standard deviations of constraints applied to ionospheric delays from SSR ionospheric corrections.

Results plotted in Figure 58 show that the mean of constraints provided with ionospheric delays is between 0.08 m and 0.40 m. Standard deviations are between 0.07 m and 0.22 m. Corrections derived from dense network have constraints slightly stronger than those derived from sparse network. These constraints can represent the precision of ionospheric corrections verified in section 14.3.2. It is important to keep in mind that some satellites will receive ionospheric delays with constraints stronger than others, according to their precisions. This is possible, thanks to modifications realized in PPP-Wizard 1.3, otherwise fixed values would have to be established which would hardly represent the precision of ionospheric corrections and its variation over time.

14.4. User side: positioning performances

Once atmospheric corrections are assessed, their use at the user positioning is analyzed as well. First, in section 14.4.1, this study focuses on stations for which changes in topology between dense and sparse network are significant. All parameters involved for typical cold-starts are visualized and briefly discussed. Further, results considering all the simulated rovers stations are assessed statistically for positioning and ambiguity fixing rate, respectively, in sections 14.4.2 and 14.4.3.

14.4.1. Individual processing results

The location of two simulated user stations, STBR and CORZ, and their nearest Reference Stations used to generate atmospheric corrections are presented in Figure 59, for

dense and sparse configurations. Rover is marked with a star and reference stations used to generate SSR corrections are highlighted with triangles. Rover is marked with a star and Reference Stations are highlighted with triangles. Remaining Rovers and Reference Stations are also represented by orange and green circles, respectively.

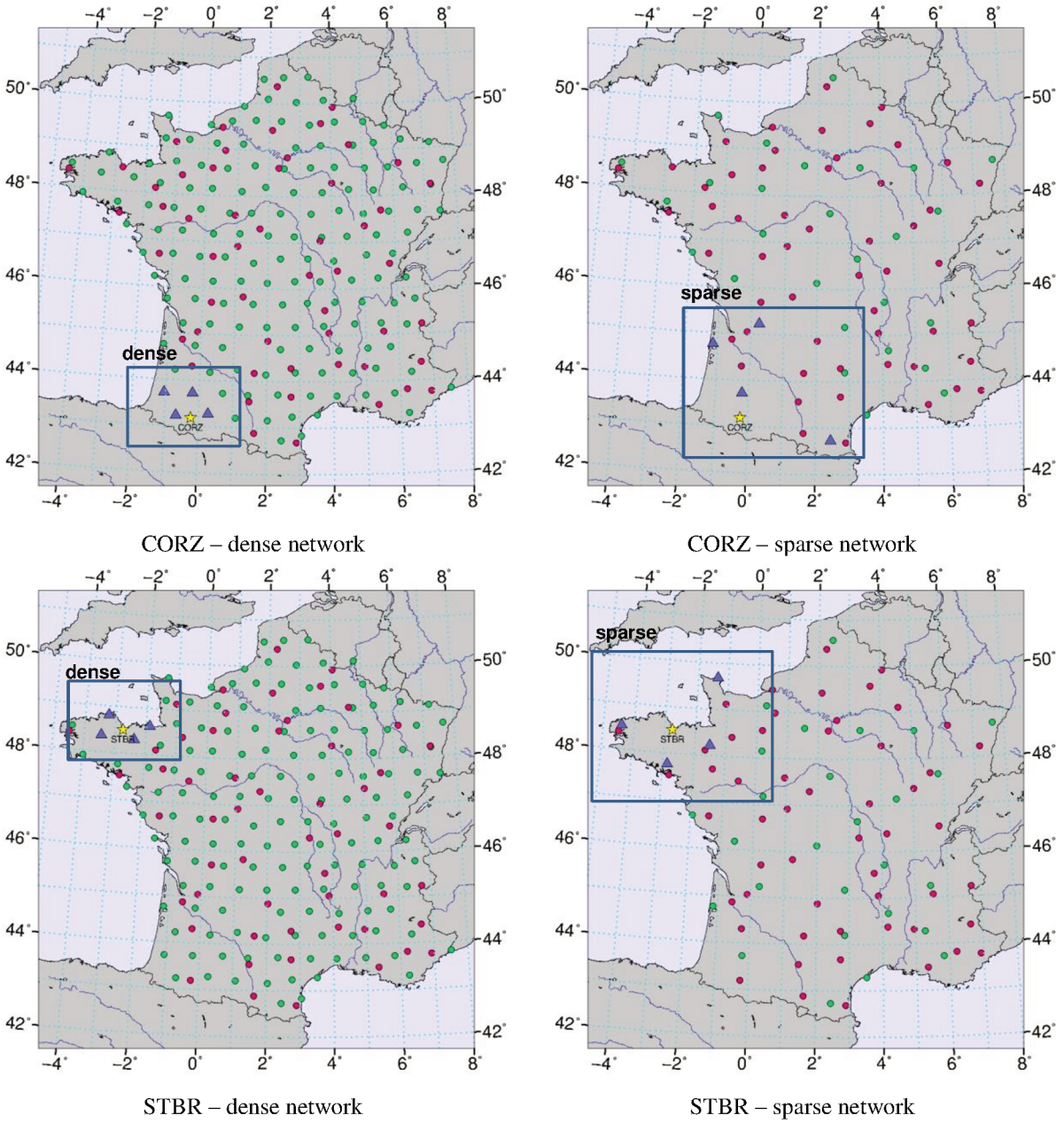

CORZ – dense network

CORZ – sparse network

STBR – dense network

STBR – sparse network

Figure 59 - Topology of Reference Stations (left: dense network; right: sparse network) used to process atmospheric delays at Rover Stations STBR (bottom) and CORZ (top).

14.4.1.1. Positioning

Figure 60 shows positioning errors with respect to reference coordinates (ITRF2008) on East, North, and Up components respectively. Such results are obtained after a cold start at 13 h on day 174/2015, for the stations STBR and CORZ, without atmospheric corrections (Standard RT-IPPP) and with atmospheric SSR corrections (PPP-RTK methods). These corrections are computed with dense and sparse networks respectively. Results obtained with atmospheric delays previously estimated thanks to standard RT-IPPP processing and re-injected are also included.

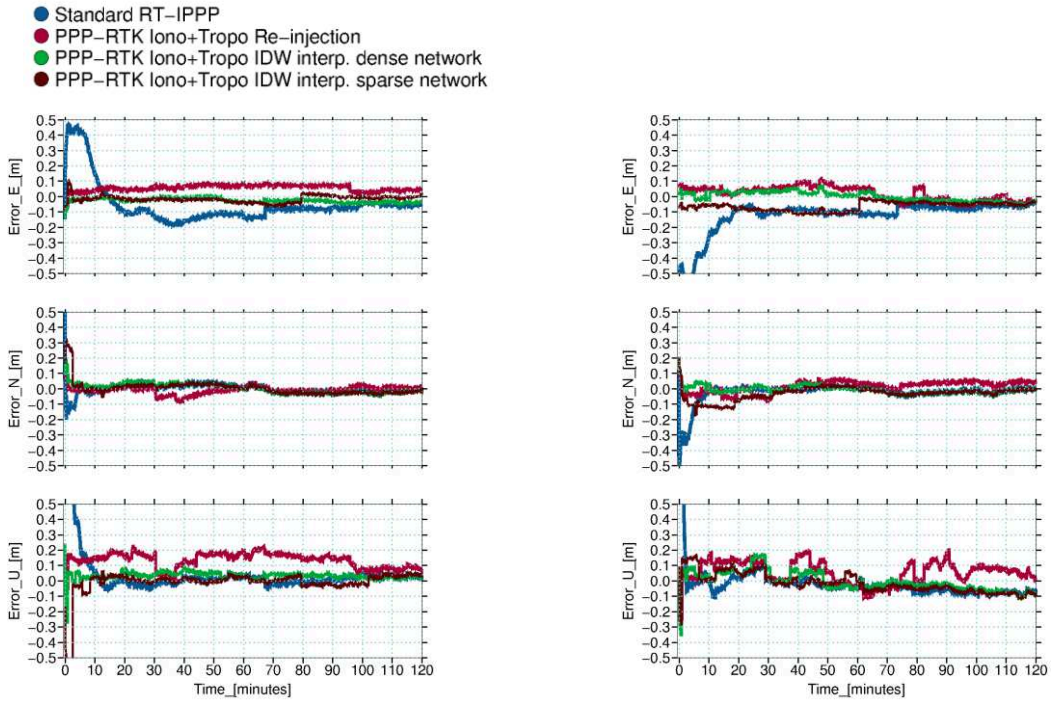

Station STBR Station CORZ

Figure 60 – Positioning errors on East (up), North (middle), and Up (bottom) components, after cold start on day 174/2015 at STBR and CORZ stations without atmospheric corrections (Standard RT-IPPP), with atmospheric delays re-injected, and with atmospheric SSR corrections (PPP-RTK methods).

Results in Figure 60 show a faster convergence of methods using atmospheric corrections, in comparison to Standard RT-IPPP. The reference method, Re-injection, presents the best performances. Centimeter-level accuracy for horizontal positioning is achieved during first epochs. On the other hand, the Up component converges slowly and its errors remain quite significant, compared to horizontal ones.

Formal post-fit standard deviations are presented in Figure 61. Such information has substantial interest to assess positioning quality when user computes its own positions without any precise a priori information.

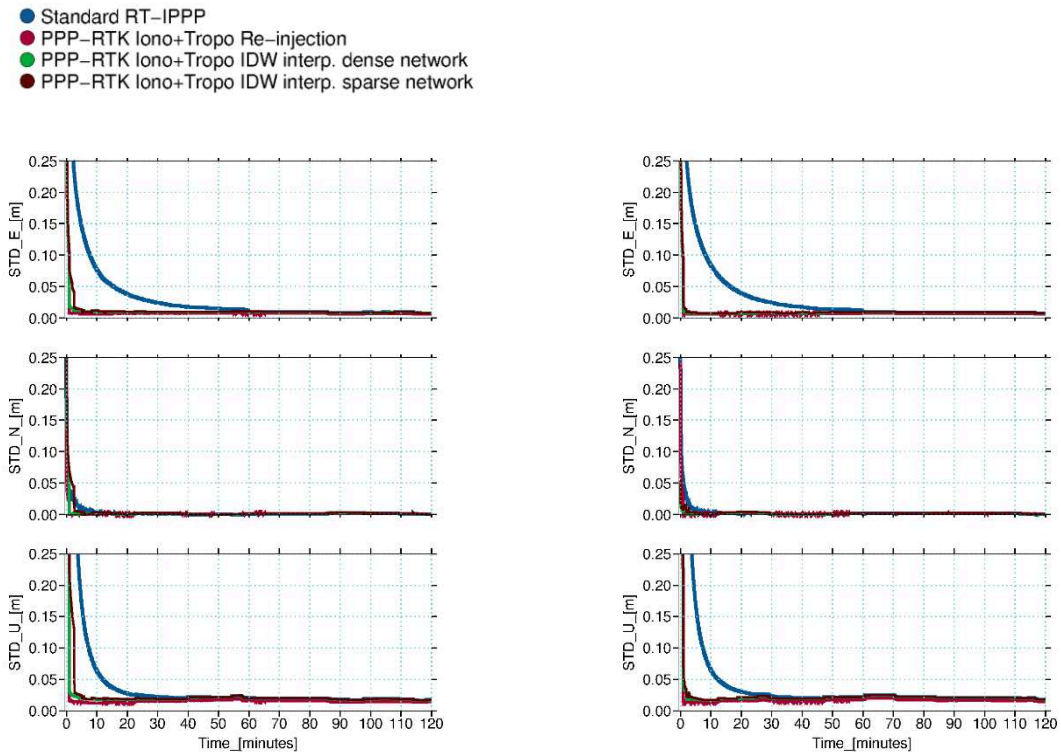

Station STBR Station CORZ

Figure 61 - Formal post-fit standard deviations of positions of stations STBR (left) and CORZ (right) without atmospheric corrections (Standard RT-IPPP) and with atmospheric SSR corrections (PPP-RTK solutions) at 13 h of day 174/2016.

Quality of positioning based on post-fit standard deviation presents comparable performances with those observed in positioning errors of Figure 60. PPP-RTK solutions converge instantaneously thanks to external information provided with atmospheric corrections.

14.4.1.2. Ambiguity fixing

Figure 62 presents the number of WL and NL ambiguities fixed to integer values during the processing of STBR and CORZ data. Ambiguity fixing for RT-IPPP starts after 60 min. This time is reduced to 1 min for other methods. Ambiguity fixing is only done on GPS phase measurements. A significant rate of fixed WL ambiguities is achieved with all methods.

NL ambiguities are harder to fix due to their small wavelength and Re-injection method presents a better rate of fixed NL most of the time. Variations of the number of fixed ambiguities is important, especially for NL ambiguities because PPP-Wizard 1.3 fix a new set of ambiguities every epoch to avoid staying a long time with a bad fixed solution. So, an ambiguity can be fixed to integer at an epoch but not at the following.

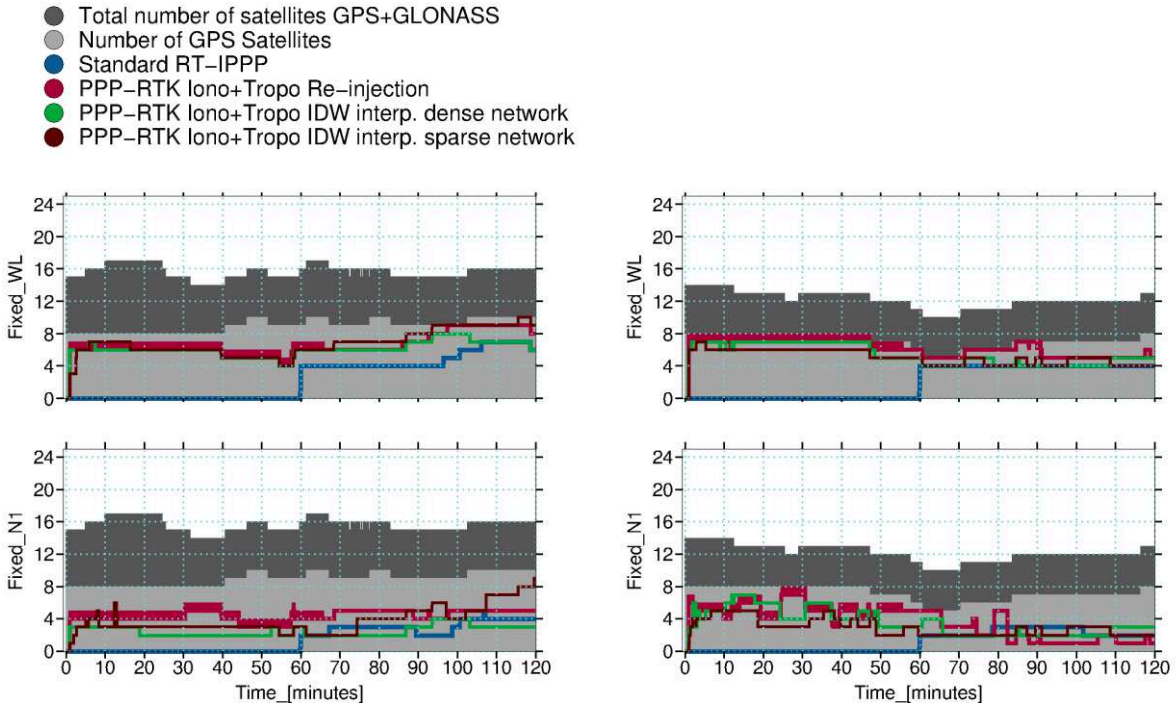

Station STBR Sation CORZ

Figure 62 – Number of integer WL and NL (N_1) ambiguities fixed to integer values, after cold start on day 174/2015 at stations STBR (left) and CORZ (right) without atmospheric corrections (Standard RT-IPPP) and with atmospheric SSR corrections (PPP-RTK methods).

WL ambiguities and their corresponding post-fit standard deviations are presented in Figure 63. In these figures, fixed ambiguities are plotted using darker colors. WL ambiguities have similar behavior for all the methods and no bias is observed. Regarding corresponding post-fit standard deviations, excepting two satellites, float ambiguities of Standard RT-IPPP present higher values in comparison to other methods. Besides, it of interest to mention that ambiguities fixed to integers have their variations set to zero, therefore post-fit standard deviations for integer ambiguities cannot be observed.

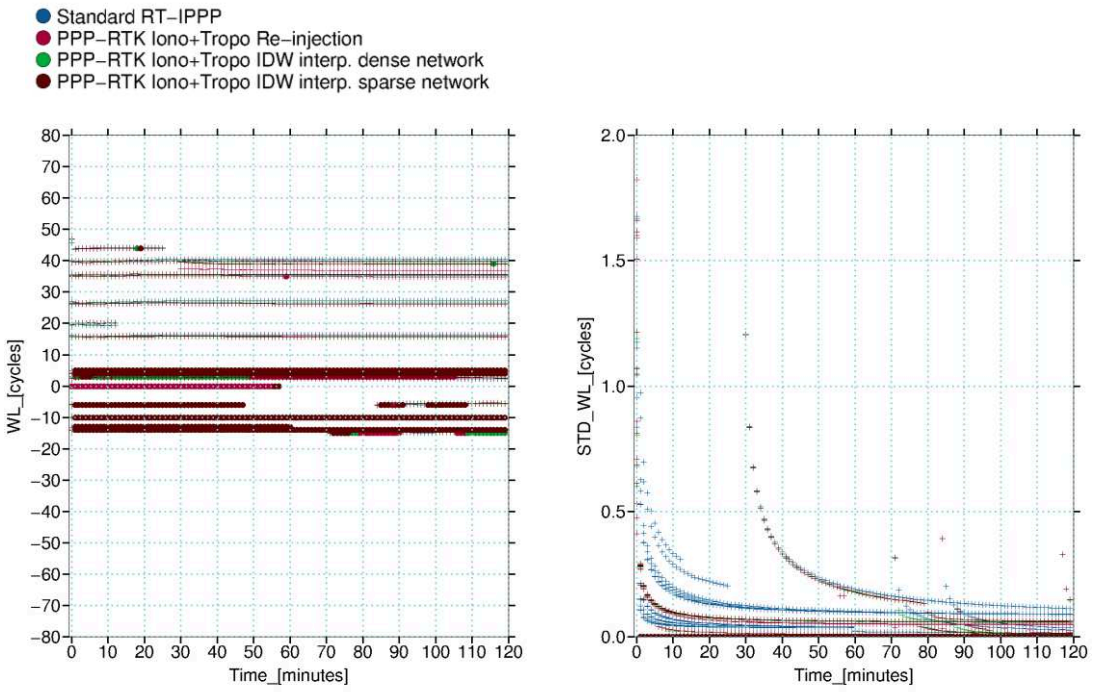

CORZ-WL ambiguities

CORZ-WL ambiguities post-fit standard deviations

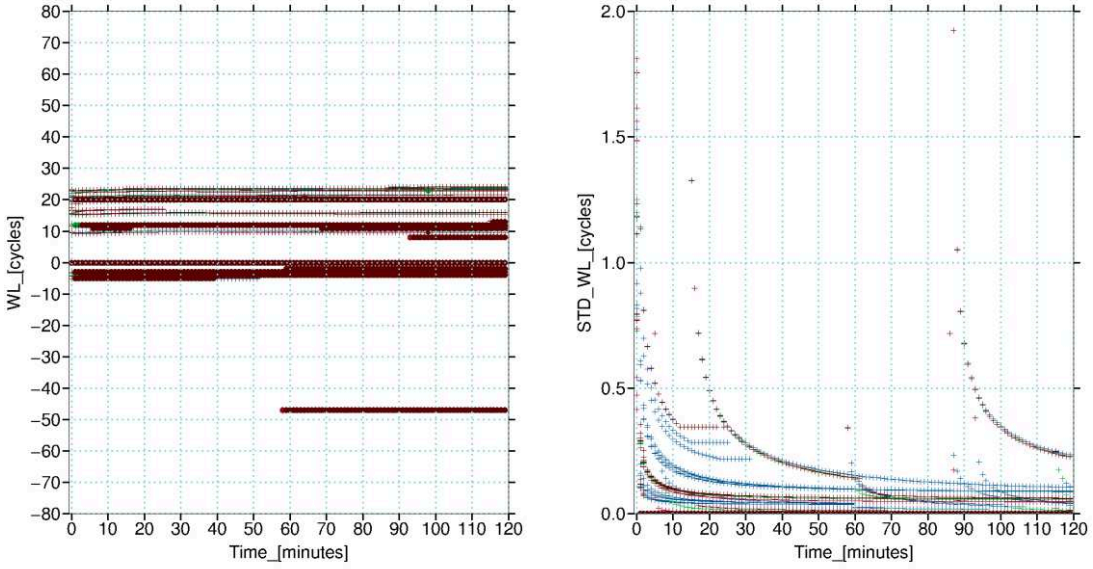

STBR-WL ambiguities

STBR-WL ambiguities post-fit standard deviations

Figure 63 - WL ambiguities estimates of STBR (bottom) and CORZ (top) stations on day 174/2015.

In Figure 64, NL ambiguities and corresponding post-fit standard deviations are presented. In this figure, again float ambiguities of RT-IPPP methods present the highest post-fit standard deviations, even after ambiguity fixing at 60 min. It is also possible to see the slower convergence of the ambiguities estimated with RT-IPPP with respect to all other methods.

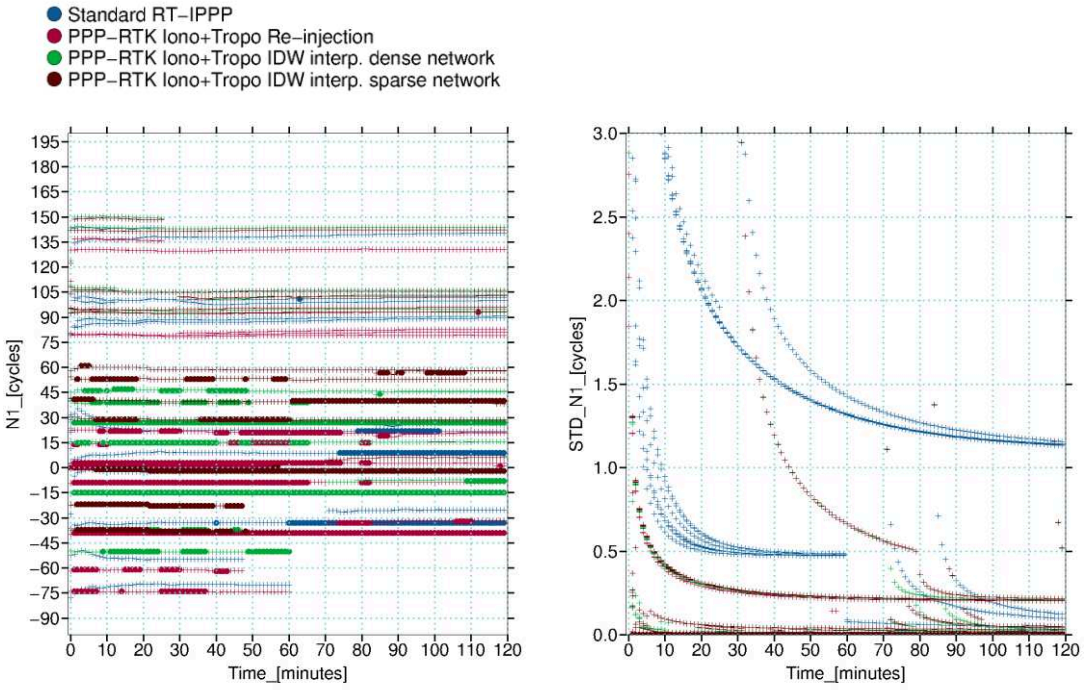

CORZ-Estimated N_1 ambiguities

CORZ-N_1 ambiguities post-fit standard deviations

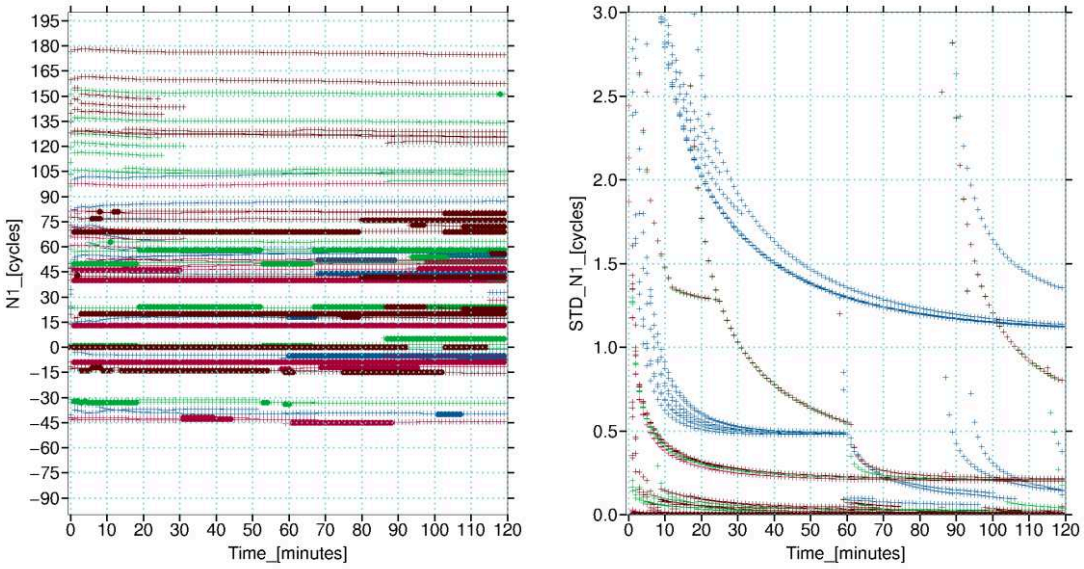

STBR-Estimated N_1 ambiguities

STBR-N_1 ambiguities post-fit standard deviations

Figure 64 - NL (N_1) ambiguities estimates of STBR (bottom) and CORZ (top) stations on day 174/2015.

NL ambiguities differ significantly between the method using external atmospheric corrections, and those estimated with atmospheric delays coming from Standard RT-IPPP. The two latter, Re-injection and Standard RT-IPPP, agree more between them with small differences of one or two cycles. Such differences, with respect to ambiguities estimated with external atmospheric corrections, indicate that estimated NL can also absorb part of the ionospheric biases. More detailed investigations about the biases influences on NL

ambiguities must be realized in future works. Even though receiver clock offset absorbs most part of them (section 14.3) and NL ambiguities are still fixed, with solution able to provide accurate positions, as verified in results of Figure 60.

14.4.1.3. Receiver clock offsets

Figure 65 shows GPS receiver clock offsets, as well as their post-fit standard deviations. Receiver clock offsets estimated with Re-injection and Standard RT-IPPP present very similar values. GPS receiver clock offsets of PPP-RTK methods converge quickly as that from re-injection method. Although, for station CORZ they are different of about ~3 m (dense) and ~5 m (sparse) with respect to Standard RT-IPPP or Re-injection. For station STBR these values correspond to ~1 m with dense network and ~4 m with sparse.

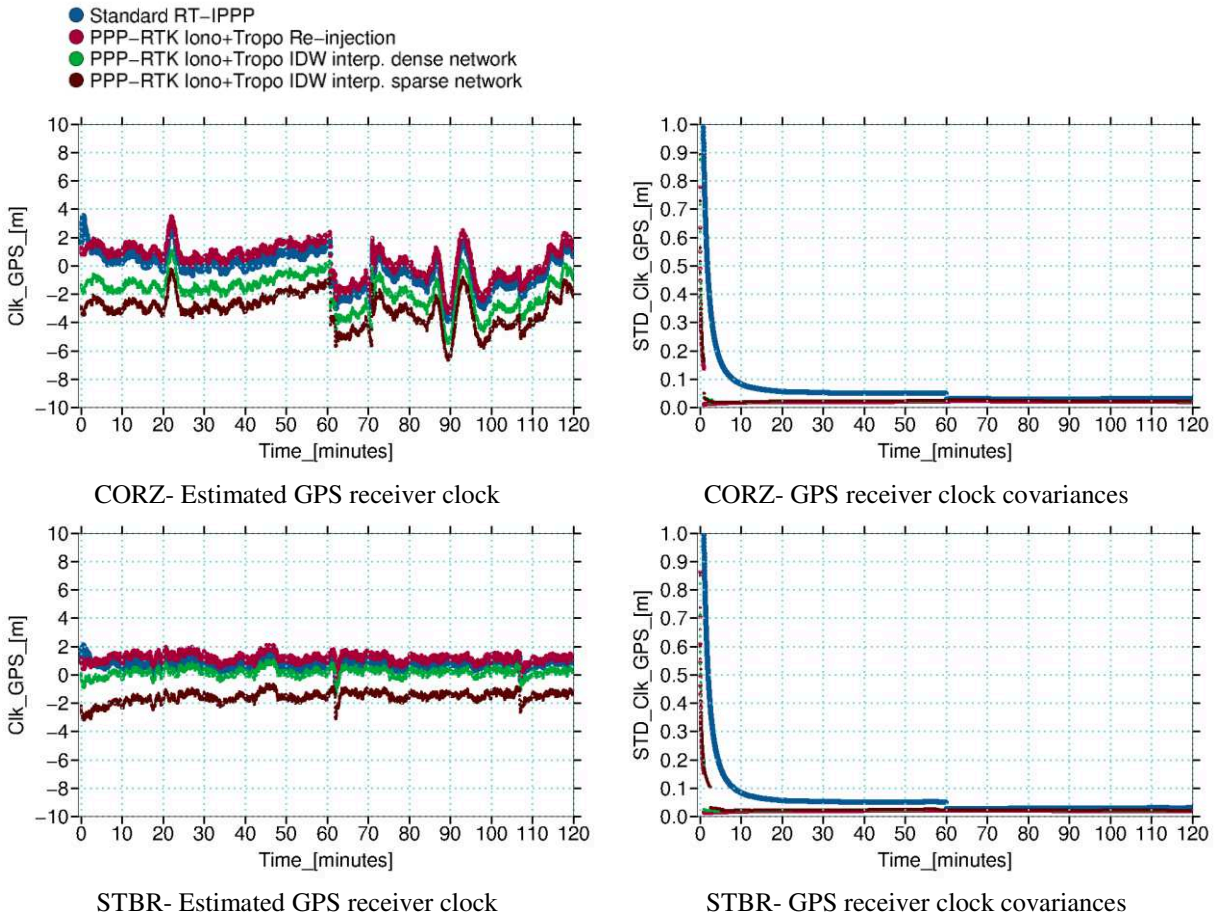

CORZ- Estimated GPS receiver clock

CORZ- GPS receiver clock covariances

STBR- Estimated GPS receiver clock

STBR- GPS receiver clock covariances

Figure 65 – GPS receiver clock offsets (left) and their standard deviations (right) of stations STBR (bottom) and CORZ (top), 13 h at day 174/2015.

As discussed in section 14.3, such discrepancies are caused by biases present in ionospheric corrections. These biases are different for dense and sparse network solutions because reference stations employed are not the same. Therefore, receiver hardware biases affecting ionospheric corrections are different, leading to different biases in ionospheric corrections from dense or sparse network solution.

Estimated GLONASS receiver clock offsets are not shown, however they presented similar behavior as those from GPS, except for the gains in precision convergence promoted by ambiguity fixing.

In PPP-Wizard 1.3, receiver clock offsets for GPS and GLONASS are estimated as the sum: $h_{r_{P_1}} = (cdt_r + b_{r_{P_1}})$ (section 6.2.3). Remaining hardware code and phase biases (b_{P2}, $b_{L_1}$and b_{L_2}) are estimated in separated parameters of PPP-Wizard 1.3 filter. Their estimates over the time are presented next section.

14.4.1.4. Receiver hardware biases

In Figure 66 are illustrated the GPS receiver hardware biases, b_{P_2}, $b_{L_1}$and b_{L_2} estimated in processing sessions in study of stations CORZ and STBR. Considering same reasons as for receiver clocks, the receiver estimated uncombined biases for GLONASS are not illustrated.

Phase biases, $b_{L_1}$and b_{L_2}, present small values in comparison to estimated biases in GPS receiver clock offset (Figure 65). Differences among all methods are observed. At station CORZ, estimated biases with Re-injection method are those with closest values to Standard RT-IPPP ones. Indeed, results using external atmospheric corrections (i.e. dense or sparse) are those that present higher differences, especially the sparse solution. On the other hand, this is not the case for all biases estimated at station STBR.

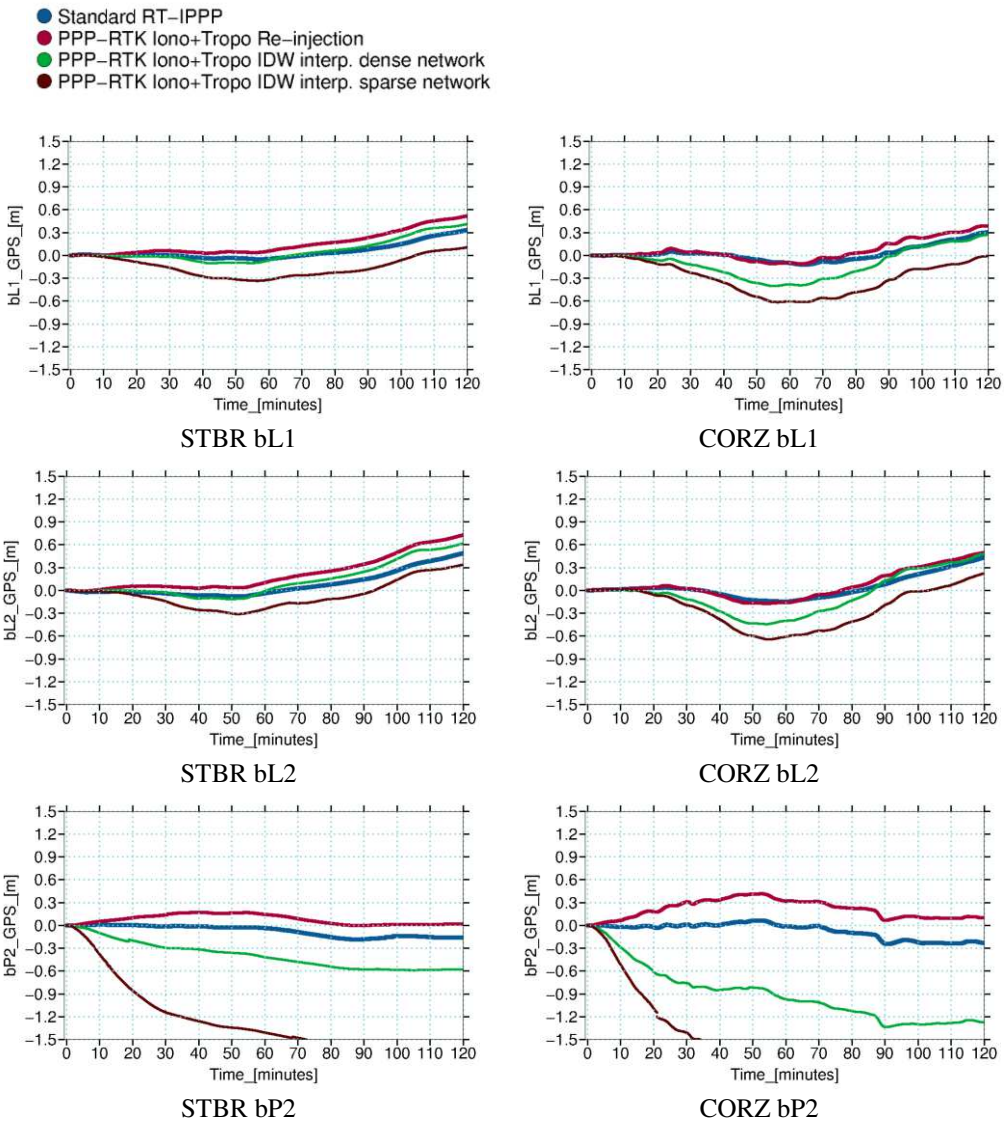

STBR bL1 | CORZ bL1

STBR bL2 | CORZ bL2

STBR bP2 | CORZ bP2

Figure 66 – Receiver hardware biases for GPS at stations STBR (left) and CORZ (right) on day 174/2015.

Hardware biases discrepancies among different methods (Figure 66), are probably related to those differences observed for ambiguities and receiver clock offset estimations. This statement includes the differences observed between estimated receiver hardware biases when using dense or sparse network corrections. Such differences are possibly provoked by receiver hardware biases present in ionospheric corrections (c.f. section 13.7), considering that not the same reference stations are used to generate the corrections of both methods (dense or sparse). The impact of this differences in estimated biases must to be further studied, especially with regard to positions estimation and performances of atmospheric corrections.

14.4.1.5. Ionospheric delays

SSR corrections for slant ionospheric delays are shown in Figure 67-top for all processing methods. The estimated ionospheric delays (Figure 67-middle) and corresponding post-fit standard deviations (Figure 67-bottom) are also illustrated. In these figures results for all GPS and GLONASS satellites are shown.

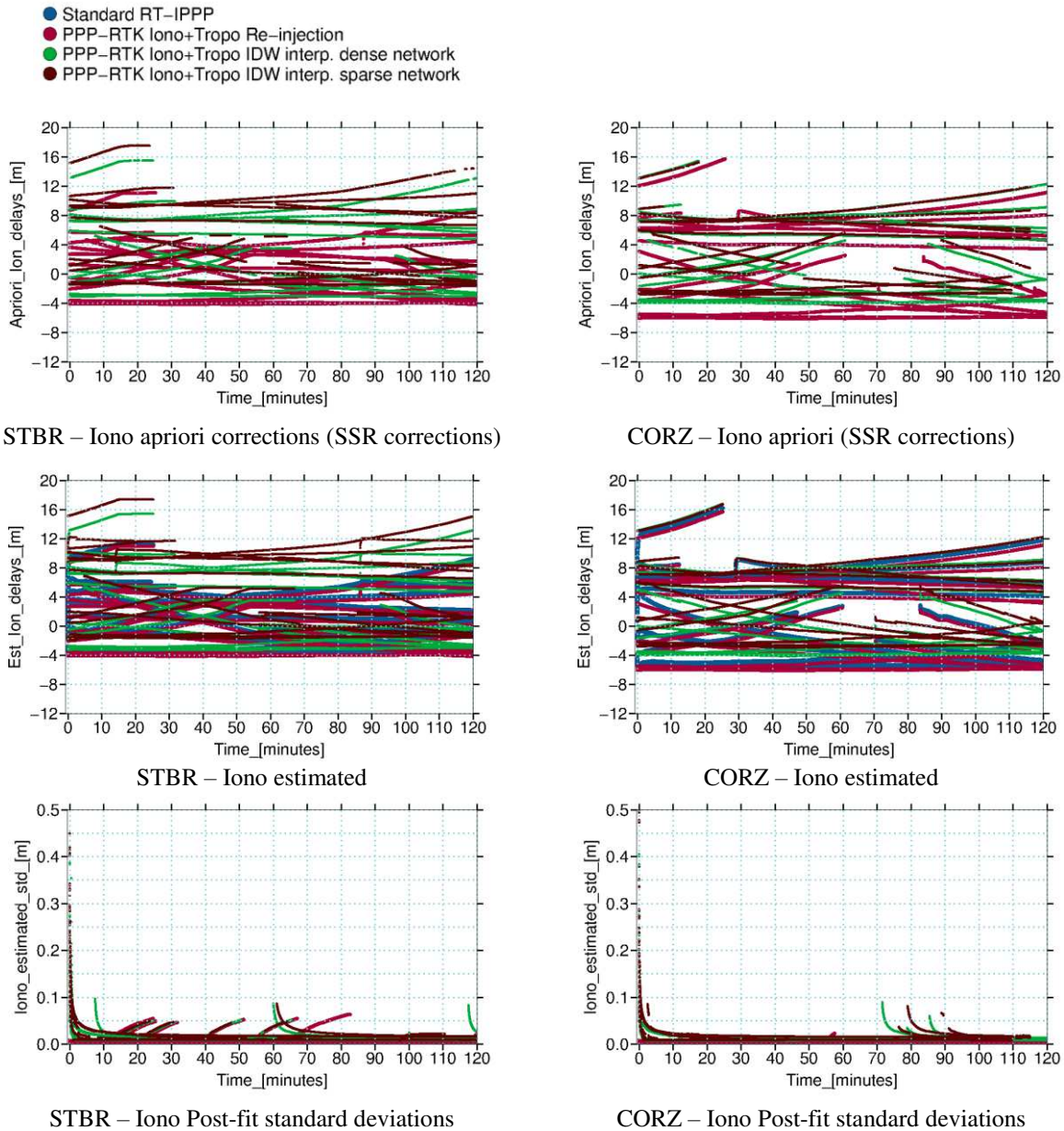

STBR – Iono apriori corrections (SSR corrections)

CORZ – Iono apriori (SSR corrections)

STBR – Iono estimated

CORZ – Iono estimated

STBR – Iono Post-fit standard deviations

CORZ – Iono Post-fit standard deviations

Figure 67 – SSR corrections for slant ionospheric delays (top), and estimated ionospheric delays (middle) with corresponding post-fit standard deviations, at stations STBR (left) and CORZ (right) on day 174/2015.

Differences (biases) between the different a priori corrections and the corresponding estimated ionospheric delays are stable. These differences correspond to those

extensively discussed in this chapter, which are provoked by receiver hardware biases at reference stations and are different for dense and sparse network. Post-fit standard deviations of estimated ionospheric delays are better than 10 cm most of time for all PPP-RTK methods.

14.4.1.6. Tropospheric delays

A priori corrections for tropospheric delays, as well as estimated values with post-fit standard deviations are plotted in Figure 68.

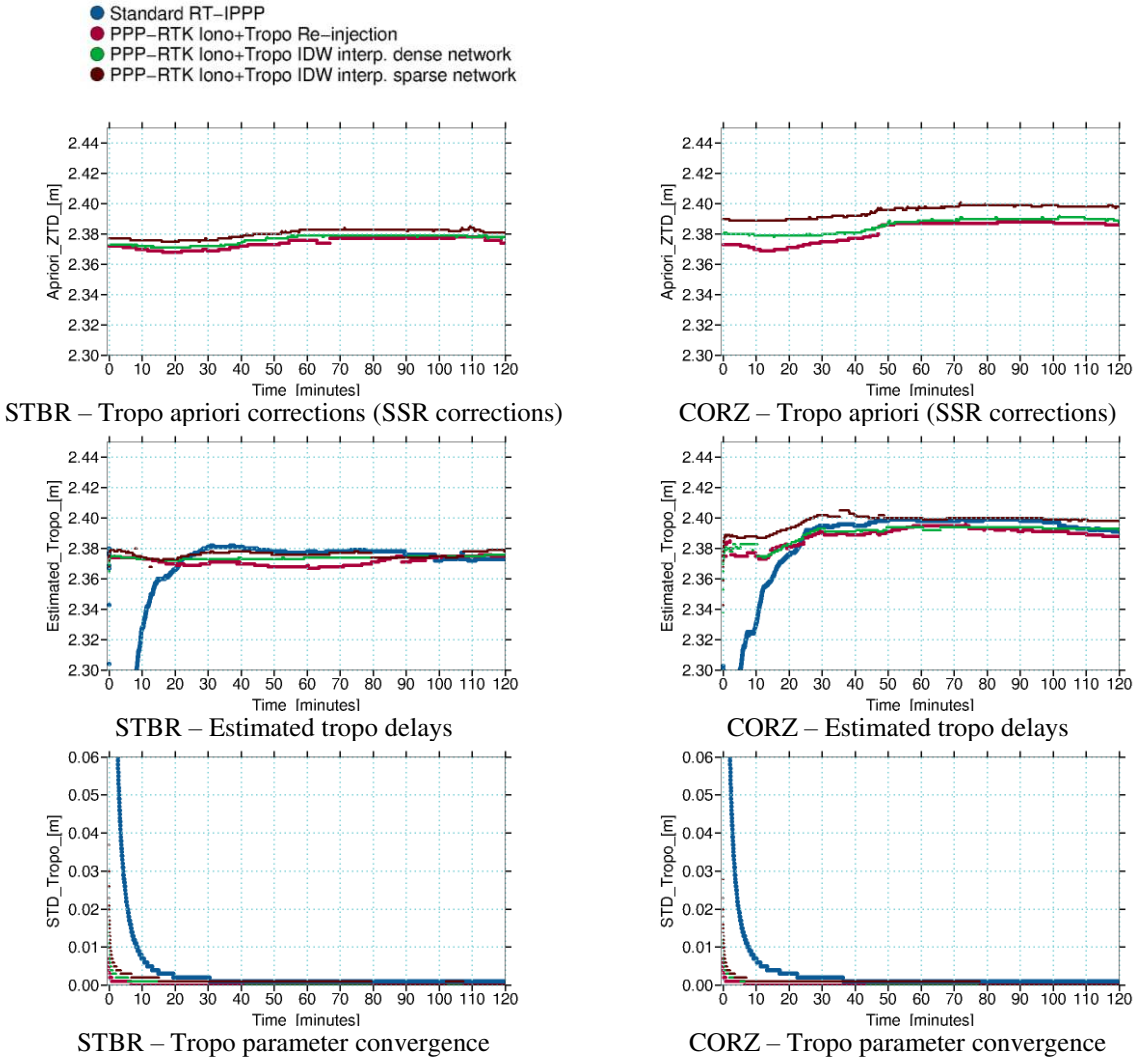

STBR – Tropo apriori corrections (SSR corrections)

CORZ – Tropo apriori (SSR corrections)

STBR – Estimated tropo delays

CORZ – Estimated tropo delays

STBR – Tropo parameter convergence

CORZ – Tropo parameter convergence

Figure 68 – Tropospheric delays estimated at stations STBR and CORZ on day 174/2015.

In Figure 68-top, external a priori tropospheric corrections of station STBR fit better to Re-injection tropospheric a priori corrections in comparison to those used in station CORZ, in particular for the sparse solution of STBR. This shows possible impacts of

topology used in sparse network of station STBR (Figure 59), which is better than that used for CORZ. However, all solutions using tropospheric corrections converge fast, while Standard RT-IPPP takes about 8 min to achieve repeatability better than 2 cm.

14.4.1.7. Positioning performances for all sessions

Results presented above illustrated results for a single cold-start at stations STBR and CORZ at 13 h on day 174/2015. Positioning results for these two stations considering all processing sessions on day 174/2015 are presented in Figure 69 and Figure 70.

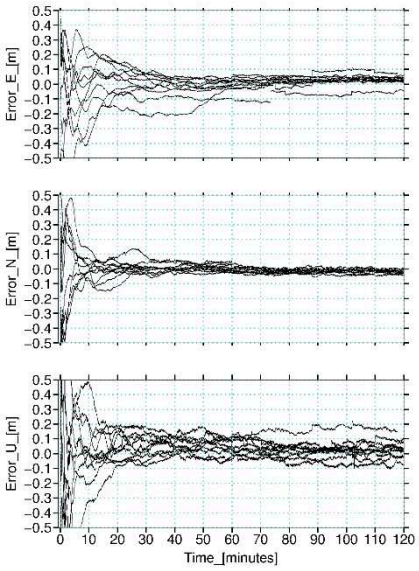

CORZ-Standard RT-IPPP

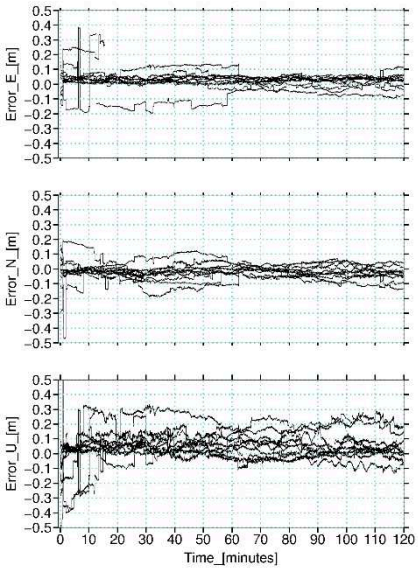

CORZ-Re-injection

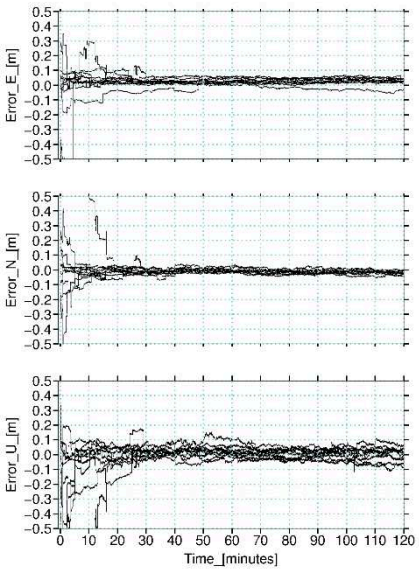

CORZ - PPP-RTK dense

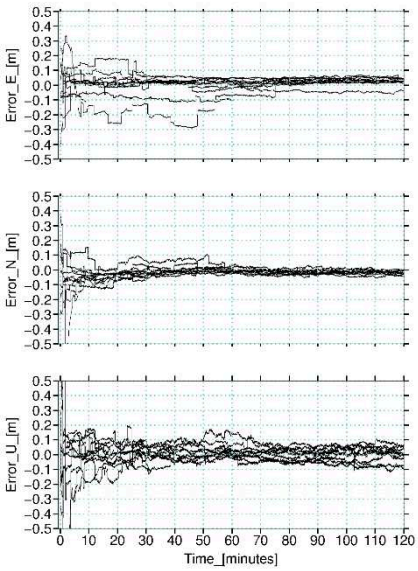

CORZ - PPP-RTK sparse

Figure 69 – Positioning errors of station CORZ from all cold-starts processed on day 174/2015.

In these results all four processing methods (Standard RT-IPPP, Re-injection, PPP-RTK with dense network, and PPP-RTK with sparse network) are illustrated. Positioning errors are shown for horizontal and vertical components. Solutions using atmospheric corrections presented a faster convergence in most of sessions. But in some cold-starts they took considerable time to convergence.

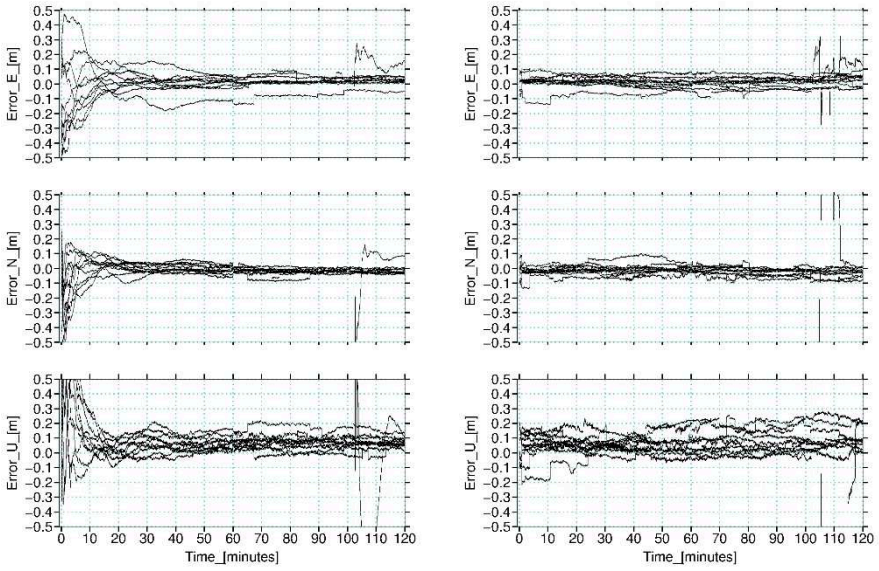

STBR-Standard RT-IPPP STBR- re-injection

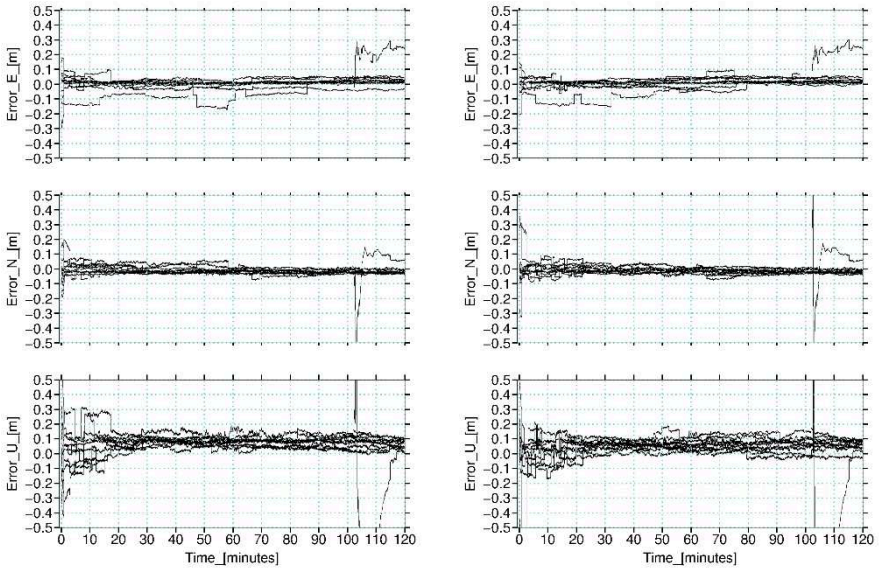

STBR-Iono+Tropo dense STBR-Iono+Tropo sparse

Figure 70 – Positioning errors of station STBR from all cold-starts processed on day 174/2015.

A data gap for a session of STBR station, induces a cold start after solution convergence, at 103 min, and affects the results of all processing methods, with or without ionospheric and tropospheric corrections. To get realistic statistics about positioning performances, a significant amount of data must be used to reduce significantly impacts of such event (data gaps/cycle-slips).

14.4.2. Impacts on positioning accuracy

Figure 71 presents medians and 68%-quantiles of absolute positioning errors calculated over the whole Rover Network. These statistics involve 60 stations during the 10 days of experiment with 10 cold-starts per day. Vertical bars in these figures indicate the time when positioning achieve an accuracy of 10 cm. Detailed results are listed in Table 22.

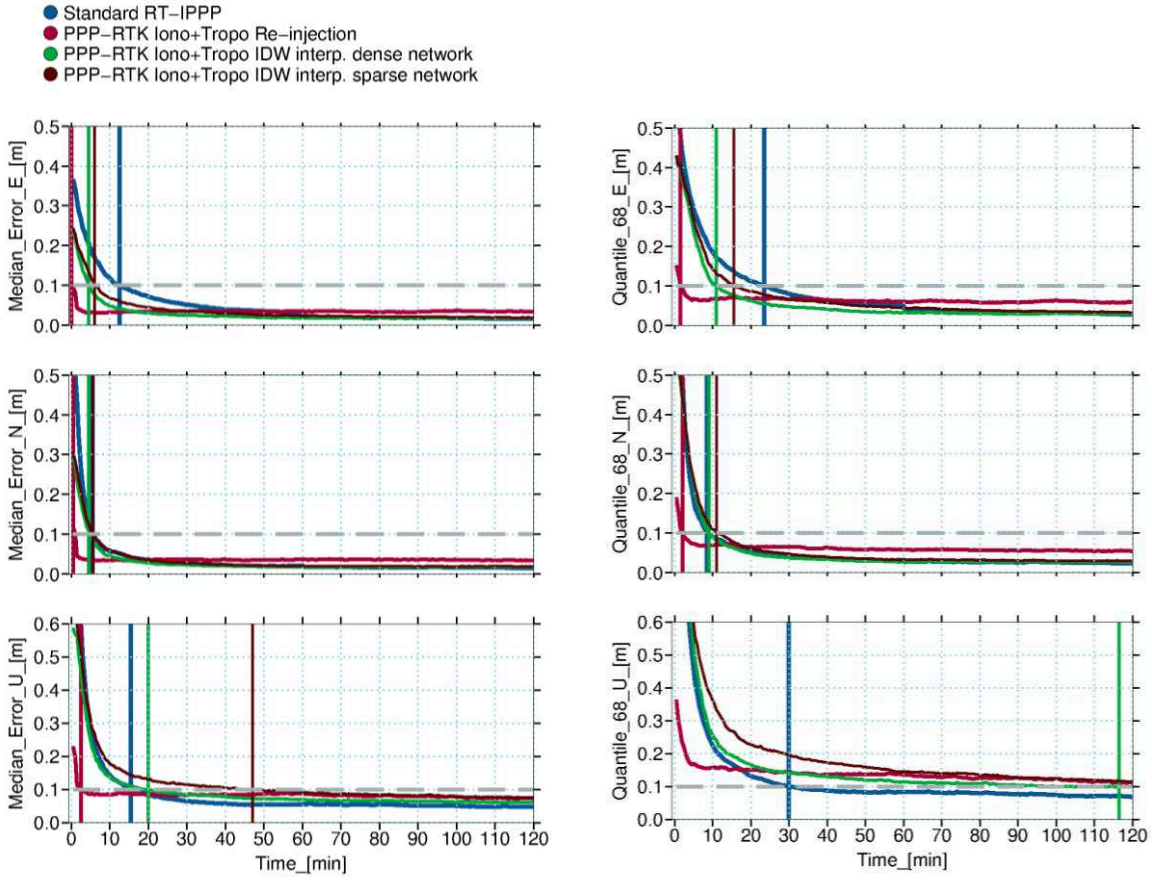

Figure 71 **-** Medians (left) and 68% quantiles (right) of PPP-RTK absolute positioning errors per epoch at simulated rover stations; statistics involve all 60 Rover Stations, during the 10 days of experiment with 10 cold-starts per day.

Median of absolute positioning errors using atmospheric corrections, dense and sparse, presents convergence to 10 cm accuracy on the East component of 6 min and 4 min, respectively. On North component these values are 4.5 min and 5 min. Such numbers represent gains in horizontal convergence time of 58% with dense and 43% sparse network solutions, in comparison to Standard RT-IPPP solution. For the reference method (Re-injection) this gain is around 95%. Only Re-injection method promoted gains in Up positioning (87%). PPP-RTK using external atmospheric corrections has degradation in Up, especially for the sparse solution.

Concerning 68%-quantiles, East and North components take 24 min and 8.5 min to achieve 10 cm convergence without atmospheric corrections (Standard RT-IPPP). When using dense network corrections, East and North converge within 10.5 min and 9 min. This characterizes a horizontal positioning 47% better than Standard RT-IPPP. With the sparse network, such horizontal positioning gain in 68%-quantiles convergence is equivalent 24%, since East and North components take 16 min and 11 min to converge. Re-injection performs a gain of 85%, showing the performances that a perfect modeling could reach. Once again, degradation is verified for the Up component, and even the Re-injection solution does not really achieve 10 cm accuracy.

Table 22 - Convergence times of PPP-RTK positioning errors (GPS+GLONASS).

Method	Median Convergence time [min]			68%-quantiles Convergence time [min]		
	E	N	U	E	N	U
Standard RT-IPPP	13.5	5.0	16.5	24.0	8.5	30.0
PPP-RTK Re-injection	0.5	0.5	2.0	2.0	3.0	No conv.
PPP-RTK Dense network	4.0	4.5	19.5	10.5	9.0	117.0
PPP-RTK Sparse network	6.0	5.5	47.0	16.0	11.0	No conv.

PPP-RTK with Re-injection performs better than all solutions, which justifies the use of this method as reference. However, in the end of 68%-quantiles convergence (120 min) its horizontal errors (East, North) remain a few centimeters higher than other solutions. A possible reason is that even if Re-injection atmospheric corrections are estimated at the station itself, they can have a range of different precisions larger than the 3 levels of accuracies defined in PPP-Wizard 1.3 (section 13.6). More investigations with Re-injection using the strategy of constraints applied for external atmospheric corrections are necessary to verify this.

The degradations found in Up convergence, when using atmospheric corrections, also must be further studied. There are two different points to consider: 1) the possible errors in IDW interpolation algorithm, since dense network provides better results than the sparse one; and 2) influence of receiver hardware biases present in ionospheric corrections. However, the improvements in horizontal positioning, when using the external SSR atmospheric corrections from dense or sparse network are promising.

14.4.3. Impacts on ambiguity fixing rate

The number of fixed ambiguities with each assessed method is also analyzed. Figure 72 presents statistics in terms of mean and standard deviation of the number of WL and NL ambiguities fixed at the rover stations.

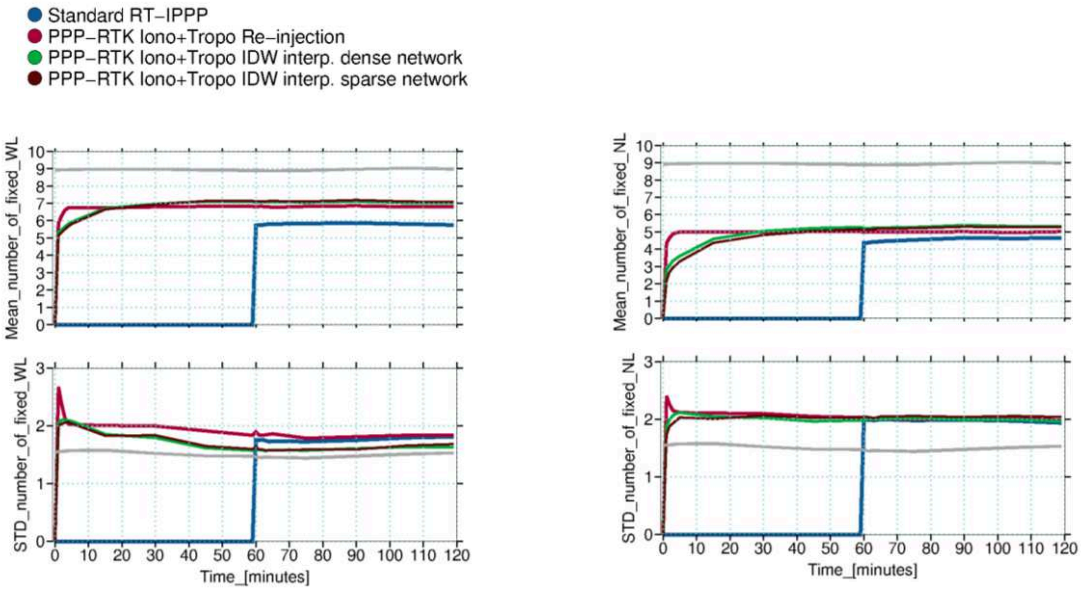

Figure 72 –Mean (top) and standard deviation (bottom) of the number of WL (left) and NL (right) ambiguities fixed to integer values; grey line is the number of GPS satellites available.

In Figure 72, results show that re-injection solution achieves a mean of about 7 WL (77%) and 5 NL (54%) fixed within 3 min. Methods using atmospheric corrections take 12 min to achieve same performances. Such results are quite consistent with the time taken by these methods to achieve the accuracy of 10 cm (Figure 71). A positive aspect is that with PPP-RTK more ambiguities are fixed than with RT-IPPP, and this number is stable since all methods present similar standard deviations on the number of fixed ambiguities.

15. Summary of Part III

In Part III, the results and discussions have encountered the generation of tropospheric and ionospheric corrections with an algorithm compatible with the RTCM standard ionospheric and tropospheric SSR corrections. A strategy to generate such by-products using Orphéon stations has been assessed, presuming that atmospheric corrections can shorten the convergence time of rover positions when provided with good quality.

The PPP-Wizard 1.3 package is employed to estimate ionospheric and tropospheric delays using GNSS data from Orphéon stations at the server side. The estimated atmospheric delays are used as input for IDW interpolation algorithm to generate corrections. The ionospheric delays are especially complicated to deal with, given that they are biased by receiver clock offsets. This problem is presented and discussed. However, changes in estimated NL ambiguities and receiver hardware biases have been observed as well and the subject deserves careful attention in order to better understand the consequences for the user, provoked by hardware biases affecting ionospheric delays.

Once ionospheric and tropospheric corrections are generated, they are introduced as a priori information not only for the first epoch (like in Part II), but for every new epoch and used as constrained parameter in PPP-Wizard engine. PPP-Wizard is modified to allow more flexibility in the application of constraints for atmospheric corrections. Such modifications made possible to introduce more realistic values to constrain atmospheric corrections.

The topology of the network with dense and sparse configuration to generate atmospheric corrections is assessed. Standard RT-IPPP takes ~25 min to achieve 10 cm horizontal accuracy, this time is improved 46% (~14 min) with dense and 24% (~19 min) with sparse network. Although, vertical positioning has its convergence slow especially when using corrections from sparse network solution. Degradations provoked in Up convergence, must be further studied, considering the mitigation of receiver hardware biases present in ionospheric corrections, and more developments in implemented interpolation/modeling algorithms, especially for ionospheric delays. Another possible explanation for the Up convergence degradation observed in experiments of Part III is the way that corrections and

constraints to atmospheric parameters are applied (a new correction every epoch) which is different from that used in Part II (a new correction for every cold start), where such problem did not occurred. However, the improvements in PPP-Wizard 1.3 horizontal positioning with external SSR atmospheric corrections from dense or sparse network are promising and can be useful for applications that depend on horizontal positioning.

CONCLUSIONS AND PROSPECTS

16. Conclusions

The feasibility of a real-time positioning service based on PPP and SSR modeling was investigated. A bibliographic revision about the main aspects involved in this thematic was carried out (Part I). Such review focused in GNSS positioning and ambiguity fixing, as well as the influences of atmospheric effects on GNSS signals. Methods and outcomes were presented in two stages which used different solutions. First stage (Part II) concentrates efforts on tropospheric corrections. In the second one (Part III), tropospheric and ionospheric corrections are used.

In Part II, a modified version of RTKLib 2.4.3 (beta) package is used to take into account network tropospheric corrections. First-order ionospheric effects were eliminated by the iono-free combination and ZTDs are estimated. Thus, tropospheric corrections were used as constrained a priori values to improve RT-PPP, by this way performing the so-called Float PPP-RTK. Concerning the generation of tropospheric corrections, an adaptive modeling based on optimal fitting coefficients (OFC) was implemented to describe the troposphere delays behavior over France. For that, tropospheric delays estimates at Orphéon stations are used to feed the modeling. This solution was adopted because it allows mono-directional communication link between server and user sides. In comparison with previous works (Shi et al., 2014), our study is done on a larger area that requires one to go further by using the second order degree of their mathematical model, what has not been presented before.

The performances between network topology and positioning quality are discussed. Regarding this aspect, it is assessed the use of different configurations of a dense and regular GNSS network existing in France, the Orphéon network. This network has about 160 sites and it is owned by Geodata-Diffusion, subsidiary of the group Hexagon Geosystems and directly involved in this project.

To assess tropospheric corrections, 20 days distributed in four main periods along the year 2014 are selected. These periods were chosen according to the seasons and the annual temperature variations in France as published by Météo-France. As an independent external reference, the IGN ZTD products are used to assess tropospheric ZWD modeled by OFCs. The modeled ZWDs present an accuracy of around 1.3 cm with respect to IGN ZTDs. In

addition, a good consistency between the RMS of residuals and the differences with respect to the IGN products is found.

Improvements of convergence time when using tropospheric corrections for float PPP-RTK are quantified. In terms of 68%-quantiles, gains on convergence time are 1% on East, about 20% on North, and about 5% on Up components when using GPS only. Introducing GLONASS data shortens by about 50% the convergence time of all components. However, adding tropospheric corrections when processing GPS+GLONASS data only improves horizontal positioning by about 2% on East and about 6% on North components but Up is improved by about 12%. The reduction in the number of reference stations by using a sparser network configuration does not degrade the generated tropospheric corrections derived from OFCs, and similar performances are achieved between the two configurations.

In second step (Part III) PPP-RTK is performed thanks to the CNES PPP-Wizard 1.3 package and CNES orbit, clock and phase biases products. Uncombined processing is realized and slant ionospheric effects are estimated simultaneously with positioning. Therefore, the modeling of ionospheric effects is now applicable too. Thus, ionospheric and tropospheric corrections are introduced as constrained a priori parameters at user side. In order to deliver corrections compatible with the RTCM standards for SSR parameters, a standard Inverse Distance Interpolation (IDW) algorithm is chosen.

Ionospheric delays were especially complicated to deal with, given that they are affected by hardware biases. This challenge was widely discussed and results showing that biases in ionospheric corrections are highly correlated with receiver clock offsets were found. However, substantial changes in estimated NL ambiguities and receiver hardware biases have been observed as well and the subject deserves careful attention in order to better understand the consequences for the user, provoked by hardware biases affecting ionospheric delays.

Once ionospheric and tropospheric corrections are generated, they were introduced as a priori information and constrained at the user side. PPP-Wizard 1.3 was improved to allow more flexibility in the application of constraints for atmospheric corrections. Such modifications made possible to introduce more realistic values to constrain atmospheric corrections and to consider their quality variation in time.

The topology of the network with dense and sparse configuration used to generate atmospheric corrections is assessed again. Standard RT-IPPP takes ~25 min to achieve 10 cm horizontal accuracy, this time is improved 46% (~14 min) with dense and 24% (~19 min) with sparse network. Although, vertical positioning has its convergence time increased, especially when using corrections from sparse network solution. However, the improvements in PPP-Wizard 1.3 horizontal positioning with external SSR atmospheric corrections from dense or sparse network are promising and can be useful for applications that depend mainly on horizontal positioning.

Finally, a key point to be learned from this thesis, is whether estimating troposphere and ionosphere delays along with the estimation of the other parameters and on whether the information from the regional network can be used as constraint at the beginning of the estimation (cold-start) as realized in Part II, or as constraint throughout the estimation (e.g. every epoch) like in Part III. This is an important aspect that could lead to the differences between achievements found in these two parts, especially for Up component, nevertheless more experiments are required to infer about the best alternative.

17. Prospects

Some points evoked along this report, are highlighted in this section to provide directions for next works.

Concerning the tropospheric modeling, it must be considered more recent empirical models, such as GPT2w (Böhm et al., 2015; Kalita and Rzepecka, 2017) as well as NWP models (Böhm et al., 2011; Urquhart and Santos, 2011). The combination of these solutions with tropospheric corrections from GNSS networks, like those implemented in this thesis can improve substantially the quality of SSR corrections.

Regarding ionospheric corrections, one major challenge remains the strategy for dealing with receiver hardware biases to model delays at a network scale. Degradations found in Up convergence must be further studied, considering the mitigation of receiver hardware biases present in ionospheric corrections, and more developments in implemented interpolation/modeling algorithms. Additionally, limitations of ionospheric mapping functions must be considered as well, and the use of ionospheric mapping functions based on the electron density field derived from IRI can be an interesting alternative (Zus et al., 2017).

Improvements on quality control strategy used for selection of ionospheric and tropospheric delays employed for IDW algorithm (Part III) should be improved to allow fixing or strongly constrain coordinates at reference stations. This may provide fast convergence of such atmospheric parameters at the network side and increase their quality.

The application of constraints to atmospheric corrections used as input in GNSS processing should be assessed deeply, with the aim to make a conclusive statement on the best option: to apply constrained a priori corrections only at the beginning of the estimation, or for every new epoch, or even to consider an ideal interval of application (e.g. every 15 min) which also could be different for tropospheric and ionospheric corrections.

The experiments realized in Part III with integer ambiguity resolution, should be carried out considering a float solution. On the other hand, results of Part II should be verified

considering ambiguity fixing. These changes on strategy can surely improve the understanding of the impacts promoted by the use of atmospheric corrections in such studies.

PPP performances, i. e. accuracy-level and required time necessary for its convergence, will improve significantly with the availability of more accurate GNSS measurements as well as the addition of more carrier frequencies with GPS modernization and new systems in deployment. Such positive aspects must be strongly explored to achieve the best of the method. Thus, it is highly recommended to study the benefits of using atmospheric corrections with the addition of other GNSS constellations, such as Galileo and BDS systems.

References

Askne, J., Nordius, H., 1987. Estimation of tropospheric delay for microwaves from surface weather data. Radio Sci. 22, 379–386. doi:10.1029/RS022i003p00379

Bertiger, W., Desai, S.D., Haines, B., Harvey, N., Moore, A.W., Owen, S., Weiss, J.P., 2010. Single receiver phase ambiguity resolution with GPS data. J. Geod. 84, 327–337. doi:10.1007/s00190-010-0371-9

Bierman, G.J., 1975. Measurement updating using the U-D factorization, in: 1975 IEEE Conference on Decision and Control Including the 14th Symposium on Adaptive Processes. Presented at the 1975 IEEE Conference on Decision and Control including the 14th Symposium on Adaptive Processes, pp. 337–346. doi:10.1109/CDC.1975.270702

Bilitza, D., Brown, S.A., Wang, M.Y., Souza, J.R., Roddy, P.A., 2012. Measurements and IRI model predictions during the recent solar minimum. J. Atmospheric Sol.-Terr. Phys. 86, 99–106.

Blewitt, G., 2006. The Fixed Point Theorem of Ambiguity Resolution for Precise Point Positioning of GPS Networks: Theory and Applications. AGU Fall Meet. Abstr. 43.

Blewitt, G., 1989. Carrier phase ambiguity resolution for the Global Positioning System applied to geodetic baselines up to 2000 km. J. Geophys. Res. Solid Earth 94, 10187–10203.

Boehm, J., Heinkelmann, R., Schuh, H., 2007. Short Note: A global model of pressure and temperature for geodetic applications. J. Geod. 81, 679–683. doi:10.1007/s00190-007-0135-3

Boehm, J., Niell, A., Tregoning, P., Schuh, H., 2006. Global Mapping Function (GMF): A new empirical mapping function based on numerical weather model data. Geophys. Res. Lett. 33. doi:10.1029/2005GL025546

Boehm, J., Schuh, H., 2004. Vienna mapping functions in VLBI analyses. Geophys. Res. Lett. 31, L01603. doi:10.1029/2003GL018984

Böhm, J., Möller, G., Schindelegger, M., Pain, G., Weber, R., 2015. Development of an improved empirical model for slant delays in the troposphere (GPT2w). GPS Solut. 19, 433–441. doi:10.1007/s10291-014-0403-7

Böhm, J., Schuh, H., Urquhart, L., Steigenberger, P., Santos, M., 2011. Troposphere Delay Modeling Based On Numerical Weather Models, in: Proceedings of the 3rd International Colloquium Scientific and Fundamental Aspects of the Galieleo Programme. Copenhagem, Denmark.

Caissy, M., Agrotis, L., 2011. IGS Real-time Working Group and IGS Real-time Pilot Project.

Camargo, P. de O., 2009. Quality of TEC Estimated with Mod_Ion Using GPS and GLONASS Data. Math. Probl. Eng. 2009, 1–16. doi:10.1155/2009/794578

Camargo, P., Monico, J.F.G., Ferreira, L.D.D., 2000. Application of ionospheric corrections in the equatorial region for L1 GPS users. Earth Planets Space 52, 1083–1089.

Chen, C.Y., Singh, M.J., 2014. Comparison of tropospheric scintillation prediction models of the Indonesian climate. Earth Planets Space 66, 1–12.

Collins, P., 2008. Isolating and estimating undifferenced GPS integer ambiguities, in: Proceedings of ION NTM-2008. Institute of Navigation, San Diego, California, p. pp 720-732.

Collins, P., Bisnath, S., Lahaye, F., Héroux, P., 2010. Undifferenced GPS ambiguity resolution using the decoupled clock model and ambiguity datum fixing. Navigation 57, 123–135.

Coordination Scientific Information Center, 2008. Global Navigation Satellite System - GLONASS - Interface Control Document (No. 5.1).

Dach, R., Lutz, S., Walser, P., Fridez, P., 2015. Bernese GNSS software version 5.2. University of Bern, Bern Open Publishing.

Davies, K., 1990. Ionospheric Radio. IET.

Davis, J.L., Elgered, G., Niell, A.E., Kuehn, C.E., 1993. Ground-based measurement of gradients in the “wet” radio refractivity of air. Radio Sci. 28, 1003–1018. doi:10.1029/93RS01917

Davis, J.L., Herring, T.A., Shapiro, I.I., Rogers, A.E.E., Elgered, G., 1985. Geodesy by radio interferometry: Effects of atmospheric modeling errors on estimates of baseline length. Radio Sci. 20, 1593–1607. doi:10.1029/RS020i006p01593

De Jonge, P.G., 1998. A processing strategy for the application of the GPS in networks. TU Delft, Deflt.

de Oliveira, P.S., Morel, L., Fund, F., Legros, R., Monico, J.F.G., Durand, S., Durand, F., 2017. Modeling tropospheric wet delays with dense and sparse network configurations for PPP-RTK. GPS Solut. 21, 237–250. doi:10.1007/s10291-016-0518-0

Dousa, J., Elias, M., 2014. An improved model for calculating tropospheric wet delay. Geophys. Res. Lett. 41, 4389–4397.

Duquenne, F., Botton, S., Peyret, F., Bétaille, D., Willis, P., 2005. GPS: localisation et navigation par satellites. Hermès Science Publications, Paris.

El-Gizawy, M.L., 2003. Development of an ionosphere monitoring technique using GPS measurements for high latitude GPS users. University of Calgary.

ESA, 2016. European GNSS (Galileo) Initial Services: open services definition document.

Ferenc, M., 2014. GPS observation of geophysical deformations induced by non tidal loading. Paris, CNAM.

Fotopoulos, G., Cannon, M.E., 2001. An overview of multi-reference station methods for cm-level positioning. GPS Solut. 4, 1–10.

Fund, F., 2009. Observations GPS et retards troposphériques : modélisations et application aux effets de surcharge océanique dans l'Ouest de la France. Université de Nantes, Le Mans.

Fund, F., Morel, L., Mocquet, A., Boehm, J., 2011. Assessment of ECMWF-derived tropospheric delay models within the EUREF Permanent Network. GPS Solut. 15, 39–48. doi:10.1007/s10291-010-0166-8

Fund, F., Perosanz, F., Testut, L., Loyer, S., 2013. An Integer Precise Point Positioning technique for sea surface observations using a GPS buoy. Adv. Space Res. 51, 1311–1322. doi:10.1016/j.asr.2012.09.028

Gao, Y., Chen, K., 2004. Performance analysis of precise point positioning using rea-time orbit and clock products. J. Glob. Position. Syst. 3, 95–100.

Ge, M., Douša, J., Li, X., Ramatschi, M., Nischan, T., Wickert, J., 2012. A Novel Real-time Precise Positioning Service System: Global Precise Point Positioning With Regional Augmentation. J. Glob. Position. Syst. 11, 2–10. doi:10.5081/jgps.11.1.2

Ge, M., Gendt, G., Rothacher, M., Shi, C., Liu, J., 2008. Resolution of GPS carrier-phase ambiguities in Precise Point Positioning (PPP) with daily observations. J. Geod. 82, 389–399. doi:10.1007/s00190-007-0187-4

Gelb, A., 1974. Applied Optimal Estimation. MIT Press.

Geng, J., Shi, C., Ge, M., Dodson, A.H., Lou, Y., Zhao, Q., Liu, J., 2012. Improving the estimation of fractional-cycle biases for ambiguity resolution in precise point positioning. J. Geod. 86, 579–589. doi:10.1007/s00190-011-0537-0

Geng, J., Teferle, F.N., Meng, X., Dodson, A.H., 2011. Towards PPP-RTK: Ambiguity resolution in real-time precise point positioning. Adv. Space Res. 47, 1664–1673. doi:10.1016/j.asr.2010.03.030

Geng, J., Teferle, F.N., Shi, C., Meng, X., Dodson, A.H., Liu, J., 2009. Ambiguity resolution in precise point positioning with hourly data. GPS Solut. 13, 263–270. doi:10.1007/s10291-009-0119-2

Grinter, T., Roberts, C., 2013. Real time precise point positioning: are we there yet, in: IGNSS Symposium. Citeseer.

Gupta, H., 2011. Encyclopedia of Solid Earth Geophysics. Springer Science & Business Media.

Hadas, T., Kaplon, J., Bosy, J., Sierny, J., Wilgan, K., 2013. Near-real-time regional troposphere models for the GNSS precise point positioning technique. Meas. Sci. Technol. 24, 055003. doi:10.1088/0957-0233/24/5/055003

Herring, T.A., 1992. Modeling atmospheric delays in the analysis of space geodetic data, in: Proceedings of Refraction of Atmospheric Signals in Geodesy, Eds. JC De Munck and TA Spoelstra. Netherlands Geodetic Commission.

Hofmann-Wellenhof, B., Lichtenegger, H., Wasle, E., 2008. GNSS -- global navigation satellite systems: GPS, GLONASS, Galileo, and more. Springer, Wien ; New York.

Ibrahim, H.E., El-Rabbany, A., 2011. Performance analysis of NOAA tropospheric signal delay model. Meas. Sci. Technol. 22, 115107.

Julier, S.J., Uhlmann, J.K., 2004. Unscented filtering and nonlinear estimation. Proc. IEEE 92, 401–422. doi:10.1109/JPROC.2003.823141

Kalita, J.Z., Rzepecka, Z., 2017. Impact of the initial tropospheric zenith path delay on precise point positioning convergence during active conditions. Meas. Sci. Technol. 28, 045102. doi:10.1088/1361-6501/aa5742

Kalman, R.E., 1960. A new approach to linear filtering and prediction problems. J. Basic Eng. 82, 35–45.

Kaplan, E.D., Hegarty, C. (Eds.), 2006. Understanding GPS: principles and applications, 2nd ed. ed, Artech House mobile communications series. Artech House, Boston.

Khodabandeh, A., Teunissen, P.J.G., 2016. PPP-RTK and inter-system biases: the ISB look-up table as a means to support multi-system PPP-RTK. J. Geod. 90, 837–851. doi:10.1007/s00190-016-0914-9

Kintner, P.M., Ledvina, B.M., de Paula, E.R., 2007. GPS and ionospheric scintillations: GPS AND IONOSPHERIC SCINTILLATIONS. Space Weather 5, n/a-n/a. doi:10.1029/2006SW000260

Kouba, J., Héroux, P., 2001. Precise point positioning using IGS orbit and clock products. GPS Solut. 5, 12–28.

Lanyi, G., 1984. Tropospheric Delay Affecting in Radio Interferometry (Telecommunications and Data Acquisition Progress Rep. Jet Propulsion). Jet Propulsion Laboratory, Pasadena.

Laurichesse, D., 2016. PPP software package (version 1.3) - User guide.

Laurichesse, D., 2008. Phase biases for ambiguity resolution: from an undifferenced to an uncombined formulation.

Laurichesse, D., Blot, A., 2016. Fast PPP Convergence Using Multi-Constellation and Triple-Frequency Ambiguity Resolution, in: Proceedings of ION GNSS 2016. Portland.

Laurichesse, D., Langley, R., 2015. Handling the Biases for Improved T riple-Frequency PPP Convergence. GPS World, Innovation clumn.

Laurichesse, D., Mercier, F., 2007. Integer ambiguity resolution on undifferenced GPS phase measurements and its application to PPP., in: Proceedings of the 20th International Technicalmeeting of the Satellite Division of the Institute of Navigation. Presented at the ION GNSS 2007, p. pp 839–848.

Laurichesse, D., Mercier, F., BERTHIAS, J.-P., 2010. Real-time PPP with undifferenced integer ambiguity resolution, experimental results, in: Proceedings of ION GNSS 2010. Portland.

Laurichesse, D., Mercier, F., Berthias, J.-P., Broca, P., Cerri, L., 2009. Integer Ambiguity Resolution on Undifferenced GPS Phase Measurements and its Application to PPP and Satellite Precise Orbit Determination. Navigation. Navigation 56.

Laurichesse, D., Privat, A., 2015. An Open-source PPP Client Implementation for the CNES PPP-WIZARD Demonstrator, in: Proceedings of ION GNSS. Tampa.

Leandro, R., Landau, H., Nitschke, M., Glocker, M., Seeger, S., Chen, X., Deking, A., BenTahar, M., Zhang, F., Ferguson, K., others, 2011. RTX positioning: the next generation of cm-accurate real-time GNSS positioning, in: ION GNSS.

Leandro, R.F., Santos, M.C., 2006. Wide area based precise point positioning, in: Proceedings of ION GNSS. pp. 26–29.

Leick, A., 2004. GPS Satellite Surveying. John Wiley & Sons.

Lejeune, S., Wautelet, G., Warnant, R., 2012. Ionospheric effects on relative positioning within a dense GPS network. GPS Solut. 16, 105–116. doi:10.1007/s10291-011-0212-1

Li, J., Jiantong Zhang, Bingqi Zhang, Bing Shen, 2015. Operation and development of BeiDou Navigation Satellite System. IEEE, pp. 1–6. doi:10.1109/IAIN.2015.7352218

Li, X., Dick, G., Ge, M., Heise, S., Wickert, J., Bender, M., 2014a. Real-time GPS sensing of atmospheric water vapor: Precise point positioning with orbit, clock, and phase delay corrections. Geophys. Res. Lett. 41, 2013GL058721. doi:10.1002/2013GL058721

Li, X., Ge, M., Douša, J., Wickert, J., 2014b. Real-time precise point positioning regional augmentation for large GPS reference networks. GPS Solut. 18, 61–71. doi:10.1007/s10291-013-0310-3

Li, X., Zhang, X., Guo, F., 2014c. Predicting atmospheric delays for rapid ambiguity resolution in precise point positioning. Adv. Space Res. 54, 840–850. doi:10.1016/j.asr.2013.07.021

Lima, C.M.D.A., 2015. PPP com Solução de ambiguidades interas no contexto de Rede GPS. Sao Paulo State University (Unesp), Presidente Prudente.

Liu, F., Gao, Y., 2017. Triple-Frequency GPS Precise Point Positioning Ambiguity Resolution Using Dual-Frequency Based IGS Precise Clock Products. Int. J. Aerosp. Eng. 2017, e7854323. doi:10.1155/2017/7854323

Liu, G.C., 2001. Ionosphere weighted global positioning system carrier phase ambiguity resolution. University of Calgary.

Loyer, S., Perosanz, F., Mercier, F., Capdeville, H., Marty, J.-C., 2012. Zero-difference GPS ambiguity resolution at CNES–CLS IGS Analysis Center. J. Geod. 86, 991–1003. doi:10.1007/s00190-012-0559-2

Ma, G., Maruyama, T., 2003. Derivation of TEC and estimation of instrumental biases from GEONET in Japan, in: Annales Geophysicae. pp. 2083–2093.

Marini, J.W., 1972. Correction of Satellite Tracking Data for an Arbitrary Tropospheric Profile. Radio Sci. 7, 223–231. doi:10.1029/RS007i002p00223

Marques, H.A., 2012. PPP em tempo real com estimativa das correções dos relógios dos satélites no contexto de rede GNSS. Sao Paulo State University (Unesp), Presidente Prudente.

Matsuoka, T., 2007. Influência de diferentes condições da ionosfera no posicionamento por ponto com GPS: Avaliação na região brasileira. Sao Paulo State University (Unesp), Presidente Prudente.

McNamara, L.F., 1991. The Ionosphere: Communications, Surveillance, and Direction Finding. Krieger Publishing Company.

Mercier, F., Laurichesse, D., 2008. Zero-difference ambiguity blocking, Properties of satellite/receiver widelane biases, in: Proceedings of the ENC-GNSS 2008.

Mervart, L., Lukes, Z., Rocken, C., Iwabuchi, T., 2008. Precise Point Positioning with ambiguity resolution in real-time, in: Proceedings of ION GNSS. pp. 397–405.

Mervart, L., Rocken, C., Iwabuchi, T., Kanzaki, M., 2013. Precise Point Positioning with Fast Ambiguity Resolution – Prerequisites, Algorithms and Performance, in: Proceedings of the 26th International Technical Meeting of The Satellite Division of the Institute of Navigation (ION GNSS+ 2013). Nashville, pp. 1176–1185.

Mitas, L., Mitasova, H., 1999. Spatial interpolation. Geogr. Inf. Syst. Princ. Tech. Manag. Appl. 1, 481–492.

Monico, J.F.G., 2008. Posicionamento pelo GNSS descrição, fundamentos e aplicações. Editora UNESP, São Paulo.

Morel, L., 2015. Influence des stratégies de traitement en géodésie spatiale (Dossier d'Habilitation à Diriger des Recherches). Conservatoire National des Arts et Métiers.

Morel, L., Fund, F., Legros, R., Durand, S., Flacelière, B., 2014. PPP, la maturité? Revue XYZ.

Niell, A., Petrov, L., 2003. Using a numerical weather model to improve geodesy, in: arXiv Preprint Physics/0401118. Presented at the The State of GPS Vertical Positioning Precision, Separation of Earth Processes by Space Geodesy, Belgium.

Niell, A.E., 1996. Global mapping functions for the atmosphere delay at radio wavelengths. J. Geophys. Res. Solid Earth 101, 3227–3246.

Nievinski, F.G., 2009. Ray-tracing Options to Mitigate the Neutral Atmosphere Delay in GPS. University of New Brunswick, Department of Geodesy and Geomatics Engineering.

NOAA, 2017. F10.7 cm Radio Emissions [WWW Document]. URL http://www.swpc.noaa.gov/phenomena/f107-cm-radio-emissions (accessed 7.18.17).

Odijk, D., Teunissen, P.J.G., Khodabandeh, A., 2014. Single-Frequency PPP-RTK: Theory and Experimental Results, in: Earth on the Edge: Science for a Sustainable Planet. Springer, Berlin, Heidelberg, pp. 571–578. doi:10.1007/978-3-642-37222-3_75

Park, J., Lee, Y.J., Choi, M., Jang, J.-G., Sung, S., 2016. Feasibility Study on Tropospheric Attenuation Effect of Ku/V Band Signal for Korean Satellite Navigation System. Int. J. Aeronaut. Space Sci. 17, 80–88. doi:10.5139/IJASS.2016.17.1.80

Parkinson, B.W., Spilker, J.J., 1996. Global Positioning System: Theory and Applications. AIAA.

Perosanz, F., Mercier, F., Loyer, S., Petit, G., Marty, J.-C., 2016. A review of “integer” PPP applications, in: EGU General Assembly Conference Abstracts. p. 2940.

Petit, G., Kanj, A., Harmegnies, A., Loyer, S., Delporte, J., Mercier, F., Perosanz, F., 2014. GPS frequency transfer with IPPP, in: 2014 European Frequency and Time Forum (EFTF). Presented at the 2014 European Frequency and Time Forum (EFTF), pp. 451–454. doi:10.1109/EFTF.2014.7331533

Petit, G., Luzum, B., 2010. IERS Conventions (2010) (IERS Technical Note No. 36). Verlag des Bundesamts für Kartographie und Geodäsie, Frankfurt.

Petrie, E.J., King, M.A., Moore, P., Lavallée, D.A., 2010. Higher-order ionospheric effects on the GPS reference frame and velocities. J. Geophys. Res. Solid Earth 115, B03417. doi:10.1029/2009JB006677

Petrovski, I.G., 2014. GPS, GLONASS, Galileo, and BeiDou for Mobile Devices: From Instant to Precise Positioning. Cambridge University Press.

Rizos, C., Janssen, V., Roberts, C., Grinter, T., 2012. PPP versus DGNSS. Geomat. World 20, 18–20.

Rovira-Garcia, A., Juan, J.M., Sanz, J., Gonzalez-Casado, G., 2015. A Worldwide Ionospheric Model for Fast Precise Point Positioning. IEEE Trans. Geosci. Remote Sens. 53, 4596–4604. doi:10.1109/TGRS.2015.2402598

Rüeger, J.M., 2002. Refractive Index Formulae for radio Waves, in: Proceedings of the FIG XXII International Congress. Washington, D. C. USA.

Saastamoinen, J., 1972. Atmospheric correction for the troposphere and stratosphere in radio ranging satellites, in: Henriksen, S.W., Mancini, A., Chovitz, B.H. (Eds.), Geophysical Monograph Series. American Geophysical Union, Washington, D. C., pp. 247–251. doi:10.1029/GM015p0247

Sanz Subirana, J., Juan Zornoza, J.M., Hernández-Pajares, M., 2013. Fundamentals and algorithms. Vol. 1. Vol. 1. ESA Communications, Noordwijk.

Sapucci, L.F., 2001. Estimativa do vapor d'água atmosférico e avaliação da modelagem do atraso zenital troposférico utilizando GPS. Sao Paulo State University (Unesp), Presidente Prudente.

Seeber, G., 2003. Satellite geodesy, 2nd completely rev. and extended ed. ed. Walter de Gruyter, Berlin ; New York.

Shi, J., Gao, Y., 2014. A comparison of three PPP integer ambiguity resolution methods. GPS Solut. 18, 519–528. doi:10.1007/s10291-013-0348-2

Shi, J., Xu, C., Guo, J., Gao, Y., 2014. Local troposphere augmentation for real-time precise point positioning. Earth Planets Space 66, 1–13.

Sreeja, V., Aquino, M., Elmas, Z.G., 2011. Impact of ionospheric scintillation on GNSS receiver tracking performance over Latin America: Introducing the concept of tracking jitter variance maps. Space Weather 9, S10002. doi:10.1029/2011SW000707

St. Laurent, A.M., 2008. Understanding Open Source and Free Software Licensing. O'Reilly Media, Inc., Sebastopol.

Stürze, A., Mervart, L., Söhne, W., Weber, G., Wübbena, G., 2012. Real-Time PPP using open CORS Networks and RTCM Standards, in: Proceedings of 3rd International Conference on Machine Control & Guidance.

Takasu, T., 2013. RTKLIB ver. 2.4.2 Manual.

Tapping, K.F., 2013. The 10.7 cm solar radio flux: F10.7. Space Weather 11, 394–406. doi:10.1002/swe.20064

Teunissen, P.J., 2001. GNSS ambiguity bootstrapping: theory and application, in: Proceedings of International Symposium on Kinematic Systems in Geodesy, Geomatics and Navigation. pp. 246–254.

Teunissen, P.J., 1995. The least-squares ambiguity decorrelation adjustment: a method for fast GPS integer ambiguity estimation. J. Geod. 70, 65–82.

Teunissen, P.J., Odijk, D., Zhang, B., 2010. PPP-RTK: results of CORS network-based PPP with integer ambiguity resolution. J Aeronaut Astronaut Aviat Ser A 42, 223–230.

Teunissen, P.J.G., Joosten, P., Tiberius, C., 2002. A comparison of TCAR, CIR and LAMBDA GNSS ambiguity resolution, in: ION GPS. pp. 2799–2808.

Teunissen, P.J.G., Khodabandeh, A., 2015. Review and principles of PPP-RTK methods. J. Geod. 89, 217–240. doi:10.1007/s00190-014-0771-3

Thornton, C.L., Bierman, G.J., 1975. Gram-Schmidt algorithms for covariance propagation, in: 1975 IEEE Conference on Decision and Control Including the 14th Symposium on Adaptive Processes. Presented at the 1975 IEEE Conference on Decision and Control including the 14th Symposium on Adaptive Processes, pp. 489–498. doi:10.1109/CDC.1975.270739

Tregoning, P., Rizos, C., 2008. Dynamic Planet: Monitoring and Understanding a Dynamic Planet with Geodetic and Oceanographic Tools. Springer Science & Business Media.

United Nations, O. for O.S., 2016. International Committee of Global Navigation Satellite Systems: The Way Forward. United Nations, S.l.

Urquhart, L., Nievinski, F.G., Santos, M.C., 2014. Assessment of troposphere mapping functions using three-dimensional ray-tracing. GPS Solut. 18, 345–354. doi:10.1007/s10291-013-0334-8

Urquhart, L., Santos, M., 2011. Development of a VMF1-like service at UNB.

Wilson, B.D., Yinger, C.H., Feess, W.A., Shank, C.C., 1999. New and Improved: the broadcast interfrequency biases. GPS World 10, 56–66.

Wu, J.T., Wu, S.C., Hajj, G.A., Bertiger, W.I., Lichten, S.M., 1992. Effects of antenna orientation on GPS carrier phase. Presented at the Astrodynamics 1991, pp. 1647–1660.

Wübbena, G., 1985. Software Development for Geodetic Positioning with GPS Using TI 4100 Code and Carrier Measurements., in: Proceedings of First Int. Symposium on Precise Position with GPS. Presented at the First Int. Symposium on Precise Position with GPS, Rockville, Maryland, pp. 403–412.

Wübbena, G., Bagge, A., Seeber, G., Böder, V., Hankemeier, P., 1996. Reducing distance dependent errors for real-time precise DGPS applications by establishing reference station networks, in: PROCEEDINGS OF ION GPS. Institute of Navigation, pp. 1845–1852.

Wübbena, G., Schmitz, M., Bagge, A., 2014. PPP with ambiguity resolution (AR) using RTCM-SSR.

Wübbena, G., Schmitz, M., Bagge, A., 2005. PPP-RTK: precise point positioning using state-space representation in RTK networks, in: Proceedings of ION GNSS. pp. 13–16.

Zaminpardaz, S., Teunissen, P.J.G., Nadarajah, N., 2016. GLONASS CDMA L3 ambiguity resolution and positioning. GPS Solut. doi:10.1007/s10291-016-0544-y

Zhang, B., Teunissen, P.J.G., Odijk, D., 2011. A Novel Un-differenced PPP-RTK Concept. J. Navig. 64, S180–S191. doi:10.1017/S0373463311000361

Zhang, H., Gao, Z., Ge, M., Niu, X., Huang, L., Tu, R., Li, X., 2013. On the Convergence of Ionospheric Constrained Precise Point Positioning (IC-PPP) Based on Undifferential Uncombined Raw GNSS Observations. Sensors 13, 15708–15725. doi:10.3390/s131115708

Zumberge, J.F., Heflin, M.B., Jefferson, D.C., Watkins, M.M., Webb, F.H., 1997. Precise point positioning for the efficient and robust analysis of GPS data from large networks. J. Geophys. Res. Solid Earth 102, 5005–5017. doi:10.1029/96JB03860

Zus, F., Deng, Z., Heise, S., Wickert, J., 2017. Ionospheric mapping functions based on electron density fields. GPS Solut. 21, 873–885. doi:10.1007/s10291-016-0574-5

Zus, F., Dick, G., Douša, J., Heise, S., Wickert, J., 2014. The rapid and precise computation of GPS slant total delays and mapping factors utilizing a numerical weather model. Radio Sci. 49, 207–216. doi:10.1002/2013RS005280

Annex 1 - RTKLIB package license

Redistribution and use in source and binary forms, with or without modification, are permitted provided that the following conditions are met:

- Redistributions of source code must retain the above copyright notice, this list of conditions and the following disclaimer.

- Redistributions in binary form must reproduce the above copyright notice, this list of conditions and the following disclaimer in the documentation and/or other materials provided with the distribution.

- The software package includes some companion executive binaries or shared libraries necessary to execute APs on Windows. These licenses succeed to the original ones of these software.

THIS SOFTWARE IS PROVIDED BY THE COPYRIGHT HOLDERS AND CONTRIBUTORS "AS IS" AND ANY EXPRESS OR IMPLIED WARRANTIES, INCLUDING, BUT NOT LIMITED TO, THE IMPLIED WARRANTIES OF MERCHANTABILITY AND FITNESS FOR A PARTICULAR PURPOSE ARE DISCLAIMED. IN NO EVENT SHALL THE COPYRIGHT HOLDER OR CONTRIBUTORS BE LIABLE FOR ANY DIRECT, INDIRECT, INCIDENTAL, SPECIAL, EXEMPLARY, OR CONSEQUENTIAL DAMAGES (INCLUDING, BUT NOT LIMITED TO, PROCUREMENT OF SUBSTITUTE GOODS OR SERVICES; LOSS OF USE, DATA, OR PROFITS; OR BUSINESS INTERRUPTION) HOWEVER CAUSED AND ON ANY THEORY OF LIABILITY, WHETHER IN CONTRACT, STRICT LIABILITY, OR TORT (INCLUDING NEGLIGENCE OR OTHERWISE) ARISING IN ANY WAY OUT OF THE USE OF THIS SOFTWARE, EVEN IF ADVISED OF THE POSSIBILITY OF SUCH DAMAGE.

Notes: Previous versions of RTKLIB until ver. 2.4.1 had been distributed under GPLv3 license.

Annex 2 - PPP-Wizard license

License PPP-Wizard-User version 1.3 (2016/02/15)

1 – Preamble

This license is to establish the conditions, under which you may use, modify and distribute the SOFTWARE. However, CNES remains the author of the SOFTWARE and retains the enjoyment and use of all rights attached thereto.

2 – Definition

The SOFTWARE is constituted by all successive versions of PPP-Wizard-User software and documentation developed by CNES. The latest version is : PPP-Wizard-User Version 1.2 (January 30, 2015).

The PPP-Wizard-User DERIVATIVE SOFTWARE consists of all or part of SOFTWARE you modified and/or translated and/or adapted.

The PPP-Wizard-User COMPOSITE SOFTWARE consists of all or part of the SOFTWARE that you have interfaced with software, a software package or a toolbox that you own or assign.

3 - Purpose and conditions of the SOFTWARE license

a) CNES allows you, free of charge, to reproduce, on all present and future support, source code and/or object code of the SOFTWARE without restriction, provided that appears in all copies the mention of the following copyright : 'PPP-Wizard- user (c) CNES'.

b) CNES allows you, free of charge, to fix any bugs, to make the changes required for SOFTWARE porting, and make any changes or usual functional correction provided that you insert a patch file, or you indicate by any equivalent means, the nature and date of the amendment or correction on the concerned SOFTWARE file(s).

c) CNES allows you, free of charge, to use the source code and/or object code of the SOFTWARE without restriction, provided that appears in all copies the mention of the following copyright : PPP-Wizard-User (c) CNES.

d) CNES allows you to disseminate and distribute, free of charge, source code and/or object code of the SOFTWARE on any present and future support, provided that :

- you include on all copies the following copyright notice :
- "PPP-Wizard-User (c) CNES" ;
- you disseminate or distribute the SOFTWARE under the terms of this license.
- you disseminate, free of charge, the patch files, or files containing equivalent informations about the nature and date of the amendment/correction to the concerned SOFTWARE file(s).

e) Any commercial use or commercial distribution of the SOFTWARE must be authorized by CNES.

4 - Purpose and conditions of the license covering the SOFTWARE DERIVATIVES

a) CNES allows you, free of charge, to reproduce, and modify, and/or translate, and/or adapt all or part of the source code and/or object code of the SOFTWARE, provided that you insert a patch file indicating the date and the nature of the modification, and/or translation,

and/or adaptation and the name of their authors on the SOFTWARE file(s) concerned. The modified SOFTWARE constitutes DERIVATIVES SOFTWARE. CNES allows you, free of charge, to use the source code and/or object code of the SOFTWARE without restriction, provided that appears in all copies the mention of the following copyright : PPP-Wizard-User CNES.

b) CNES allows, free of charge, to use the source code and/or object code of the SOFTWARE modified under Article 4-a) above, without restriction, provided that appears in all copies the copyright notice next: PPP-Wizard-User (c) CNES.

c) CNES allows you, free of charge, to disseminate and distribute, free of charge for non-commercial purposes, the source code and/or object code of the SOFTWARE DERIVATIVES on any present and future support, provided that you :

- state clearly "PPP-Wizard (c) CNES";
- distribute DERIVATIVE SOFTWARE under this License;
- allow recipients to access to the source code of the SOFTWARE
- distribute DERIVATIVE SOFTWARE under a name other than PPP-Wizard-User.

d) Any commercial use or commercial distribution of DERIVATIVE SOFTWARE must be authorized by CNES.

5 - Purpose and conditions of the license covering the COMPOSITE SOFTWARE

a) CNES allows you to reproduce and make the interface of all or part of the SOFTWARE, with all or part of other software packages or toolboxes which you are owners or holders, in order to obtain COMPOSITE SOFTWARE.

b) CNES allows you, free of charge, to use the source code and/or object code of the SOFTWARE included in COMPOSITE SOFTWARE, without restriction, provided that appears in all copies the mention of the following copyright : "composite software using features PPP-Wizard-User (c) CNES "

c) CNES allows you, free of charge, to disseminate and distribute, free of charge for non-commercial purposes, source code and/or object code of COMPOSITE SOFTWARE on any present and future support, provided that you :

- state clearly "composite software using features of PPP-Wizard-User (c) CNES ";
- distribute the SOFTWARE included in COMPOSITE SOFTWARE under this License;
- allow recipients to access to the source code of the SOFTWARE;
- distribute COMPOSITE SOFTWARE under a name other than PPP-Wizard-User.

d) Any commercial use or distribution of COMPOSITE SOFTWARE must be authorized by CNES.

6 - Limited Warranty

Unless otherwise agreed in writing, the SOFTWARE is provided as is without any express or implied warranties, including warranties of merchantability or fitness. You assume the entire risk as to the quality or the effects of the SOFTWARE and use. If the SOFTWARE is defective, you assume the cost of all necessary servicing, repair or correction.

7- Effect Required

This license has the binding value of a contract.
You are responsible for compliance with the license by a third party.
8 - Governing Law
This license and its effects are subject to French law and the competent French courts.

Annex 3 - Standardized and experimental SSR RTCM messages for PPP users

Table 23 - Different messages currently standardized and experimental SSR RTCM messages for PPP users.

Stage	SSR Message Name	SSR message type	Status
1	GPS Orbit Correction	1057	Standardized
1	GPS Clock Correction	1058	Standardized
1	GPS Code Bias	1059	Standardized
1	GPS Combined Orbit and Clock Corrections	1060	Standardized
1	GPS High Rate Clock Correction	1061	Standardized
1	GPS User Range Accuracy (URA)	1062	Standardized
1	GLONASS Orbit Correction	1063	Standardized
1	GLONASS Clock Correction	1064	Standardized
1	GLONASS Code Bias	1065	Standardized
1	GLONASS Combined Orbit and Clock Corrections	1066	Standardized
1	GLONASS High Rate Clock Correction	1067	Standardized
1	GLONASS URA	1068	Standardized
1	Galileo Orbit Correction	1240	Standardized
1	Galileo Clock Correction	1241	Standardized
1	Galileo Code Bias	1242	Standardized
1	Galileo Combined Orbit and Clock Corrections	1243	Standardized
1	Galileo High Rate Clock Correction	1244	Standardized
1	Galileo URA	1245	Standardized
1	QZSS Orbit Correction	1246	Standardized
1	QZSS Clock Correction	1247	Standardized
1	QZSS Code Bias	1248	Standardized
1	QZSS Combined Orbit and Clock Corrections	1249	Standardized
1	QZSS High Rate Clock Correction	1250	Standardized
1	QZSS URA	1251	Standardized
1	SBAS Orbit Correction	1252	Standardized
1	SBAS Clock Correction	1253	Standardized
1	SBAS Code Bias	1254	Standardized
1	SBAS Combined Orbit and Clock Corrections	1255	Standardized
1	SBAS High Rate Clock Correction	1256	Standardized
1	SBAS URA	1257	Standardized

1	BDS Orbit Correction	1258	Standardized
1	BDS Clock Correction	1259	Standardized
1	BDS Code Bias	1260	Standardized
1	BDS Combined Orbit and Clock Corrections	1261	Standardized
1	BDS High Rate Clock Correction	1262	Standardized
1	BDS URA	1263	Standardized
1	Satellite GPS Phase Bias	1265	Standardized
1	Satellite GLONASS Phase Bias	1266	Standardized
2	Satellite Galileo Phase Bias	1267	Standardized
2	Satellite QZSS Phase Bias	1268	Standardized
2	Satellite SBAS Phase Bias	1269	Standardized
2	Satellite BDS Phase Bias	1270	Standardized
2	SSR Ionosphere Spherical Harmonics	1264	Experimental
3	SSR Ionospheric Slant TEC	????	Planed
3	SSR Tropospheric delay	????	Planed

Source: adapted from (Stürze et al., 2012; Wübbena et al., 2014)

Paulo Sérgio DE OLIVEIRA Jr.
Definition and implementation of a new service for precise GNSS positioning

Abstract:
PPP (Precise Point Positioning) is a GNSS (Global Navigation Satellite Systems) method, based on SSR (State Space Representation) concept. Thanks to recent improvements in atmospheric models, Real-time PPP (RT-PPP) can also be improved. The main objective of this work is to study the RT-PPP and the optimized infrastructure in terms of costs and benefits to realize the method using atmospheric corrections. Therefore, different configurations of a dense and regular GNSS network existing in France, the Orpheon network, are used. This network has about 160 sites and is owned by Geodata-Diffusion (Hexagon Geosystems). Initially, 'float PPP-RTK' was evaluated, it corresponds to RT-PPP with improvements resulting from network corrections, although with ambiguities kept float. Further on, network corrections are applied to improve "PPP-RTK" where ambiguities are fixed to their integer values. For the float PPP-RTK, a modified version of the RTKLib 2.4.3 (beta) package is used to apply network corrections. First-order ionospheric effects were eliminated by the iono-free combination and zenith tropospheric delay estimated. The corrections were applied by introducing a priori constrained tropospheric parameters. Adaptive modeling based on OFCs (Optimal Fitting Coefficients) has been developed to describe the behavior of the troposphere, using estimates of tropospheric delays for Orpheon stations. This solution allows one-way communication between the server and the user. The gains achieved in convergence time to 10 centimeters accuracy were statistically quantified. Network topology was assessed by reducing the number of reference stations (up to 75%) using a sparse network configuration. In the second step, PPP-RTK is realized using the PPP-Wizard 1.3 software and CNES (*Centre National d'Etudes Spatiales*) real-time products for orbits, clocks and phase biases of satellites. The RT-IPPP (RT-*Integer* PPP) is performed with estimation of tropospheric and ionospheric delays. Ionospheric and tropospheric corrections are introduced as a priori parameters constrained in PPP-RTK. To generate ionospheric corrections, it was implemented an Inverse Distance Weighting (IDW) algorithm. Improvements achieved in horizontal positioning due to external SSR corrections from a (dense or sparse) network are promising and may be useful for applications that depend primarily on horizontal positioning.
Keywords: GNSS; PPP-RTK; ZWD; Troposphere; Ionosphere; Modeling; Reference network; Ambiguity resolution.

Résumé :
Le PPP (*Precise Point Positioning*) est une méthode GNSS (*Global Navigation Satellite Systems*), basée sur le concept SSR (*State Space Representation*). Grâce aux améliorations récentes des modèles atmosphériques, le PPP en temps réel (RT-PPP) peut être également amélioré. L'objectif principal de ce travail est d'étudier le RT-PPP et l'infrastructure optimisée en termes de coûts et d'avantages pour réaliser la méthode en utilisant des corrections atmosphériques. Pour cela, différentes configurations d'un réseau GNSS dense et régulier existant en France, le réseau Orphéon, sont utilisées. Ce réseau compte environ 160 sites, propriété de Geodata-Diffusion (Hexagon Geosystems). Dans un premier temps, le mode «PPP-RTK flottant» a été évalué, il correspond au RT-PPP avec des améliorations issues des corrections de réseau, mais avec les ambiguïtés flottantes. Ensuite, des corrections de réseau sont appliquées pour améliorer le mode « PPP-RTK » où les ambiguïtés sont fixées à leurs valeurs entières. Pour le PPP-RTK flottant, une version modifiée du package RTKLib 2.4.3 (beta) est utilisée pour prendre en compte les corrections réseau. Les effets ionosphériques de premier ordre ont été éliminés par la combinaison *iono-free* et le retard troposphérique zénithal est estimé. Les corrections ont été appliquées en introduisant des paramètres troposphériques a priori contraints. Une modélisation adaptative basée sur les OFCs (*Optimal Fitting Coefficients*) a été mise en place pour décrire le comportement de la troposphère, en utilisant des estimations des retards troposphériques pour les stations Orphéon. Cette solution permet une communication monodirectionnelle entre le serveur et l'utilisateur. Les gains réalisés sur le temps de convergence pour obtenir un positionnement de 10 centimètres de précision ont été quantifiés statistiquement. La topologie du réseau a été évaluée, en réduisant le nombre de stations de référence (jusqu'à 75%), via une configuration de réseau lâche. Dans la deuxième étape, le PPP-RTK est réalisé grâce au logiciel PPP-Wizard 1.3 et avec les produits temps réel CNES (*Centre Nacional de Estudes Spatiales*) pour les orbites, les horloges et les biais de phase des satellites. Le RT-IPPP (RT-*Integer* PPP) est réalisé avec estimation des délais troposphériques et ionosphériques. Les corrections ionosphériques et troposphériques sont introduites en tant que paramètres a priori contraints au PPP-RTK. Pour générer des corrections ionosphériques, il a été mis en place un algorithme d'interpolation à distance inversée (IDW–*Inverse Distance Weighting*). Les améliorations apportées au positionnement horizontal dues aux corrections atmosphériques SSR externes provenant d'un réseau (dense ou lâche) sont prometteuses et peuvent être utiles pour les applications qui dépendent principalement du positionnement horizontal.
Mots-clés : GNSS; PPP-RTK; ZWD; Troposphère; Ionosphère; Modèles; Réseau de référence; Résolution des ambiguïtés

Resumo:
O PPP (*Precise Point Positioning*) é um método GNSS (*Global Navigation Satellite Systems*) baseado no conceito SSR (*State Space Representation*). Graças às melhorias recentes nos modelos atmosféricos, o PPP em tempo real (RT-PPP) também pode ser aprimorado. O objetivo principal deste trabalho é estudar o RT-PPP e a infraestrutura otimizada em termos de custos e benefícios para realizar o método usando correções atmosféricas. Portanto, são utilizadas diferentes configurações de uma rede GNSS densa e regular existente na França, a rede Orphéon. Esta rede tem cerca de 160 estações, sendo propriedade da Geodata-Diffusion (Hexagon Geosystems). Inicialmente, foi avaliado o "*float* PPP-RTK", que corresponde ao RT-PPP com melhorias resultantes de correções de rede, embora mantendo as ambiguidades como *float*. Em um segundo momento, as correções de rede são aplicadas para aprimorar o "PPP-RTK", onde ambiguidades são fixadas para seus valores inteiros. Para o *float* PPP-RTK, uma versão modificada do software RTKLib 2.4.3 (beta) é empregada de modo a levar em consideração as correções de rede. Os efeitos ionosféricos de primeira ordem foram eliminados pela combinação *iono-free* e o atraso troposférico é estimado. As correções são aplicadas introduzindo parâmetros troposféricos a priori injuncionados. Uma modelagem adaptativa baseada em OFCs (*Optimal Fitting Coefficients*) foi implementada para descrever o comportamento da troposfera, utilizando estimativas de atraso troposférico para estações da rede Orpheon. Tal solução permite a comunicação unidirecional entre o servidor e o usuário. Os ganhos alcançados no tempo de convergência para acurácia de 10 centímetros foram quantificados estatisticamente. A topologia de rede foi avaliada reduzindo o número de estações de referência (até 75%) usando uma configuração de rede esparsa. Na segunda etapa, o PPP-RTK é realizado usando o software PPP-Wizard 1.3, bem como os produtos para tempo real do CNES (*Centre National d'Etudes Spatiales*) de órbitas, relógios e *biases* de fase de satélites. O RT-IPPP (RT-*Integer* PPP) é realizado com estimativa de atrasos troposféricos e ionosféricos. As correções ionosféricas e troposféricas são introduzidas como parâmetros a priori injuncionados no PPP-RTK. Para gerar correções ionosféricas, foi implementado um algoritmo baseado na ponderação pelo inverso da distância (IDW–*Inverse Distance Weighting*). As melhorias alcançadas no posicionamento horizontal com o uso das correções SSR externas de uma rede (densa ou esparsa) são promissoras e podem ser úteis para aplicações que dependem principalmente do posicionamento horizontal.
Palavras chave: GNSS; PPP-RTK; ZWD; Troposfera; Ionosfera; Modelos; Rede de Referência; Resolução das ambiguidades